BIBLIOGRAPHIC INFORMATION

PB94-103777

Report Nos: CCEER-93-1

Title: Behavior, Design, and Retrofit of Reinforced Concrete One-Way Bridge Column Hinges.

Date: Mar 93

Authors: Y. Jiang, M. Saiide, and D. N. O'Connor.

Performing Organization: Nevada Univ., Reno. Center for Civil Engineering Earthquake Research.

Sponsoring Organization: *National Science Foundation, Washington, DC.

Grant Nos: NSF-CES-870062

Supplementary Notes: See also PB92-189109. Sponsored by National Science Foundation, Washington, DC.

NTIS Field/Group Codes: 50A, 50C, 89D

Price: PC A09/MF A03

Availability: Available from the National Technical Information Service, Springfield, VA. 22161

Number of Pages: 196p

Keywords: *Bridge piers, *Hinges, *Earthquake engineering, Seismic design, Reinforced concrete, Lateral pressure, Loads(Forces), Mathematical models, Axial strain.

Abstract: The experimental program included testing of four types of specimens. The first type represents column-to-foundation connections using 1/6-scale replicas of the hinges in piers 2 and 3 of the Rose Creek Bridge. Five specimens of this type were tested. The purpose of the first four sprcimens was to determine the influence of reinforcement details in the hinge region on energy absorption capacities under cyclic loads. The fifth specimen was used in a pilot study to determine the cyclic response of hinged columns with inadequate steel development length, and to develop and test a repair method for damaged columns.

Center for Civil Engineering Earthquake Research

- Reno

Engineering Research and Development Center
College of Engineering
University of Nevada, Reno

Report Number CCEER-93-1

Behavior, Design, and Retrofit of Reinforced Concrete One-way Bridge Column Hinges

Y. Jiang and M. "Saiid" Saiidi

Edited by D. N. O'Connor

Center for Civil Engineering Earthquake Research
Department of Civil Engineering/258
University of Nevada
Reno, Nevada 89557

March 1993

Abstract

This report describes an experimental and analytical investigation of one-way reinforced concrete hinges, frequently used at the base of highway bridge columns, when subjected to axial compression, shear, and uniaxial moment transfer in the strong direction. Attempts were made to develop recommendations for more reliable hinged column design, to conduct a preliminary study of the response of hinged columns with inadequate reinforcement development length, and to develop and test a repair method for damaged columns.

Many variables, including column aspect ratio, monotonic or cyclic loading, hinge steel arrangement, and hinge thickness relative to hinge width, were examined to study their effects on hinge flexural and shear strength, energy dissipation capacity, shear slip, and hinge throat concrete confinement.

A linear finite element analysis was performed to study stress distribution in the hinge throat area. Analytical studies also included inelastic analyses of bridges with hinged columns. Focus was placed on the influence of deck torsional stiffness and abutment spring stiffness on inflection point height. The inflection point represents the point where the lateral load should be applied for the purpose of calculating lateral hinge strength.

A new approach was developed for estimating the lateral load strength of hinged columns. This approach can be used for design purpose as well as for calculating the shear capacity for existing hinged pier columns.

Acknowledgements

This study was conducted under grant number CES-870062 from the National Science Foundation. The opinions expressed in this report belong solely to the authors and do not necessarily represent the views of the National Science Foundation.

The authors are indebted to Mr. Jesus Pedroarena, Civil Engineering Technician, for his careful work in constructing, instrumenting, and testing of the specimens. Messrs. Binoy Abraham, David Straw, and Nadim Wehbe, former graduate students at the University of Nevada, are also thanked for their assistance during the testing portion of this study.

Contents

List of Tables

List of Figures

Chapter 1
Introduction

1.1 Background

Reinforced concrete hinges are frequently used at the base of bridge columns to release moment transfer in one or both principal directions. The primary benefit is reduction of the forces transferred to the foundation, thus reducing foundation cost; this cost reduction is particularly significant in bridges supported on soft soil.

Column hinges may be grouped into two categories: one-way hinges and two-way hinges (Figure 1-1). A one-way hinge will release moments in one direction while resisting moments in the other. In a two-way hinge, the moment is released in both directions. Hinged single-column bents are usually detailed with one-way hinges to maintain stability, whereas hinged multiple-column bents may utilize one- or two-way hinges.

While the results of many building system studies have been applied to bridges, there are some aspects of bridge behavior which can not readily be found in the literature on buildings. As a result, many studies have focused on bridge-specific issues related to superstructures and substructures. Reinforced concrete columns commonly used in bridges differ from building columns in slenderness, scale, cross-section, and end connections. Building columns frequently carry higher axial loads than bridge columns. The general design approach to buildings is to force plastic hinging in beams before plastic hinging occurs in columns. In contrast, development of plastic hinges in bridge columns is necessary for energy dissipation under lateral loading. The reinforcement ratio in bridge columns is also smaller than in building columns, typically less than 2 percent.

Bridge columns must allow adequate rotation under thermal loads and loads due to support settlement, transmit relatively small moments, be simple and inexpensive to construct and maintain, provide adequate shear strength, and provide adequate ductility under cyclic loads.

Various types of one-way hinges have been used since the turn of the century. The first, known as the sliding hinge, was used in three-hinged arch construction. A

member with a convex cylindrical surface rests in a cylindrical concavity of the same radius in the adjoining member. Later versions, called saddle bearings, employed unequal radii so that rotation produced rolling, rather sliding, motion between the surfaces. In order to reduce friction and obviate the need for extreme accuracy in the construction, a thin sheet of lead was usually placed between the curved surfaces.

The next type of concrete hinge was developed by a French engineer, Angustin Mesnager, at the beginning of the century, and has been used extensively since 1910.[9] This hinge consists of reinforcing bars crossing each other in a small gap between the members to be articulated. Concrete was usually used to protect the bars against corrosion; however, the contribution of the concrete to the strength of the hinge was ignored.

The realization that concrete strength was considerable in the throat of a Mesnager-type hinge led to the development of the Freyssinet hinge. In a Freyssinet hinge, little or no reinforcement passes through the throat and the throat concrete is recognized to withstand compressive stresses considerably greater than the unconfined compressive strength. Figure 1-2 shows the hinges of various types.

Recent earthquakes have caused severe damage, and even collapse, in a number of concrete bridges.[10,12,30] The 1971 San Fernando earthquake resulted in the collapse of five highway bridges and caused major damage to forty-two other bridges.[21] The primary causes of column damage were identified as: (1) insufficient ductility of bridge columns to absorb the inelastic displacements experienced, (2) shear failures in shorter columns, and (3) longitudinal reinforcement anchorage failure in the plastic hinge regions at the base of columns.

As a consequence, there has been a considerable increase in research and design activities to produce effective and economical measures for seismic design and retrofit of bridges. Reinforced concrete one-way hinges are designed to prevent a build-up of flexural stresses on the foundations in one direction. In the transverse direction, the hinge must be designed to prevent a shear or flexural failure such as could be caused by excessive wind pressures or inertial forces due to an earthquake. Severe earthquakes subject a bridge to many cycles of large-amplitude load reversals; therefore, connections

such as hinges must be capable of undergoing large deformations while maintaining integrity. In addition, the hinge must continue to carry the axial load of the column. Another general requirement for connections is the ability to dissipate energy during inelastic deformation cycles.

One-way hinges are currently designed using the compressive axial capacity of the section and the lateral load capacity based on the shear friction theory.[2,26] Previous research has been conducted to determine the bearing, flexural, and shear capacity of hinges under monotonic and cyclic loading in the weak direction (direction of intended hinging).[8] Additionally, research has also been conducted on the lateral behavior of concrete hinges since the late 1980s.[28,33,36,37] Recent studies demonstrate that the shear friction theory is not appropriate for hinge lateral load design because it does not produce a conservative design. A new approach for lateral load design is needed to replace the shear friction theory.

1.2 Previous Work

Although the concept of using a hinge at a column end to release moment transfer has been employed for almost a century, there appears to be very limited information regarding hinge behavior. Research was conducted in England in the late 1950s and 1960s;[6,7,8,9] however, there is virtually no research data available between that time and the time of the pilot study conducted by Saiidi and Orie in the late 1980s.[28,36]

Base[6] performed research on four one-way reinforced concrete hinges with loading in the direction of hinging. Two specimens were Freyssinet hinges with very little reinforcement through the throats, another was designed as a Mesnager hinge, and the fourth was a saddle bearing. A series of three different loadings were applied to the specimens, including axial load, combined axial and lateral load, and axial load with fatigue flexural load. The test results can be grouped into five categories:

Compressive stress under axial load: The compressive stress in the throat or contact area of the hinge was found rarely, if ever, to result in crushing of the concrete. It appeared that the concrete in the hinge throat was in a state of biaxial or triaxial compressive stress and could sustain considerably greater stresses than the unconfined compressive strength. In the Freyssinet hinges, the maximum stresses occurred near the

edges of the throat. The ratio of peak stress to average stress depended on the shape and height of the throat and the ratio of throat width to column width. In the reinforced Mesnager hinge, the stress distribution was more complex. A higher value of compressive stress might have lead to a more satisfactory hinge, capable of allowing larger rotations while transferring smaller bending moments.

Transverse stress under axial load: The compressive stress in and near the throat of the hinge reached several times the unconfined concrete compressive strength without causing crushing. This increase in strength was a result of the lateral compressive stresses induced as the force "flowed" into the throat, and by the confining effect of concrete above and below. Testing indicated that an increase of about 3 psi in the concrete strength was achieved for each 1 psi of laterally applied pressure. Tests also showed that if a standard 6-inch cube was loaded through 1 square inch at the center of one face, the bearing pressure under the loaded area might reach six times the compressive strength, and the pressure under a 6-inch by 1-inch strip load might reach twice the strength. In both cases failure was due to vertical cracking of the cube followed by wedge penetration; no crushing occurred. It was also observed that a few inches above and below the throat of hinge, the lateral stresses changed from compression to tension. It was important to locate this transition since transverse reinforcement would need to be present.

More references are available concerning biaxial and triaxial stress behavior for concrete.[5,20,29,32] A biaxial stress condition occurs if the principal stresses act only in two directions, i.e., two stresses act in a plane and the third stress is zero. Investigations conducted by Kupfer, et al.,[20] show that the strength of concrete subjected to biaxial compression may be as much as 27 percent higher than the unconfined strength. For equal biaxial compressive stress, the strength increase was approximately 16 percent. Under conditions of triaxial compression, the strength and ductility of concrete was greatly increased. Richart, et al.,[32] found the following relationship for the strength of concrete cylinders loaded axially to failure while subjected to a confining fluid pressure:

$$f'_{cc} = f'_c + 4.1 f_l \qquad (1\text{-}1)$$

where f'_{cc} is the confined compressive strength, f'_c is the unconfined compressive strength, and f_l is the lateral confining pressure.

Other tests by Balmer[7] have produced values for the lateral stress coefficient which range between 4.5 and 7.0, with an average value of 5.6, rather than the value 4.1 found by Richart. Lower lateral pressures resulted in higher coefficient values.

Crack propagation under eccentric loads: Rotation of an axially-loaded Freyssinet or Mesnager hinge superimposes bending stresses on the direct compressive stress in the throat. As loading became eccentric, the center of pressure moved away from the vertical axis and the stresses in and around the throat changed. As rotation was applied, the compressive stress increased on one side of the throat and decreased on the other. At a certain rotation, depending on the magnitude of the initial compressive stress at the throat, a flexural crack began to penetrate the throat, and the width of the concrete section carrying the vertical load was reduced. Often, this crack was the reopening of a shrinkage crack formed before the hinge was loaded. The flexural crack was also influenced by the length of time the hinge was vertically loaded before rotation occurred and by the rate of rotation.

Fatigue testing: The rotation of a concrete hinge usually consists of a permanent rotation due to shrinkage, dead load, and creep of the structure, rotation due to annual temperature cycles, and small cycles due to short term temperature changes, and rotation due to live loads on the structure. For cyclic testing, it was assumed that a small number of rapidly applied large rotations would be more severe than those encountered in practice. Large rotations would actually occur very slowly, and creep would probably give considerable stress relief. In general, fatigue loadings equivalent to hundreds of years of life did not cause significant damage except for spalling and cracking in some specimens, which could result in corrosion of the transverse reinforcement. Such spalling could probably have been prevented by better detailing, particularly by ensuring that the potential spalling zones were anchored by lateral reinforcement.

Shear testing: Shear tests showed that concrete hinges, in general, had shear resistance and that Freyssinet hinges without any throat reinforcement, in particular, could carry shear loads much greater than those likely to be seen in practice. Shear reinforcement through the throat of Freyssinet hinge appears to be necessary only for absorption of impact shear force. A considerable amount of well-anchored cross-bar reinforcement would be required.

A pilot study of reinforced concrete one-way hinges subjected to loading in the strong direction was completed in 1988 by Saiidi and Orie.[8,9] The primary objective of that preliminary study was to investigate the behavior of bridge column-to-foundation one-way hinges subjected to uniaxial moment transfer with loading applied in the strong direction. For simplicity, the effect of axial force was not included. Four 1/8-scale specimens, representing the Rose Creek Bridge (Figure 1-3), were built and tested (Figure 1-4). Three specimens, with shear span-to-depth ratios (aspect ratios) of 1, 2 and 3, were tested monotonically. The fourth specimen, with an aspect ratio of 3, was tested cyclicly. Another objective of the investigation was to determine the effect of shear span variation on the lateral load and flexural capacity of the hinge and to determine if the shear friction theory was valid for this type of application. The shear effect became dominant when the shear span was decreased. The cyclic test was designed to obtain a general insight into the effects of load reversals on flexural strength and to give an indication of energy dissipation. The study showed that, even for an aspect ratio of 1, flexure controlled the load capacity. The results also indicate that the shear friction theory significantly overestimated the lateral load strength; the lateral load failure mechanism of the hinge region was very different from that assumed in the shear friction theory. The cyclicly-loaded specimen showed that when cracks developed over the entire hinge throat section, significant shear slip between the column and the footing could take place, reducing the energy absorption capacity of the hinge. Dowel action was noticed only after a large deflection had occurred; until this, shear resistance was provided by aggregate interlock within the compression zone. Under large deflections, the depth of the compression zone became smaller, thus limiting the resistance and increasing the shear stress in the reinforcing bars.

As a continuation of this early work, Saiidi and Straw[21,22] tested four 1/6-scale specimens (Figure 1-5). Two test variables were considered in the study: loading type (cyclic versus monotonic), and shear span-to-depth (aspect) ratio. A constant axial force was applied to the column, simulating the weight of the superstructure. This research showed that the current ACI shear friction method does not give a reasonable estimate of lateral hinge strength. Primary shear resistance developed only in the compression zone of the hinge interface and only for small deflections; dowel action occurred only after noticeable deformations. It was also found that as the aspect ratio was decreased, the energy dissipation capacity of the hinge also decreased. Displacement ductility levels were as high as 4.0 and 5.3 for specimens with aspect ratios of 1 and 2, respectively. Specimen load-deflection curves exhibited moderate pinching, indicating a relatively small energy absorption capacity.

Lim and McLean[23,24] tested 1/20- and 1/5-scale two-way hinges (Figures 1-6 through 1-8). The 1/20-scale specimens predicted the general characteristics, behavioral trends, and failure mechanisms observed in the 1/5-scale tests; however, the rates of stiffness deterioration within force-reversal regions were higher in the 1/20-scale tests as a result of weak bond between the reinforcement and the concrete. Despite the limitations, the 1/20 scale testing program provided insight into the behavior, and guided the selection of parameters for use in the 1/5-scale testing program. The specimens were tested with two different details: a hinge detail providing horizontal discontinuity only (used in California), and another incorporating a hinge detail providing both vertical and horizontal discontinuity (used in Washington) (Figure 1-6). It was expected that the plastic hinge would concentrate along a horizontal plane at the interface of the column and the foundation in the California detail, and would be distributed over a larger vertical distance in the Washington detail. Load-carrying capacities of columns incorporating the Washington detail were approximately 10 percent lower than with the California detail. The hysteresis curves for columns with the California detail were slightly more pinched than those with the Washington detail. The authors concluded that the two-way hinges with both details exhibited stable moment-deflection hysteresis curves and continued to absorb energy even at a

displacement ductility of 12. Flexure dominated the behavior in all columns, including those with an aspect ratio of 1.35; however, greater strength degradation was observed in columns with higher aspect ratios.

Recently, Haroun, et al.,[14] tested six 2/5-scale two-way hinged columns (Figure 1-9). The columns were based on a scaled down version of the standard details employed by the California Department of Transportation (Caltrans) with appropriate rounding-off to ensure compliance with standard bar size and concrete tolerances. The variables examined include hinge details with and without shear keys, levels of ductility, and application of axial load. The repeatability of test results strongly suggest that the presence or absence of a depressed key has very little effect on lateral resistance. The ultimate strength of the hinged column was governed by the strength of the column; the failure mechanism was a diagonal shear failure in the column. It was also found that the measured shear resistance of the column pins was in close agreement with the theoretically calculated values.

1.3 Objective and Scope

The first objective of the current study was to develop a better understanding of the behavior of pinned reinforced concrete columns subjected to combined axial and lateral forces, and flexure in the strong direction, and to determine if alternate reinforcement details could improve the behavior. While the primary source of axial force may be gravity, lateral load and flexure may be due to partial live load across the bridge, water pressure, wind pressure, or earthquake loads. Axial forces produced by seismic loads were not considered in this study.

The second objective was to develop a preliminary recommendation for lateral load design of one-way hinges using the results of the first part of this study.

The third objective was to conduct a preliminary study of the cyclic response of hinged columns with bars with inadequate development length, and to formulate and test a repair method for damaged columns. The repair strategy should restore the strength and ductility capacity of the hinge to the level of a hinge with adequate steel anchorage.

Many variables were considered in the testing, including aspect ratio, type of loading (monotonic or cyclic), arrangement of steel in the hinge region, and hinge throat thickness relative to hinge width. The purpose of varying these parameters was to study their effects on hinge flexural and lateral strength, energy absorption capacity, shear slip, and compressive strength of concrete in the hinge.

To address the variables and their effects, a variety of specimens were constructed and tested. Relative to dimensions of the actual bridge columns, the specimens were of small scale (1/8 and 1/6), but were sufficiently large to be built with normal weight concrete and deformed reinforcing steel, as used in actual bridge construction. The maximum concrete aggregate size used was 1/2-inch instead of 3/4-inch normally used in bridge construction.

In addition to the experimental study, linear finite element analyses of selected specimens were performed to study the stress distribution and confining stresses in the hinge throat area. Analytical studies also included inelastic analysis of bridges with hinged columns. Focus was placed on the influence of deck torsional stiffness on the aspect ratio of hinged bridge columns. A new approach for estimating the lateral load strength of the hinged columns was developed. The results were evaluated based on the test results reported herein and elsewhere.

Chapter 2

Experimental Program

2.1 General Remarks

The experimental program included testing of four types of specimens. The first type represents column-to-foundation connections using 1/6-scale replicas of the hinges in piers 2 and 3 of the Rose Creek Bridge. Five specimens of this type were tested. The purpose of the first four specimens was to determine the influence of reinforcement details in the hinge region on energy absorption capacities under cyclic loads. The fifth specimen was used in a pilot study to determine the cyclic response of hinged columns with inadequate steel development length, and to develop and test a repair method for damaged columns.

Unlike the single row of equally spaced bars usually used in one-way hinges, the first four specimens utilized bundled or diagonal bars. All reinforcing bars were provided with adequate development length as required by current ACI and AASHTO codes.[1,2] Variables studied included reinforcing details in the hinge region and the aspect ratio. All four specimens were subjected to a constant axial load, representing the superstructure dead load, and cyclic lateral loads up to a displacement ductility of 4. The fifth specimen was also a 1/6-scale column. To simulate the existing anchorage in the Rose Creek Bridge, short reinforcing bars were equally distributed in the hinge region. This specimen was tested to a displacement ductility factor of 2 using a load history similar to that used for the other four specimens. The specimen was then repaired and cyclically loaded to a ductility of 4.

The second and third specimen types were designed to study the effects of hinge depth on hinge behavior. These specimens included three shear specimens and three compression specimens, all tested under either pure shear or pure axial load. The effect of concrete confinement in the hinge on the compressive strength was determined by testing a fourth group of 24 plain concrete specimens incorporating hinges with different thicknesses.

This chapter describes the first four test columns, shear specimens, compression specimens, and the plain concrete hinge specimens. The fifth test column is discussed in Chapter 8.

2.2 Column Specimens

Previous testing was conducted on 1/8- and 1/6-scale hinges incorporating uniformly distributed reinforcing bars.[28,37] In these specimens, the reinforcing bars were sufficiently anchored to develop their yield stress. As tensile yielding propagated to the second and third steel layer, the amount of crack opening was very significant and reduced shear friction forces that could develop. One possible approach to reduce the excessive opening of the crack is to bundle bars near the two edges of the section while keeping the total amount of steel constant. By comparing the results with those corresponding to one row of equally spaced steel, it is possible to quantify the improvement.

It was also observed that the energy dissipation characteristics for these specimens were not quite satisfactory, as indicated by a relatively strong pinching effect on the load-deflection hysteresis curves. The cause of pinching was a relatively large slip between the column and the base. To reduce the slip, use of diagonal bars, rather than equally spaced straight bars, may be helpful.

Four column specimens were built and tested with modified details, BB1C, BB2C, DB1C, and DB2C. Figures 2-1 and 2-2 show the dimensions and details of these specimens. The hinge sections measured 2.5 inches by 16 inches, which is approximately 1/6-scale of the pier hinges in the Rose Creek Bridge. BB stands for bundled bars; DB stands for diagonal bars. The numeral refers to the shear span-to-depth ratio (aspect ratio). The last letter, C, identifies the loading type as cyclic loading.

The hinged column specimens consisted of two concrete segments. The first was a 24-inch by 14.5-inch by 18-inch footing segment, which was identical in size for all four specimens. The column segment measured 16 inches by 6.5 inches by 22 inches for specimens BB1C and DB1C, and 16 inches by 6.5 inches by 38 inches for specimens BB2C and DB2C.

For each specimen, six No. 3 Grade 60 deformed bars were used to connect the footing to the column. The reinforcing steel had 90 degree, standard hooks on both ends and had a straight of 8 inches above and below the hinge. The reinforcing bars had a concrete cover of 1 inch over the outer steel. This practice was repeated for all four specimens.

For specimens BB1C and BB2C, the reinforcing bars were bundled at two ends of the hinge section, and the inner bars were spaced at 4.4 inches, on center. The column ties were No. 2 plain bars spaced at 3 inches, on center.

For specimens DB1C and DB2C, four inner reinforcing bars were symmetrically inclined 45 degrees relative to the vertical direction, and the outer bars were straight. Bars were placed in such a way that they were equally spaced at the interface between the column and the foundation. No. 2 plain bars spaced 3 inches, on center, were used for column ties. Eight No. 3 U-Stirrups were used for the footing reinforcement.

For all four specimens, the connection between the footing and the column was a hinge region formed using a 2.5-inch by 16-inch by 1/2-inch shear key. The hinge throat region was fabricated with a 1-inch deep by 2.5-inch wide by 16-inch long piece of styrofoam placed in the base section prior to concrete placement. Two 1/2-inch thick styrofoam inserts were put on either side of the shear key to ensure that no bonding between the bottom surface of the column to the footing would take place during placement of the concrete for the column. After the base was poured and cured for three days, the hinge throat area was scraped to a depth of approximately 0.5 inch before the column was poured.

2.3 Shear Specimens

One-way hinges are designed to allow rotation about the weak axis due to thermal loads and support settlement. An increase in hinge depth allows more rotation without developing moments; however, this may reduce the degree of concrete confinement in the hinge throat, thus reducing hinge strength. To determine the influence of hinge throat thickness on behavior under pure shear, three shear specimens were built and monotonically tested.

The three shear specimens, SSP1, SSP2, and SSP3, were identical in configuration except for hinge depths, which were 0.5 inch, 1.0 inch, and 1.5 inch, respectively (Figure 2-3). The hinge cross section of each specimen measured 2.5 inches by 8 inches, one-half of the length of the hinge throats in the column specimens. The specimens consisted of two L-shaped stubs with the hinge formed on the inner side of one of the two stubs. The reinforcement consisted of three No. 3 Grade 60 bars placed in a row in the strong direction. Standard 90-degree hooks with required development lengths allowed yielding of the steel. The specimens were cast horizontally and tested vertically.

2.4 Compression Specimens

When a one-way hinge is subjected to a lateral force at the top of the column in the strong direction, the interface between the column and the footing will have a tension zone and a compression zone. The reinforcement will be subjected to a tensile force in the tension zone; however, both concrete and steel will contribute to the strength in the compression zone. The compression zone affects the overall behavior of the hinge. An increase in hinge depth may reduce concrete confinement and the compressive strength in the hinge, and reduce the lateral loading-carrying capacity of the column.

Three compression specimens, CS1, CS2, and CS3, were built and tested to determine the effect of hinge thickness on compressive strength (Figure 2-4). These specimens had identical overall configurations; the only variable was the hinge thickness, 0.5 inch for CS1, 1.0 inch for CS2, and 1.5 inches for CS3. The hinge sections measured 2.5 inches by 6 inches.

The compression specimens consisted of two concrete segments. The footing measured 12 inches by 10 inches by 8 inches; the column measured 6.5 inches by 5 inches by 9 inches. The sizes of both segments were identical for all three specimens. For each specimen, two No. 3 Grade 60 deformed bars were used as hinge reinforcement. Because the overall size of the specimens were small, 1/2-inch steel mesh was used as ties for the column. Four No. 3 U-stirrups were used as

reinforcement in the base. The specimens were built and cured under the same conditions as the column specimens.

2.5 Plain Concrete Hinge Specimens

Because the concrete in the hinge throat is in a triaxial state, the concrete is confined. This confinement is indicated by the high attainable compressive stresses in the hinge throat.[5,7,20,29,32] To quantify the concrete confinement, 24 small-scaled hinged specimens were tested (Figure 2-5). These specimens were not reinforced and were cast in standard cylinder molds. Hinges were formed using two pieces of styrofoam, one on each side of the hinge. Because of the high compressibility of the styrofoam, it was not necessary to remove the pieces. Hinge thickness ranged from 0.25 inch to 2 inches, while hinge width was constant at 1.5 inches, creating width-to-thickness ratios ranging from 0.75 to 6 (the ratios in the Rose Creek Bridge are 3 for piers 1 and 4, and 3.75 for piers 2 and 3). Three specimens were fabricated for each ratio.

2.6 Material and Fabrication

Grade 60, No. 3 deformed bars were used as reinforcing dowels for all column specimens, shear specimens, and compression specimens. Horizontal ties used in the specimens were either Grade 40 No. 2 plain bars or 1/2-inch steel mesh.

For column specimens and plain concrete hinge specimens, a normal weight ready-mix concrete with an average compressive strength of 4150 psi was used (Table 2-1). The maximum coarse aggregate size was 1/2 inch.

The concrete for shear and compression specimens was designed with a target 28-day strength of 4000 psi, using Type I-II low alkali cement. The coarse and fine aggregates used were obtained from a local source. The coarse aggregate was sieved to remove all materials larger that 1/2 inch.

The concrete was mechanically mixed for approximately 10 minutes. Compressive strength, using standard 6-inch by 12-inch cylinders, was determined at 7 days, 28 days, and on the day of testing. Table 2-1 shows the concrete strength for all specimens.

The two portions for all but the plain concrete hinge specimens were poured separately to simulate field construction by first pouring the foundation and then the

column. For the shear specimens, the left segment in Figure 2-3 was poured first, followed by the other segment.

The footing of each specimen was poured and moist cured for three days. The specimen was removed from moist curing and the styrofoam keyway form was removed. A chisel was used to roughen the concrete surface to a depth of approximately 0.5 inch to ensure a good bond between the foundation and the column. The column was poured and moist cured for an additional four days. At the end of seven days, the specimen was taken out of the moist room, the forms were removed, and the specimen was allowed to dry cure at room temperature until the time of testing.

2.7 Instrumentation

A microcomputer data acquisition system was used to record electrical-resistance strain gage readings, linear variable differential transformer (LVDT) measurements, and lateral loads. The computer program *PIERHINGE*[37] was used to collect and store the test data. Axial load was applied using a 300-kip load frame. Lateral loads were applied using a 55-kip displacement controlled hydraulic actuator with a stroke of ±3 inches.

The resistance-type strain gages (Measurements Group EA-06-240LZ-120) were mounted on the reinforcing bars located within each specimen as shown in Figures 2-6 though 2-11.

Two 2-inch LVDTs (Schaevitz 2000HPD) were used to measure the rotation of the column section relative to the footing and one 1-inch LVDTs (Schaevitz 1000HPD) was used to measure the horizontal slip of the column with respect to the footing (Figures 2-6 and 2-7). Two 2-inch LVDTs were used for measuring vertical displacements for the shear specimens and the compression specimens (Figures 2-8 and 2-9). Figures 2-6 to 2-9 show the actual number and location of the strain gages and the locations of LVDTs. A dial gage was used to measure the vertical displacement for plain concrete hinge specimens (Figure 2-10). Figure 2-11, obtained from Ref. 37, shows the instrumentation for the standard (SD) column specimens. This

figure is included because some of the test results for SD specimens were used in this study.

The column specimens were connected to the testing frame (Figure 2-12) by means of eight 1.25-inch diameter, 125-ksi threaded rods which passed through pre-cast holes in the footing and were bolted to the frame setup. A 1-inch thick steel bearing plate was used to distribute the loads from the threaded rods (Figure 2-12). A steel collar was used to transfer the load from the hydraulic ram to the column (Figure 2-13).

2.8 Test Procedure

2.8.1 Column Specimens

The testing procedure for all column specimens was identical. The first step was to apply an axial load of 26 kips (which produced the same dead load stress level in the hinge throat as that in the piers of the Rose Creek Bridge) in approximately 5-kip increments. Once the total axial load was applied, the threaded anchor rods were tightened and the lateral hydraulic ram was fastened to the column collar. There was approximately a 0.1-inch gap between the column face and the hydraulic ram collar, resulting in a larger measured displacement than actual.

Cyclic lateral loads were applied using displacement control. A predetermined displacement was applied slowly to the specimen, held, and the computer triggered to record the test data. The measured axial load was kept nearly constant throughout the test within ±1 kip of the target load; however, the actual load varied due to the nature of the test setup (Figure 2-12). The load cell built into the test frame measures load on the platform; although the test frame was very stiff, overturning effects increased or decreased the actual load. When the top of the column was pushed to the left, the column base was pushed against the platform of the compression machine, making the actual load less than the measured load; when the column was pulled to the right, the actual load was larger than the measured value.

All specimens were subjected to several cycles of increasing displacement amplitude and ductility. Figures 2-14 and 2-15 illustrate the displacement histories for the column specimens. No particular earthquake history was simulated.

2.8.2 Shear and Compression Specimens

The only load applied to shear specimens and compression specimens was a monotonically increasing point load as shown in Figures 2-8 and 2-9. The load was applied statically in small increments. The shear force and average shear displacement on two opposite sides were recorded and the shear force versus shear displacement diagram was plotted. All specimens were loaded to failure, defined as the point for which the load-carrying capacity of the specimen dropped to 85 percent of the maximum load.

2.8.3 Plain Concrete Hinge Specimens

The cylindrical plain concrete hinge specimens were axially loaded in small increments to failure. A dial gage assembly was connected to the specimen to measure the average displacement in the hinge; the load and the corresponding displacement were recorded for each load increment.

Chapter 3

Test Results

3.1 General Remarks

The experimental results and observed behavior of each test are presented in this chapter. Results that are presented are the deflection, rotation, horizontal slip, and reinforcement strain strain for each column specimen as a function of the lateral load. The results for the shear specimens include the slippage and the steel strains as afunction of shear. Axial load versus axial deformation and load versus strain for compression specimens are also described. Plain concrete hinge specimen data are presented as relationships between hinge strength and width-to-depth ratio.

3.2 Column Specimens

Before testing, a visual inspection of each specimen was performed to note any unusual cracks; there were no major visible cracks in any of the specimens. All four specimens were subjected to several cycles of increasing lateral displacements and ductilities; however, no particular earthquake loading was simulated. Figures 3-1 and 3-2 show the numbering system used for the reinforcing steel located within each specimen.

3.2.1 Specimen BB1C

Specimen BB1C (with bundled bars, aspect ratio of 1, cyclically loaded) was subjected to nine cycles of displacement reversals at four amplitudes (Figure 2-14). Figures 3-3 and 3-4 are photographs taken at the end of testing. The column had separated from the footing, indicating that the joint had failed. There were no significant cracks observed outside the hinge area; the only crack was a vertical crack at the bottom of one end of the column which led to a 3-inch long spalling of the concrete cover. This crack resulted from local compressive stresses at the end of the hinge. When the final cycle began, another crack was observed at the base of the specimen where LVDT No. 1 (Figure 2-6) was attached. The LVDT moved slightly, resulting in readings that were offset by a constant value.

3.2.1.1 Load-Deflection Response

Figure 3-5 shows the load-deflection response for specimen BB1C. Initially, two cycles at a displacement of ±0.1 inch were applied to capture the cracking point. Two cycles of amplitude ±0.25 inch displacement, representing the apparent yield point of the specimen, were then applied. Three lateral displacement cycles were applied at a ductility level of 2 (±0.5-inch deflection) to monitor the effects on strength degradation of cyclic displacement with a moderate degree of nonlinearity. Figure 3-5 shows some pinching effects on the hysteresis loops, indicating a reduction in energy absorption capacity even at a ductility level of two. Finally, a ductility level of 4 (±1.0-inch deflection) was applied for two cycles; even more significant pinching was noted in the hysteresis loops.

The largest lateral load applied was 28.4 kips in the positive direction (away from the actuator) and 30.7 kips in the negative direction (toward the actuator). On the last cycle a maximum load of 22.8 kips, in the positive direction, and 28.1 kips, in the negative direction, was reached. These values indicate a strength degradation of 19.7 percent and 8.0 percent for the positive and negative directions, respectively. The reasons for the differences are explained in the next chapter.

3.2.1.2 Load-Rotation Response

Figure 3-6 shows the load-rotation response of specimen BB1C. The rotation in the positive direction was always larger than in the negative direction for each cycle. As a result of the sudden movement of LVDT No. 1 at the beginning of the final cycle, the rotation value shifted by approximately 0.0043 radian.

The maximum rotation in the positive direction was 0.0463 radian and in the negative direction 0.0243 radian, taking into account the LVDT shift during the last cycle. The maximum apparent rotation ductility was 26.0 in the positive direction and 8.7 in the negative direction.

The magnitude of rotation is a function of the lateral displacement as well as the loading history, and is especially pronounced at large displacements. For a displacement ductility factor of 4 (lateral displacement of 1.0 inch), the maximum rotation for the first cycle in the positive direction was 0.0463 radian, and 0.0234 radian in the negative

direction. However, for the second cycle, the maximum rotation was 0.0361 radian for the positive side and 0.0243 radian for the negative side. The values for the second cycle were corrected to include the shifting of the curve.

3.2.1.3 Load-Slip Response

Figure 3-7 illustrates the load-slip response. The slip increased substantially with an increase in lateral displacement. The maximum slip was 0.197 inch in the positive direction and 0.411 inch in the negative direction. The load-slip response was symmetric up to a displacement ductility of 2, but was unsymmetric when the ductility factor approached 4, with the negative slip approximately twice the positive slip. A possible explanation of this behavior is provided in the next chapter.

There was a good correlation between the load-rotation response and the load-slip response. For positive lateral loads, the rotations were high and the slips were low. For the negative loads, the rotations were low and the slips were high.

Given the measured rotation and slip, and knowing the distance between the lateral load and the base and assuming rigid-body rotation and displacement, the approximate lateral deflection due to hinge rotation and slip can be calculated. This calculated deflection can then be added to the deflections due to flexure and shear to obtain the approximate lateral deflection at a given load. Shear deformation was small enough to be ignored in the calculation.

The calculated deflection was 0.943 inch for the positive direction and 0.805 inch for the negative direction. In determining the flexure deflection, the concrete modulus of elasticity was calculated according to the ACI building code,[2] using the concrete compressive strength determined on the day of testing. The calculated values are different for the two directions and both values are less than 1.0 inch, which was measured in both directions. The measured rotations used in the above calculations were relative rotations between the column and the footing of the specimen; the rotations between the footing the test platform were not considered. The rotation between the footing and the platform is relatively small when the column is subjected to the load in the positive direction, because the footing was pushed into the platform; conversely,

the rotation is relatively large when the column is subjected to the load in the negative direction.

3.2.1.4 Load-Strain Response

Figures 3-8 through 3-19 show the load-strain relationships and the location of strain gages for specimen BB1C. Tensile strains are shown as positive quantities. Due to gage failures after yielding in some cases, some of the load-strain curves show only a part of the entire response; however, these curves are sufficient to indicate the trend in load-strain relationships.

Figures 3-8 and 3-9 show the load-strain histories of the two exterior bars in the hinge region. Both bars yielded in tension (yield strain was 2000 μ-in./in.) and experienced several reversals of tension and compression. The trend between lateral load and strain was nearly linear. The outer and next inner bars were bundled in-line with the strong axis and were expected to exhibit similar behaviors; however, it appears (Figures 3-10 and 3-11) that the inner bars behaved quite differently. Most of the curves fall in the positive strain regions, except at the initial stages of testing. Once the bars yielded, they remained in tension, indicating that the inner bars were near the neutral axis.

Figures 3-12 and 3-13 show the response for the two inner-most bars in the hinge. These bars primarily experienced tension and were in compression only when the lateral load was small relative to the axial load.

Figures 3-14 through 3-19 show the load-strain relationships for the gages outside the hinge throat. Figures 3-14 and 3-15 are for the two outer bars, 3 inches above the hinge. Both bars yielded in tension. The load-strain relationships for the two next inner bars are shown in Figures 3-16 and 3-17. The strain data in Fig. 3-16 is not complete because the gage failed near the beginning of testing; because of symmetry, Figure 3-17 is believed to represent the strain behavior at both locations. The bars yielded in tension. The strain behavior for the two outer bars at a location 6 inches above the hinge is shown in Figures 3-18 and 3-19. The outer bars yielded, indicating that the plastic hinge spread well into the column.

All bars in the hinge region were subjected to significant tension. The hinge section was subjected to a combination of shear and flexure, but dominated by shear after tensile yielding in the steel. For such a short column (aspect ratio of 1), it was not unexpected that shear would have a major impact on overall behavior; however, significant shear slip was preceded by significant tensile yielding of the longitudinal bars.

3.2.2 Specimen BB2C

Specimen BB2C (bundled bars, aspect ratio of 2, cyclically loaded) was subjected to ten and one-quarter cycles of displacement reversals at five amplitude levels (Figure 2-15). Figures 3-20 and 3-21 are photographs taken at the end of testing. The column separated from the footing, indicating that the joint had failed. There were generally no cracks observed outside the hinge area on the column; however, at the final stages, there were some cracks radiating from the anchor rods near the top of the base.

3.2.2.1 Load-Deflection Response

Figure 3-22 shows the load-deflection response. Two small cycles at a displacement of ±0.1 inch were completed to capture the cracking point. Next, two cycles of ±0.25-inch displacement were applied, followed by three cycles at a displacement ductility of 2 (±0.5 inch) to monitor the effect on strength degradation of cyclic displacements with a moderate degree of nonlinearity. A ductility level of 4 (±1.0 inch) was applied for three cycles to simulate the effect of a strong earthquake. Finally, one-quarter cycle was applied to fail the specimen at a displacement of 1.5 inches (ductility factor of 6).

The largest load applied was 13.8 kips in the positive direction and 15.9 kips in the negative direction. On the last cycle, a maximum value of 13.4 kips was reached in the positive direction and a value of 15.2 kips was reached in the negative direction, strength degradations of 2.9 percent and 4.4 percent, respectively.

There was no appreciable strength degradation in the connection, as indicated by the overlapping cycles. At a displacement ductility of 2, some slight pinching was

evident on the hysteresis curves. At a ductility of 4, moderate pinching was apparent in the hysteresis loops, indicating a loss of energy absorption capacity.

3.2.2.2 Load-Rotation Response

Figure 3-23 shows the load-rotation response of specimen BB2C. Similar to that observed for specimen BB1C, the rotation in the positive direction is always larger than in the negative direction for each cycle. The curves for BB2C were generally smoother than those for BB1C.

The maximum rotation in the positive direction was 0.0267 radian and in the negative direction 0.0225 radian. The maximum rotation ductility was 6.8 in the positive direction and 7.3 in the negative direction.

For specimen BB2C, the magnitude of rotation is a function only of lateral displacement. There was no apparent relationship between the magnitude of rotation and the loading history, as indicated by the well-overlapped cycles on the load-rotation curves.

3.2.2.3 Load-Slip Response

Figure 3-24 is the load-slip response for specimen BB2C. The maximum slip was 0.046 inch in the positive direction and 0.085 inch in the negative direction. The load-slip response was symmetric up to a displacement ductility of 2; however, it was unsymmetric when the ductility approached 4, with the negative slip being approximately twice the positive slip.

Based on the measured maximum rotation and slip, the calculated maximum lateral deflections, excluding base-platform rotation, were 0.920 inch for the positive direction and 0.828 inch for the negative direction. As per the same reasons cited in Section 3.2.1.3, the two values are different and are less than 1.0 inch, which was measured in both directions.

3.2.2.4 Load-Strain Response

Figures 3-25 and 3-26 illustrate the load-strain responses for the two exterior bars in the hinge. Both bars yielded both in compression and tension, with the strains in compression greater than those in tension. The general trend for both bars in the hinge region was similar, and both showed evidence of strain hardening.

The outer and first inner bars were bundled in-line with the strong axis. As expected, the two bundled bars exhibited somewhat similar behaviors, as shown in Figures 3-27 and 3-28. The only major difference was that the strains corresponding to the positive loads in the first inner bars were approximately 20 to 60 percent lower than those in the outer bars. Figures 3-29 and 3-30 are for the two inner-most bars in the hinge. These two bars experienced reversals of tension and compression up to the first half of the load history, after which they were primarily subjected to tension.

Figures 3-31 through 3-36 present the load-strain relationships for the gages located outside the hinge throat. Figures 3-31 and 3-32 are for the two outer bars, 3 inches above the hinge. Both bars yielded in tension. In Figure 3-32, the strain gage failed before the end of testing. The load-strain relationships for gages located on the two first inner bars, 3 inches above the hinge, are shown in Figures 3-33 and 3-34. These two figures show somewhat different behavior in the negative regions. Loading to the left put bar 2 in tension (Figure 3-33), but loading to the right led to compression in Bar 5 (Figure 3-34). This indicates that the depth of the compression zone was larger in the later case, and confirms that the axial load was larger when the specimen was pulled towards the actuator. The strain behavior of the two outer bars, 6 inches above the hinge, can be seen in Figures 3-35 and 3-36. Tensile yielding in the outer bars extended 6 inches upward into the column; compressive yielding was limited to the hinge throat.

Based on the measured response, all four exterior bars in the hinge region were subjected to reversals of tension and compression. The two interior bars experienced mostly tension, indicating that the hinge behavior was dominated by flexure. For such a column as BB2C (aspect ratio of 2), it was expected that flexure would dominate the overall behavior. However, some shear slip did take place following significant tensile yielding of the bars.

3.2.3 Specimen DB1C

Specimen DB1C (diagonal bars, aspect ratio of 1, cyclically loaded) was subjected to nine cycles of displacement reversals at four amplitudes (Figure 2-14). Figures 3-37 and 3-38 are photographs taken after testing. The column had separated

from the footing, indicating that the joint had failed. There were no major cracks outside the column's hinge area; however, some cracks developed on top of the base near the final stages of testing. These cracks originated at the anchor rods (Figure 3-38).

3.2.3.1 Load-Deflection Response

Figure 3-39 shows the load-deflection response for the specimen. Specimen DB1C was loaded using the same loading history as BB1C. Figure 3-39 shows notable pinching at a ductility factor of 2, with more significant pinching at a ductility factor of 4. The largest load applied was 23.6 kips in the positive direction and 26.6 kips in the negative direction. On the last cycle, the maximum value was 21.2 kips in the positive direction and 24.5 kips in the negative direction, strength degradations of 10.1 percent 7.9 percent, respectively.

3.2.3.2 Load-Rotation Response

Figure 3-40 shows the load-rotation response of the specimen. The rotation was always larger in the positive direction of each displacement cycle.

The maximum rotation was 0.0564 radian in the positive direction and 0.0422 radian in the negative direction. The maximum rotation ductility was 21.0 in the positive direction and 10.1 in the negative direction.

Unlike the load-rotation response for specimen BB1C, the hysteresis loops for specimen DB1C were stable at a displacement ductility of 4.

3.2.3.3 Load-Slip Response

Figure 3-41 shows the load-slip response. Similar to the previous specimens, the slip increased with an increase in lateral displacement. The maximum slips were 0.175 inch in the positive direction and 0.104 inch in the negative direction.

The calculated maximum deflection, based on the measured rotation and slip between the column and the footing plus the flexural deflection, was 1.082 inches for the positive direction and 0.784 inch for the negative direction. The calculated deflections for the two directions are different because rotation between the footing and the test platform was not considered. When comparing this result with the calculated deflections for specimen BB1C, the calculated deflection shows more offset in the

positive direction, attributable to the gap between the column face and the ram collar on one side of the column.

3.2.3.4 Load-Strain Response

Figures 3-42 and 3-43 are the load-strain responses for the two exterior bars at the hinge throat. Both bars experienced reversals of tension and compression and yielded in tension. The general trend was a nearly-linear relationship between load and strain. The four interior bars primarily experienced tension in the hinge region, as shown in Figures 3-44 to 3-47.

Figures 3-48 through 3-53 are the load-strain relationships for the gages located above the hinge throat. Figures 3-48 and 3-49 are for the two exterior bars, 3 inches above the hinge. Both bars yielded in tension after experiencing reversals of tension and compression. Figure 3-50 shows the response for bar 1, 6 inches above the hinge. The bar reached yielding in tension and almost reached yielding in compression. Figures 3-51 through 3-53 show the responses for three of the four interior bars, 6 inches above the hinge. There was no significant strain at these locations; all were subjected to small tensile strains, far from the yield point. Figures for the two strain gages at locations symmetric to the gages in Figures 3-50 and 3-51 are not available because the data were not properly recorded.

All bars in the hinge region were subjected to significant tension, except for the two exterior bars which were subjected to tension and compression reversals. Similar to specimen BB1C, shear dominated the response after tensile yielding of the steel.

3.2.4 Specimen DB2C

Similar to BB2C, specimen DB2C (diagonal bars, aspect ratio of 2, cyclically loaded) was subjected to ten and one-quarter cycles of displacement reversals at five amplitude levels (Figure 2-15). Figures 3-54 and 3-55 are photographs taken at the end of testing. The column separated from the footing, indicating failure of the hinge. There were generally no cracks observed outside the hinge area on the column; however, at the final stages, there were some cracks on top of the base near the anchor rods (Figure 3-55).

3.2.4.1 Load-Deflection Response

Figure 3-56 shows the load-deflection response for the specimen. Even at a displacement ductility factor of 2 (±0.5 inch displacement), some slight pinching of the hysteresis loops is present. At a lateral ductility of 4 (±1 inch displacement), moderate pinching is apparent, indicating a loss of energy absorption capacity.

The largest load applied was 12.2 kips in the positive direction and 13.7 kips in the negative direction. On the last cycle, a maximum of 11.8 kips was applied in the positive direction and 12.8 kips applied in the negative direction, strength degradations of 3.3 percent and 6.6 percent, respectively.

3.2.4.2 Load-Rotation Response

Figure 3-57 shows the load-rotation response. Similar to specimen BB1C, the positive rotation during each cycle was always larger.

The maximum rotation was 0.0297 radian in the positive direction and 0.0223 radian in the negative direction. The maximum rotation ductility was 17.1 in the positive direction and 9.0 in the negative direction.

For specimen DB2C, the magnitude of rotation was a function of lateral displacement only, as indicated by the overlapping cycles at the same ductility level.

3.2.4.3 Load-Slip Response

Figure 3-58 shows the load-slip response for specimen DB2C. The maximum slip was 0.052 inch in the positive direction and 0.073 inch in the negative direction. The load-slip response was generally unsymmetric with the slip in the negative direction larger than in the positive direction.

Maximum deflections can be estimated using the measured rotations and slips and the flexure and shear deflections of the column. Shear deflection was very small and was neglected. Rotation between the footing and the platform was not measured and, thus, could not be used in calculating the deflection. The calculated deflection was 1.020 inches in the positive direction and 0.806 inch in the negative direction. The difference in the two values is due to the rotation between the footing and the platform and the gap between the column face and the ram collar.

3.2.4.4 Load-Strain Response

Figures 3-59 through 3-71 show the load-strain relationships for specimen DB2C; corresponding strain gage locations are also shown.

Figures 3-59 and 3-60 are the load-strain responses of the two exterior bars in the hinge region. Both bars experienced reversals of tension and compression and yielded in both tension and compression. The strain in Bar 1 exceeded 2.5 times the yield strain. Bar 6 also yielded in both directions, however, the extent of yielding can not be determined because both strain gages failed during testing.

The load-strain relationships for the two inner bars in the hinge region are shown in Figures 3-61 and 3-62. Although the bars are located symmetrically, bar 2 experienced primarily tension while bar 5 experienced reversals of tension and compression. As discussed in Section 2.8.1, the actual axial load on the column was smaller when the column was laterally loaded in the positive direction and larger when loaded in the negative direction. This resulted in a shift in the location of the neutral axis.

Figures 3-63 and 3-64 are for bars 3 and 4. The anomalous shift in Figure 3-63 occurred after three cycles, when the reading from one gage substantially increased for an unknown reason. Figure 3-64 shows that the steel experienced reversals of tension and compression and yielded only in tension.

Figures 3-65 through 3-72 are the load-strain relationships for the gages located outside the hinge throat. Figures 3-65 and 3-66 are for the two exterior bars, 3 inches above the hinge. Both bars yielded in tension before the strain ganges failed. Figures 3-67 and 3-68 are for the two exterior bars, 6 inches above the hinge. Yielding progressed 6 inches upward into the column. Figures 3-69 through 3-72 show that there was no yielding 6 inches above the hinge in the four interior bars.

All six bars at the hinge throat were subjected to reversals of tension and compression and yielded in tension. The two interior bars experienced mainly tension with some compression. As expected, flexure dominated the overall behavior; however, some shear slip resulted following tensile yielding of the bars, indicating some loss of shear resistance.

3.3 Shear Specimens

The three shear specimens, SSP1, SSP2, and SSP3, were identical in configuration except for hinge depths of 0.5 inch, 1.0 inch and 1.5 inches, respectively. All three specimens were monotonically loaded to failure by an incrementally-applied point load, as shown in Figure 2-8. A photograph of a failed shear specimen is shown in Figure 3-73.

3.3.1 Load-Deformation Response

Figures 3-74 through 3-76 show the load-deformation responses for the shear specimens. The slip axis shows the relative vertical displacement of the left and the right sides of the specimen. The peak shear force experienced by all three specimens was close to 40 kips. The response histories can be broken into three regions: (1) a very-stiff linear relationship before the peak shear force was reached (typical for "push-off" shear specimens); (2) a sudden drop (approximately 50 percent) in shear force immediately after reaching the peak force; and (3) after a shear deformation of approximately 0.3 inch, an increase in shear force to a second peak at a deformation of approximately 0.9 inch. This increase in shear force was a result of strain-hardening in the reinforcing steel. The ratio of the second peak to the first peak was 78 percent for SSP1, 71 percent for SSP2, and 62 percent for SSP3.

Under pure shear, the shear capacities of the 3 specimens before cracking were identical. The peak shear force was twice the value calculated from the shear friction method[2] for all specimens. This strength is not a dependable value since it represents the uncracked condition. After a relatively large slip (0.8 to 1.0 inch), an increase in shear force occurred in all specimens. At this stage, a crack had developed at the hinge throat and the shear friction mechanism prevailed. The second peak was largest in SSP1 and smallest in SSP3. This is believed to be a result of a higher degree of concrete confinement in the hinge throat with the thinner hinge.

The large magnitude of the second peak following relatively large slips may not be significant under monotonic loading; however, it may affect the ability of the hinge to sustain large-amplitude cyclic deformations that may be caused by seismic loads.

3.3.2 Load-Strain Response

Figures 3-77 through 3-85 are the load-strain relationships for the shear specimens; corresponding strain gage locations are also shown.

All bars yielded in the hinge region, and major strain activities occurred before the peak shear forces were reached. The load-strain curves consist of four regions: (1) a small initial strain (roughly 60 μ-in./in.) resulting from the self-weight of the specimen before loading; (2) a nearly-linear relationship up to approximately 45 percent of the peak shear force with a slight increase in strain; (3) an increase in shear force corresponding to a large increase in strain (approximately 2100 μ-in./in.); and (4) a small increase in strain with a large drop in shear force for specimens SSP1 and SSP2 and a small decrease in shear force for specimen SSP3.

3.4 Compression Specimens

Three compression specimens were tested to determine the effects of hinge thickness on confined concrete compressive strength. Three compression specimens, NCS1, NCS2, and NCS3, were identical in configuration except for hinge depths of 0.5 inch, 1.0 inch and 1.5 inches, respectively. Loading was applied incrementally by a point load, as shown in Figure 2-9. Because of the relatively small cross section and large amount of steel, the column regions were very congested; some internal air pockets may have been present.

Because of the high degree of confinement in the hinge region, the column segments failed before the hinges. A failed specimen is illustrated in Figure 3-86. Failure was initiated from cracking in the middle of the column. Figures 3-87 through 3-89 show the load-deformation histories for the specimens. The peak axial loads were 149.5 kips and 140.0 kips for both specimens NCS1 and NCS2, and specimen NCS3, respectively.

The peak loads were used to back-calculate the lower bound of the confined concrete strength in the hinge region; by doing so, the confined strength was found to be 8500 psi for NCS1 and NCS2, and 7900 psi for NCS3. The apparent hinge concrete strength to the cylinder concrete strength ratios were 1.50 for NCS1 and NCS2, and 1.40 for NCS3.

Figures 3-90 through 3-95 show the load-strain relationships and gage locations for the compression specimens. Both bars in NCS1 at the hinge throat behaved linearly up to yielding in compression. The two bars in NCS2 also behaved linearly at the hinge throat, but only one yielde The load-strain relationship for NCS3 in the hinge throat was also linear, but neither bar yielded.

3.5 Plain Concrete Hinge Specimens

Plain concrete hinge specimens were axially loaded to failure to quantify the confinement provided by concrete immediately above and below the hinge (Figure 2-10). The failed specimens are shown in the photograph in Figure 3-96. Failure consisted of vertical cracking in the concrete, followed by penetration of a wedge into the concrete.

Table 3-1 shows the average strength of each group of specimens, the concrete compressive strength on the day of testing, and the ratios relating hinge strength to unconfined compressive strength. Figure 3-97 presents the test results for all hinged specimens and the average hinge strength-to-unconfined compressive strength. The figure also shows a dashed line which is the recommended hinge strength-to-concrete strength ratio of 1.25 for design purpose. The hinge strength was always higher than the unconfined compressive strength; however, there is no clear indication that the magnitude of hinge width to thickness (height) ratio had a significant influence on compressive strength in the hinge throat. The strength ratio varied from 1.27 to 1.61 with an average of 1.38 and a standard deviation of 0.147. The ratio of 1.25, which is approximately the mean value less one standard deviation, was deemed a conservative and appropriate value.

Chapter 4

Analysis of Test Results

4.1 General Remarks

This chapter discusses analysis of the test data presented in Chapter 3, a detailed explanation of the more important results is also presented. A comparison of column energy absorption capacities under cyclic loading, slip response of specimens with different reinforcing details, and flexural analysis of the hinged column specimens in the strong direction is also described. Additionally, the influence of the variation of applied axial load on the behavior of the specimen is discussed.

4.2 Energy Absorption Capacity Comparison

The energy absorbed by a column during a loading cycle is represented by the area enclosed by the load-displacement hysteresis curve. The effectiveness of energy dissipation provides a basis for comparison between column specimens incorporating different hinge details.

The energy absorption capacity for each cycle was calculated for each specimen by integrating the area within the load-deflection curve. The load-deflection curves for bundled bar (BB) and diagonal bar (DB) specimens are shown in Figures 3-5, 3-22, 3-39 and 3-56. The curves for standard detail (SD) specimens, obtained from Ref. 37, are shown in Figures 4-1 and 4-2.

Figure 4-3 shows the energy absorption per individual load cycle for the specimens with an aspect ratio of 1. Specimen BB1C possesses a higher energy absorption capacity at larger displacements (cycles 8 and 9). Specimen DB1C shows a lower energy absorption capacity at nearly all displacements compared to the standard specimen (SD1C).

The energy absorption comparison for the specimens with an aspect ratio of 2 is shown in Figure 4-4. The standard specimen showed higher energy dissipation at nearly all displacement amplitudes. Specimen BB2C exhibited lower energy dissipation than BB1C, indicating that bundled bar details can improve energy characteristics in hinges where shear dominates.

The energy absorption comparison did not take into account the effects of variation in concrete strength. It was believed that small variations in concrete compressive strength would not have a significant influence on the energy absorption characteristics.

The energy dissipated by a perfectly elasto-plastic system during a complete displacement cycle, as shown in Figure 4-5, is the area of the parallelogram BCDE. For a particular displacement ductility factor, u, the ideal plastic energy dissipated, E_p, can be calculated as:

$$E_p = 4(u - 1) V_p d_y \qquad (4\text{-}1)$$

where l is the distance between the applied lateral load and the hinge, V_p is the maximum shear force, and d_y is the displacement.[4]

The measured energy dissipation, E, can be divided by E_p for the same displacement ductility factor. Instead of using "energy absorbed" as the vertical axes in Figures 4-3 and 4-4, a ratio of E/E_p can be used. The above equation is not valid for u less than 1.0 since, in a perfectly elasto-plastic system, no energy absorption occurs prior to yielding; therefore, the E/E_p ratio can be calculated only for cycles 4 through 9.

Figure 4-6 is a comparison of the relative absorbed energy during individual load cycles for the specimens with an aspect ratio of 1. The observations are identical to those in Figure 4-3; the column incorporating the bundled bar detail exhibits higher energy absorption at larger displacement amplitudes. The specimen with diagonal reinforcement shows lower energy absorption at nearly all displacements, compared to the standard detail specimen.

The relative energy absorption comparison for specimens with an aspect ratio of 2 is shown in Figure 4-7. Again, the standard specimen exhibited a higher level of energy dissipation at almost all displacement amplitudes.

The comparison confirmed that the specimens with bundled bar arrangement exhibited higher energy dissipation at a lower aspect ratio, but not at a higher aspect

ratio; this indicates that bundled bar details can improve energy characteristics for hinges where shear dominates the behavior, irregardless of concrete strength variations.

4.3 Flexural Analysis

Flexural analysis of the specimens was performed using the computer program *UTCNR*, reinforced concrete analysis program that computes the moment and curvature at the yield point of a specified layer of steel and at different values of concrete strains. The program assumes that plane sections remain plane after bending and that the stress-strain curves for concrete and steel are known. The Hognestad model,[28] consisting of a parabola and a linear segment, is used as the concrete constitutive relationship (Figure 4-8). A bilinear stress-strain relationship with elastic and strain hardening branches is used for the reinforcing steel. The input data for the program consists of concrete and steel properties as well as the geometric section properties and the existing axial load.

Figures 4-9 and 4-10 show the interaction diagrams for the BB and DB specimens, respectively. These curves correspond to a maximum concrete strain of 0.004. The 26 kip axial load applied to each specimen during testing is indicated on the figures. Measured concrete and steel properties were used in the analysis.

For the bundled bar specimens (Figure 4-9), a moment of 392 kip-inch was reach with a 26 kip axial load. The measured average moments for the positive and negative directions were 473 kip-inch for BB1C and 475 kip-inch for BB2C. For the diagonal bar specimens (Figure 4-10), the moment corresponding to an axial load of 26 kips was 335 kip-inch. The measured average moments for the positive and negative directions were 402 kip-inch for DB1C and 414 kip-inch for DB2C. In each case, the measured moment was about 20 percent higher than calculated, indicating that the specimens were stronger than the computer model predicted.

Because of confinement, the concrete strength in the hinge region was higher than the measured concrete compressive strength. To account for this confinement, a value of $1.25f'_c$ was used for the hinge concrete strength. A value of 0.004 in./in. was used as the ultimate concrete compressive strain; however, due to confinement, the actual crushing strain was higher than 0.004. The study presented in Ref. 37 shows that the concrete in the hinge throat is capable of developing strains up to 0.03 in./in., 7.5

times larger than assumed for this analysis. A higher value of concrete strain results in a higher moment on the interaction diagram.

The interaction diagrams for a concrete strength of $1.25f'_c$ and an estimated ultimate concrete strain of 0.02 are shown in Figures 4-11 and 4-12. The moment corresponding to an axial force of 26 kips are marked in the figures. The calculated moments were 461 kip-inch for the bundled bar specimens and 396 kip-inch for the diagonal bar specimens. The measured values match extremely well, with a maximum difference of less than 5 percent.

Figures 4-13 and 4-14 are the moment-curvature responses for bundled bar and diagonal bar specimens, using the measured concrete strengths. The diagrams for increased concrete strength and ultimate strain are shown in Figures 4-15 and 4-16. All of these curves are very similar; therefore, Figure 4-13 will be used to describe the data. There are five distinct break points, indicated by the letters A through E. Point A is the cracking point of the concrete, which occurred at a moment of 124 kip-inch. Points B and C are the yield points of the bundled bars, which yielded in tension (Figure 3-1). Point D corresponds to yielding of bar 3. Finally, the ultimate point (E) corresponds to the crushing of concrete at an ultimate strain of 0.004 in./in.

4.4 Effects of Variation in Axial Loading

As described in Section 2.8.1, the axial load applied to the column specimens was intended to be kept constant, but the actual load varied due to the nature of the test setup. The load cell in the testing machine measures total load on the platform. Although the test frame was very stiff, overturning effects increased or decreased the load on the platform. This variation in actual axial load resulted in differences between the measured capacity in opposite directions.

To estimate the actual difference in the column axial load, the load-moment interaction diagrams can be used. A tangent line drawn on the interaction curve through the point corresponding to the axial load of 26 kips gives an approximate relationship between the variation in moment and axial load (Figures 4-11 and 4-12). The slope of the line is 0.325 kip/kip-inch in Figure 4-9 and 0.302 kip/kip-inch in Figure 4-10. The difference in shear capacities can be multiplied by the height of the lateral loading to

obtain the difference in moment capacities. The difference in axial loading in two directions can be obtained by multiplying the moment difference by the slope of 0.325 kip/kip-inch for BB specimens and 0.302 kip/kip-inch for DB specimens. Differences resulting from eccentricity in the axial load was negligible.

Table 4-1 lists a summary of these calculations. The difference in axial load is 12.0 kips for BB1C and 14.5 kips for DB1C. Specimen BB1C was actually subjected to an axial load which varied between 20.0 kips in the positive direction and 32 kips in the negative direction (with an average of 26 kips). Specimen DB1C experienced a axial load of 18.7 kips in the positive direction and 33.3 kips in the negative direction.

Similarly, the difference in axial load was 21.8 kips for BB2C and 20.9 kips for DB2C. This means that the axial load on BB2C varied from 15.1 kips in the positive direction and 36.9 kips in the negative direction. Specimen DB2C experienced an axial load of 16.8 kips in the positive direction and 35.2 kips in the negative direction.

The difference between load variations for specimens of the same aspect ratio may be attributed to approximations in the interaction diagrams and crudeness in drawing the tangent lines.

4.5 Slip Response Comparison

The slip response histories for the column specimens are shown in Figures 3-7, 3-24, 3-41, and 3-58. Table 4-2 summarizes the maximum slips for these specimens. The results for SD1C and SD2C were obtained from Ref. 37.

The load-slip responses were symmetric for positive and negative loadings up to a displacement ductility of 2; however, they were unsymmetric when the ductility approached 4.

The slip difference in the positive and negative directions resulted from variations in axial load. Higher axial loads restrict column rotation; to achieve the same deflection at the top of the column with a smaller rotation, the slip must increase. At small displacement levels, the variation in axial load was small and the slip in both directions was approximately the same. At larger displacement levels, the difference in axial load became significant, and its effect on rotation became considerable.

For specimen BB1C, the positive slip was comparable to other specimens with the same aspect ratio, but the negative slip was much larger. Table 4-2 lists the slip of specimen DB1C in the positive direction as 0.175 inch, comparable to the slip for specimens BB1C and SD1C in the same direction (0.197 inch and 0.22 inch, respectively); however, the negative slip of DB1C, 0.104 inch, was considerably less than BB1C and SD1C (0.611 inch and 0.25 inch, respectively).

To compare the maximum slip response for all specimens, the average slip in both directions is a reasonable representation of the response. The average slips are also listed in Table 4-2. For the specimens with an aspect ratio of 1, specimen DB1C exhibited the lowest average slip, a result of the diagonal reinforcement in the hinge. It appears that the diagonal reinforcement can also reduce the slip for an aspect ratio of 2, albeit not significantly.

Chapter 5

Finite Element Studies

5.1 General Remarks

A finite element analysis was performed to investigate the stress distribution and intensity in the hinge region of column specimens, shear specimens and compression specimens. The results provide evidence of concrete confinement in the hinge throat under various loading conditions, before cracking takes place. A nonlinear finite element analysis would provide the stress distribution under various stages of precracking, post-cracking, and post-yielding stages; however, available programs do not adequately address the important factors. Development of a new nonlinear finite element program was beyond the scope of this study.

The variables involved in the finite element models were variation in hinge thickness for column specimens and compression specimens, and variation of hinge thickness and footing slope for compression specimens. Sloped footings were investigated as a way of allowing greater rotation between the column and the foundation.

The commercial finite element package *IMAGES-3D*[16] was used to perform the analysis. *IMAGES-3D* is a three-dimensional general purpose finite element analysis program for IBM® and compatible personal computers.

Because of symmetry, only one-half of each specimen needed to be modeled; planes of symmetry were restrained to provide proper boundary conditions. The finite element models were composed of many rectangular solid elements of various sizes, smaller elements near the hinge. Where the element size changed, discontinuities occurred; these discontinuities should not be a concern since they occurred relatively far from the hinge region

The concrete modulus of elasticity used in the program was based on a compressive strength of 4000 psi; Poisson's ratio was assumed to be 0.25. Reinforcing bars were not considered in the modeling.

5.2 Column Specimen Models

The finite element model of the column specimen is shown in Figure 5-1. Each model consisted of 292 solid elements, of which eight elements represented the hinge throat. Nodes on the plane of symmetry (x-z plane) were restrained in the translational y-direction. Nodes on the bottom of the footing were restrained in the translational z-direction. The node located at the origin was restrained in all directions to make the system stable. All other degrees-of-freedom in the model were unrestrained. The figures presented in the following sections show relative stress magnitudes under various loading conditions. The stresses correspond to the stress at the center of the elements in the hinge throat.

The model (Figure 5-1) was loaded at the two nodes corresponding to the locations of the applied vertical and lateral loads on the test specimens. Both point loads were 13 kips, equivalent to 26 kips were the whole specimen modeled. In this analysis, the hinge thickness (dimension in the z-direction) had values of 0.5 inch, 1.0 inch, and 1.5 inches, to examine the effect of hinge depth on stress distribution.

Figures 5-2 through 5-4 show the hinge normal stress distributions (σ_x, σ_y, σ_z) with respect to hinge depth. Figure 5-5 shows the shear stress distribution (τ_{xy}). For the normal stresses, positive values indicate tension, while negative values represent compression.

The concrete in the compression region of the hinge throat is confined by concrete immediately above and below as a result of the reduced cross section. This is evident in Figure 5-3, which shows the stresses in the y-direction. The stresses increase from the center to the edge in both compression and tension, although the increase in the tension zone is of no practical significance. As the hinge thickness was reduced from 1.5 inches to 0.5 inch, the confinement stress increased approximately 40 percent in element 8 and 27 percent in element 7. The change in depth did not significantly affect stresses in the x-direction (Figure 5-2) for the inner elements; however, it did have some effects on the outer elements. The y-stress component increased about 22 percent for a hinge thickness of 0.5 inch. The hinge thickness had little influence on the

stresses in the vertical direction (Figure 5-4). The stress distribution in all three directions deviated slightly from linear; this was attributed to mesh size.

The magnitudes of confining stresses in the y-direction were approximately 47 percent, 38 percent, and 31 percent of the vertical stress for hinge depths of 0.5 inch, 1.0 inch and 1.5 inches, respectively, in the intermediate elements 4 through 7, and 39 percent, 32 percent, and 28 percent, respectively, for element 8. The confining stresses in the x-direction were approximately 40 percent, 35 percent, and 32 percent of the vertical stress for hinge depths of 0.5 inch, 1.0 inch and 1.5 inches, respectively, in elements 4 through 7, and 31 percent, 27 percent, and 24 percent, respectively, in element 8. For a given direction, the lesser the hinge thickness, the greater the confinement; for a given hinge thickness, the y-direction confinement is greater than the x-direction confinement.

Figure 5-5 shows the relationship between shear stresses in the hinge region and hinge depth. The shear stresses are markedly higher in the edge elements than in the interior elements. Shear stress distributions in the inner elements were relatively uniform. Shear resistance in the hinging direction was non-uniform, with a large concentration at the edges.

5.3 Shear Specimen Models

Figure 5-6 shows the finite element models of shear specimens SSP1, SSP2, and SSP3 (with hinge depths of 1, 2, and 3 inches, respectively). Each model consisted of 512 solid elements. The only difference between the models was the size of the six elements in the hinge throat, which produced the three different hinge thickness. The nodes on the plane of symmetry (x-y plane) were restrained in the translational z-direction. The nodes on the base plane (x-z plane) were restrained in translational y-direction. All other degrees-of-freedom were unrestrained. The origin node was restrained in all directions to make the system stable. The load on the models was a 1 kip point load applied to the top of the model (Figure 5-6).

Figures 5-7 through 5-9 show the hinge normal stress distributions (σ_x, σ_y, σ_z) with respect to hinge depth. Figure 5-10 shows the shear stress distribution (τ_{xy}). For

normal stresses, positive values indicate tension and negative values represent compression.

Figure 5-7 shows the normal stress distribution in the x-direction. This stress is primarily tension, with compression in the edge elements when the hinge was subjected to pure shear in the direction of hinging. The segments on either side of the hinge separated from each other, except near the edges, where the two segments pressed into each other. There were no significant stress differences accompanying the change in hinge thickness.

The normal stress distribution in the y-direction is shown in Figure 5-8. All elements experienced compression, with higher magnitudes at the edge elements, especially at the top edge. The compressive stress in the top element decreased 17 percent between SSP1 and SSP2 and 36 percent between SSP1 and SSP3. The normal stress in z-direction was primarily tension. Compression existed in the top elements for all three models, and in the bottom element for SSP1. In the z-direction, compressive stress in the top element decreased 32 percent between SSP1 and SSP2 and 71 percent between SSP1 and SSP2. Tensile stresses in the intermediate elements were linear, with a 27 percent increase between SSP3 and SSP2 and between SSP2 and SSP1.

Figure 5-10 shows the shear stress distribution in the hinges. There were no stress changes in the intermediate elements resulting from a change in hinge depth. Some differences existed at the top and bottom elements, with the highest values in specimen SSP1.

5.4 Compression Specimen Models

Figure 5-11 shows the finite element mesh used to model the compression specimens NCS1, NCS2, and NCS3 (hinge depths of 1, 2, and 3 inches, respectively). Each specimen was modeled with 266 solid elements, of which six represented the hinge throat. The nodes on the plane of symmetry (x-z plane) were restrained in the translational y-direction. The base nodes (x-z plane) were restrained in the translational z-direction. The node at the origin was restrained in all directions to make the system stable. All other degrees-of-freedom were unrestrained. The model was loaded with a 1 kip point load.

Figures 5-12 through 5-14 show the hinge normal stress distributions (σ_x, σ_y, σ_z) with respect to hinge depth. For all normal stresses, the distribution along the hinge was generally uniform, except for the edge elements. Stresses in the x- and y-directions were confinement stresses in the hinge. Confinement stresses in both directions decreased as hinge depth was increased. As indicated in Figure 5-12, the interior element normal stresses in the x-direction dropped 9 percent between NCS1 and NCS2 and 16 percent between NCS1 and NCS3. These percentages were 22 percent and 35 percent, respectively, for the edge elements. The y-direction normal stresses for the interior element (Figure 5-13) decreased 14 percent between NCS1 and NCS2 and 28 percent between NCS1 and NCS3. These percentages were 22 percent and 35 percent, respectively, for the edge elements.

The vertical normal stress distribution for the compression specimens is shown in Figure 5-14. The hinge depth did not appear to significantly affect the stress in the vertical direction. The stress level for NCS1 was slightly higher in the edge elements and lower in the interior elements than in specimens NCS2 and NCS3.

The rotation allowed by a one-way hinge depends primarily on the thickness of the hinge (dimension in the z-direction, Figure 5-11). The thicker the hinge, the greater the allowed rotation. The concrete in thicker hinges is less confined, and will directly influence hinge strength. To allow more rotation in a one-way hinge without reducing confinement, the top surface of the foundation may be sloped.

Finite element analyses focusing on the influence of footing slope were also conducted. Figures 5-15 and 5-16 are the finite element models with different slopes in the top surface of the footing. The models were based on the compression specimen NCS1 (0.5 inch hinge thickness).

Figures 5-17 through 5-19 compare the normal stresses for the flat footing to footings with different slopes. The sloped footings did not appreciably affect confinement stresses in the hinge throat (under precracking conditions).

5.5 Concluding Remarks

The finite element analysis results shed some light on the behavior of specimens under precracking condition. Focus was placed on the influence of hinge depth on

confining stresses in the hinge throat. Under pure axial load or under combined axial and lateral loads, the confinement decreased as the hinge depth was increased; however, there was no indication of such influence when the hinge was subjected to pure shear. As an alternative to increasing hinge depth when it is desirable to allow a greater rotation, the top surface of the footing may be sloped; this sloping will maintain the desired level of confinement in the hinge throat.

Chapter 6

Lateral Strength of Hinged Columns

6.1 Introductory Remarks

Recent earthquakes have caused substantial damage to reinforced concrete bridge columns due to large induced lateral forces. Much of the damage directly resulted from lateral failure of short columns, insufficient ductility to withstand the imposed inelastic displacements, and anchorage failure of longitudinal reinforcement in regions of plastic hinging.[11,17] If there was a one-way hinge connection between the bridge deck and the supporting column or between the column and the foundation, damage was likely to occur in the hinge region because of the reduced cross-section.

The most commonly used reinforced concrete one-way hinge in bridge columns is the Freyssinet hinge.[9,36] In this type of hinge, little or no reinforcement passes through the hinge throat. The strength of the concrete in the hinge is considerable, and is sufficient to resist internal forces due to vertical loads and thermal movements. Reinforcing steel is used to provide shear resistance as well as to increase bearing strength. A hinge throat depth of 1 to 4 inches is normally used to allow rotation about the weak axis.

Bridge designers have used the shear friction method[2,26] to calculate the lateral strength of hinged columns in the strong direction, assuming that all the bars at the hinge throat yield in tension and that aggregate interlock occurs over the entire hinge region. In reality, lateral forces are introduced into bridge columns through loads acting primarily at the deck level; there can be significant flexural cracking at the hinge throat, making this assumption questionable.[36]

This chapter introduces the compressive force path method (CFPM) to calculate the lateral strength of reinforced concrete one-way hinged columns in the strong direction, and compares the CFPM with the shear friction method. The experimental investigations discussed in Chapters 2 through 4 and in Refs. 28 and 37 were used to evaluate this new method.

6.2 Shear Friction Method

The shear friction method has been widely applied in design since its incorporation into the ACI building code[2] in 1971. This theory assumes that as the concrete segments on the two sides of a initially-cracked section slide relative to each other, they introduce tension in the steel crossing the crack because of the roughness of the aggregate. The reaction from this tension is a compressive force normal to the crack; to this force, any applied compressive force is added. The product of the compressive force and a friction factor results in the shear resistance (Figure 6-1).

The behavior of the hinge throat in a pinned bridge column is considerably different (Figure 6-2). Normally, substantial flexural cracking of concrete is expected, limiting the contact area to the compression zone of the section. The extent of flexural cracking is a function of the hinges's aspect ratio (the ratio of the inflection point height to the hinge depth). To make a realistic prediction of shear strength, the effects of flexure must be considered.

6.3 Compressive Force Path Method

Kotsovs[19] introduced a new method for predicting the ultimate shear strength of reinforced concrete beams. This method is based on the compressive force path which was observed during experimental investigation of simply-supported reinforced concrete beams with various arrangement of stirrups. The compressive force path is a reasonably assumed "flow" line for compressive stresses with varying cross-sections perpendicular to the direction of path. The key to this method is developing a path model capable of providing a realistic description of the features which can cause failure of the column. Failure is associated with the development of tensile stresses in the path region, perpendicular to the compressive stresses. Tensile stresses may develop due to a number of reasons, including an abrupt change in the column cross-section.

A sudden change in compressive stress field intensity along the path in the hinge region appears to be a major cause of failure in hinged columns. Compressive stresses reach a critical level in the hinge region where the cross-section is the smallest and the stress intensity is the largest.

Figure 6-3 shows the assumed compressive force path for a hinged specimen. The path is a bilinear curve with a horizontal path accounting for the application of lateral force. In determining the path, two lines are first drawn by extending the directions of the vertical and lateral forces to the point where they intersect; this point is then connected to the center of the hinge compression zone. If the lateral force is applied as shear at the top of the column, the suggested compressive force path would be a line directly connecting the point where the axial force is applied to the center of the hinge compression zone; an equivalent lateral force can be applied horizontally at the top of the column.

Assuming that the steel yields both in tension and in compression at the ultimate state, the lengths of the tension and compression zones are determined by considering equilibrium in the vertical direction. Equilibrium in the vertical direction leads to the following equation:

$$P_y + (1 \quad \xi)A_s f_y - \xi A_s f_y + 0.85\xi(whf_c)\cos^2\gamma \qquad (6\text{-}1)$$

where P_y is the applied axial force, ξ is the ratio a/h (where a is the length of compression zone of the hinge and h is the dimension of the hinge in the strong direction), w is the dimension of the hinge in the weak direction, A_s is the total area of reinforcing steel in the hinge, f_y is the yield strength of the reinforcing steel, f'_c is the specified concrete compressive strength, f_c is the concrete compressive strength in the hinge throat ($1.25f'_c$), and γ is the angle of the compressive force path relative to the vertical axis.

The parameter P_y may be taken as the unfactored dead load acting on the column. The compressive strength of the concrete in the hinge region is assumed to be 25 percent higher than the specified compressive strength because of confinement. This increase was justified by the testing described in Chapter 3, and is conservative. The angle γ is a function of ξ and may be written as such; however, such a substitution will complicate the equation. In subsequent sections it will be shown that γ may be taken as the arc tangent of $h/2l$ with little effect on the calculated shear strength. Based on this simplification, ξ can be determined from Eq. (6-1).

The lateral load capacity of the column can be calculated by taking the moments about the center of compression zone:

$$V_c l = 0.5 P_s (1 - \xi) h + 0.5 (1 - \xi) A_s f_y h \qquad (6\text{-}2)$$

where V_c is the lateral load capacity of the hinged column and l is the distance from the lateral force to the hinge.

6.4 Testing Program

Experimental results were used to evaluate the compressive force path method for estimating lateral strength of hinged specimens. The evaluation consisted of two parts: (1) to determine the actual lateral strength of the hinge specimens, and (2) to determine the ultimate concrete strength in the hinge throat.

6.4.1 One-Eighth Scale Column Specimens

As discussed in Ref. 28, four specimens with one-way hinge details were tested to failure (Figure 1-4). The specimens were one-eighth scale representations of the hinges in the Rose Creek Bridge (Figure 1-3). The column cross-section measured 2 inches by 12 inches in the hinge area and 6 inches by 12 inches elsewhere. The hinge throat in each specimen was reinforced with six No. 2 plain bars; the aspect ratio (l/h) ranged from 1 to 3. The columns were subjected to a series of monotonic and cyclic loads, but no axial loads were applied to the specimens.

6.4.2 One-Sixth Scale Column Specimens

Eight one-sixth scale models of the Rose Creek Bridge columns were tested in (Figures 1-5, 2-1, and 2-2). The cross section of each column specimen measured 6.5 inches by 16 inches, reduced to 2.5 inches by 16 inches in the hinge region. The hinge throats in the four standard detail specimens[37] were reinforced with equally spaced bars to simulate common practice. The four bundled-bar and diagonal-bar specimens (Chapter 2) had modified reinforcing details. Reinforcing steel in all eight specimens consisted of No. 3, Grade 60 deformed bars.

Other variables considered include column aspect ratio and loading type. A nominal axial load of 26 kips was applied to the columns. This load produced an axial

stress in the hinge throat approximately the same as the dead load stress in the Rose Creek bridge. For specimens which were tested cyclically, the lateral load capacity was based on the envelop of the hysteresis curve.

6.4.3 Plain Concrete Hinge Specimen

Concrete in the hinge region is confined in a triaxial state of stress. To quantify this confinement, twenty-four small scale hinged specimens were constructed and tested in compression (Figure 2-5). To determine the effect of the hinge width-to-height ratio, the hinge thickness was varied from 0.25 inch to 2.0 inches, with a constant width of 1.5 inches; this produced width-to-thickness ratios ranging from 0.75 to 6 (the hinge width-to-thickness ratio in the Rose Creek Bridge is 4). No reinforcing steel was used in the specimens.

Table 3-1 lists the average compressive strength of each group of specimens, the unconfined compressive strength on the day of testing, and the ratio of hinge strength to unconfined compressive strength. The hinge strength was higher than the unconfined compressive strength, varying from 1.27 to 1.61; however, there is no clear indication that the height-to-width ratio had a substantial influence. The higher concrete strength in the hinge region can be incorporated into the compressive force path method. A ratio of 1.25, which is approximately the mean value less one standard deviation, was deemed to be an appropriately conservative value.

6.5 Comparison of Analytical and Experimental Results

Table 6-1 shows the comparison of measured and calculated lateral load capacities for all column specimens. The results based on the compressive force path method were determined using an approximate value for γ. The results based on the shear friction method overestimated the column strength by 230 to 500 percent. The compressive force path method led to results which were very close to the measured data. Table 6-1 also compares the lateral load capacities using different compressive strengths for the concrete in the hinge. By using strengths 25 percent greater than the unconfined compressive strength, the compressive force path method led to an excellent prediction of lateral strength for all specimens.

6.6 Effect of Approximating γ

It was noted in previous sections that the angle γ is a function of the ξ factor. To simplify this analysis, however, γ was approximated by the arc tangent of $h/2l$. Table 6-2 shows the influence of this simplification. The predicated values based on the approximate value for γ are within 3 percent of the values calculated using the exact method.

6.7 Concluding Remarks

The compressive force path method, used to determine the lateral load strength of one-way hinges in the strong direction, leads to results which are in very close agreement with the measured results for twelve column specimens. The shear friction method, currently in use by designers, was found to produce results which can be several times higher than the observed strengths. The amount of calculation involved in the compressive force path method is comparable to the shear friction method.

In the compressive force path method, the concrete compressive strength in the hinge throat can be assumed to be twenty-five percent higher than the unconfined compressive strength. This increase, a result of concrete confinement, is justified by compression testing of 24 plain concrete hinge specimens.

Chapter 7

Aspect Ratio of Bridge Columns with One-way Hinges

7.1 Introductory Remarks

The lateral load capacity of a hinged column in the strong direction depends on the shear span-to-depth ratio (aspect ratio) of the column, i.e., the ratio of inflection point distance from the hinge to the hinge depth. The behavior of one-way hinged columns change from pure shear to flexure when the aspect ratio changes from zero to a larger value. Under pure shear, the shear friction theory is valid since this theory assumes a cracked section and assumes that aggregate interlock provides shear resistance. The aspect ratio is not a parameter in the shear friction theory; however, it is a factor in the compressive force path method, which has been shown to be an accurate method of predicting lateral strengths. A rational determination of the aspect ratio is essential to an accurate predication of lateral strength.

This chapter presents the results of analytical studies of this parameter. The studies were performed on single-column bridges without expansion joints, using the computer program *ISADAB*.[35]

7.2 Computer Program *ISADAB*

The computer program *ISADAB* uses a multiple degree-of-freedom nonlinear model for analyzing the transverse response of highway bridges subjected to static lateral loads, free vibration, and earthquake motions. Nonlinear effects are accounted for by incorporating translational and rotational springs at abutments, column bases, and column foundations. The deck and columns are treated as line elements.

Two hysteresis models were used to represent the cyclic behavior of the nonlinear components: the Ramberg-Osgood model[31] for the abutment springs, and the TQ-hyst model[34] for pier and foundation springs.

Figures 7-1 and 7-2, obtained from Ref. 18, show a schematic view of one-half of a bridge system and a pier element. The pier element was assumed to consist of an infinitely rigid top part, an elastic line element, and a nonlinear rotational spring at the base. The rigid end segment represents the segment from the centroid to the bottom of

the deck. The rigidity for this segment is assumed to be infinity since the pier cap sections are considerably wider than the pier columns. The moment diagram for the pier is shown in Figure 7-2(c). The maximum moment ordinarily occurs at the base. For the columns incorporating hinges, the length of the yielded region was assumed to be equal to the length of the hinge throat. The boundary conditions and spring numbering scheme is shown in Figure 7-3.

The analytical model was found to have a reasonable correlation between the calculated and measured static and dynamic response of the Rose Creek Bridge.[18,34] In the present study, only the static analysis feature of *ISADAB* was utilized.

7.3 Aspect Ratio of Single-Column Bents

A parametric study was performed to investigate the method of determining the shear span-to-depth ratio of single-column bents. The analysis was based on the Rose Creek Bridge model presented in Ref. 34. A detailed description of the model and boundary spring properties can be found in that reference.

The column shear span-to-depth ratio appeared to be affected by deck torsional rigidity, abutment translational and rotational spring stiffnesses, and lateral load.

By comparing the top and bottom moments of a pier at a certain ductility level, the height of the inflection point can be determined. For columns in double curvature, the ratio of the top moment and the bottom moment can be used to determine the location of the inflection point on the column, at which the lateral load should be applied for the compressive force path method. For columns in single curvature, the lateral load should be applied at the centroid of the deck.

The first *ISADAB* run was made using actual member cross-section properties and assumptions as described in Ref. 34. Both exterior and interior columns flexed in double curvature. The ratios of top moment-to-bottom moment were 0.41 for the two exterior bents and 0.009 for the two interior bents (corresponding to ductilities of 1.192 and 3.728, respectively). This was expected, since the two exterior bents are closer to the abutments, where more translational and rotational resistances exist. At the two interior bents, the deck tended to flex with the top of the columns, making the ratio of top moment-to-the bottom moment substantially smaller.

The next several runs were made using independently increased abutment spring stiffnesses and deck torsional rigidity. The results show little change in the ratios for the two interior columns. The largest ratio was 0.06, when the deck torsional rigidity was increased a hundred-fold. The ductilities were comparable to those of the first run; thus, for interior columns, the total height of the column should be used in the compressive force path method.

The ratios of top moment-to-bottom moment for the two exterior columns were more sensitive to the changes in abutment stiffness and deck rigidity. In some extreme cases, the exterior columns flexed in single-curvature. The ratios ranged from zero to 0.45 depending on the parameter and the magnitude of change. As a result, it is conservative to apply the lateral load at the centroid of the deck for exterior bents as well.

Some of the stiffness and rigidity changes in the parametric study were so large as to be unrealistic. The purpose was to determine the effect of top moment-to-bottom moment ratio. The ratio appeared to be related to many factors in addition to the parameters considered in this study, such as the deck bending moment of inertia in the two principal directions. Therefore, the use of a lower inflection point height may not be justifiable. To avoid the need for a nonlinear analysis, and to simplify calculations, it is recommended that the inflection point in single column piers be conservatively located at the centroid of the superstructure.

7.3 Aspect Ratio of Multi-Column Bents

There was no static nonlinear analysis computer program available to perform a similar parametric study on the aspect ratio for bridges with multiple column bents; developing such a program was beyond the scope of this study.

Since many seismic codes implicitly include the effects of nonlinear behavior and allow the practicing engineer to use more familiar elastic analyses, it may be more practical to determine the inflection point of multiple-column bents using elastic methods. Such analysis can be performed using any general purpose finite element program. After the inflection point is located, the parameter l in the compressive force path method (Eq. (6-2)) can be determined.

7.4 Concluding Remarks

The shear span-to-depth ratio of bridge columns is an important factor in determining the lateral strength using the compressive force path method. Based on nonlinear analysis of a bridge system incorporating one-way hinges at the interface between the column and the foundation, it was concluded that the application of the lateral load at the centroid of the deck, for single-column bents, yields rational and conservative results. The inflection point height of multiple-column bents can be determined using elastic analysis.

Chapter 8

Response and Repair of an Existing Hinged Column

8.1 General Remarks

The extensive damage that occurred to bridges in the 1971 San Fernando earthquake resulted in a significant reevaluation of seismic design procedures. Since then, many improvements have been incorporated into design codes; however, many bridges were built prior to the application of this knowledge. In many existing bridges, such as the Rose Creek Bridge, the anchorage length provided for reinforcing steel is shorter than that specified in modern building codes.[7] Inadequate anchorage can result in bond failure before the reinforcement develops its yielding strength.

As discussed in previous chapters, the shear friction method assumes full development of tensile yield strength of the steel. Inadequate anchorage makes the calculated lateral strength even more unconservative.

Because it is not feasible to replace the one-way hinges in existing bridges, there is a need to develop a rational retrofitting method to improve the behavior of existing columns. As a pilot study, one column specimen with insufficient steel anchorage was constructed and tested. To investigate techniques for retrofitting existing bridges to improve their seismic performance, the test column was retrofitted after failure and once again tested.

Only limited testing was performed; the conclusions presented in this chapter are preliminary in nature.

8.2 Insufficient Development Length Column Specimen

The test specimen had overall dimensions identical to specimens BB2C and DB2C (Chapter 2); however, the six No. 3 bars used in this specimen were equally spaced short, straight bars with no hooks on either end (Figure 8-1).

The specimen was designed to model the short development length of the Rose Creek Bridge columns. Reinforcement in the bridge consists of No. 11 bars with a specified anchorage length of 3 feet above and below the hinge (Figure 1-3). In the specimen, an anchorage length of 6 inches was provided, based on the assumption that

the ratio of actual development length to required development length for No. 3 and No. 11 bars are identical. The required lengths for the bars were calculated according to the ACI building code.[3] Figure 8-2 is a photograph of the specimen taken before the column was poured.

One strain gage was bonded to each steel bar in the hinge region, and one gage bonded 3 inches above and below the hinge on both exterior bars. Three LVDTs were used to monitor rotation and slip (Figure 8-3).

The specimen was subjected to seven cycles of increasing displacement in the strong direction, under a nearly constant axial load of 26 kips, up to an apparent displacement ductility of 2. The loading history is shown in Figure 8-4.

8.3 Repaired Column Specimen

After the original specimen was tested, it was repaired with a steel plate and angle jacket system designed to transfer tensile force across the hinge. The goal was to restore the strength and ductility capacity of the hinge to the level of a hinge with adequate steel anchorage. The specimen was repaired using a jacket constructed of ASTM A36 steel angles, channels, and plates (Figures 8-5 and 8-6). The steel plates were anchored to the column and the footing using Trubolt Wedge concrete anchors. At the connection between the column and the footing, the steel angle cross-section was reduced to allow hinging in the weak direction. The width of the reduced section was calculated based on a yielding strength of 36 ksi and a maximum tensile force of approximately 30 kips, corresponding to the yield force for five No. 3 bars.[37] Actual yield strength was approximately 45 ksi, as measured by three test coupons (Figure 8-7) obtained from the angles. The measured stress-strain curve is shown in Figure 8-8.

To reduce the deflection of the horizontal plate as a result of forces acting in the weak direction, the plates were stiffened by welding a channel to both plates. The number of anchor bolts used was based on test data provided by the manufacturer, with a safety factor of approximately 1.5. Based on the manufacturer's data, the 3/8-inch anchor system, embedded 4.5 inches in 4000 psi concrete, has an ultimate pullout capacity of 5.9 kips and an ultimate shear capacity of 4.6 kips; the 1/2-inch anchor, embedded 4.125 inches in 4000 psi concrete, has an ultimate pullout capacity of 7.3

kips and an ultimate shear capacity of 7.4 kips. The minimum specified spacing for 3/8-inch anchor is 3.75 inches, on center, and 1.875 inches from the edge; spacing for the 1/2-inch anchor is 5 inches, on center, and 2.5 inches from the edge. These spacing requirements were barely satisfied, due to the narrow column section. Figures 8-9 and 8-10 are photographs of the steel jacket taken before it was attached to the column.

After being repaired, the specimen was subjected to ten and one-quarter cycles of displacement reversals at four displacement amplitudes (Figure 8-11). Again, a nominally constant axial load of approximately 26 kips was applied to the column to simulate the superstructure dead load.

8.4 Original Specimen Testing Results

Figures 8-12 and 8-13 show the original specimen after testing. Because of the relatively small displacements applied, there was no dramatic visible damage to the column, and few cracks observed outside the hinge.

8.4.1 Load-Deflection Response

Figure 8-14 shows the load-deflection response for the specimen. The largest load applied at a displacement ductility factor of 2 was 8.6 kips in the positive direction and 10.96 kips in the negative direction. On the last cycle, a maximum value of 7.1 kips was reached in the positive direction and 9.93 kips in the negative direction, indicating strength degredations of 17.4 percent and 9.4 percent, respectively. The load appeared to be still increasing; however, stiffness substantially decreased between ductility factors of 1 and 2, indicating that reinforcement bond failure had occurred. The differences in the maximum loads and the variation in stiffness for the positive and negative directions are attributed to the variation of applied axial load in different directions (see Section 4.4).

Figure 4-2 shows the load-deflection response for specimen SD2C.[37] The only difference between this specimen and SD2C was the inadequate development length. Comparing Figures 4-2 and 8-14, the response for this specimen shows a much stronger pinching effect at a ductility factor of 2; this was a result of the bond failure in the short reinforcing bars.

8.4.2 Load-Rotation Response

Figure 8-15 shows the load-rotation response. The maximum rotation was 0.012 radian in the positive direction and 0.014 radian in the negative direction. As with the other specimens (see Chapter 3), the maximum rotation in the positive direction was larger than in the negative direction; however, because of the small displacements, the difference was relatively small.

Similar to Figure 8-14, the load-rotation response also shows strong pinching due to loss of bond between the concrete and the reinforcing steel.

8.4.3 Load-Slip Response

Figure 8-16 shows the load-slip response. The maximum slip was 0.0138 inch in the positive direction and 0.0148 inch in the negative direction. Similar to specimens BB2C and DB2C (Figures 3-24 and 3-58), the slip contributed only a small fraction of the lateral displacement.

8.4.4 Load-Strain Response

Figures 8-17 and 8-18 are the responses for the two exterior bars, 3 inches above the hinge. Both bars experienced strain reversals, but neither bar yielded. The general trend between load and strain was linear. Figures 8-19 and 8-20 show the corresponding responses 3 inches below the hinge. Similar behavior was observed, although the strains were larger.

Figures 8-21 through 8-26 show the load-strain histories in the hinge. All bars experienced reversals of tension and compression. The four exterior bars yielded in tension; the two interior bars did not yield.

Neither of the two exterior bars developed their yield strength 3 inches above or below the hinge; however, it was reported that both exterior bars of SD2C developed their yield strength at the 3 inch point;[37] again indicating that bond failure has occurred between the concrete and the steel.

8.5 Results of Repaired Column Testing

Figures 8-27 and 8-28 are photographs of the repaired specimen after testing. All major cracks initiated at the steel jacket anchors. Relative displacement between the

steel plate and the footing was observed; this was a result of oversized holes, used to avoid interfering with the steel reinforcement.

8.5.1 Load-Deflection Response

Figure 8-29 shows the load-deflection response after repair. The largest load applied was 13.9 kips in the positive direction and 20.2 kips in the negative direction. On the last cycle (ductility factor of 4) the maximum load was 11.85 kips in the positive direction and 18.4 kips in the negative direction, a strength degradation of 15.0 percent and 9.1 percent, respectively. The difference in maximum loads for positive and negative directions are attributed to the variation of applied axial load (see Chapter 4).

The stiffness in both directions decreased significantly after the first cycle due to the enlarged anchor holes. Better stiffness behavior could be expected if there were no such weak connections.

The repaired column showed a relatively small energy dissipation capacity and a strong pinching effect, indicated by the very narrow hysteresis response (Figure 8-29); nevertheless, the repair method did restore the strength and ductility capacity to the level of a hinge with adequate steel anchorage.

8.5.2 Load-Rotation Response

Figure 8-30 shows the load-rotation response after repair. The maximum rotation was 0.022 radian in the positive direction and 0.020 radian in the negative direction. As with the other specimens (Chapter 3), the rotation in the positive direction was slightly larger than in the negative direction.

8.5.3 Load-Slip Response

Figure 8-31 shows the load-slip response after repair. The maximum slip was 0.027 inch in the positive direction and 0.039 inch in the negative direction. There were clear correlations between load-rotation response and load-slip response. Based on the measured rotation and slip, the approximate lateral deflection was calculated to be 0.97 inch in the positive direction and 1.03 inches in the negative direction. Both values are very close to 1.0 inch value measured during testing.

8.5.4 Load-Strain Response

Figures 8-32 and 8-33 show the load-strain responses for the two exterior bars, 3 inches above the hinge. Both bars experienced reversals of tension and compression, but, even at a ductility factor of 4, neither bar yielded. The general trend in the hinge region for both bars was nearly linear. Figures 8-34 and 8-35 show the histories for the gages located 3 inches below the hinge; similar behaviors were observed. The low strain was expected, since the retrofit steel collar is taking most of the force.

Figures 8-36 through 8-41 show the load-strain histories for the gages located in the hinge. All bars were subjected to reversals of tension and compression. The four internal bars yielded in tension; the front exterior bar (Figure 8-36) did not yield in tension but did yield in compression, while the back exterior bar (Figure 8-37) just reached the yield level.

8.6 Comparison of Original and Repaired Results

Figure 8-42 shows the envelopes of the lateral load-deflection curves for the original and the repaired specimens. The repair method restored and improved the strength and ductility of the specimen; however, the stiffness of the retrofitted specimen was lower, a result of loosened connections between be retrofitted steel plate and the footing. Other means of attaching the steel plates to the column, such as high strength adhesives, need to be explored. A better bond between the steel plates and the concrete most probably would have improved the stiffness of the repaired column. Another alternative would have been to attach a complete jacket around the column. When hinge retrofit is accompanied with strengthening of the footing, the horizontal segment of the steel assembly may be embedded in the reinforced concrete jacket which is placed on the top of the footing.

8.7 Concluding Remarks

Inadequate reinforcement development length in the hinge region caused a loss of strength and stiffness at a displacement ductility of 2. The proposed retrofit method improved the strength and ductility capacity of the hinge; however, an improved method is needed to attach the retrofit to a damaged column.

Chapter 9

Summary and Conclusions

9.1 Summary

This report describes an experimental and analytical investigation of one-way Freyssinet-type reinforced concrete hinges subjected to axial compression, shear, and uniaxial moment transfer in the strong direction. This type of hinge is used at the base of many highway bridges to provide a pinned detail, which is designed to release moments in the weak direction. The overall goal of this study was to develop a better understanding of the behavior of hinged columns. Attempts were made to develop recommendations for more reliable hinged column design, to conduct a preliminary study of the response of hinged columns with inadequate reinforcement development length, and to develop and test a repair method for damaged columns.

Thirty-five specimens were constructed and tested. Many variables were considered in the design, including aspect ratio, loading type (monotonic or cyclic), steel arrangement in the hinge, and hinge thickness relative to hinge width. These parameters were examined to study their effects on hinge flexural and shear strength, energy dissipation capacity, hinge shear slip, and concrete confinement in the hinge throat.

Among the thirty-five specimens were five 1/6-scale column specimens: two with an aspect ratio of one and three with an aspect ratio of two. Three types of reinforcement details were used: a bundled bar arrangement (BB specimens), a diagonal bar arrangement (DB specimens), and short dowels (the repaired specimen). All five specimens were axially-loaded to simulate dead load stress and were subjected to several cycles of lateral displacement at increasing amplitudes and ductility levels. No particular earthquake load history was simulated.

To determine the influence of hinge throat thickness on pure shear and pure axial load behavior, two other types of specimens were constructed and tested: three shear specimens, three compression specimens, and twenty-four small-scale, plain concrete hinges designed to quantify concrete confinement in the hinge. The only variable considered in these specimens was hinge thickness.

In addition to the experimental study, a linear finite element analysis was performed to study stress distribution in the hinge throat area. Analytical studies also consisted of an inelastic analysis of bridges with hinged columns. Focus was placed on the influence of deck torsional stiffness and abutment spring stiffness on inflection point height. The inflection point represents the point where the lateral load should be applied for the purpose of calculating lateral hinge strength.

A new approach was developed for estimating the lateral load strength of hinged columns. The results were evaluated based on test results reported herein and elsewhere. The new approach can be used for design purpose as well as for calculating the shear capacity for existing hinged pier columns.

9.2 Observations

The reinforced concrete analysis program *IAUNR* produced a conservative flexural hinge capacity in the strong direction when a twenty-five percent increase in specified concrete strength ($1.25f'_c$) and an ultimate concrete strain of 0.02 were used to account for concrete confinement.

Significant flexural deformations occurred in all column specimens, even in specimens with an aspect ratio of 1. Reasonable ductility was also noted.

Shear resistance was provided by friction forces only in the compression zone, and not along the entire section depth as assumed in the ACI shear friction method.

9.3 Conclusions

1) When subjected to cyclic inelastic displacements under a nearly constant axial load, columns with modified details (bundled bars and diagonal bars) displayed a hinging behavior similar to that of an unmodified column with identical dimensions and a similar reinforcement ratio.

2) For specimens with an aspect ratio of 1, the column specimen incorporating bundled bars exhibited a higher capacity for energy absorption at large displacements. The specimen with diagonal reinforcement showed a slightly lower energy absorption capacity at almost all displacements. The bundled bar detail appears to slightly improve energy characteristics where shear dominates the behavior.

3) For specimens with an aspect ratio of 2, the standard detail column (equally spaced bars) exhibited higher energy dissipation at almost all displacements.

4) A 25 percent increase in specified concrete strength ($1.25f'_c$) in the hinge region, to account for concrete confinement, was a lower-bound, conservative value.

5) The current method of analysis for determining shear capacity of the hinge, based on the shear friction theory, can lead to a false sense of conservatism. Shear friction type failure was not observed in any of the columns even when the column aspect ratio was one. The lateral strength of hinged column specimens in the strong direction was controlled by the flexural strength of the hinge.

6) The proposed method of analysis based on the compressive force path concept yielded an excellent and conservative estimate of lateral strength. The strength was provided by compression in the hinge, the magnitude of which depends on several factors, such as inflection point height, hinge width, and concrete strength.

7) For single-column bents, the inflection point may be assumed to be at the centroid of the superstructure. For multiple-column bents, the inflection point may be determined using elastic analysis, or by assuming double curvature bending using the top and bottom nominal moment capacities.

8) Under pure axial loading or under combined axial and lateral loading in the elastic range, concrete confinement decreases as hinge depth increases. There was no indication of such influence when the hinge was subjected to pure shear loading.

9) As an alternative to increasing the hinge depth to allow more rotation, the top of the footing may be sloped to maintain the desired level of confinement in the hinge throat.

10) The repair method presented in this study can restore the strength and ductility capacity of damaged hinges with inadequate reinforcement development length. The strength of the repaired column was comparable to that of a hinge with adequate development length.

References

1. AASHTO. 1989. *Standard specifications for highway bridges.* 14ed. Washington, D.C.: American Association of State Highway and Transportation Officials.

2. ACI Committee 318. 1989. *Building code requirements for reinforced concrete (ACI 318-89) and commentary ACI318R-89.* Detroit: American Concrete Institute.

3. Anderson, A. R., and S. E. Moustafa. 1970. "Ultimate strength of prestress concrete piles and columns." *ACI Journal* 68(8):620-635.

4. Ang, B. G., M. J. N. Priestley, and T. Pauley. 1985. "Seismic shear strength of circular bridge piers." *Research Report 85-5.* Christchurch, N.Z.: University of Canterbury, Department of Civil Engineering.

5. Balmer, G. G. 1949. "Shearing strength of concrete under high triaxial stresses—computation of Mohr's envelope as a curve." *Structural Research Laboratory Report No. SP-23.* Washington, D.C.: U.S. Bureau of Reclamation.

6. Base, G. D. 1959. "Some tests on a particular design of reinforced concrete structural hinge." *Technical Report TRA/325.* London: Cement and Concrete Association, London.

7. Base, G. D. 1961. "Tests on a particular design of reinforced concrete rocker bearing for motorway bridges." *Technical Report TRA/351.* London: Cement and Concrete Association.

8. Base, G. D. 1962. "Tests on a reinforced concrete hinge with a large design rotation." *Technical Report TRA/359.* London: Cement and Concrete Association.

9. Base, G. D. 1965. "Tests on four prototype reinforced concrete hinges." *Research Report No. 17.* London: Cement and Concrete Association. 1-28.

10. Buckle, I. G., et al. 1990. "Bridge structures." "Loma Prieta earthquake reconnaissance report." *Earthquake Spectra* 6(Supplement):151-187.

11. Cheok, G. S., and W. C. Stone. 1991. "Behavior of 1/6 scale model bridge columns subjected to inelastic cyclic loading." *ACI Structural Journal* 87(6):630-638.

12. Fung, G. G. et al. 1971. "Field investigation of bridge damage in the San Fernando earthquake." Sacramento: California Department of Transportation, Bridge Department.

13. Furlong, R. W. 1971. "Column slenderness and charts for design." *ACI Journal* 618(1):9-17.

14. Haroun, M. A., G. C. Pardoen, R. Shepherd, A. C. Costley, R. P. Lazanjy, and S. A. Mourad. 1991. "Strength of column piers at the base of elevated road ways." *Proceedings of the First Annual Seismic Research Workshop* Sacramento: California Department of Transportation, Division of Structures. 125-143.

15. Hognestad, E. 1951. "A study of combined bending and axial load in reinforced concrete members." *Bulletin Series No 399* Urbana: University of Illinois Engineering Experimental Station.

16. *Images-3D* 1985. Berkeley, Calif.: Celestial Software.

17 Iwasaki, T., et al. 1985. "Experimental investigation on hysteretic behavior of reinforced concrete bridge pier columns." *Proceedings of the Second US-Japan Workshop* 165-175.

18. Jiang, Y., M. Saiidi, and D. Straw. 1990. "Behavior of R/C one-way bridge pier hinges." *Proceeding of the Second Workshop on Bridge Engineering Research in Progress.* Washington, D.C.: National Science Foundation. 273-276.

19. Kotsovos, D. 1988. "Compressive force path concept: Basis for reinforced concrete ultimate limit state design." *ACI Structural Journal* 84(1):68-75.

20. Kupfer, H., H. K Hilsdorf, and H. Rusch 1969. "Behavior of concrete under biaxial stress." *ACI Journal* 66(8):656-666.

21. Lew, H. S., E. V. Leyendecker, and R. D. Dikkers. 1971. "Engineering aspects of the 1971 San Fernando earthquake." *NBS Building Science Series No 40.*

22. Lim, K. Y., and D. McLean. 1991. "Scale model studies of moment-reducing hinge details in bridge columns." *ACI Structural Journal* 88(4):465-474.

23. MacGregor, J. G., J. E. Breen, and E. O. Pfrang. 1970. "Design of slender columns." *ACI Journal* 68(1):6-28.

24. Maruama, K., H. Ramirez, and J. O. Jirsa. 1984. "Short RC columns under bilateral load histories." *[ASCE] Journal of Structural Engineering* 110(1):120-137.

25. McLean, D., and K. Y. Lim. 1989. "Plastic hinges details for the bases of architecturally oversized bridge columns." *Proceedings of the First Workshop on Bridge Engineering Research in Progress.* Washington, D.C.: National Science Foundation. 251-154.

26. Moese, J. C. "Column key design calculations." Sacramento: California Department of Transportation.

27. Nathan, N. D. 1983. "Slenderness of prestressed concrete columns." *PCI Journal*. 50-77.

28. Orie, J. L., and M. Saiidi. 1987. "A preliminary study of one-way reinforced concrete pier hinges subjected to shear and flexure." *Report No. CCEER-87-3*. Reno: University of Nevada, Department of Civil Engineering.

29. Pauley, T., and R. Park. 1975. *Reinforced concrete structures*. New York: Wiley.

30. Priestley, M., and J. Nigel. 1988. "Damage of the I-5/I-605 separator in the Whittier earthquake of October 1987." *Earthquake Spectra* 4(2):389-405.

31. Rainberg, W., and W. T. Osgood. 1943. "Description of stress-strain curves by three parameters." *NACA Technical Note No. 902*.

32. Richart, F. E., A. Brandtzaeg, and R. L. Brown. 1928. "A study of concrete under combined compressive stresses." *Bulletin Series No. 185*. Urbana: University of Illinois Engineering Experimental Station.

33. Saiidi, M., D. Bergman, and D. Straw. 1989. "Scaled model testing of bridge hinged piers subjected to lateral loads." *Proceedings of the First Workshop on Bridge Engineering Research in Progress*. Washington, D.C.: National Science Foundation. 305-308.

34. Saiidi, M., J. Hart, and B. Douglas. 1984. "Inelastic static and dynamic analysis of short R/C bridges subjected to lateral loads." *Report No. CCEER-84-03*. Reno: University of Nevada, Department of Civil Engineering.

35. Saiidi, M., R. Lawver, and J. Hart. 1984. "User's manual for ISADAB and SIBA, computer programs for nonlinear transverse analysis of highway bridges subjected to static and dynamic lateral loads." *Report No. CCEER-86-2*. Reno: University of Nevada, Department of Civil Engineering.

36. Saiidi, M., J. L. Orie, and B. Douglas. 1988. "Lateral load response of reinforced concrete bridge columns with a one-way pinned end." *ACI Structural Journal* 85(6):609-616.

37. Straw, D., and M. Saiidi. 1992. "Scaled model testing of one-way reinforced concrete pier hinges subjected to combined axial force, shear and flexure." *Report No. CCEER-92-1*. Reno: University of Nevada, Department of Civil Engineering.

38. Wood, B. R., D. Beaulieu, and P. F. Adams. 1976. "Column design by p-delta method." *[ASCE] Journal of the Structural Division* 102(ST).

Table 2-1. Specimen Concrete Unconfined Compressive Strength.

Specimen		Bundled Bar Specimens (psi)	Diagonal Bar Specimens (psi)	Retrofit Specimen (psi)	Shear Specimens (psi)	Compression Specimens (psi)	Cylinder Specimens (psi)
Column or Hinge	7 Days	2500	2450	2390	3960	3200	2020
	28 Days	4250	4030	3210	5450	4690	3630
	Day of Testing	4300	4350	4250	6080	5660	3680
Footing	7 Days	2370	2210	2230	3820	3420	
	28 Days	3980	3800	3000	5810	4880	
	Day of Testing	4050	4000	4070	6760	5840	

Table 3-1. Hinge Concrete Confined Compressive Strength.

	Hinge Width-to-Thickness Ratio							
	0.75	0.86	1.0	1.2	1.5	2.0	3.0	6.0
Confined Compressive Strength, f''_c	5350	5290	4750	4690	5840	5190	4440	4830
Unconfined Compressive Strength, f'_c	3680	3680	3680	3680	3680	3680	3680	3680
f''_c / f'_c	1.45	1.44	1.29	1.27	1.59	1.41	1.21	1.31

Table 4-1. Variation of Applied Axial Load.

	Specimen BB1C	Specimen DB1C	Specimen BB2C	Specimen DB2C
Positive-Direction Shear (kips)	28.4	23.6	13.8	11.8
Negative-Direction Shear (kips)	30.7	26.6	15.9	13.7
Difference in Shear (kips)	2.3	3.0	2.1	1.9
Difference in Moment (kip-in.)	36.8	48.0	67.2	60.8
Difference in Axial Load (kips)	12.0	14.5	21.8	18.4
Minimum Axial Load (kips)	20.0	18.7	15.1	16.8
Maximum Axial Load (kips)	32.0	33.3	36.9	35.2

Table 4-2. Maximum Slips.

Direction	Specimen BB1C	Specimen DB1C	Specimen SD1C	Specimen BB2C	Specimen DB2C	Specimen SD2C
Positive (in.)	0.197	0.175	0.220	0.046	0.052	0.078
Negative (in.)	0.411	0.104	0.250	0.085	0.073	0.122
Average (in)	0.304	0.140	0.240	0.066	0.063	0.100

Table 6-1. Comparison of Lateral Load Capacities.

	Specimen											
	CH1 (kips)	CH2 (kips)	CH3 (kips)	CH4 (kips)	SD1M (kips)	SD1C (kips)	JB1C (kips)	DB1C (kips)	SD2M (kips)	SD2C (kips)	BB2C (kips)	DB2C (kips)
Shear Friction Method (SFM)	12.9	12.9	12.9	12.9	65.6	65.6	65.6	57.9	65.6	65.6	65.6	57.9
Compressive Force Path Method (CFPM), using f'_c	1.93	2.35	5.58	1.90	22.4	22.0	21.8	21.4	12.0	11.5	11.4	11.2
Compressive Force Path Method (CFPM), using $1.25f'_c$	1.96	2.90	5.72	1.94	23.8	23.4	23.2	22.9	12.6	12.2	12.1	11.9
Measured	2.57	3.33	6.90	1.87	25.3	28.7	29.6	25.1	13.4	14.9	14.9	13.0
Measured / SFM	0.2	0.26	0.53	0.15	0.39	0.44	0.45	0.43	0.20	0.23	0.22	0.22
Measured / CFPM (f'_c)	1.33	1.17	1.24	0.98	1.13	1.30	1.36	1.17	1.11	1.30	1.31	1.16
Measured / CFPM ($1.25f'_c$)	1.31	1.15	1.21	0.96	1.06	1.22	1.28	1.10	1.06	1.22	1.23	1.09

Table 6-2. Effects of Approximating γ on Calculated Lateral Load Capacity.

	Specimen											
	CH1	CH2	CH3	CH4	SD1M	SD1C	BB1C	DB1C	SD2M	SD2C	BB2C	DB2C
Measured Lateral Load Capacity (kips)	2.57	3.33	6.90	1.87	25.3	28.7	29.6	25.1	13.4	14.9	14.9	13.0
Exact, γ_e	1.96	2.90	5.74	1.94	24.4	24.0	23.8	23.5	12.7	12.3	12.2	12.0
Approximate, γ_a	1.96	2.90	5.72	1.94	23.8	23.4	23.2	22.9	12.6	12.2	12.1	11.9
γ_a / γ_e	1.00	1.00	1.00	1.00	0.98	0.98	0.97	0.97	0.99	0.99	0.99	0.99

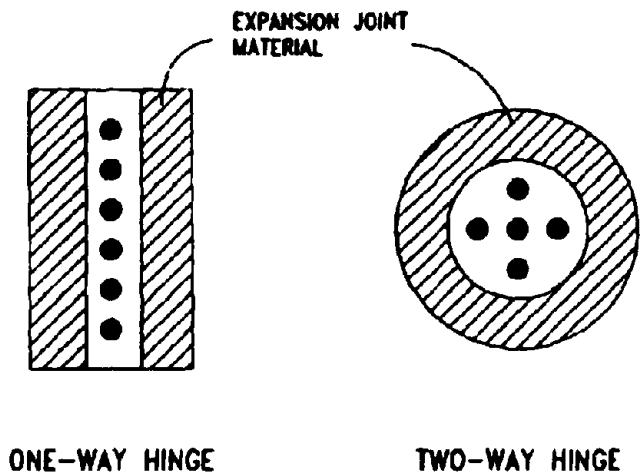

Figure 1-1. Typical Reinforced Concrete Hinge.

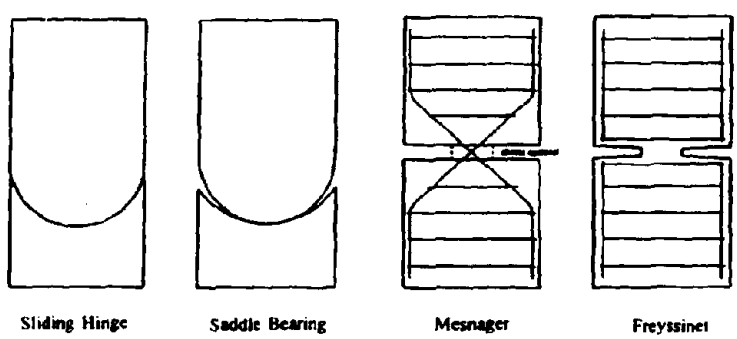

Figure 1-2. Types of Concrete Hinges (after Ref. 9).

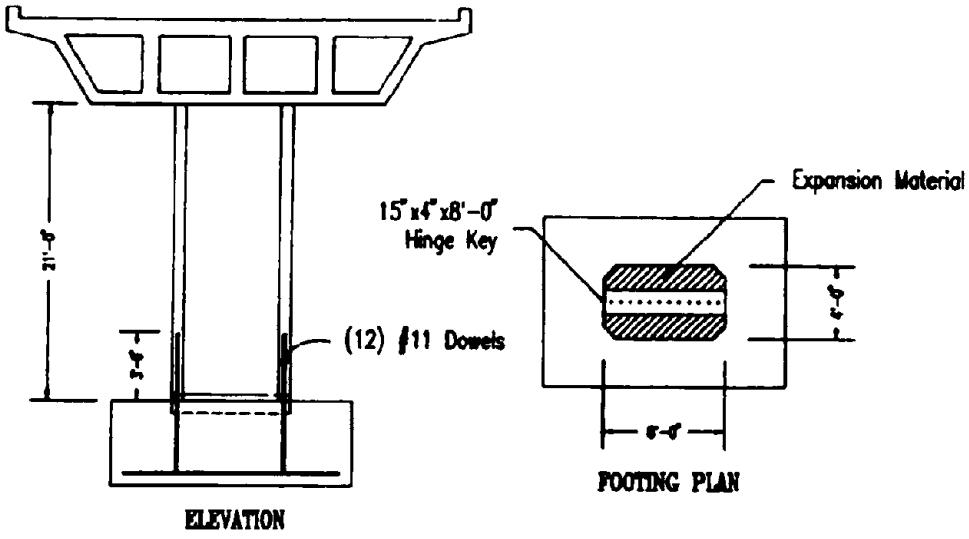

Figure 1-3. Rose Creek Bridge Bent Elevation and Hinge Cross Section.

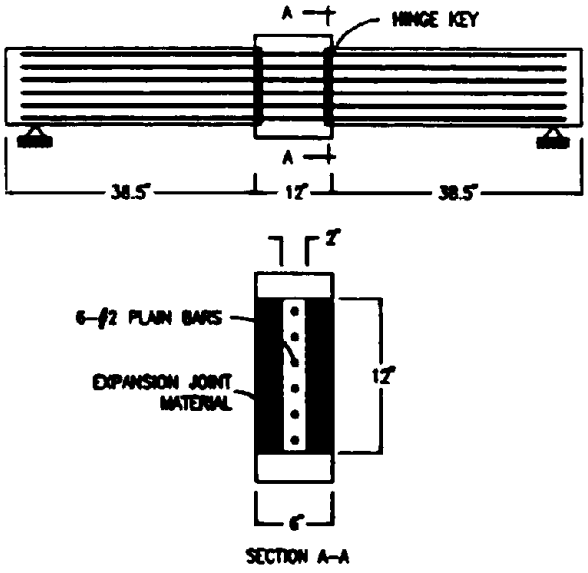

Figure 1-4. 1/8-Scale Specimen Details (after Ref. 28).

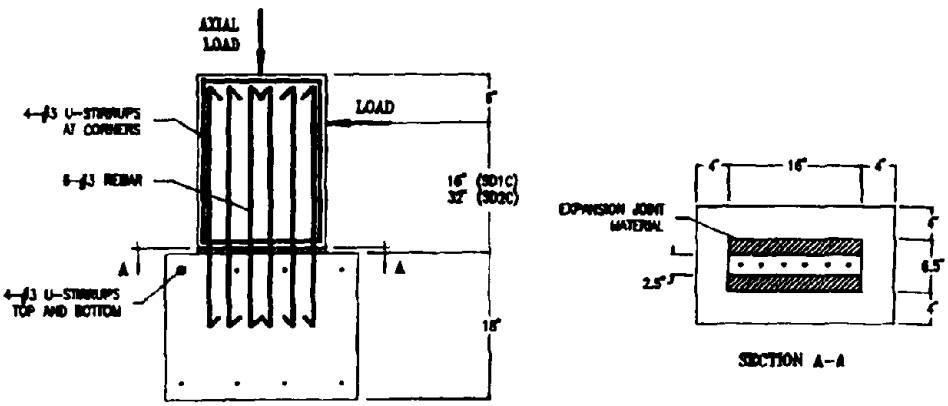

Figure 1-5. SD Specimen Details (after Ref. 37).

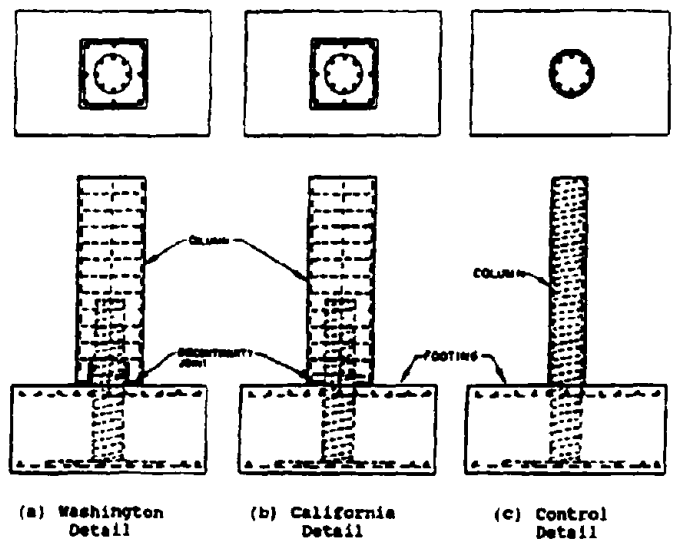

Figure 1-6. Comparison of Hinge Details (after Ref. 22).

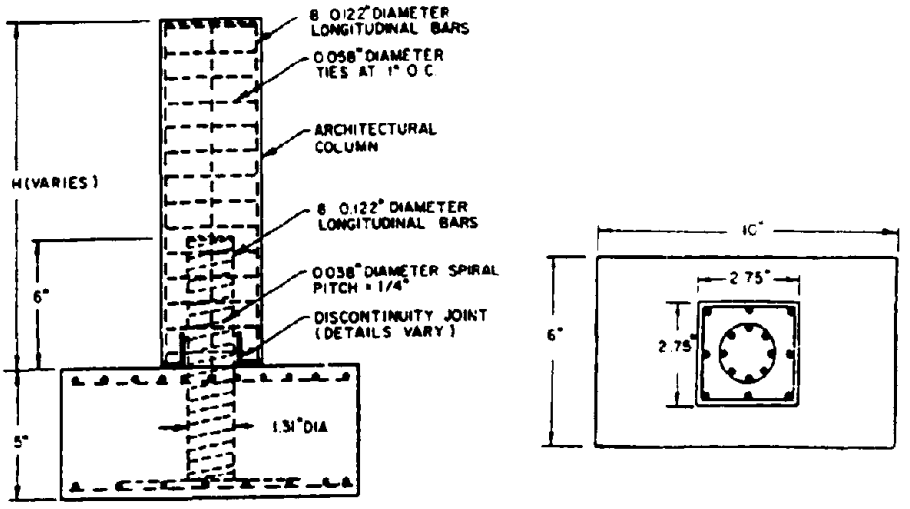

Figure 1-7. 1/20-Scale Specimen Details (after Ref. 22).

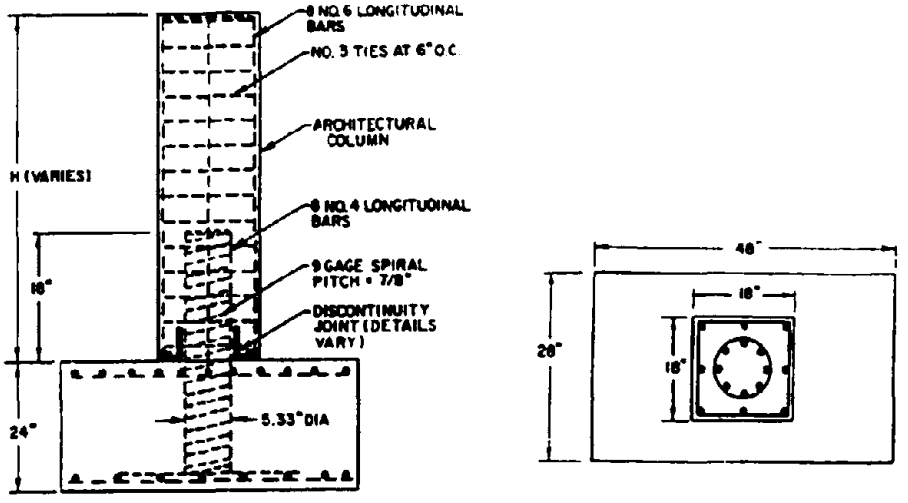

Figure 1-8. 1/5-Scale Specimen Details (after Ref. 22).

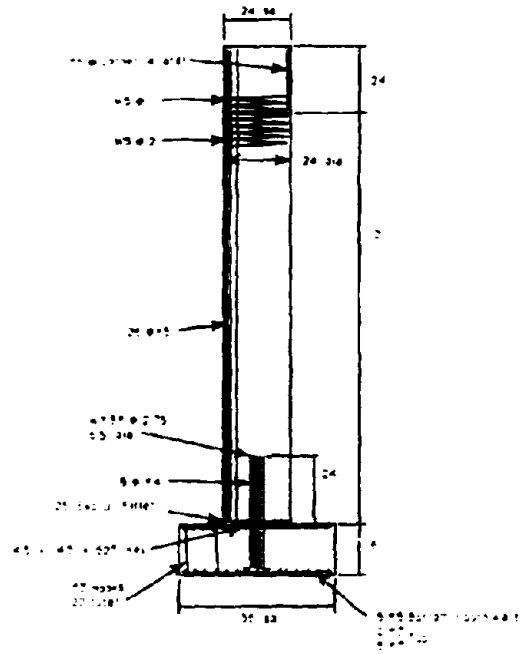

Figure 1-9. 2/5-Scale Specimen Details (after Ref. 14).

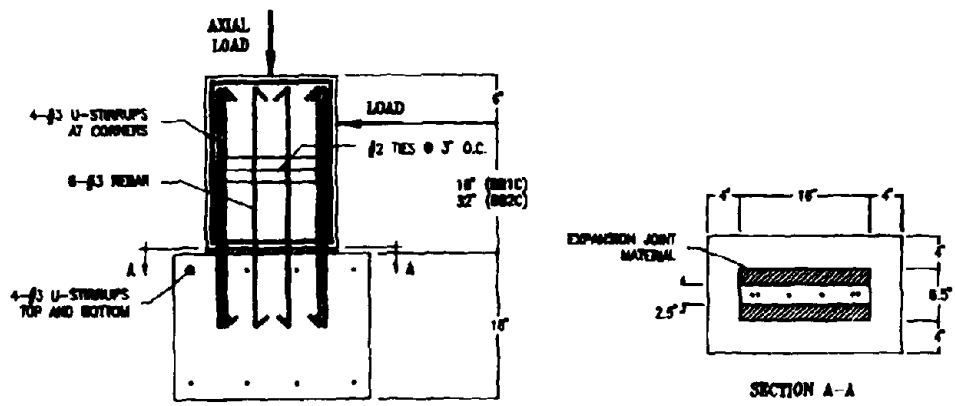

Figure 2-1. BB1C and BB2C Specimen Details.

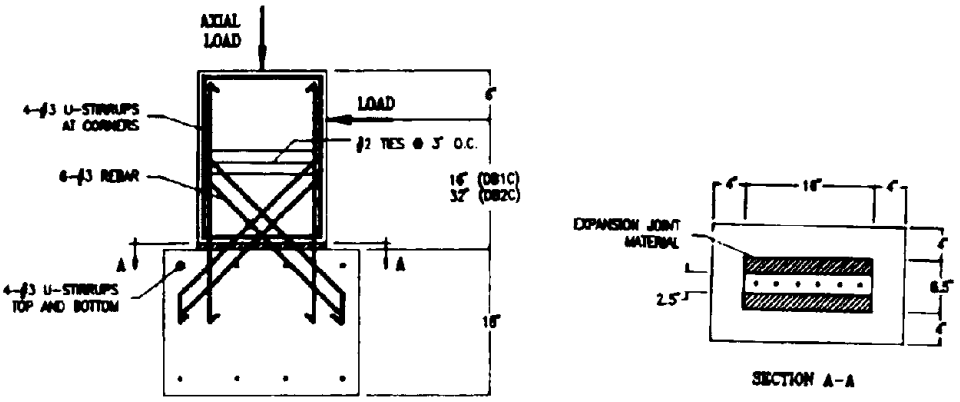

Figure 2-2. DB1C and DB2C Specimen Details.

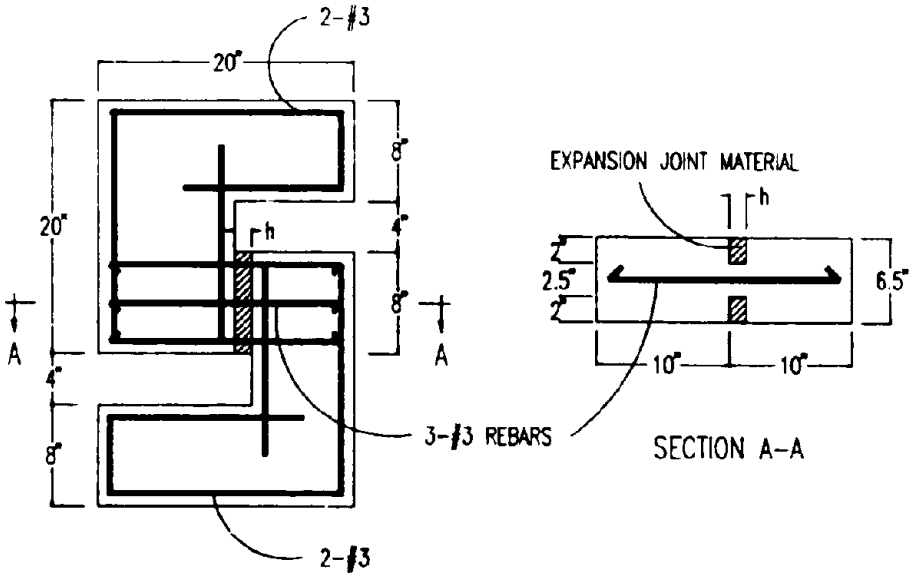

Figure 2-3. Shear Specimen Details.

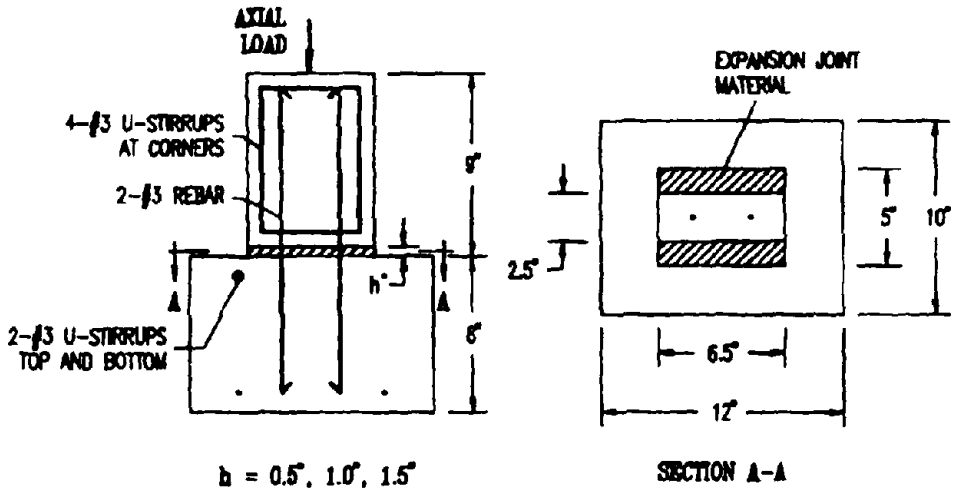

Figure 2-4. Compression Specimen Details.

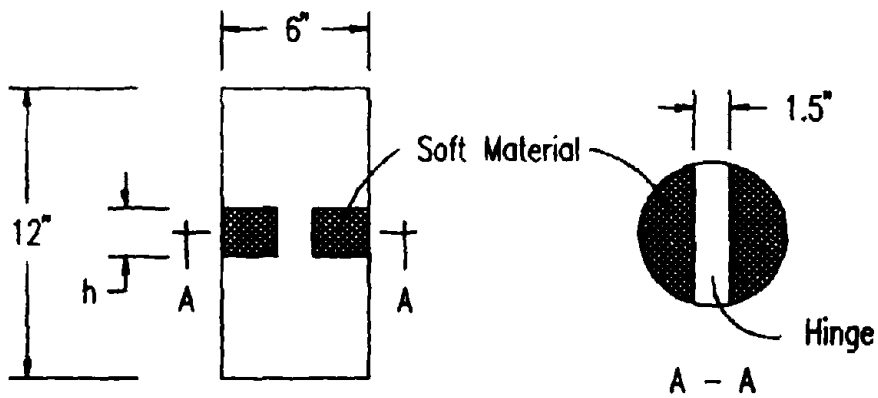

h = 0.25", 0.50", 0.75", 1.00"
1.25", 1.50", 1.75", 2.00"

Figure 2-5. Plain Concrete Hinged Specimen Details.

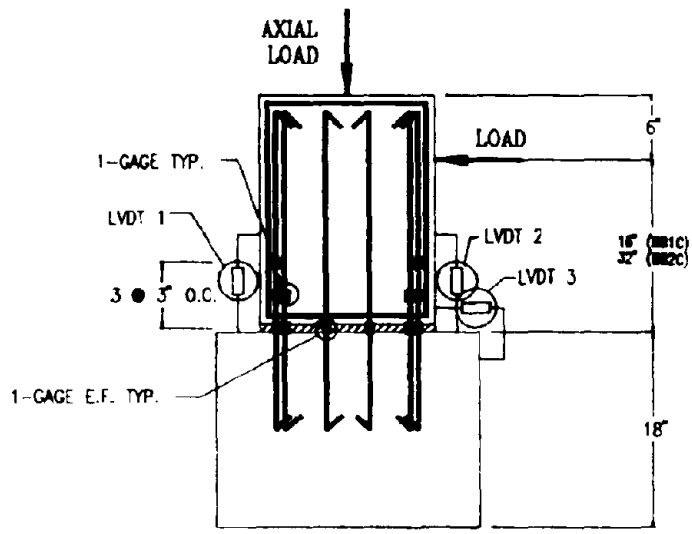

Figure 2-6. Specimens BB1C and BB2C Instrumentation Details.

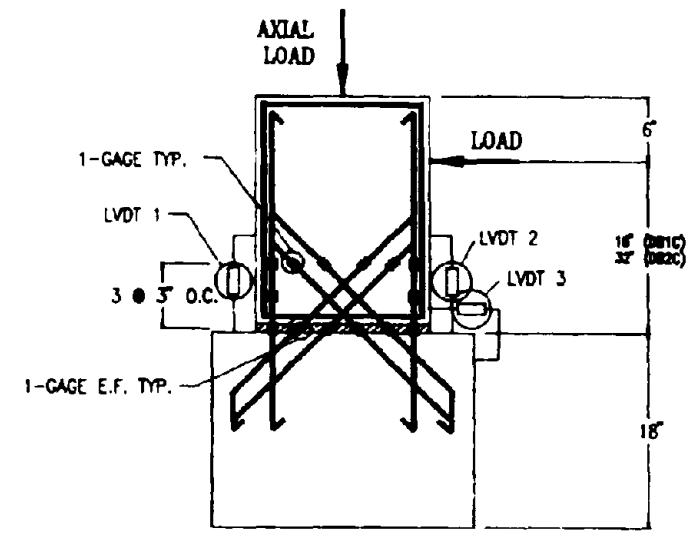

Figure 2-7. Specimens DB1C and DB2C Instrumentation Details.

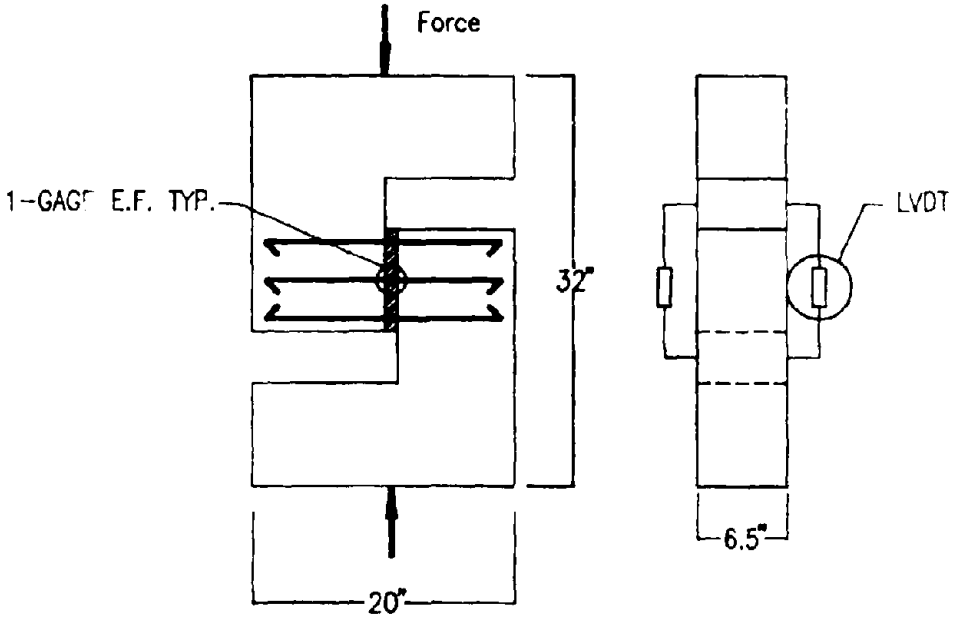

Figure 2-8. Shear Specimen Instrumentation Details.

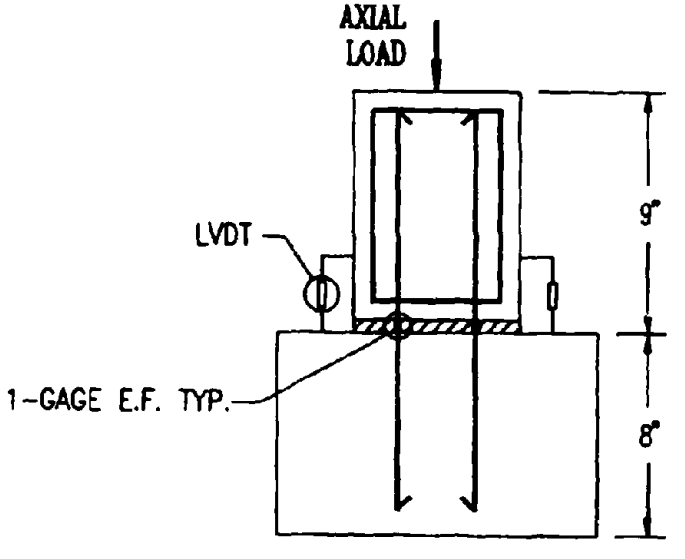

Figure 2-9. Compression Specimen Instrumentation Details.

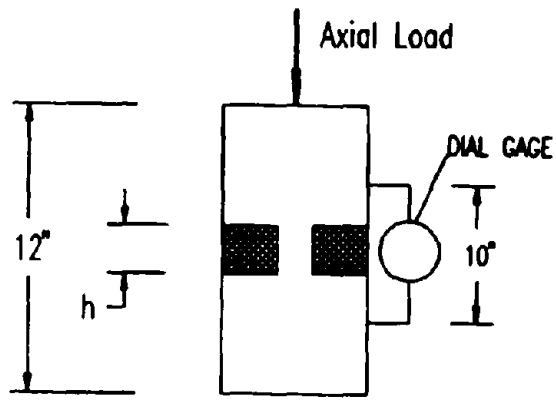

Figure 2-10. Plain Concrete Hinged Specimen Instrumentation Details.

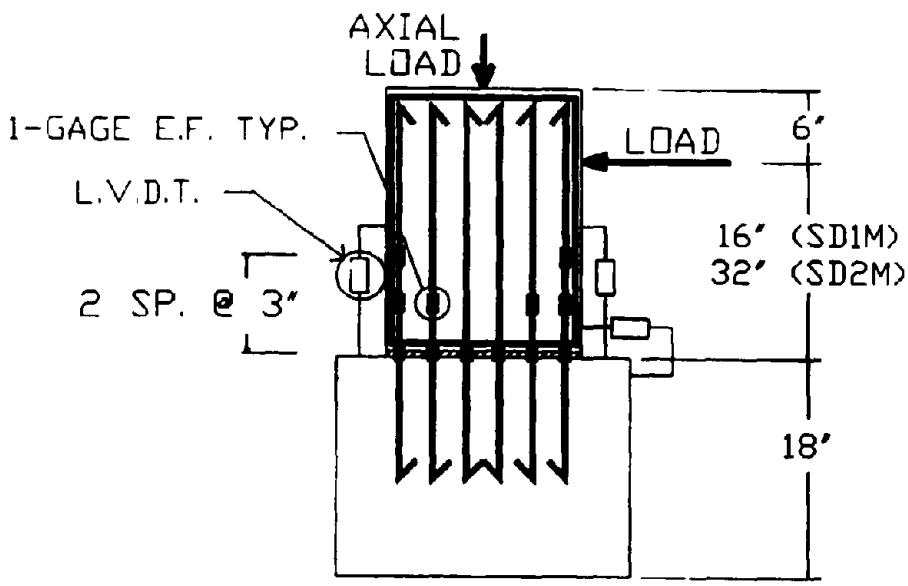

Figure 2-11. SD1C and SD2C Instrumentation Details.

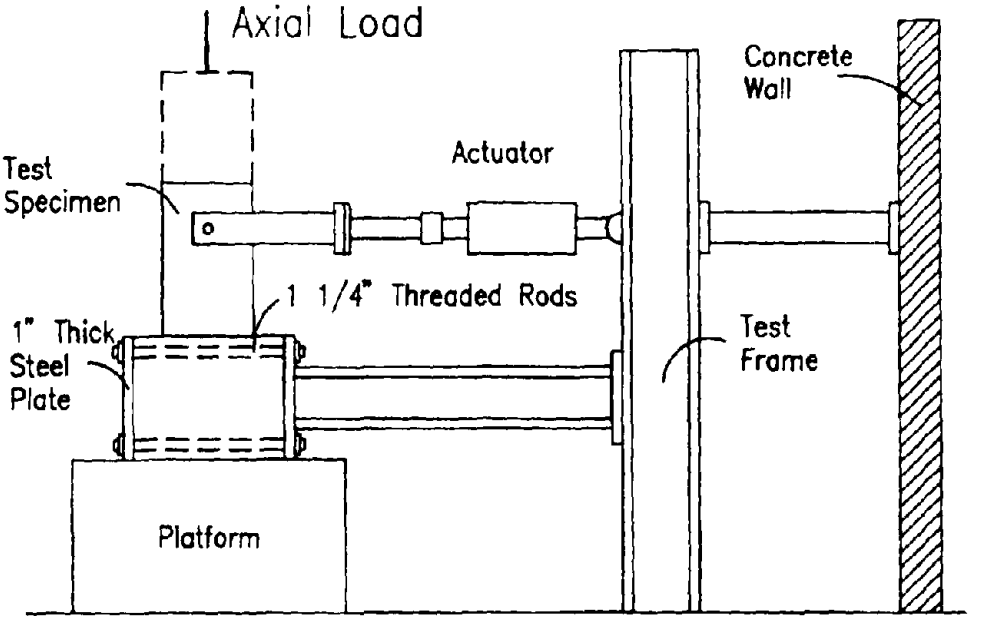

Figure 2-12. Test Frame Setup.

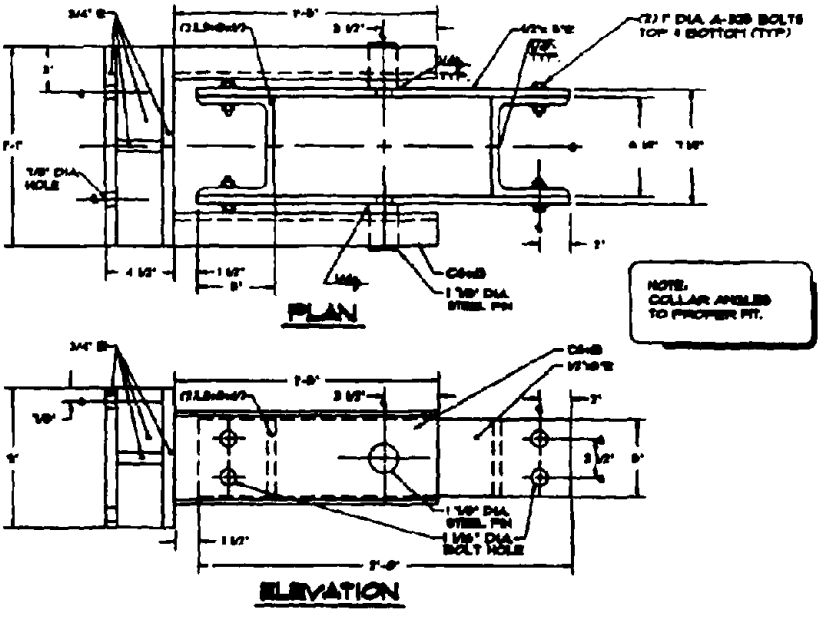

Figure 2-13. Hydraulic Ram Collar (after Ref. 23).

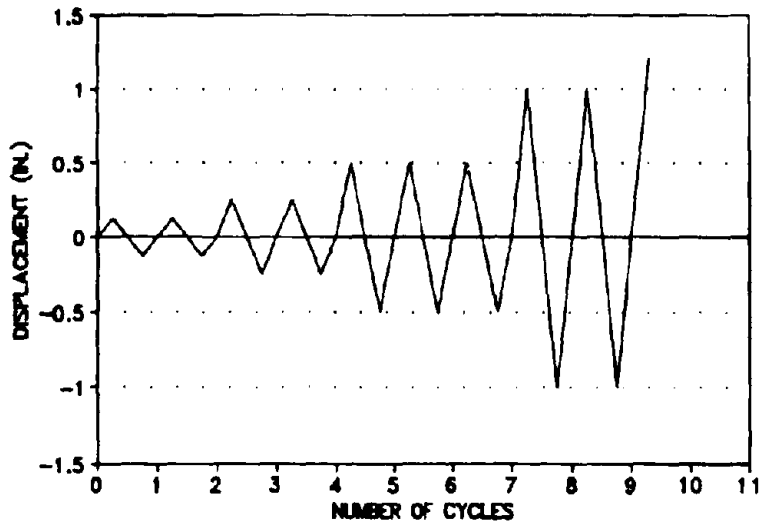

Figure 2-14. BB1C and DB1C Lateral Displacement History.

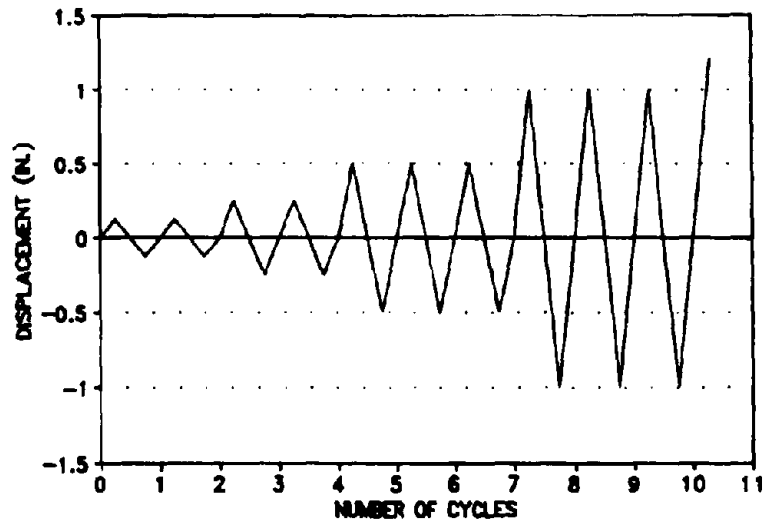

Figure 2-15. BB2C and DB2C Lateral Displacement History.

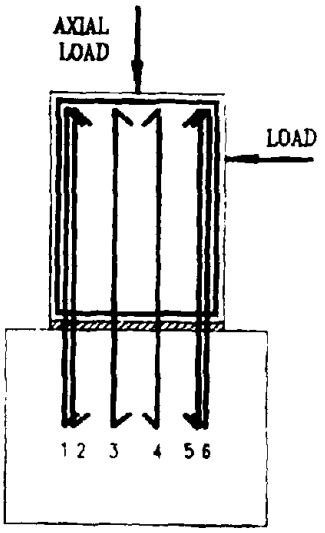

Figure 3-1. BB1C and BB2C Bar Numbering.

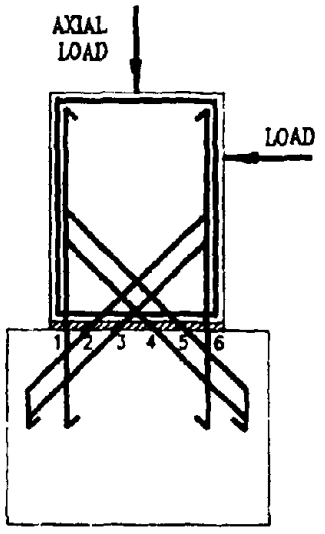

Figure 3-2. DB1C and DB2C Bar Numbering.

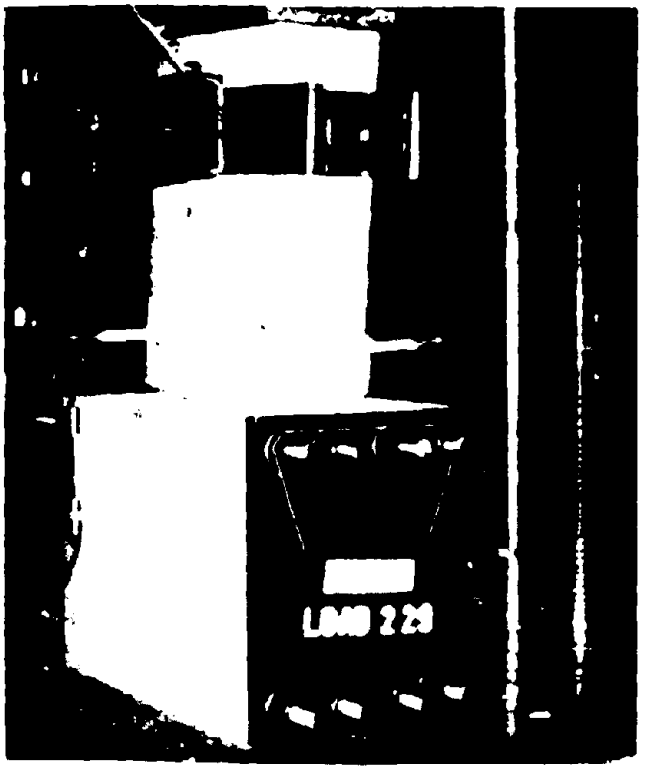

Figure 3-3. BB1C Front Elevation after Testing.

Figure 3-4. BB1C after Testing.

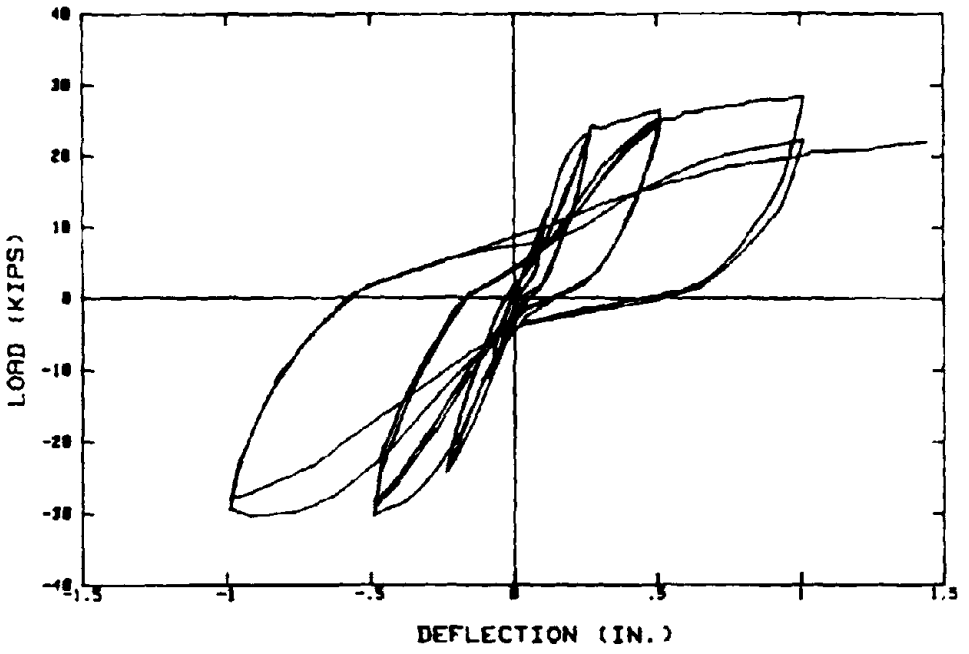

Figure 3-5. BB1C Load-Deflection Response.

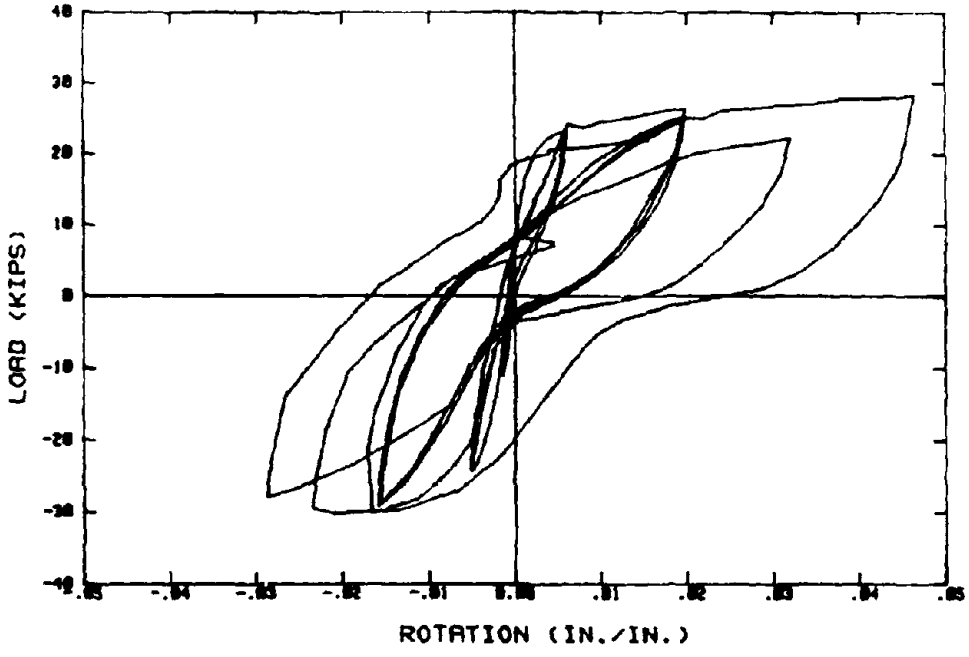

Figure 3-6. BB1C Load-Rotation Response.

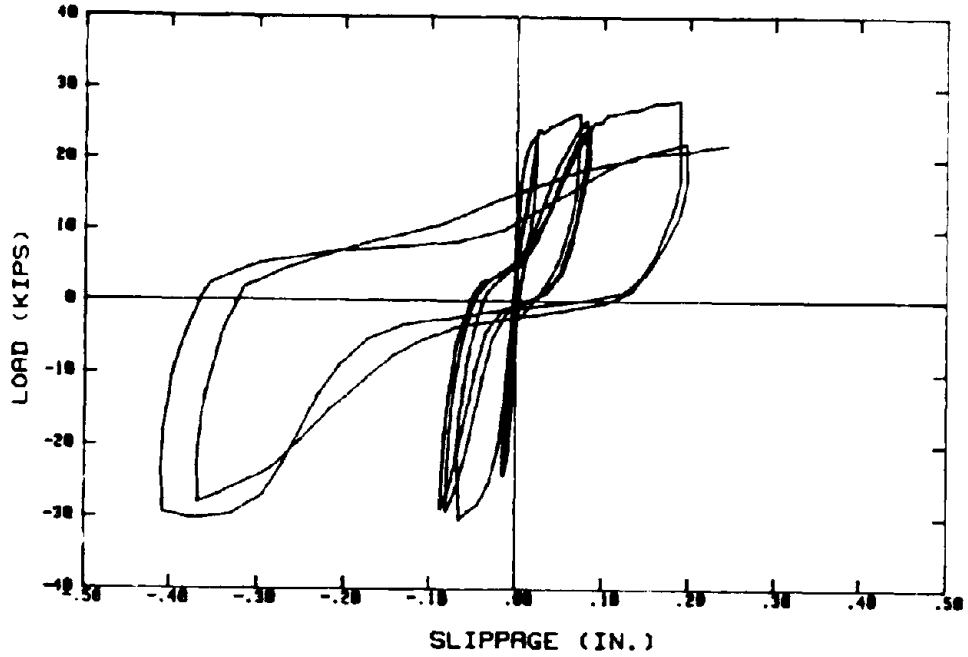

Figure 3-7. BB1C Load-Slippage Response.

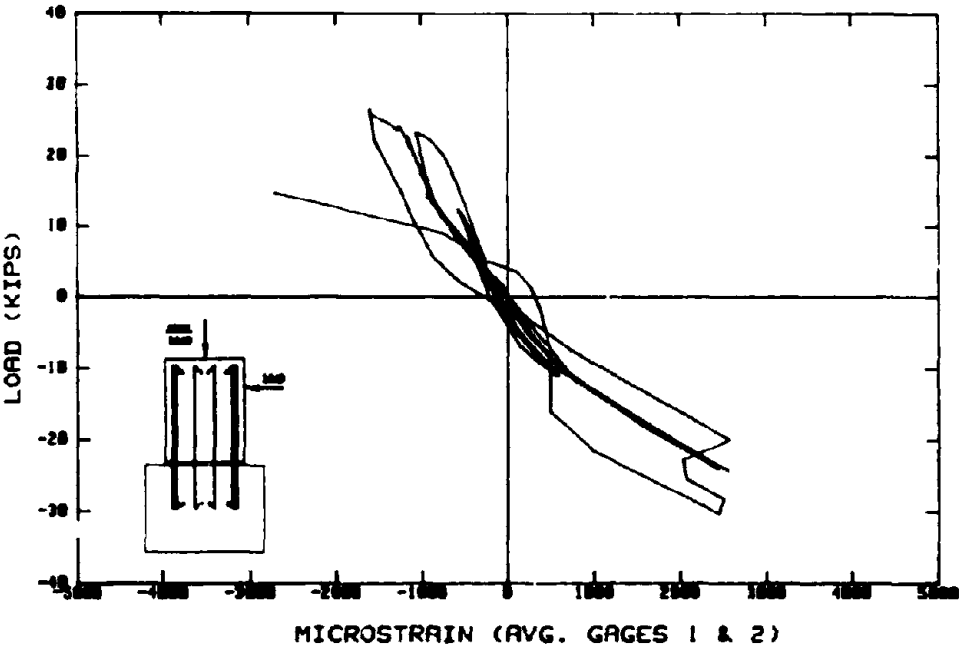

Figure 3-8. BB1C Load-Strain Response (Average of Gages 1 & 2).

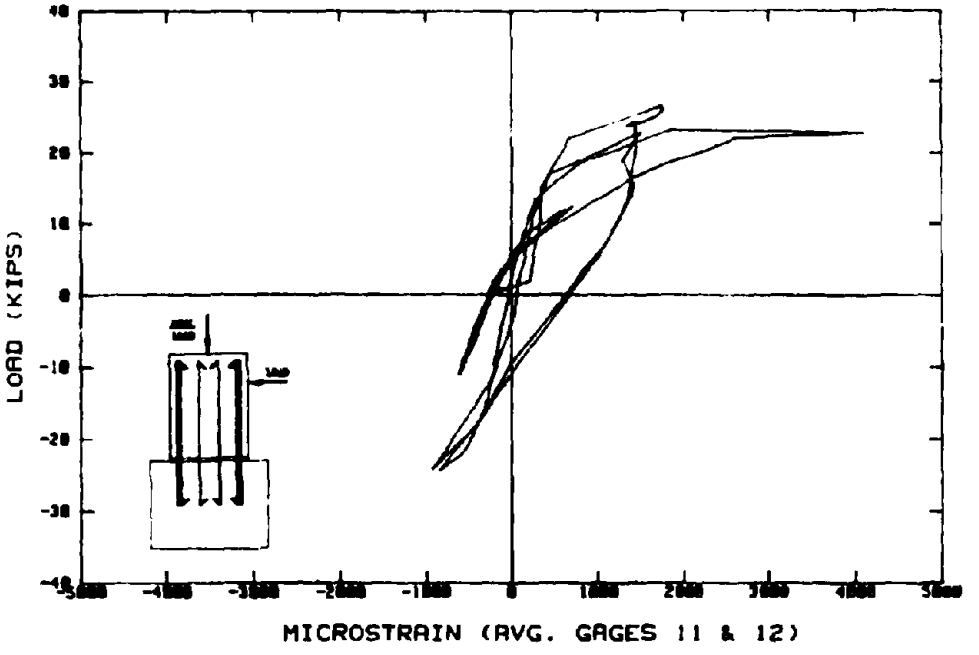

Figure 3-9. BB1C Load-Strain Response (Average of Gages 11 & 12).

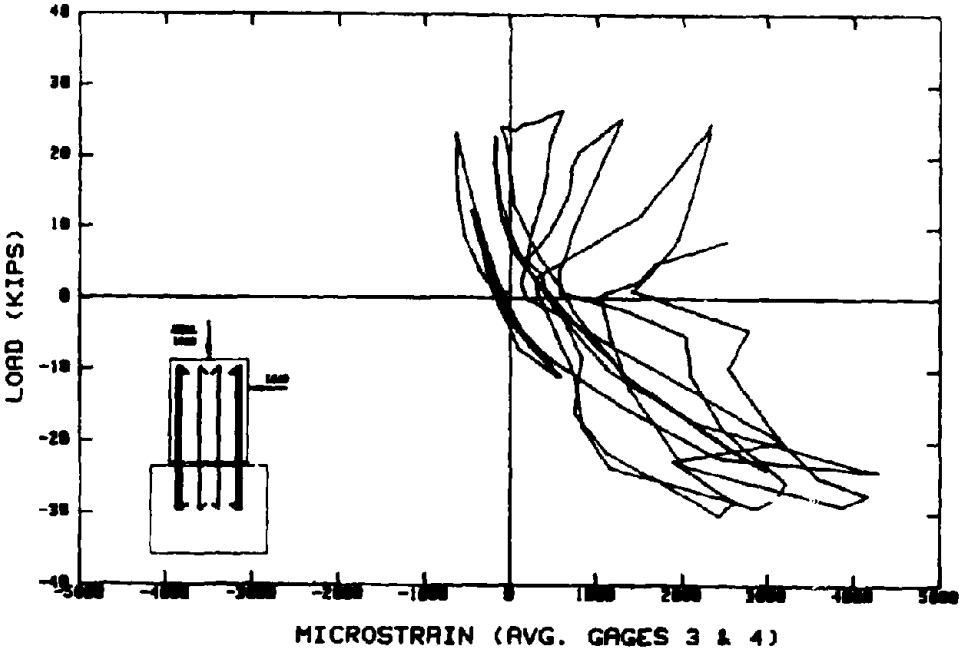

Figure 3-10. BB1C Load-Strain Response (Average of Gages 3 & 4).

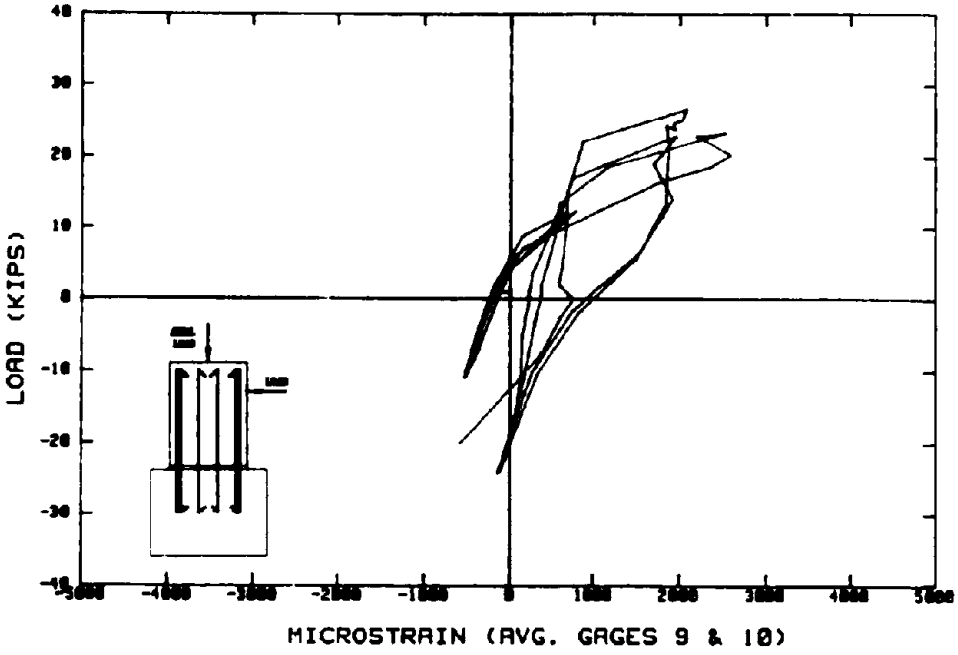

Figure 3-11. BB1C Load-Strain Response (Average of Gages 9 & 10).

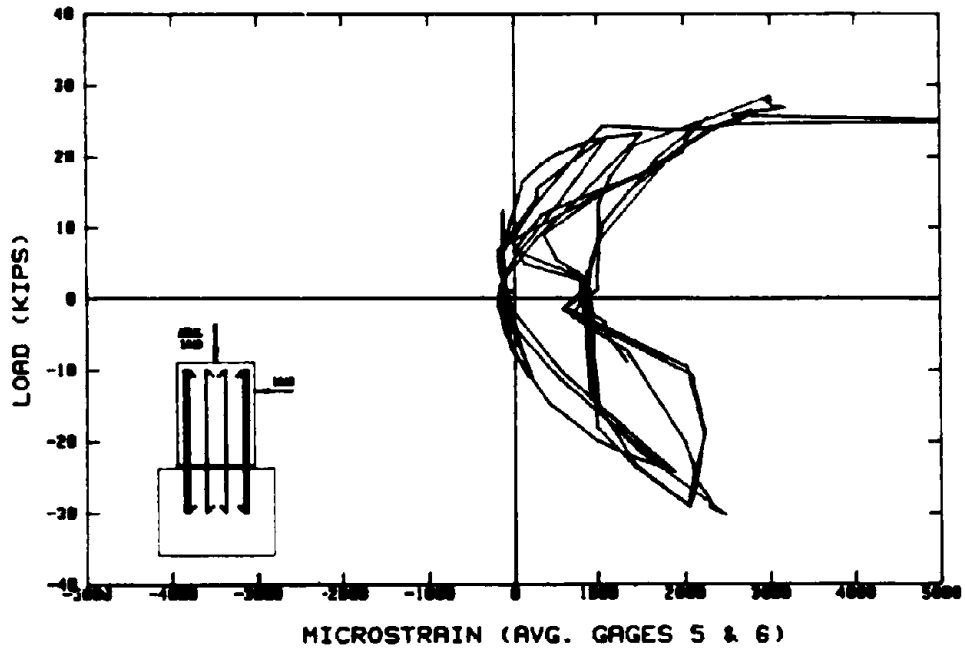

Figure 3-12. BB1C Load-Strain Response (Average of Gages 5 & 6).

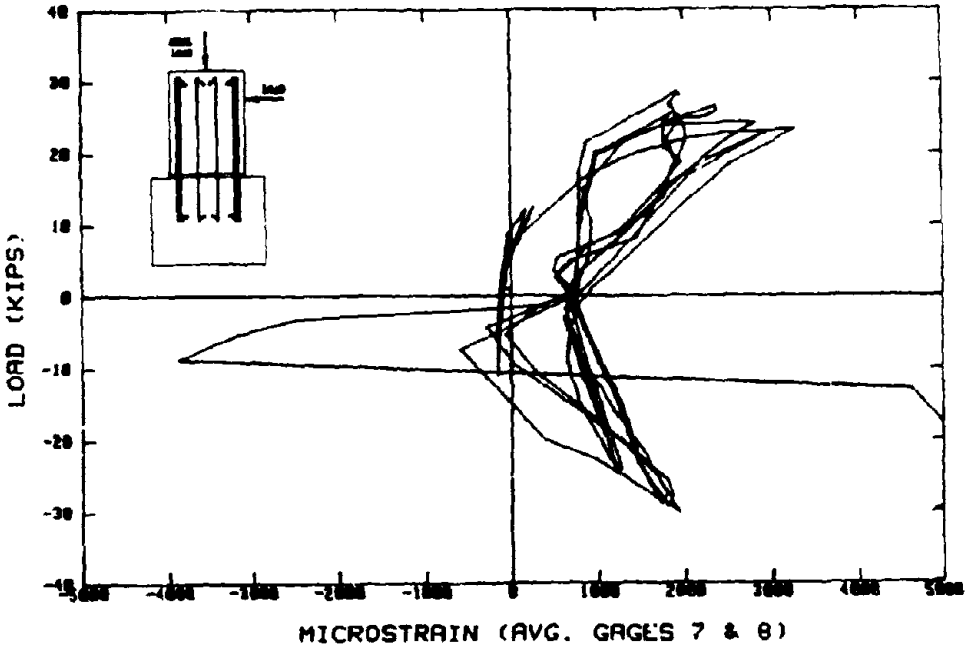

Figure 3-13. BB1C Load-Strain Response (Average of Gages 7 & 8).

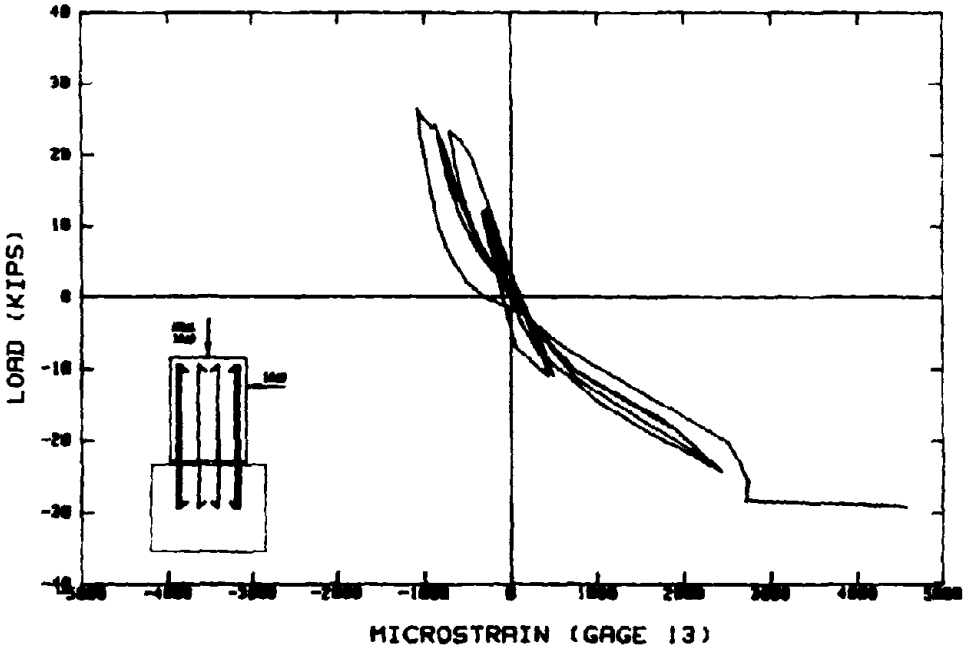

Figure 3-14. BB1C Load-Strain Response (Gage 13).

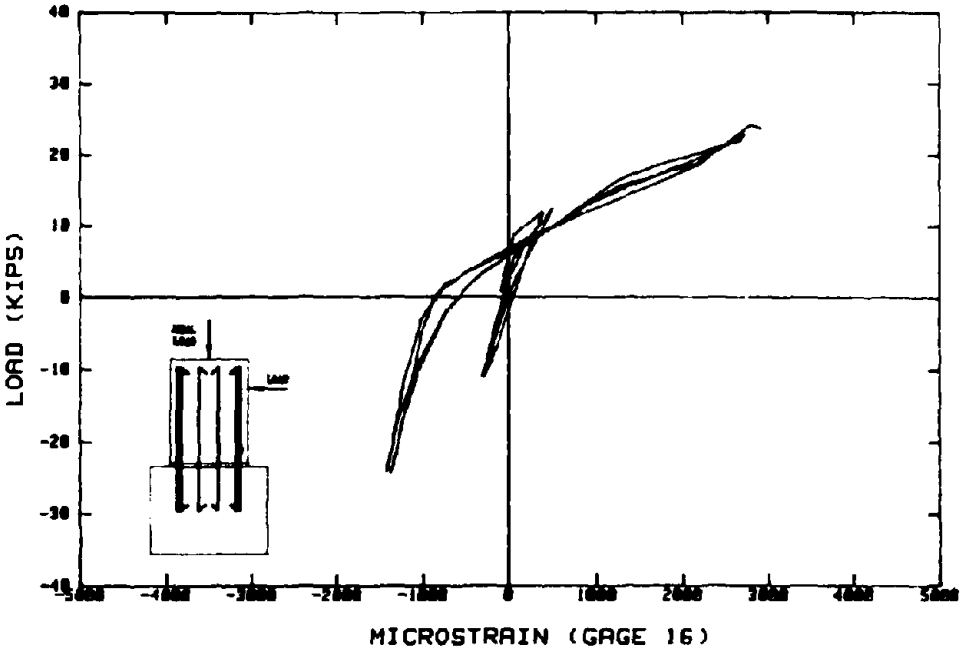

Figure 3-15. BB1C Load-Strain Response (Gage 16).

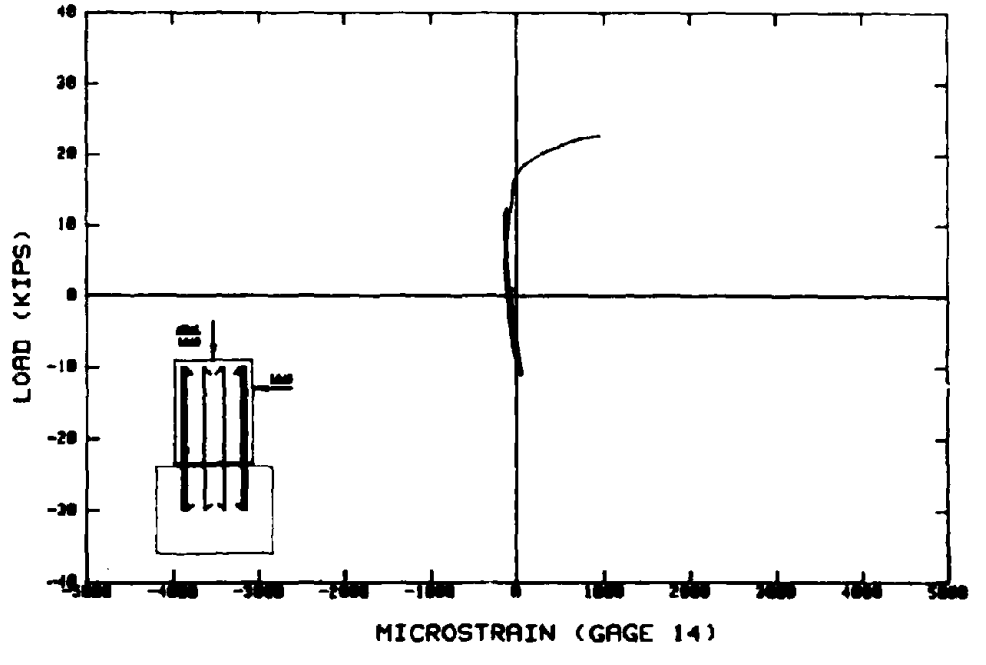

Figure 3-16. BB1C Load-Strain Response (Gage 14).

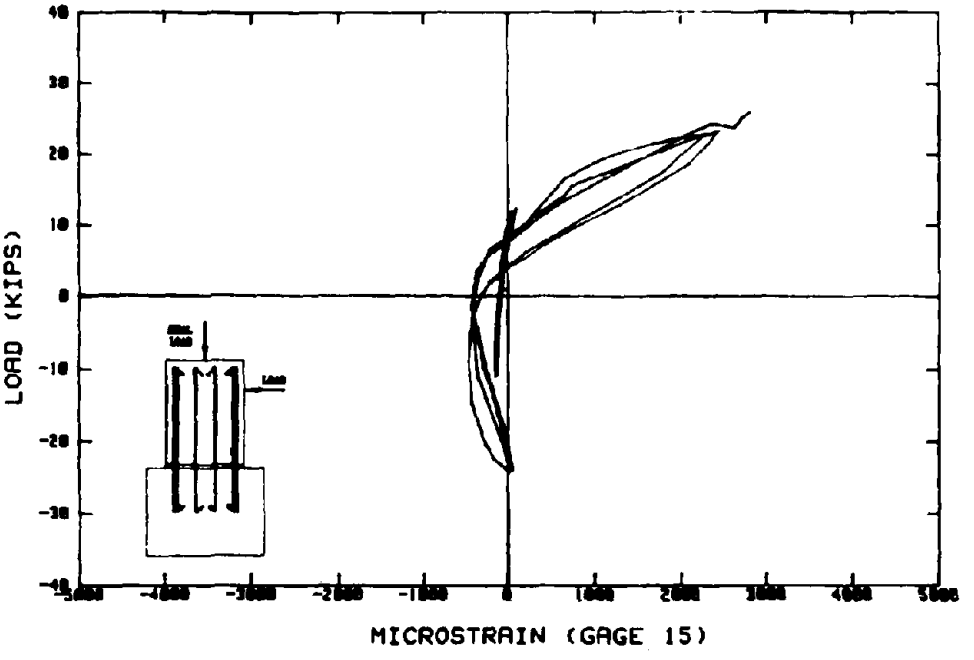

Figure 3-17. BB1C Load-Strain Response (Gage 15).

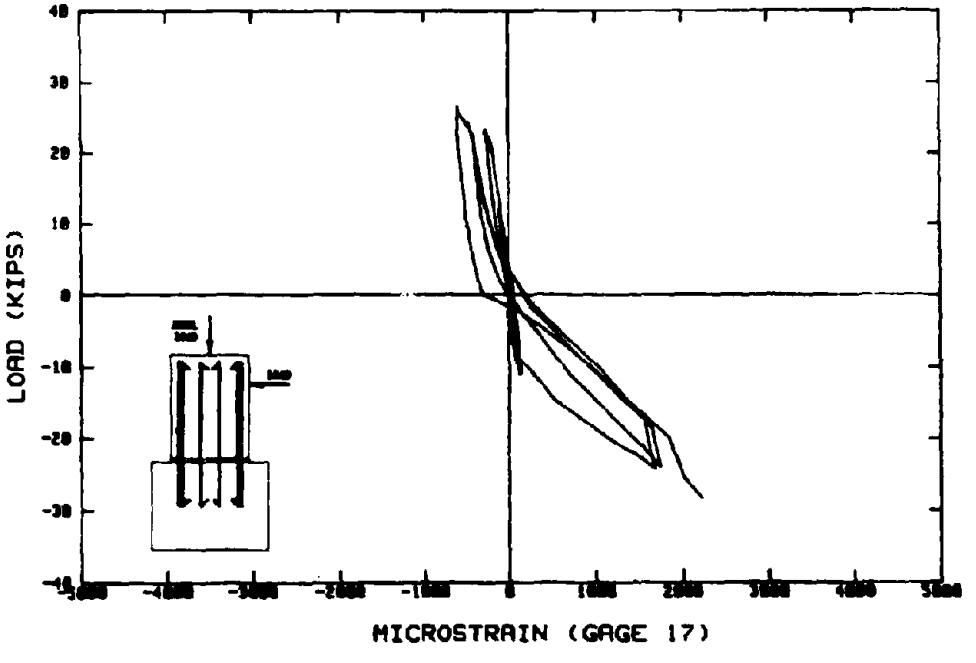

Figure 3-18. BB1C Load-Strain Response (Gage 17).

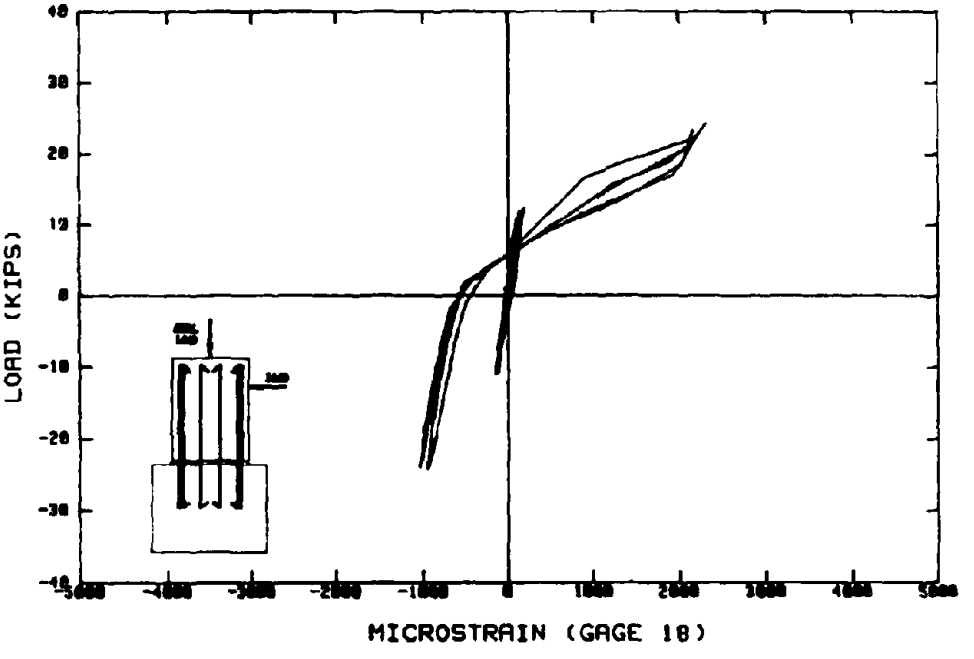

Figure 3-19. BB1C Load-Strain Response (Gage 18).

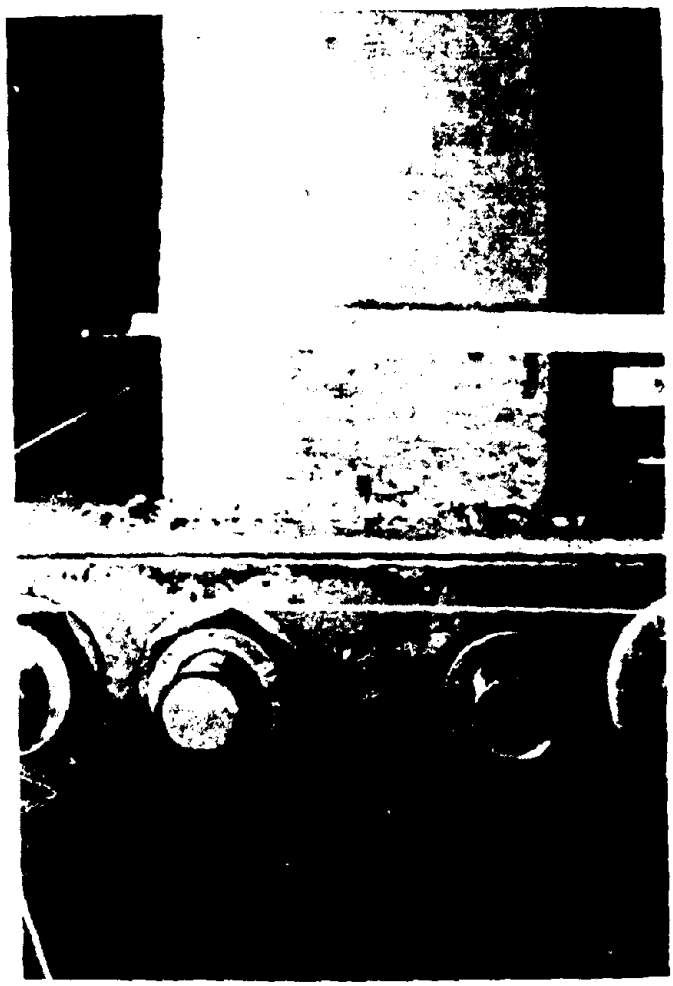

Figure 3-20. BB2C Front Elevation after Testing.

Figure 3-21. BB2C after Testing.

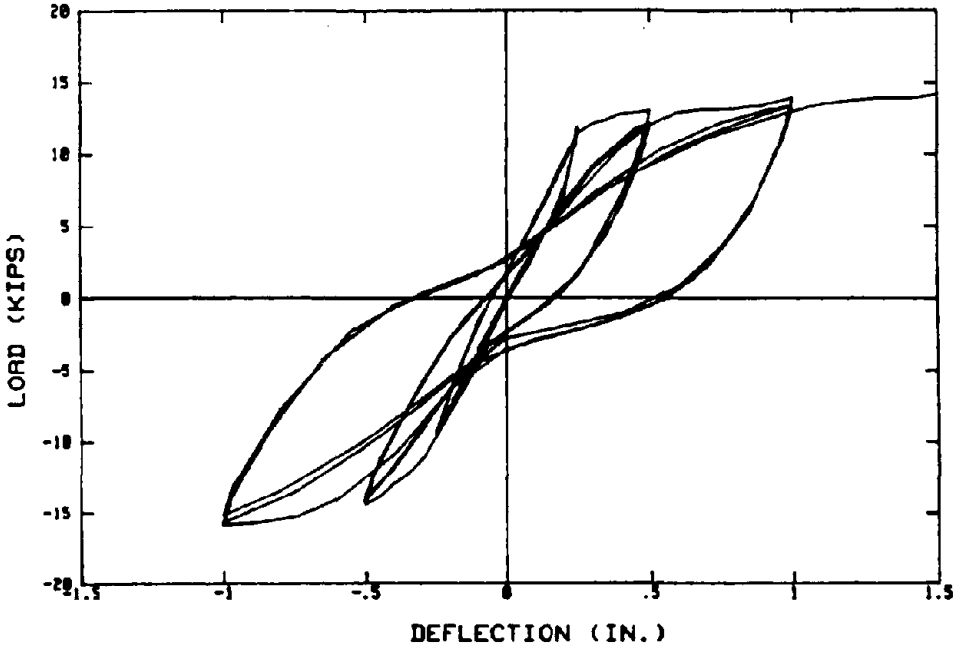

Figure 3-22. BB2C Load-Deflection Response.

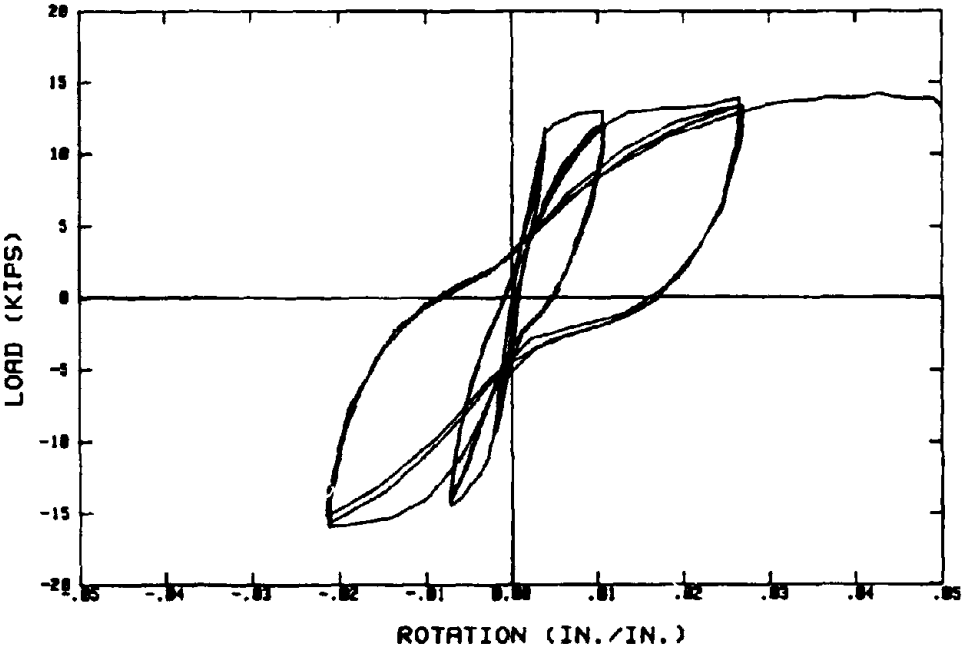

Figure 3-23. BB2C Load-Rotation Response.

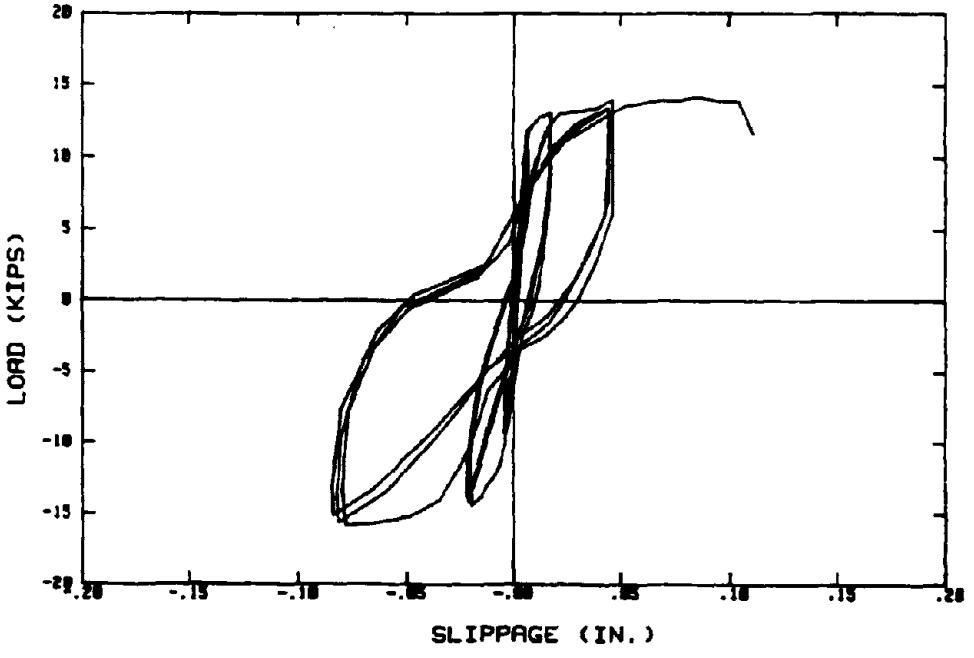

Figure 3-24. BB2C Load-Slippage Response.

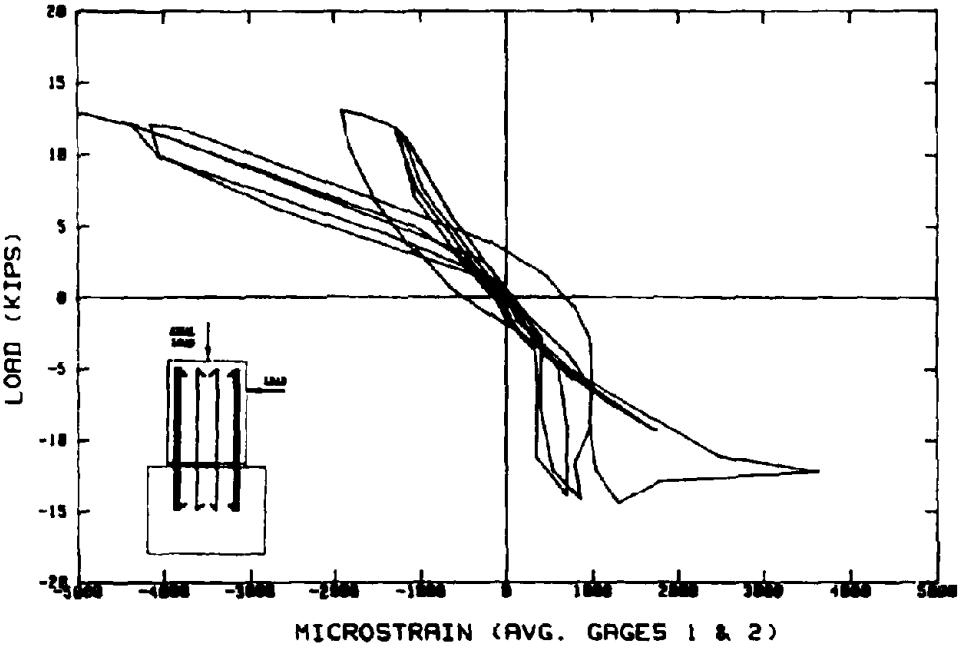

Figure 3-25. BB2C Load-Strain Response (Average of Gages 1 & 2).

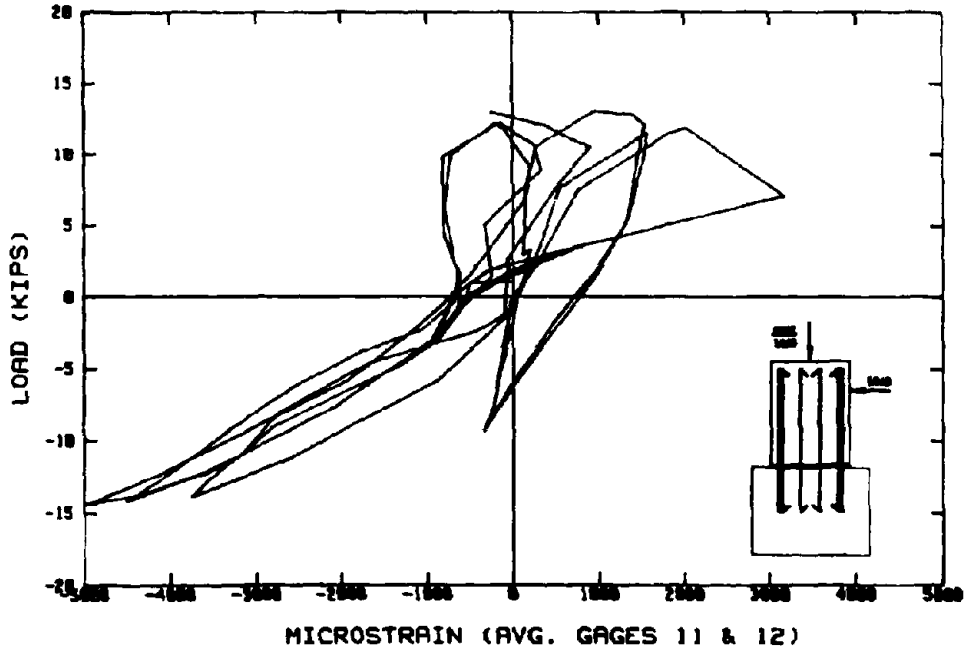

Figure 3-26. BB2C Load-Strain Response (Average of Gages 11 & 12).

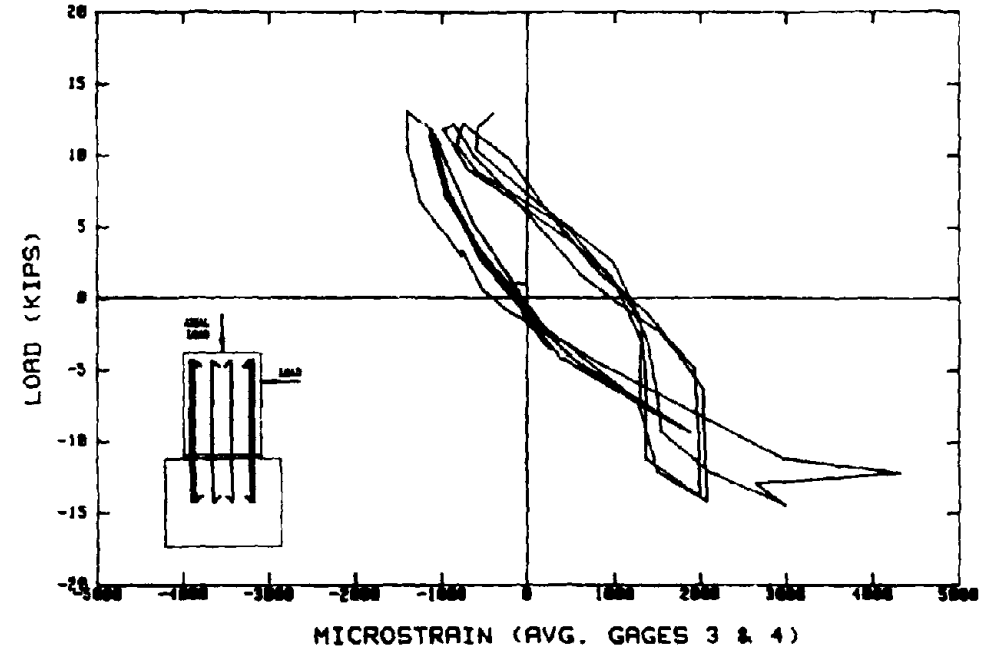

Figure 3-27. BB2C Load-Strain Response (Average of Gages 3 & 4).

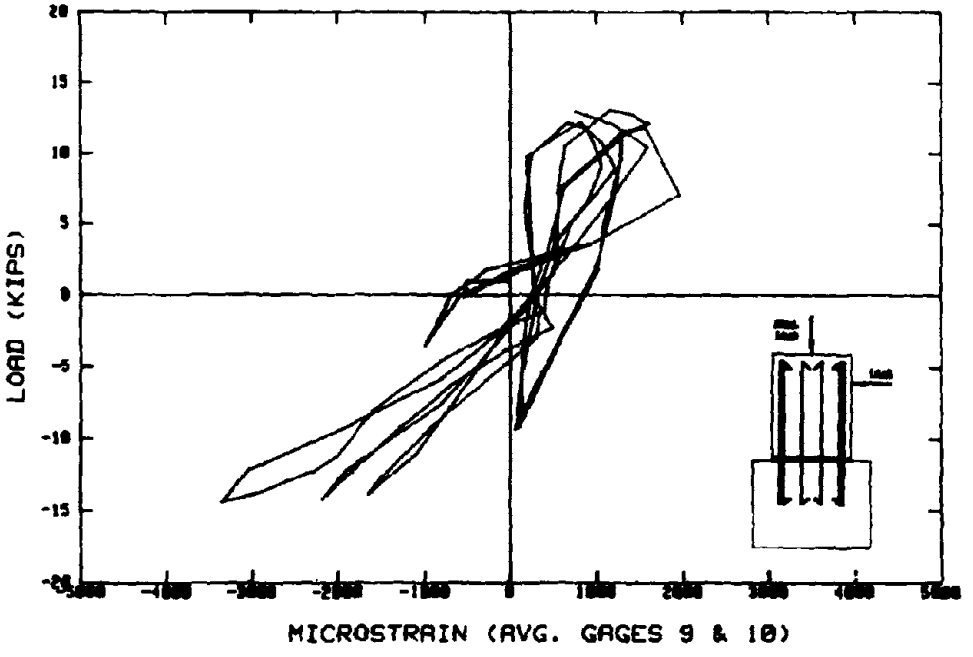

Figure 3-28. BB2C Load-Strain Response (Average of Gages 9 & 10).

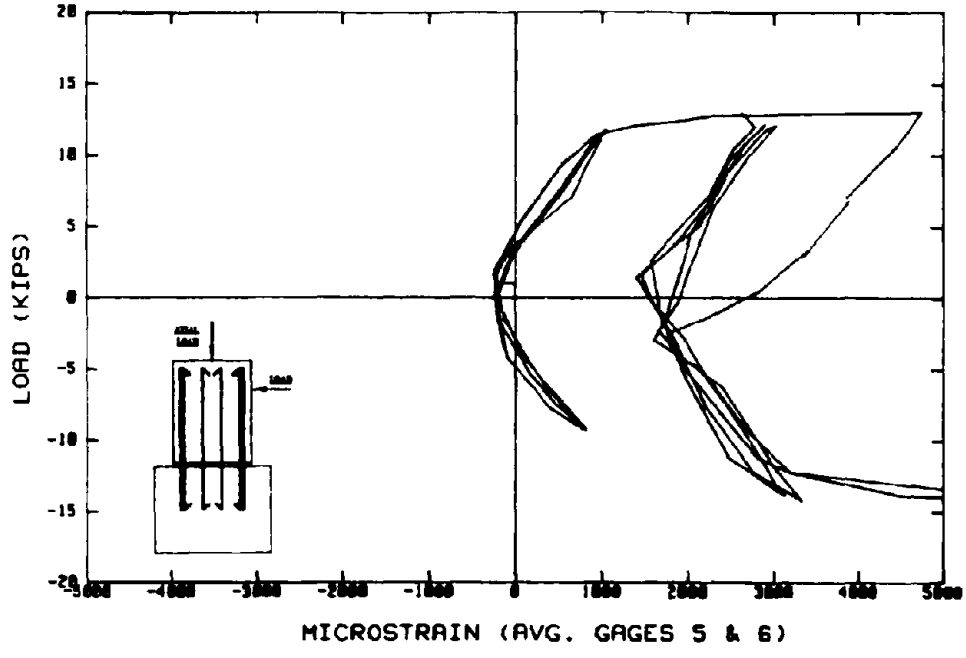

Figure 3-29. BB2C Load-Strain Response (Average of Gages 5 & 6).

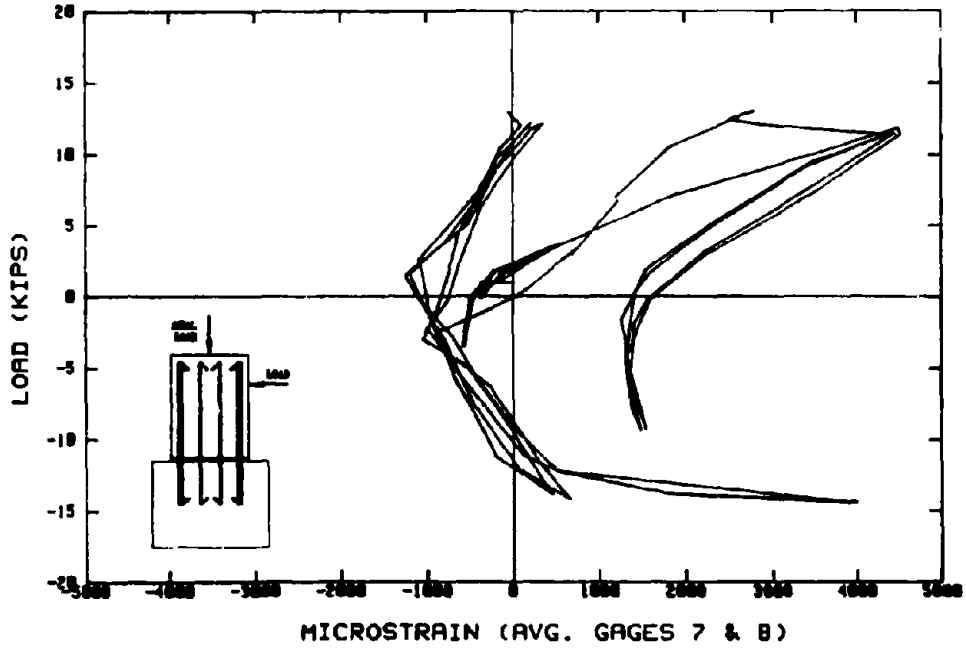

Figure 3-30. BB2C Load-Strain Response (Average of Gages 7 & 8).

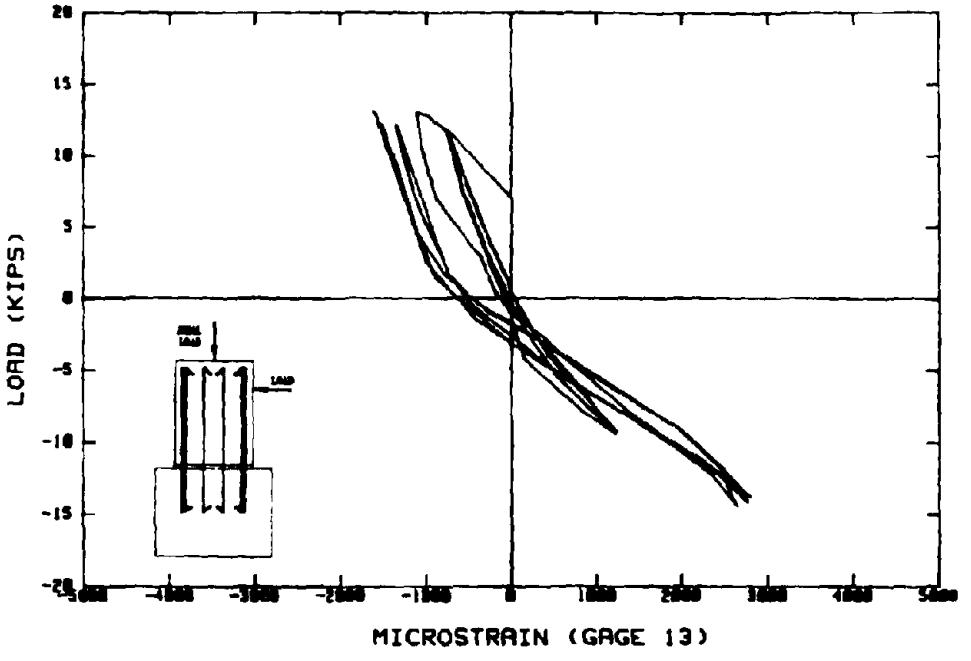

Figure 3-31. BB2C Load-Strain Response (Gage 13).

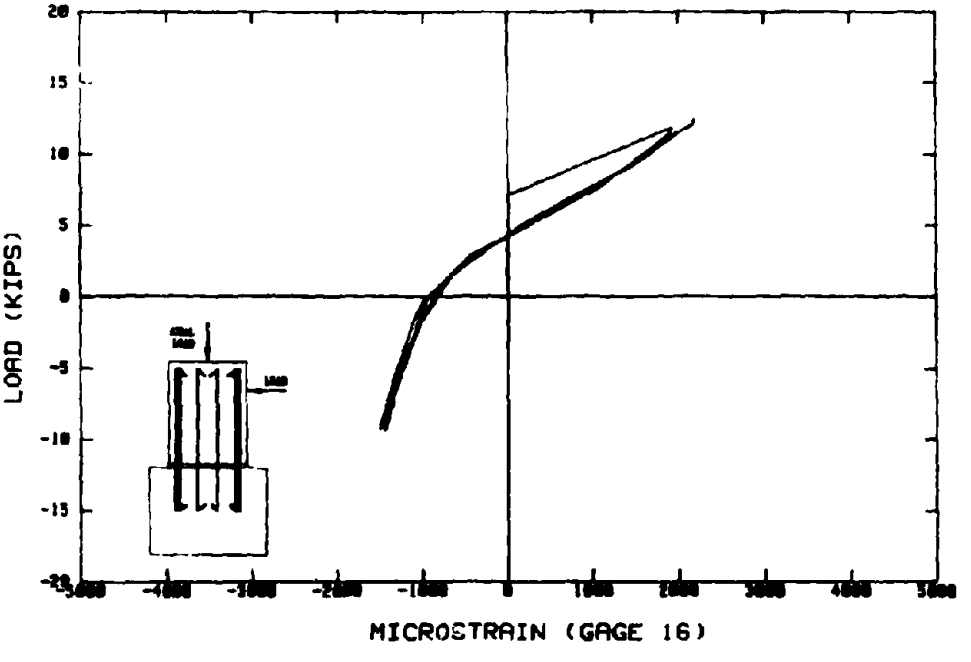

Figure 3-32. BB2C Load-Strain Response (Gage 16).

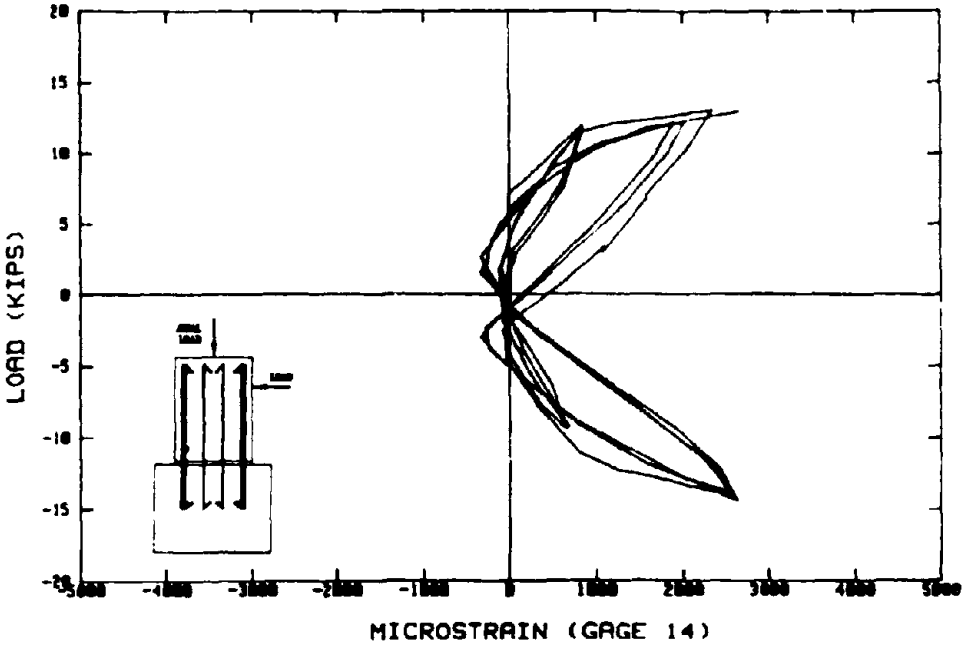

Figure 3-33. BB2C Load-Strain Response (Gage 14).

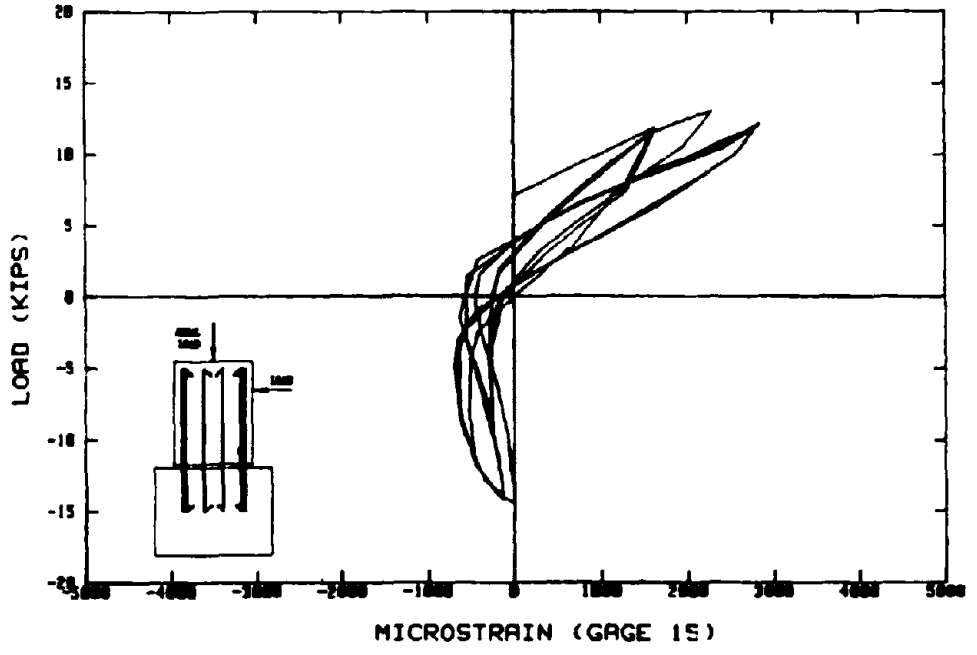

Figure 3-34. BB2C Load-Strain Response (Gage 15).

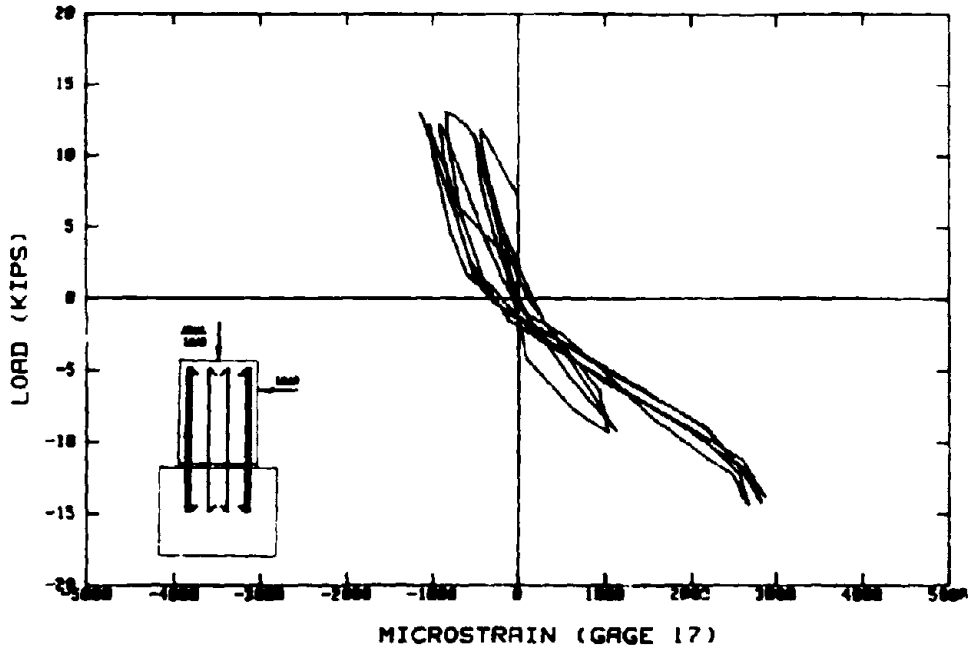

Figure 3-35. BB2C Load-Strain Response (Gage 17).

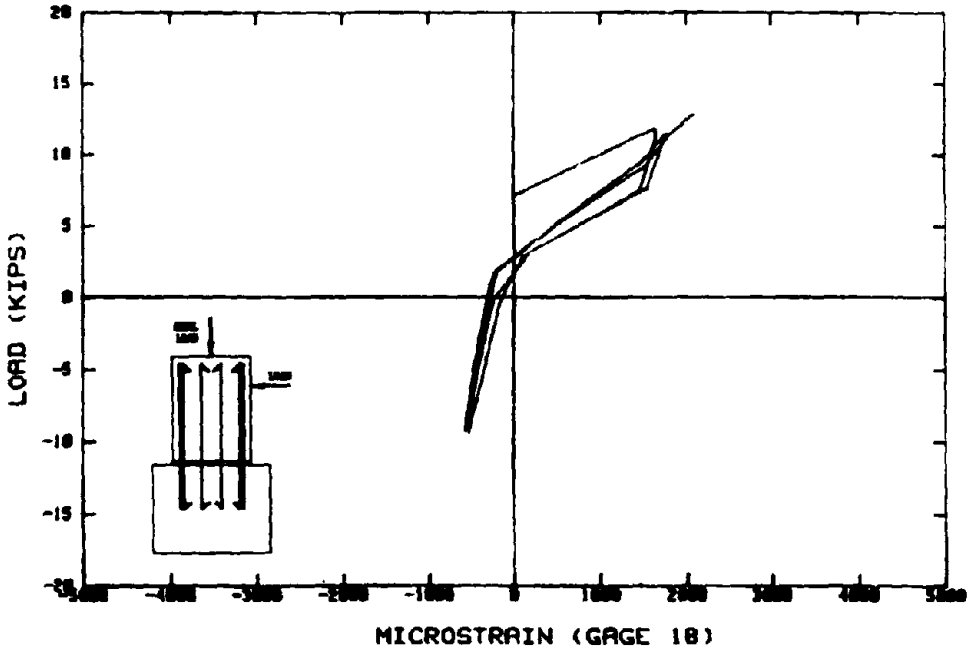

Figure 3-36. BB2C Load-Strain Response (Gage 18).

Figure 3-37. DB1C Front Elevation after Testing.

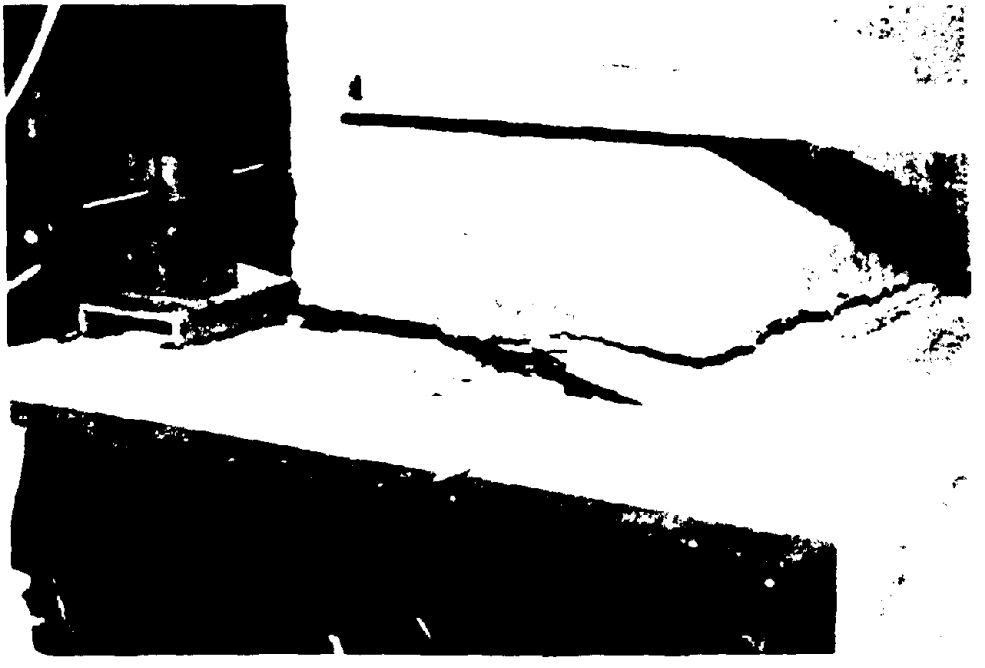

Figure 3-38. DB1C after Testing.

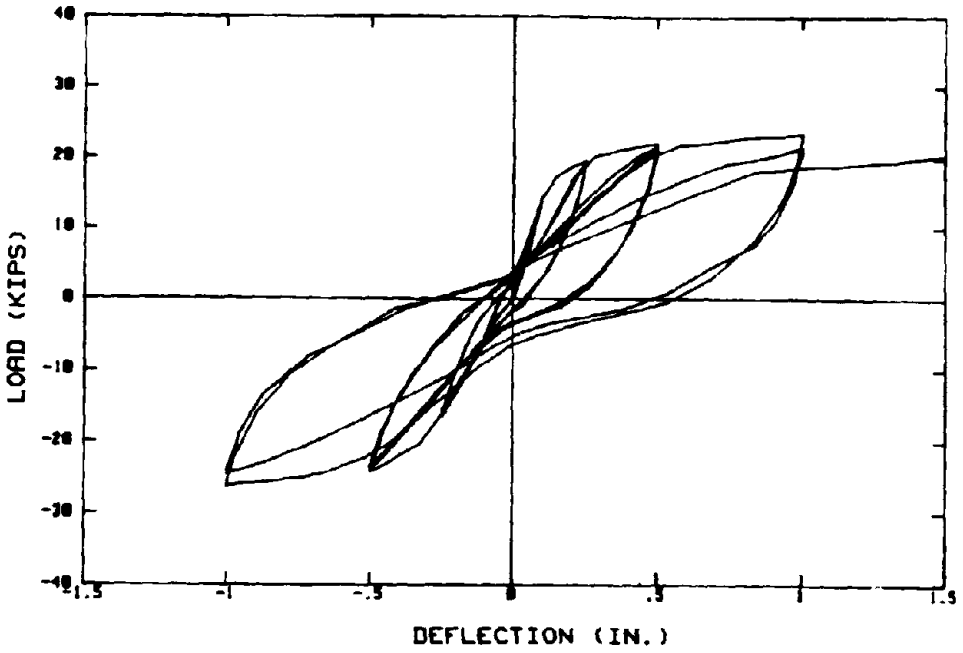

Figure 3-39. DB1C Load-Deflection Response.

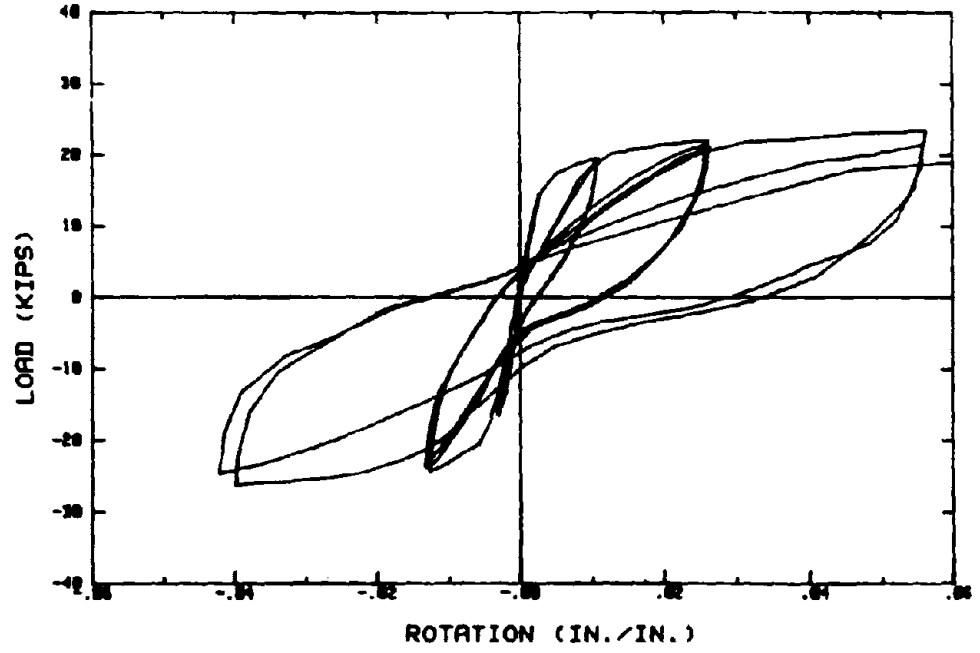

Figure 3-40. DB1C Load-Rotation Response.

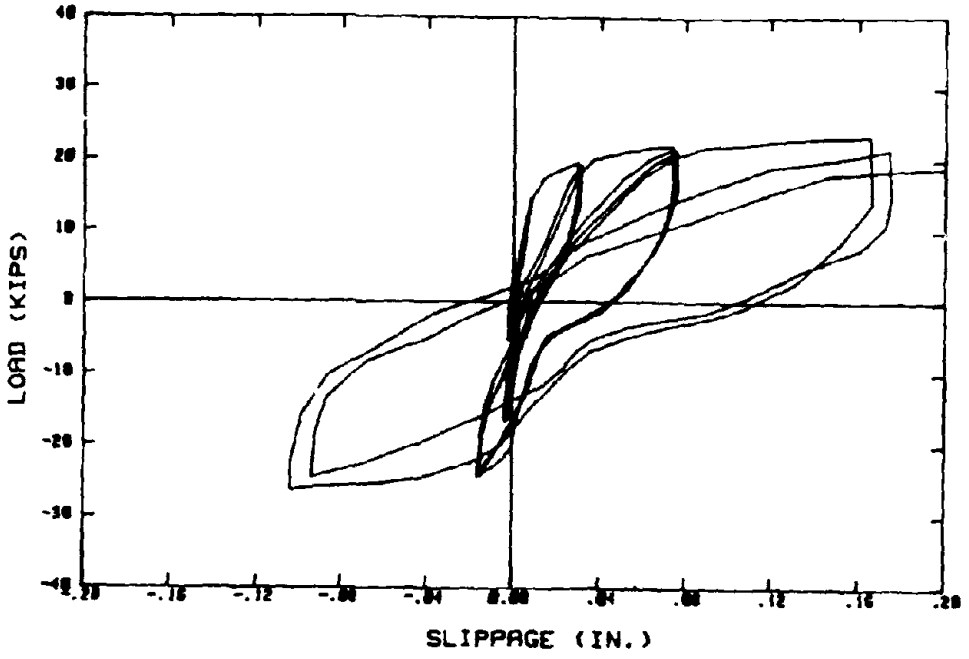

Figure 3-41. DB1C Load-Slippage Response.

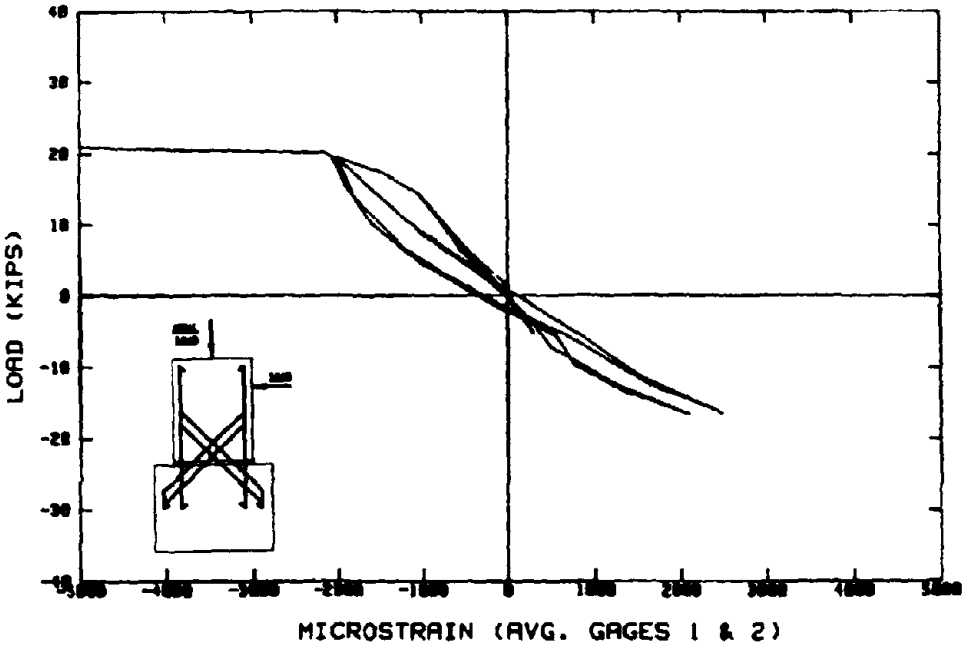

Figure 3-42. DB1C Load-Strain Response (Average of Gages 1 & 2).

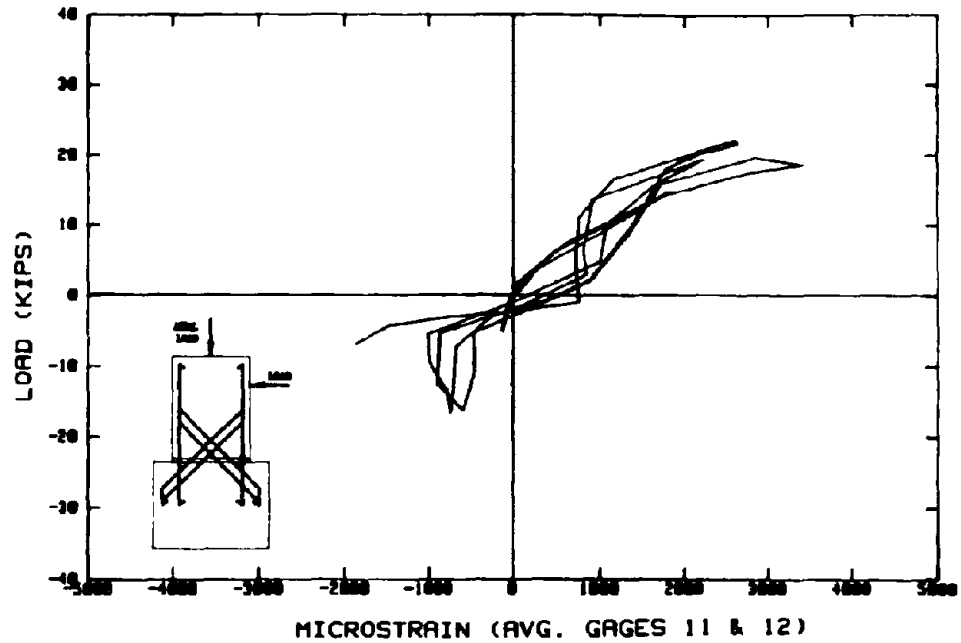

Figure 3-43. DB1C Load-Strain Response (Average of Gages 11 & 12).

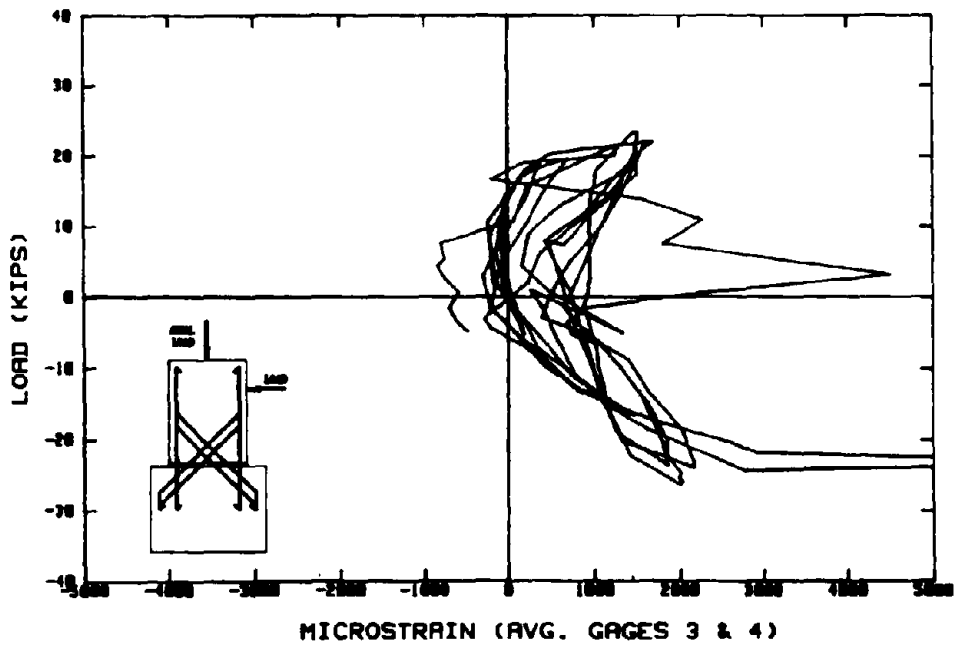

Figure 3-44. DB1C Load-Strain Response (Average of Gages 3 & 4).

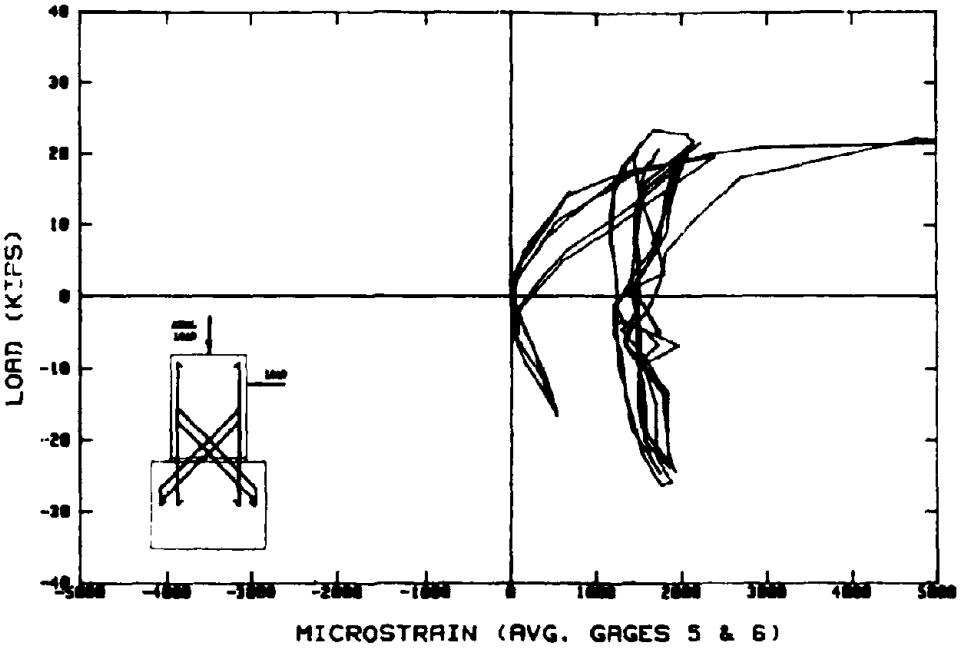

Figure 3-45. DB1C Load-Strain Response (Average of Gages 5 & 6).

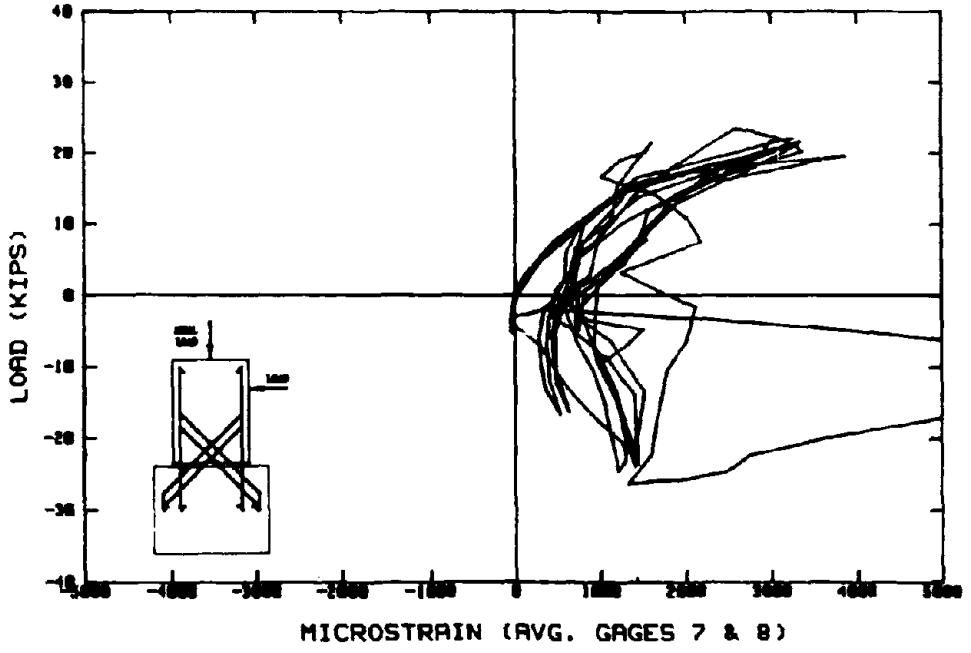

Figure 3-46. DB1C Load-Strain Response (Average of Gages 7 & 8).

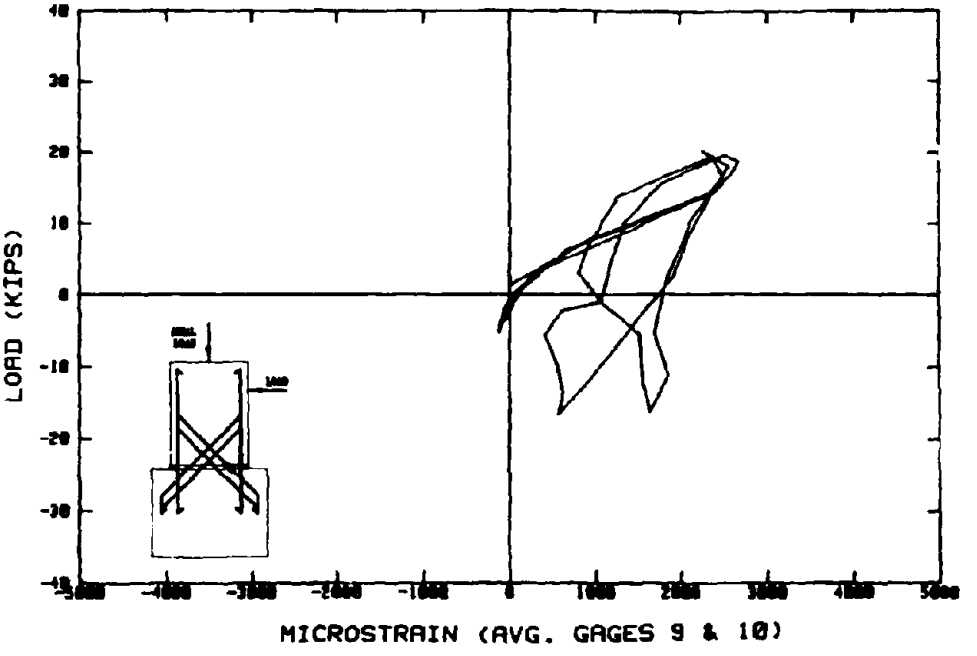

Figure 3-47. DB1C Load-Strain Response (Average of Gages 9 & 10).

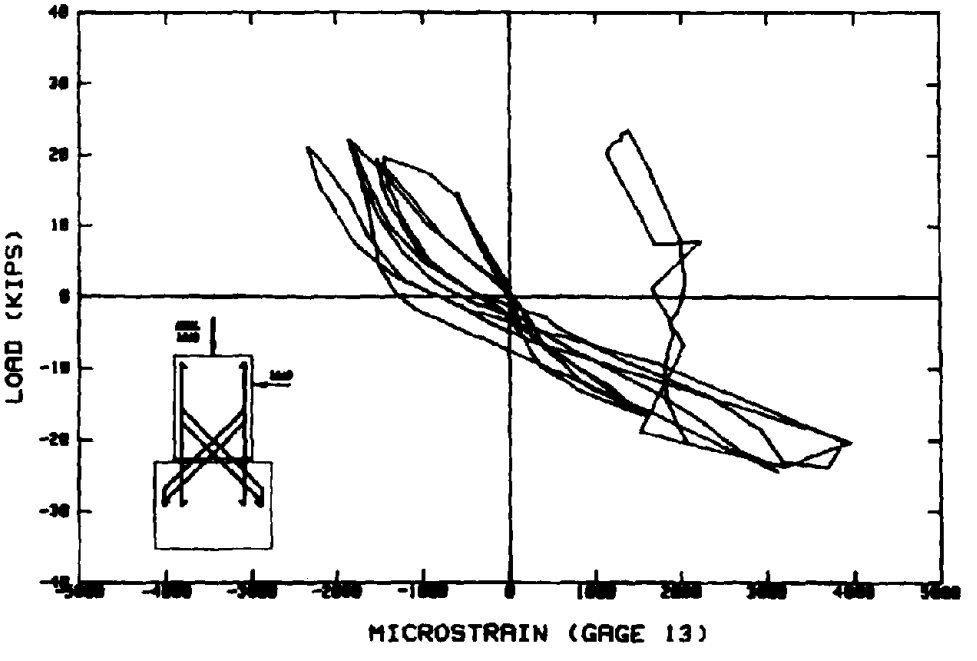

Figure 3-48. DB1C Load-Strain Response (Gage 13).

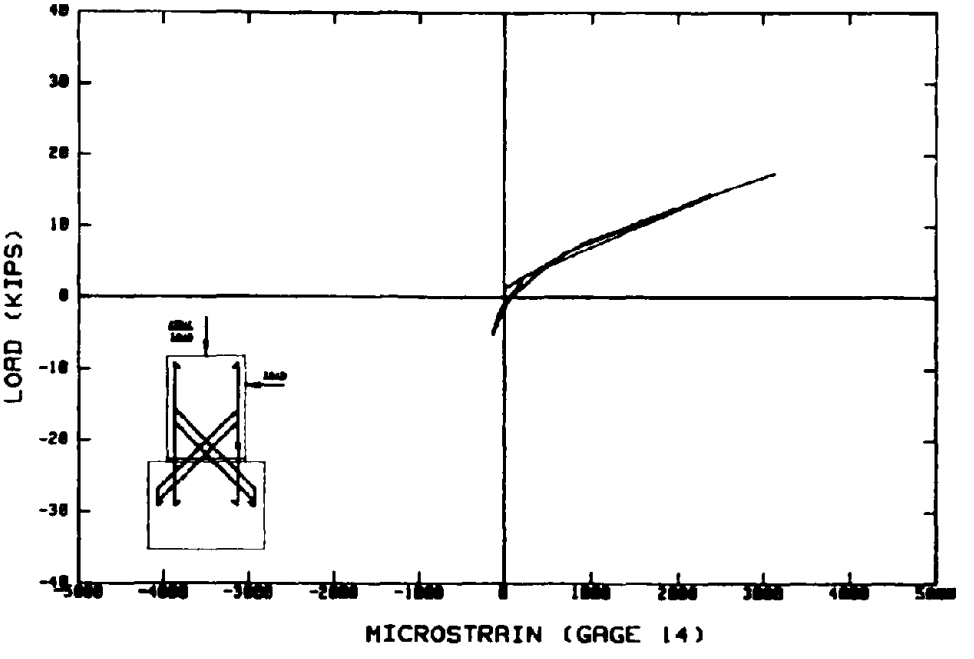

Figure 3-49. DB1C Load-Strain Response (Gage 14).

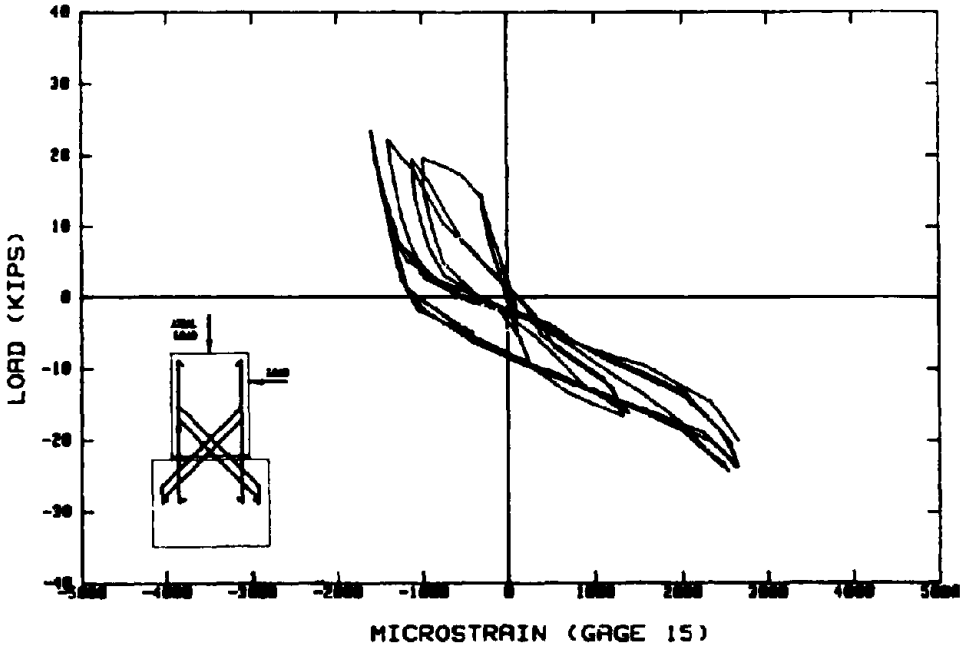

Figure 3-50. DB1C Load-Strain Response (Gage 15).

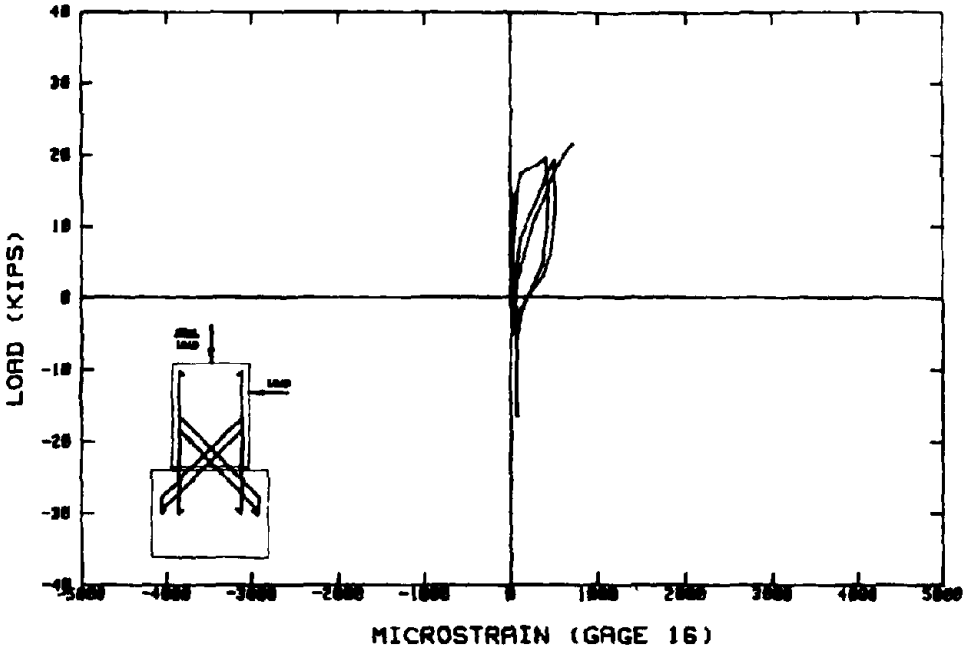

Figure 3-51. DB1C Load-Strain Response (Gage 16).

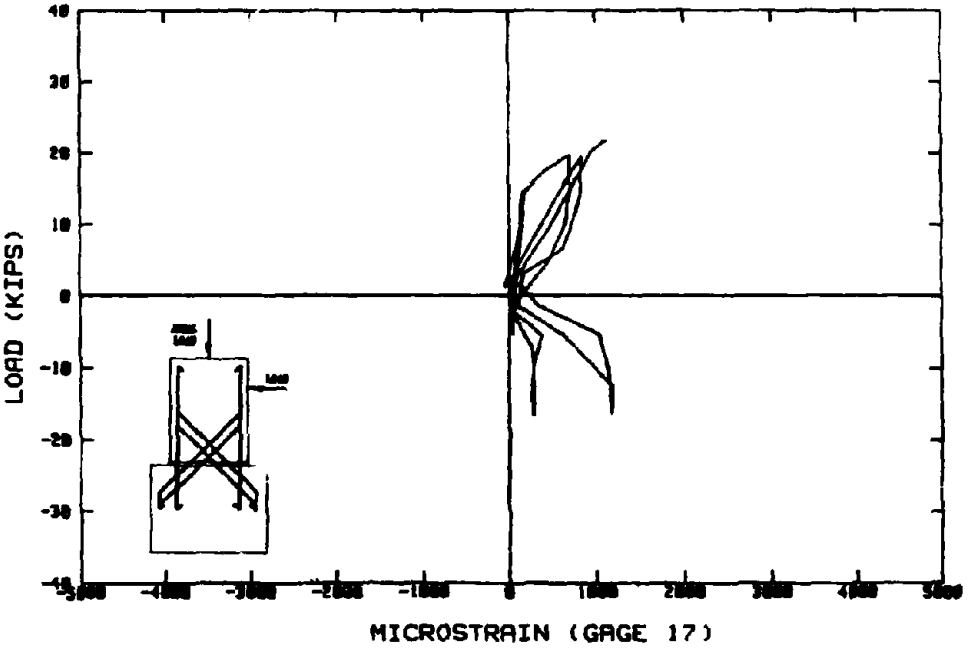

Figure 3-52. DB1C Load-Strain Response (Gage 17).

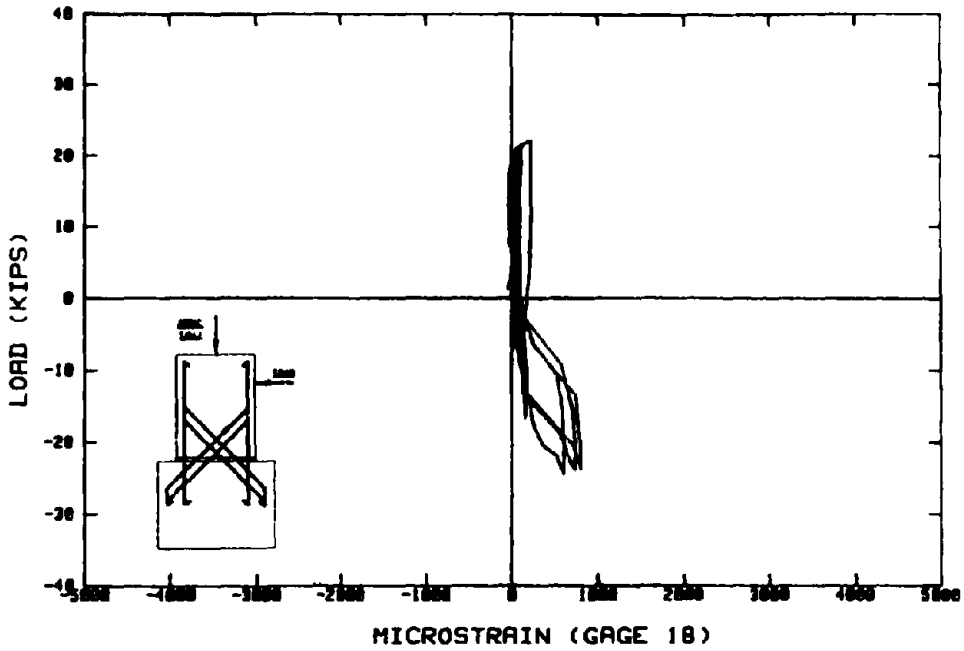

Figure 3-53. LDB1C oad-Strain Response (Gage 18).

Figure 3-54. DB2C after Testing (Tension Zone).

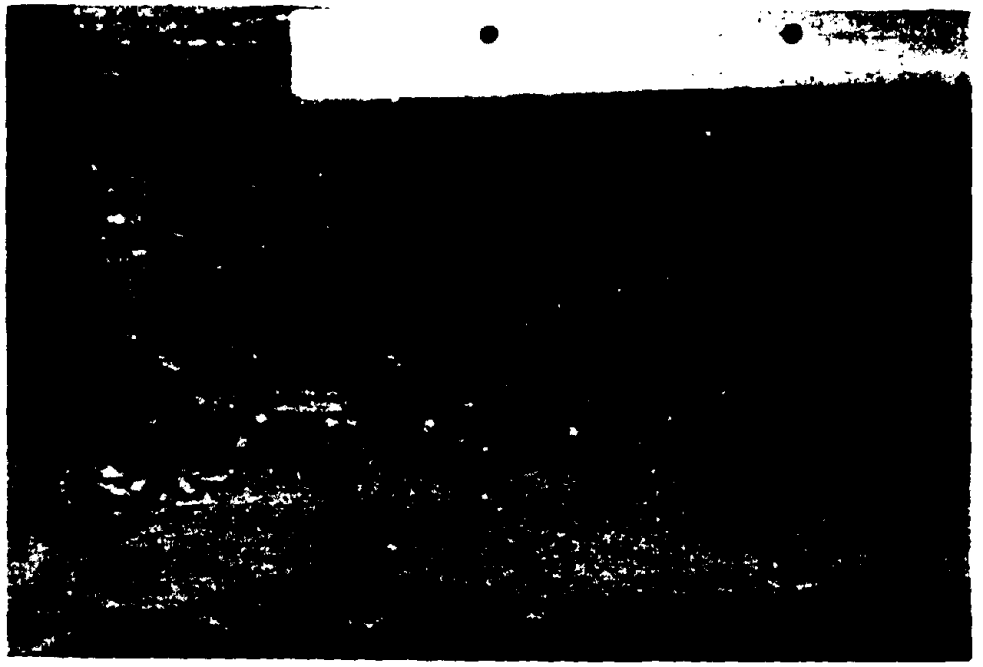

Figure 3-55. DB2C after Testing (Compression Zone).

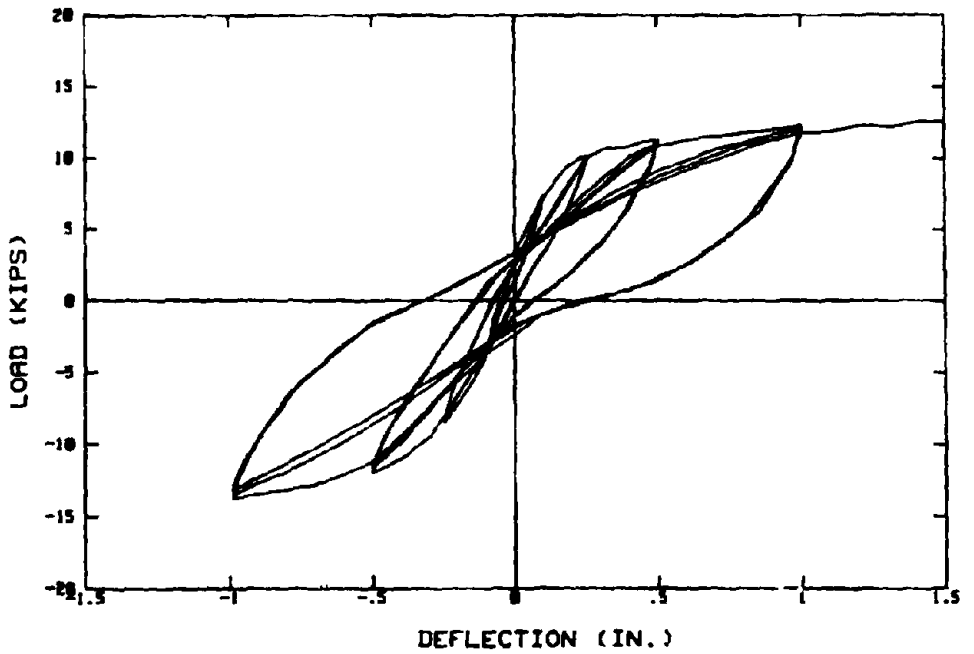

Figure 3-56. DB2C Load-Deflection Response.

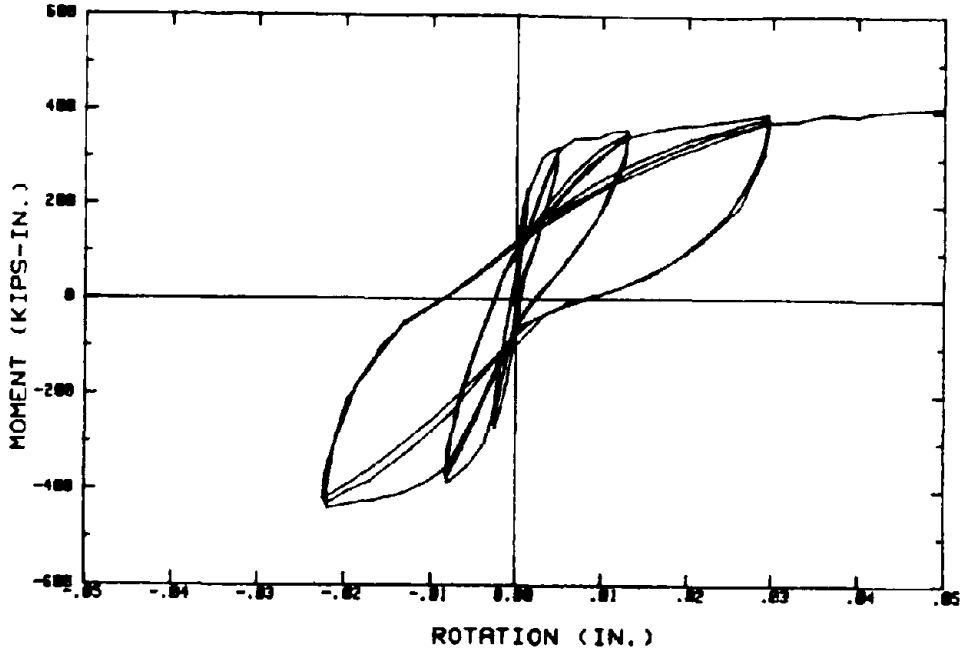

Figure 3-57. DB2C Load-Rotation Response.

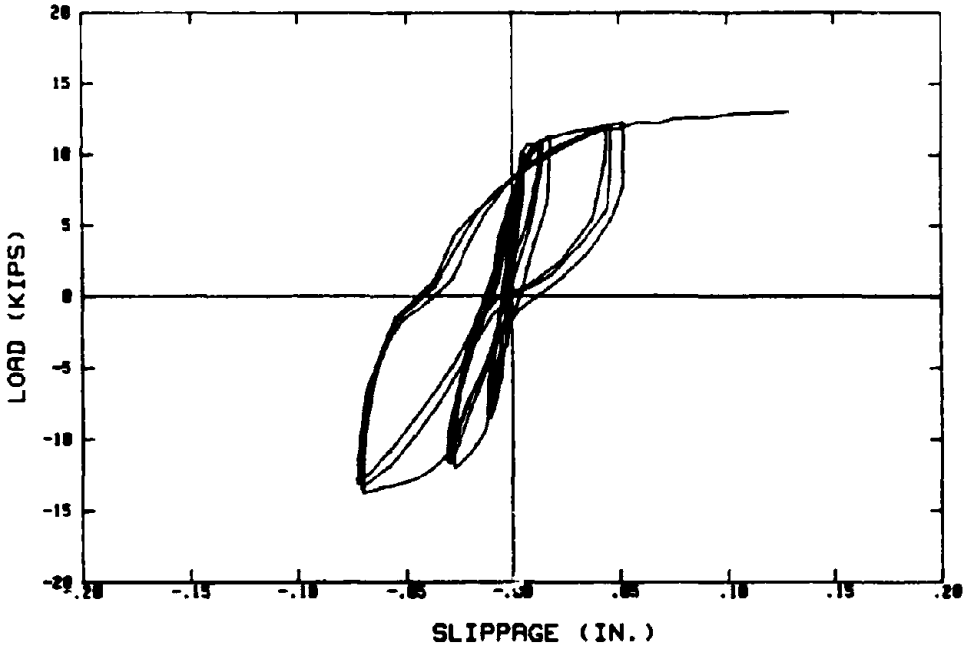

Figure 3-58. DB2C Load-Slippage Response.

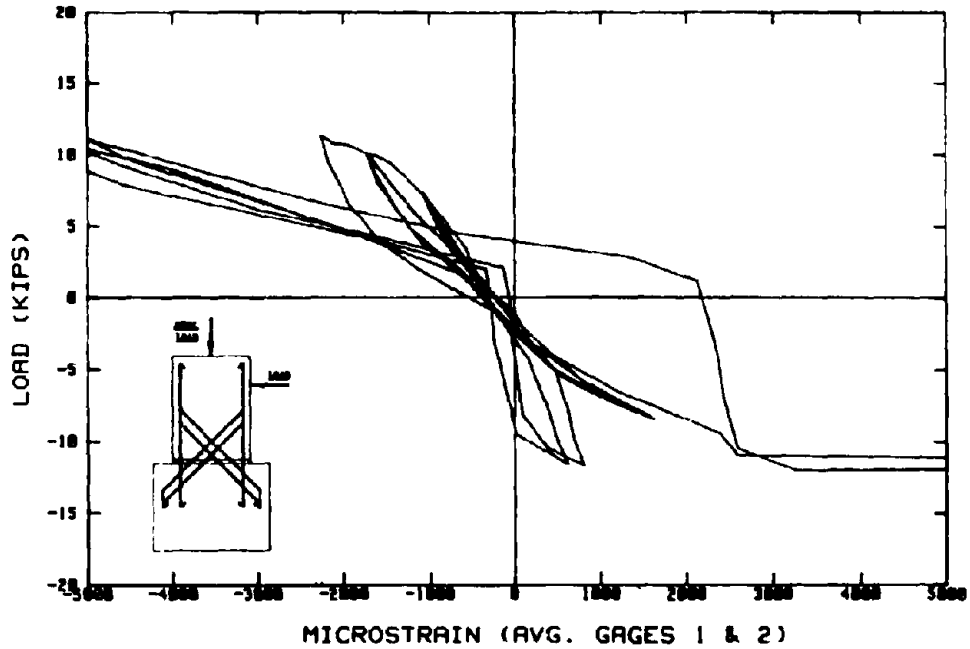

Figure 3-59. DB2C Load-Strain Response (Average of Gages 1 & 2).

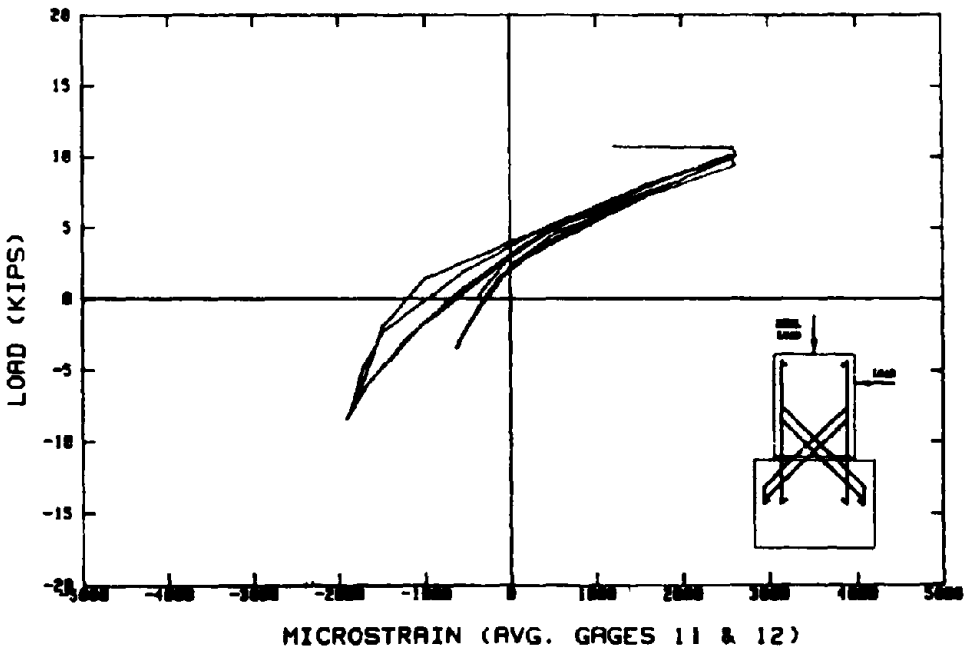

Figure 3-60. DB2C Load-Strain Response (Average of Gages 11 & 12).

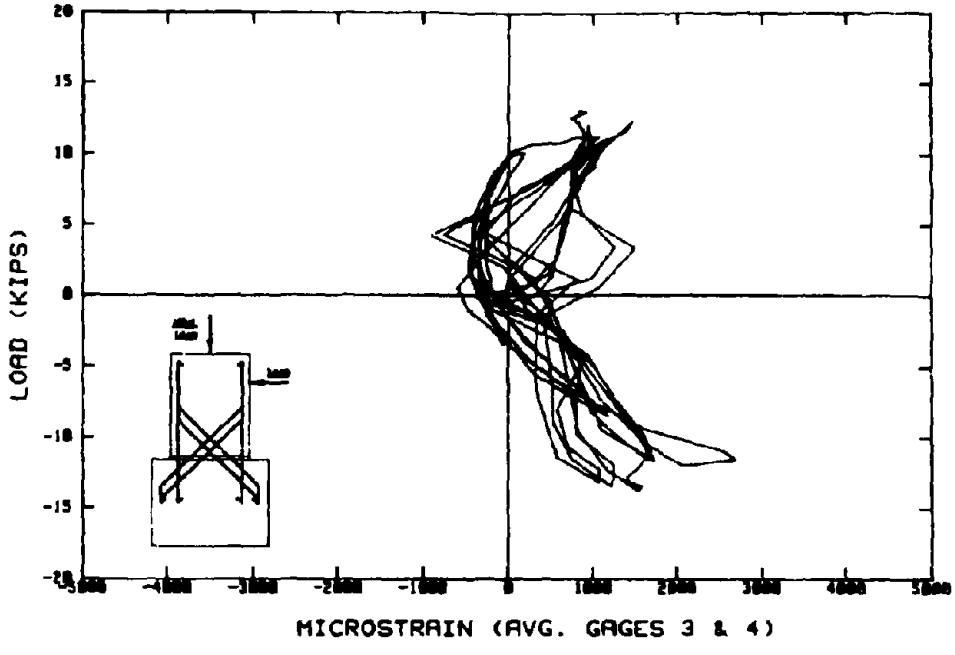

Figure 3-61. DB2C Load-Strain Response (Average of Gages 3 & 4).

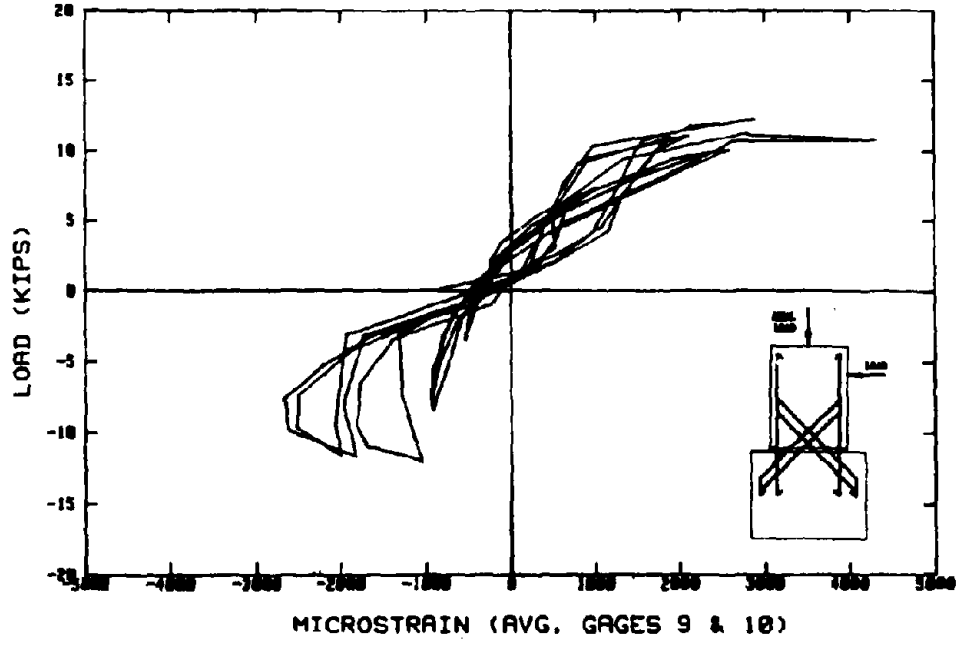

Figure 3-62. DB2C Load-Strain Response (Average of Gages 9 & 10).

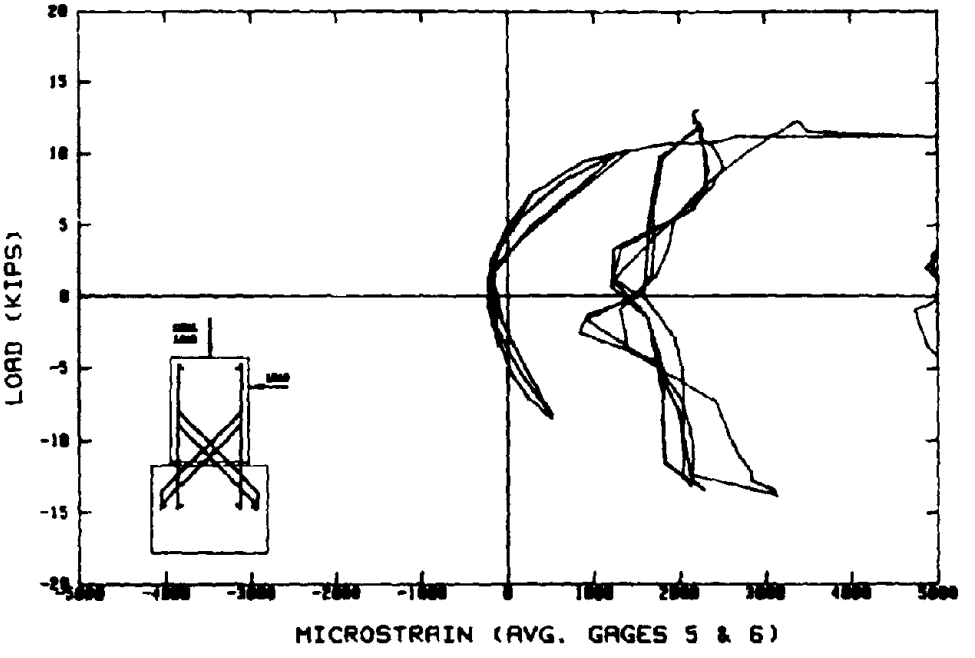

Figure 3-63. DB2C Load-Strain Response (Average of Gages 5 & 6).

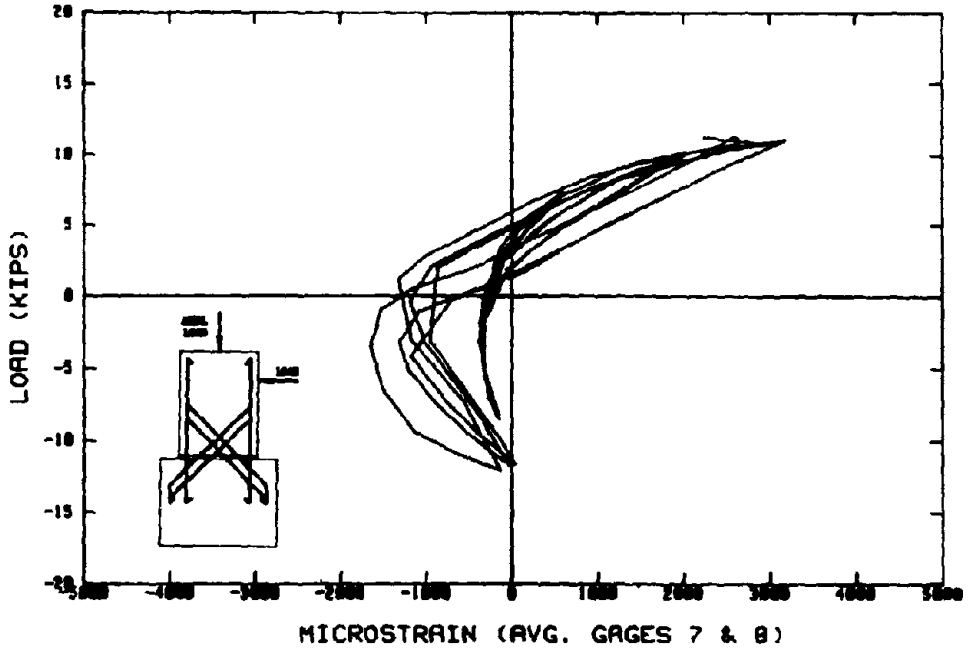

Figure 3-64. DB2C Load-Strain Response (Average of Gages 7 & 8).

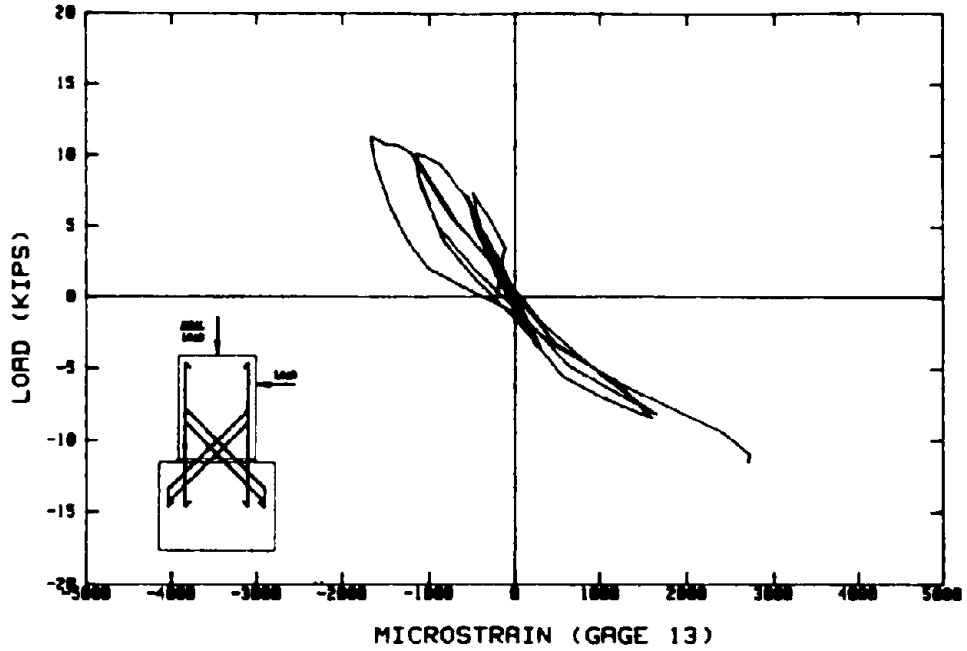

Figure 3-65. DB2C Load-Strain Response (Gage 13).

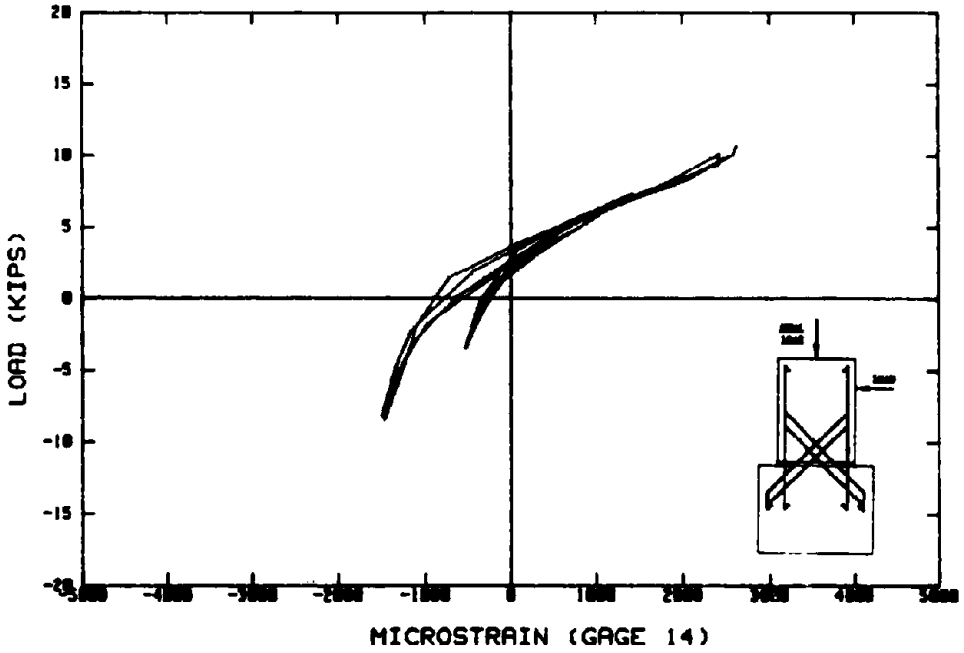

Figure 3-66. DB2C Load-Strain Response (Gage 14).

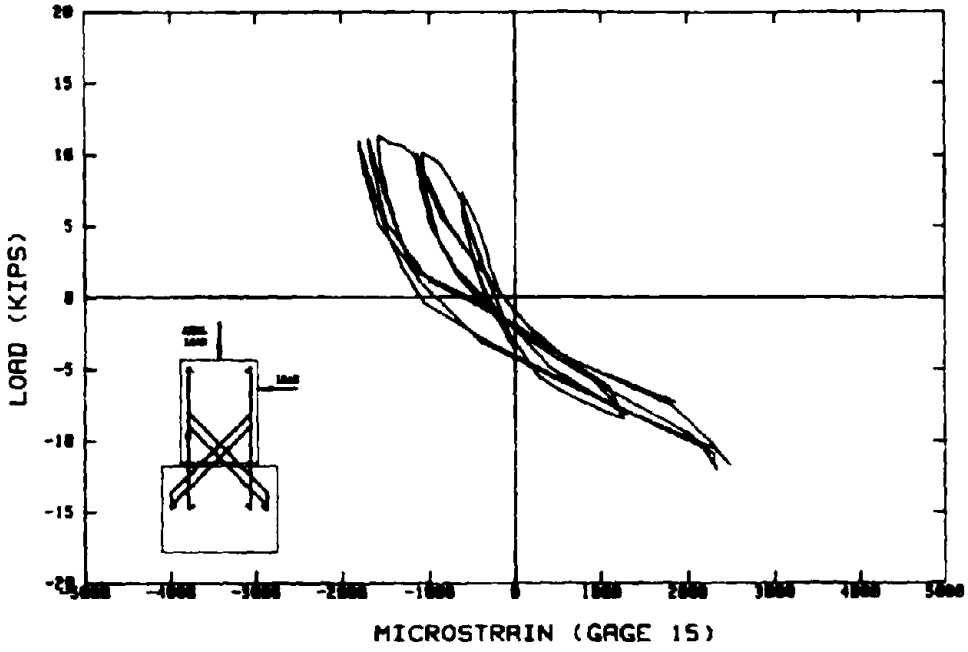

Figure 3-67. DB2C Load-Strain Response (Gage 15).

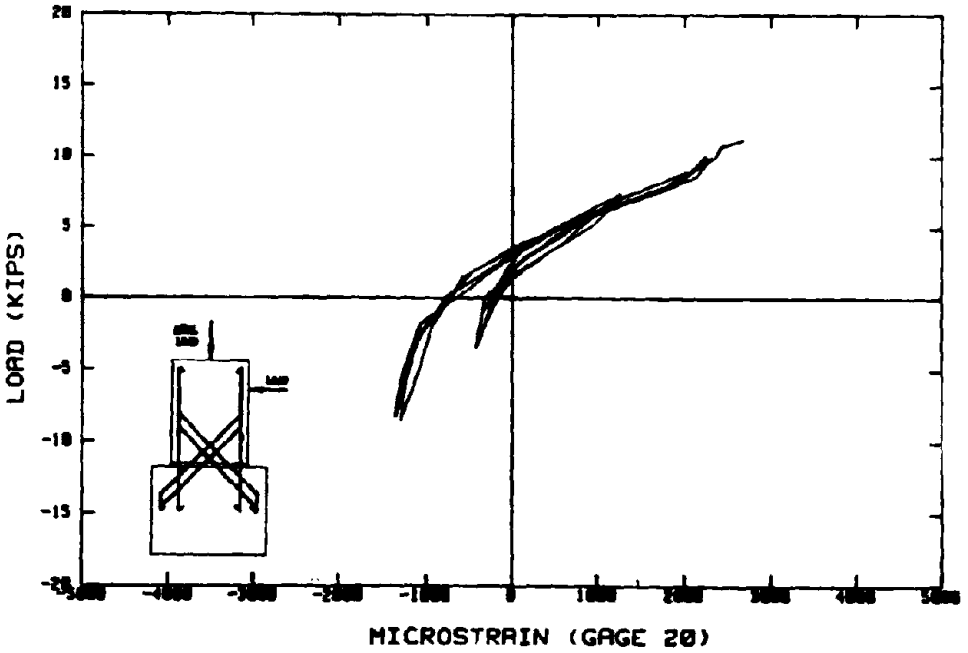

Figure 3-68. DB2C Load-Strain Response (Gage 20) .

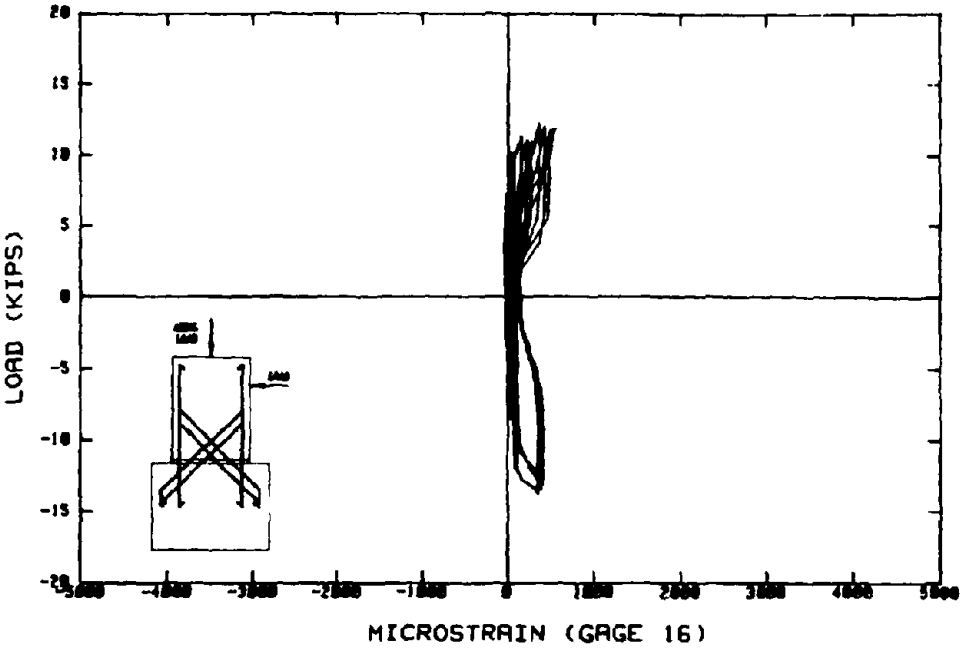

Figure 3-69. DB2C Load-Strain Response (Gage 16).

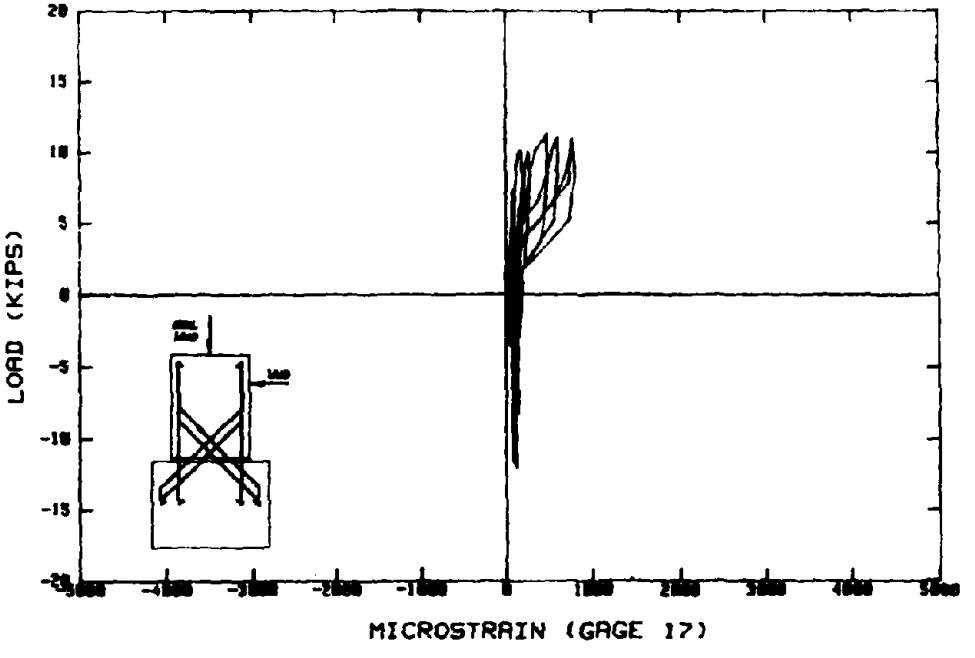

Figure 3-70. DB2C Load-Strain Response (Gage 17) .

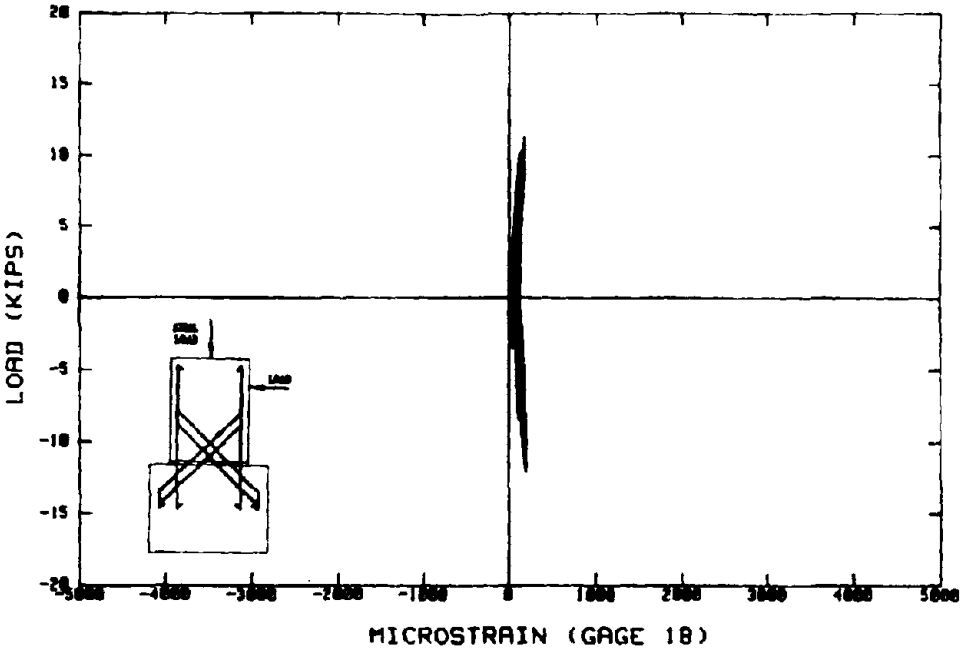

Figure 3-71. DB2C Load-Strain Response (Gage 18).

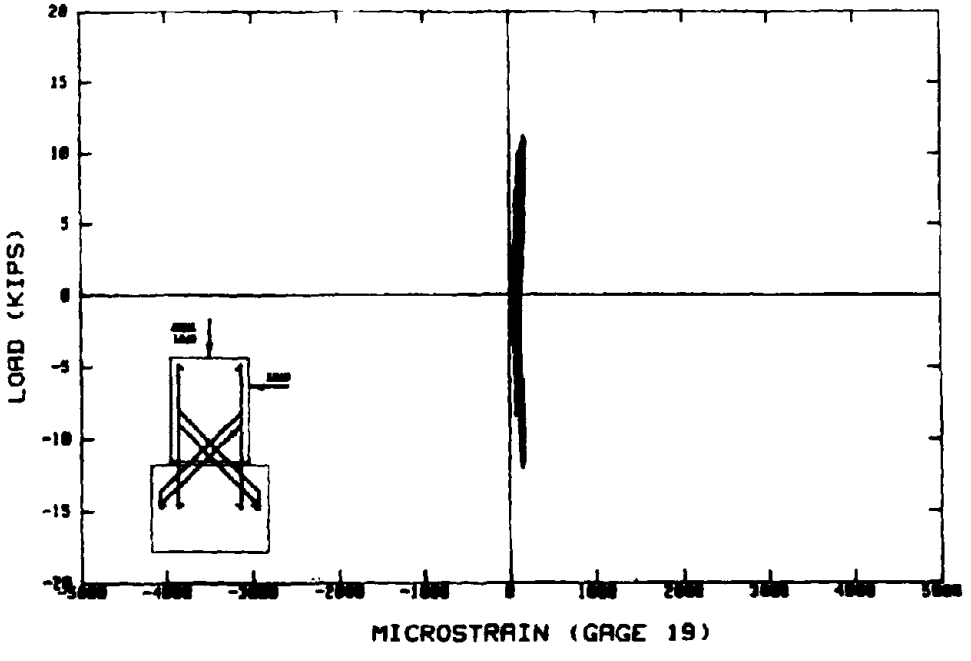

Figure 3-72. DB2C Load-Strain Response (Gage 19).

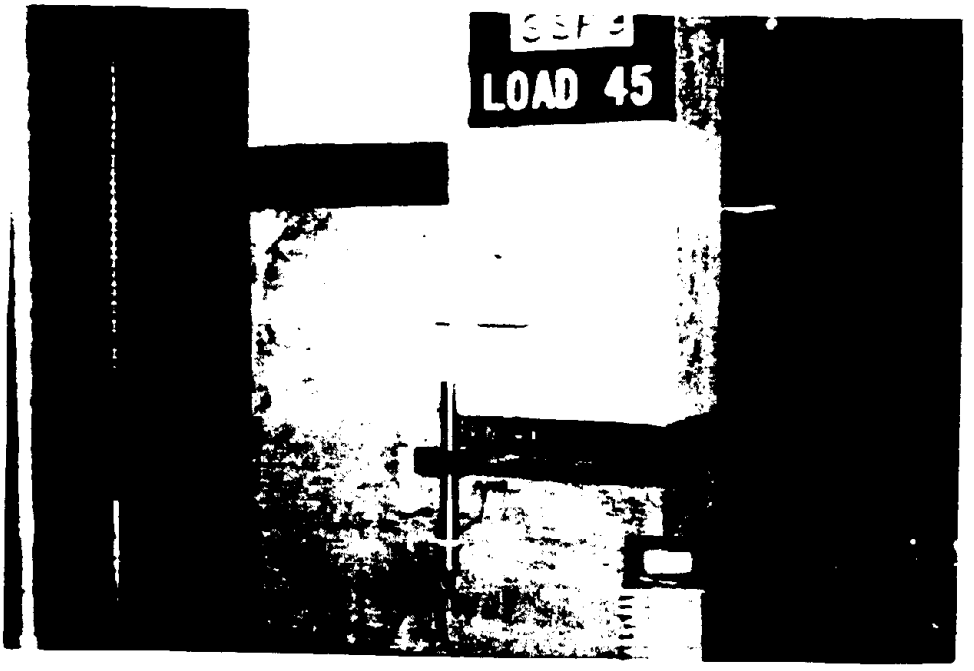

Figure 3-73. Typical Failed Shear Specimen.

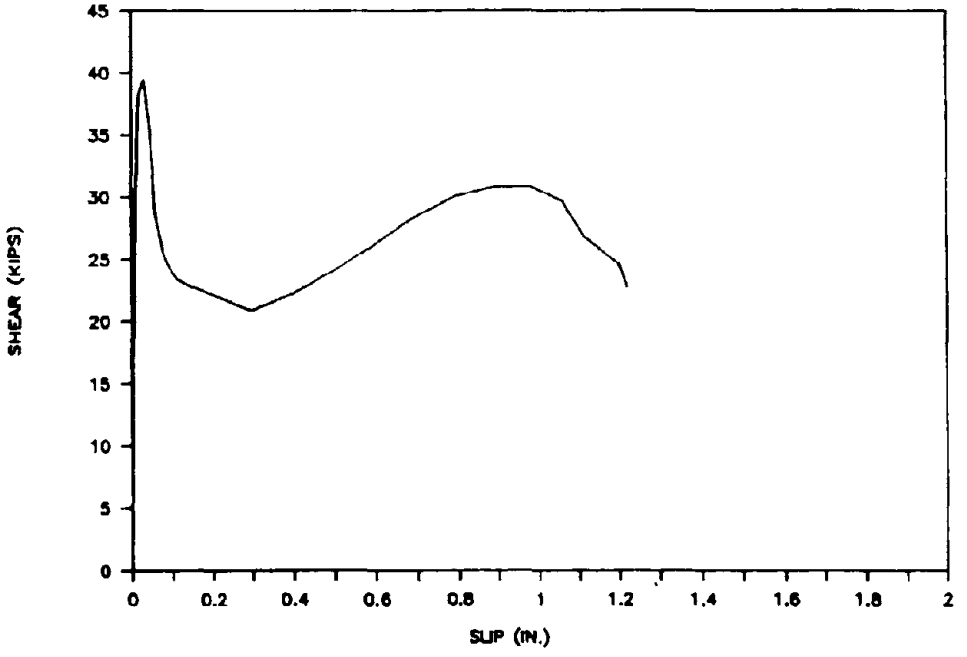

Figure 3-74. SSP1 Shear-Slip Response.

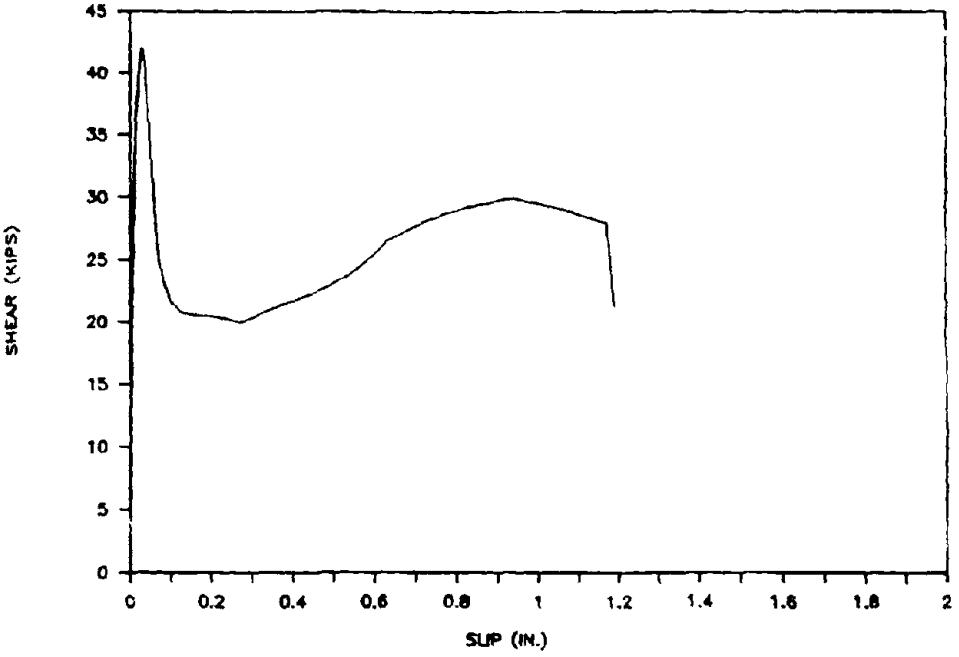

Figure 3-75. SSP2 Shear-Slip Response.

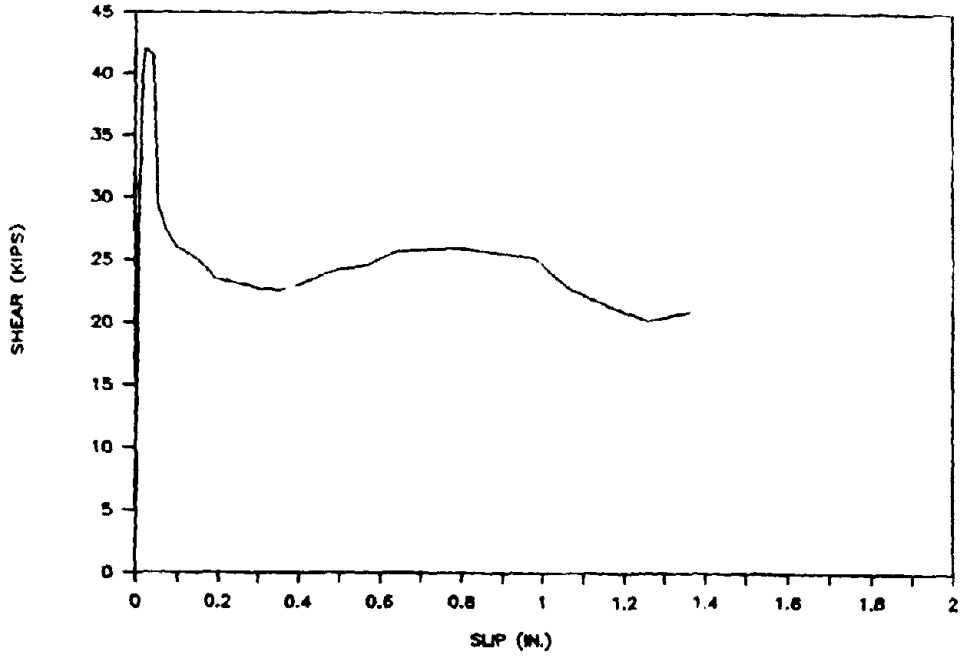

Figure 3-76. SSP3 Shear-Slip Response.

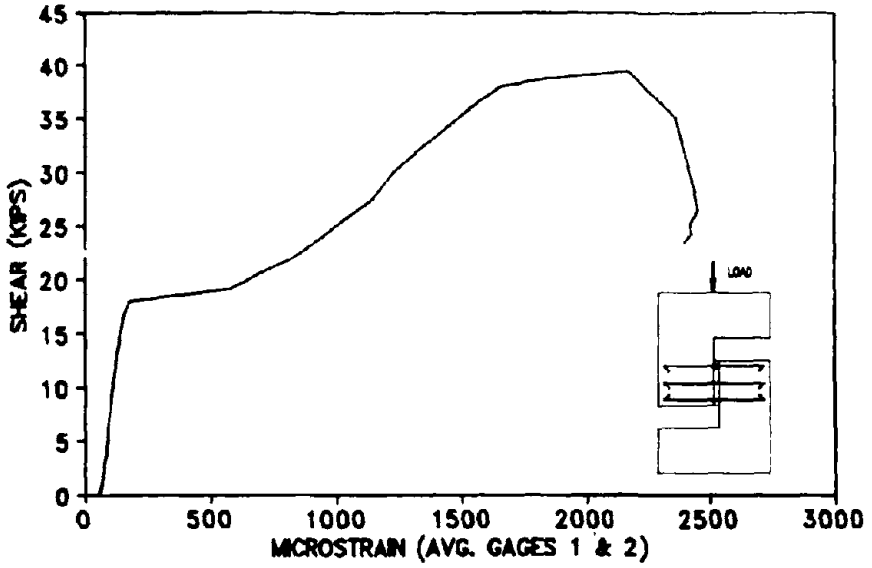

Figure 3-77. SSP1 Shear-Strain Response (Average of Gages 1 & 2).

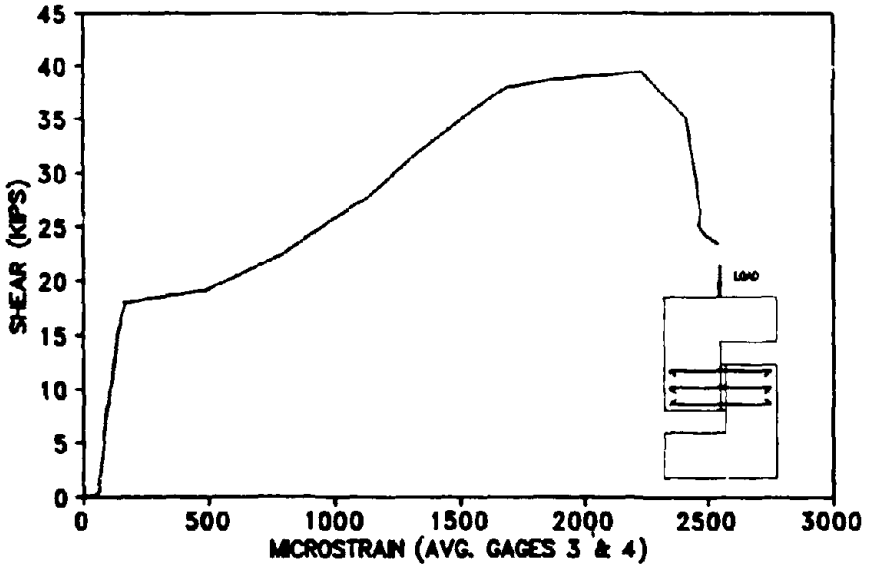

Figure 3-78. SSP1 Shear-Strain Response (Average of Gages 3 & 4).

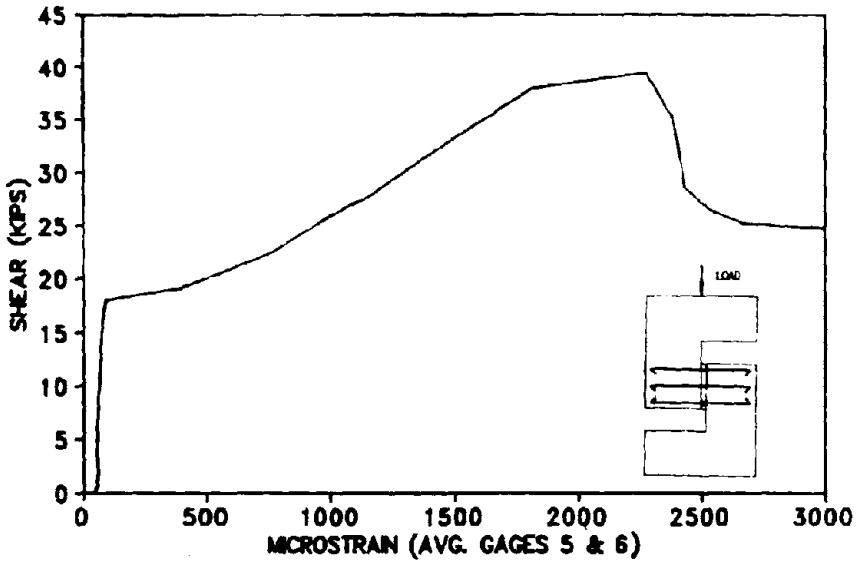

Figure 3-79. SSP1 Shear-Strain Response (Average of Gages 5 & 6).

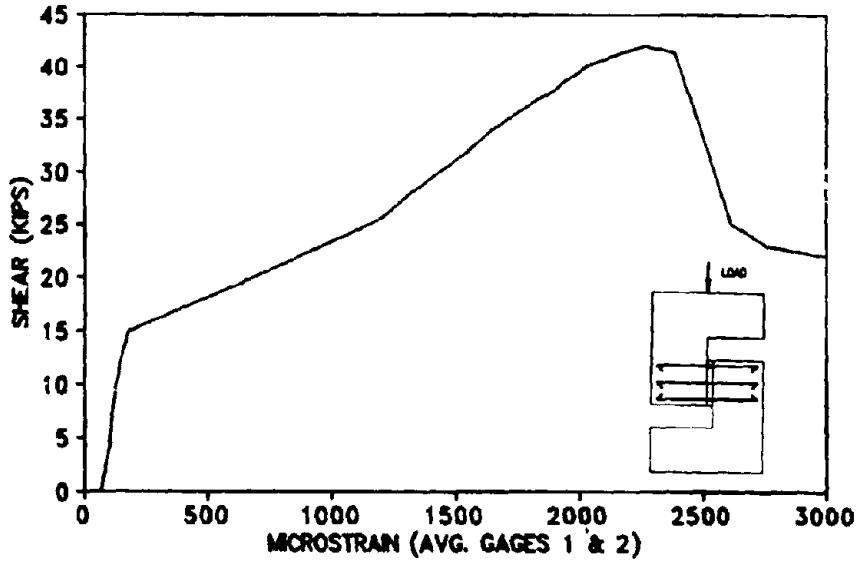

Figure 3-80. SSP2 Shear-Strain Response (Average of Gages 1 & 2).

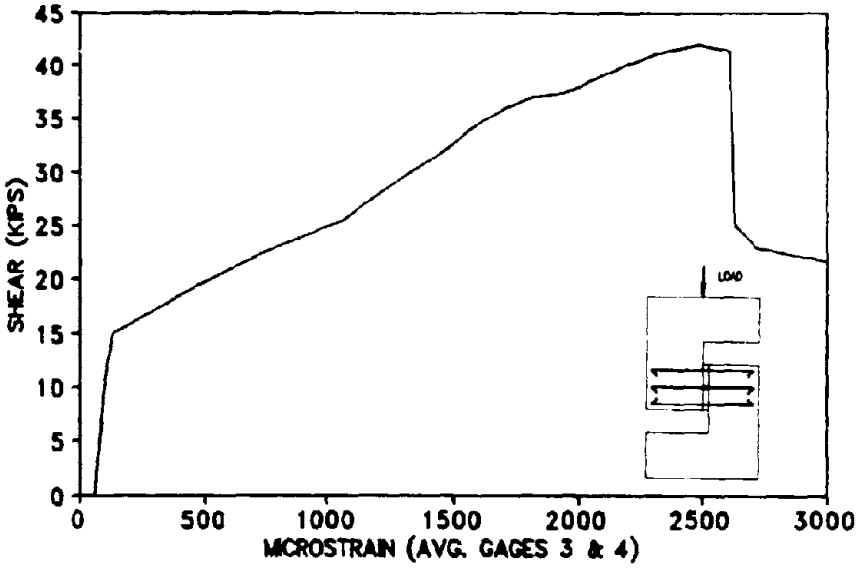

Figure 3-81. SSP2 Shear-Strain Response (Average of Gages 3 & 4).

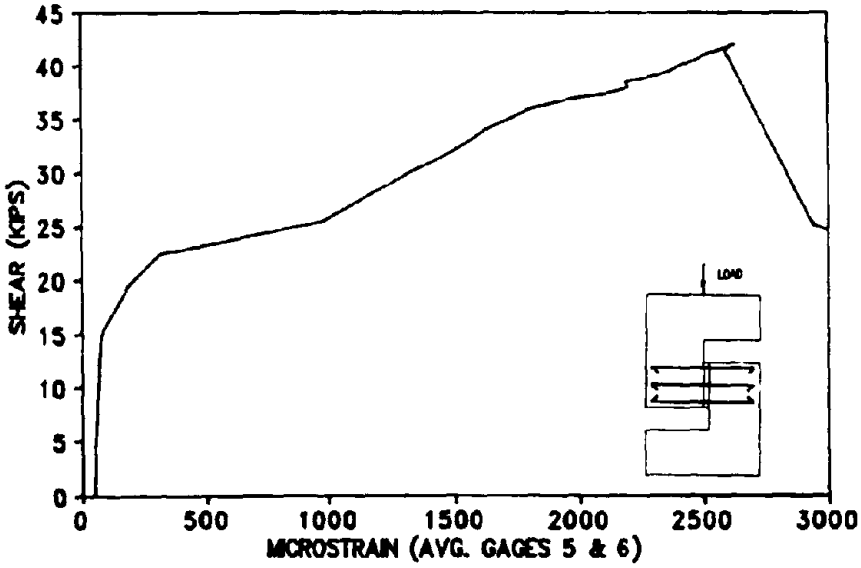

Figure 3-82. SSP2 Shear-Strain Response (Average of Gages 5 & 6).

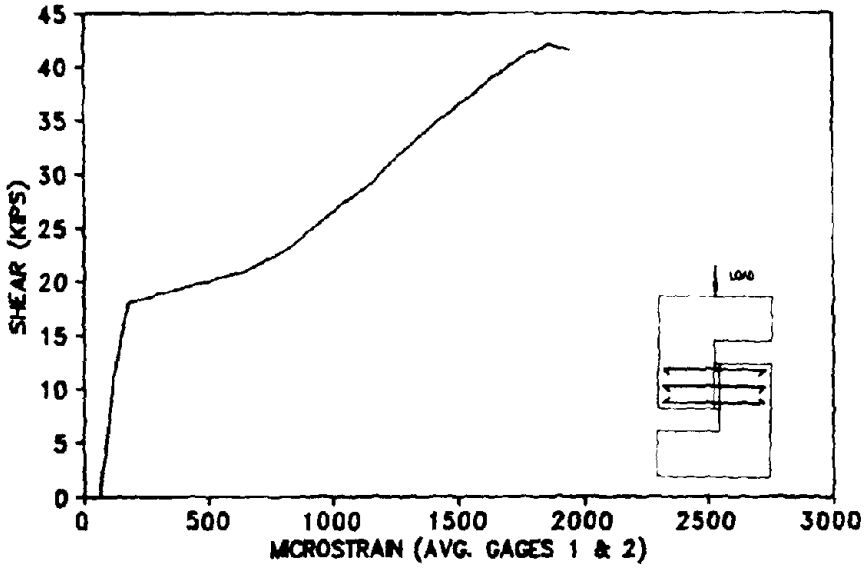

Figure 3-83. SSP3 Shear-Strain Response (Average of Gages 1 & 2).

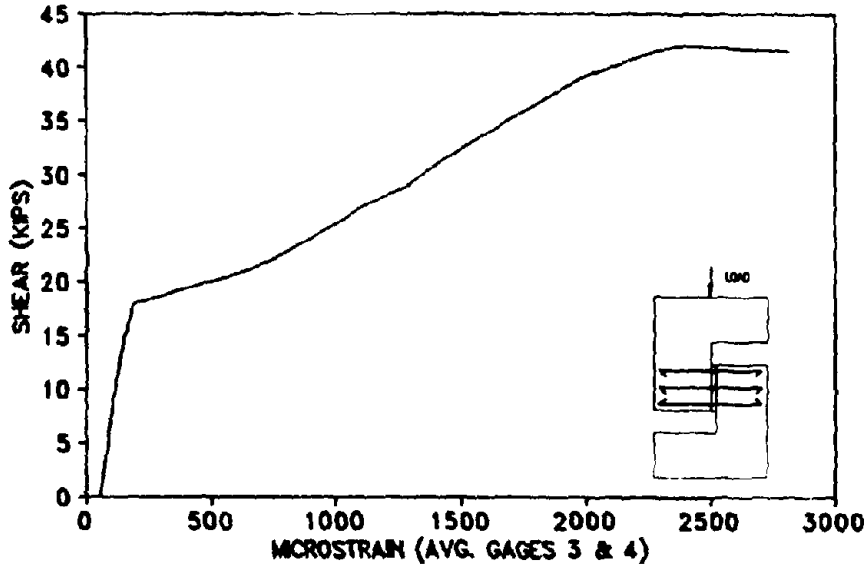

Figure 3-84. SSP3 Shear-Strain Response (Average of Gages 3 & 4).

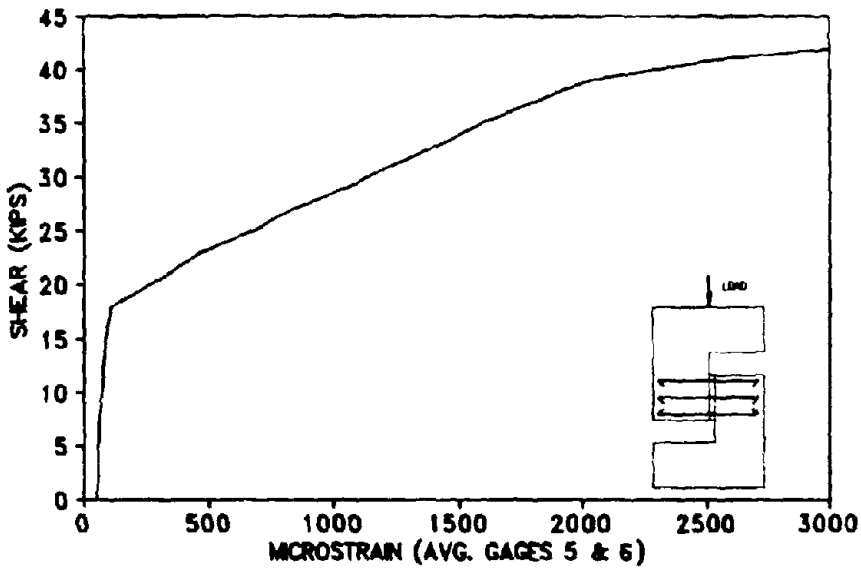

Figure 3-85. SSP3 Shear-Strain Response (Average of Gages 5 & 6).

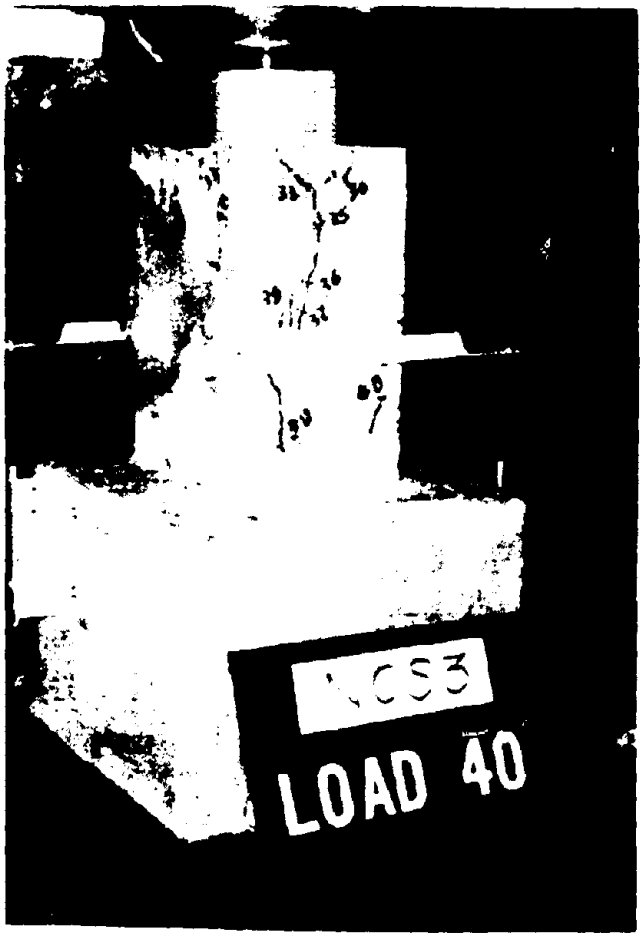

Figure 3-86. Typical Failed Compression Specimen.

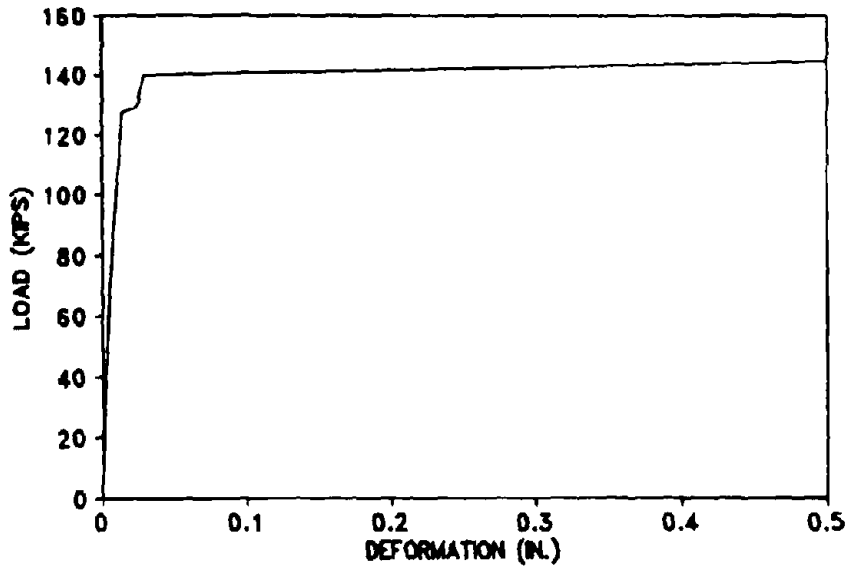

Figure 3-87. NCS1 Load-Deformation Response.

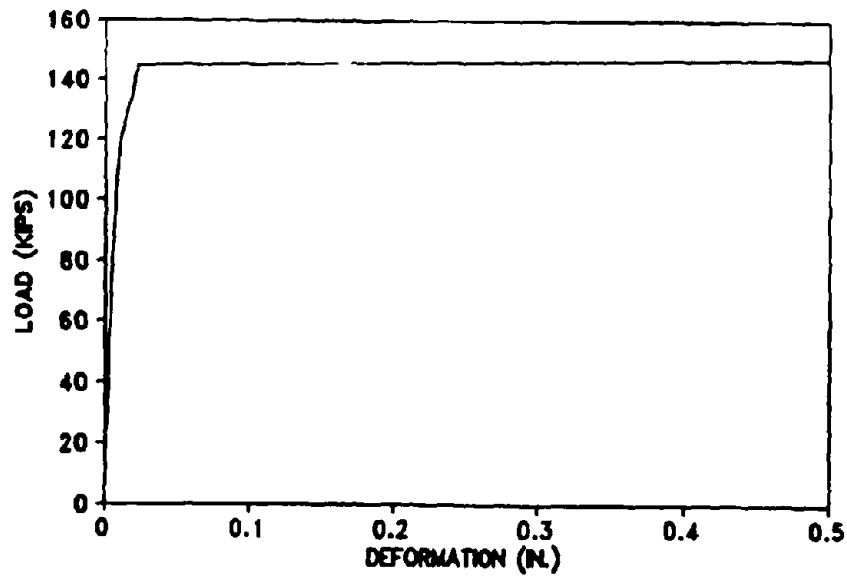

Figure 3-88. NCS2 Load-Deformation Response.

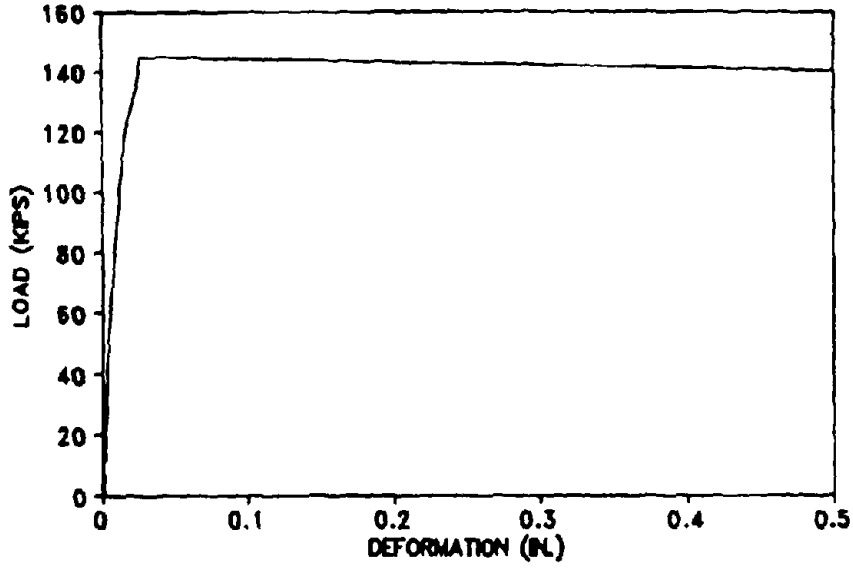

Figure 3-89. NCS3 Load-Deformation Response.

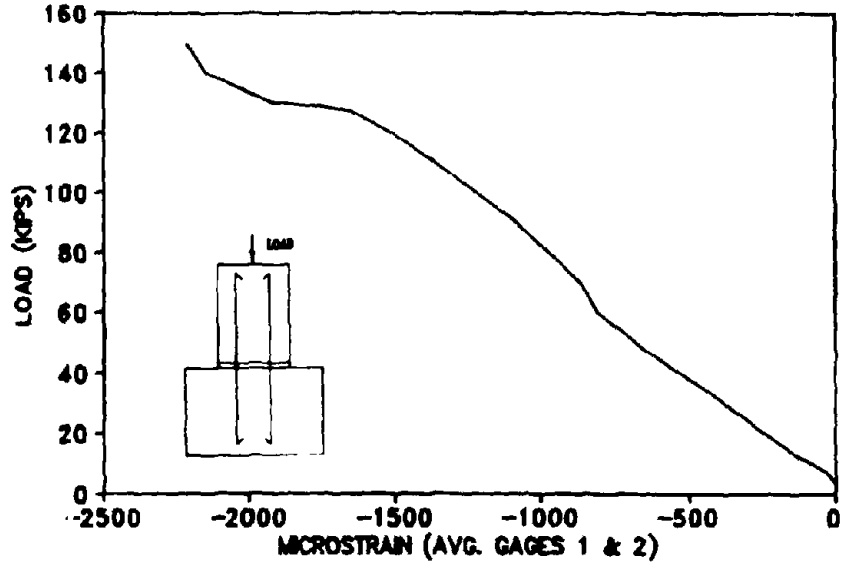

Figure 3-90. NCS1 Load-Strain Response (Average of Gages 1 & 2).

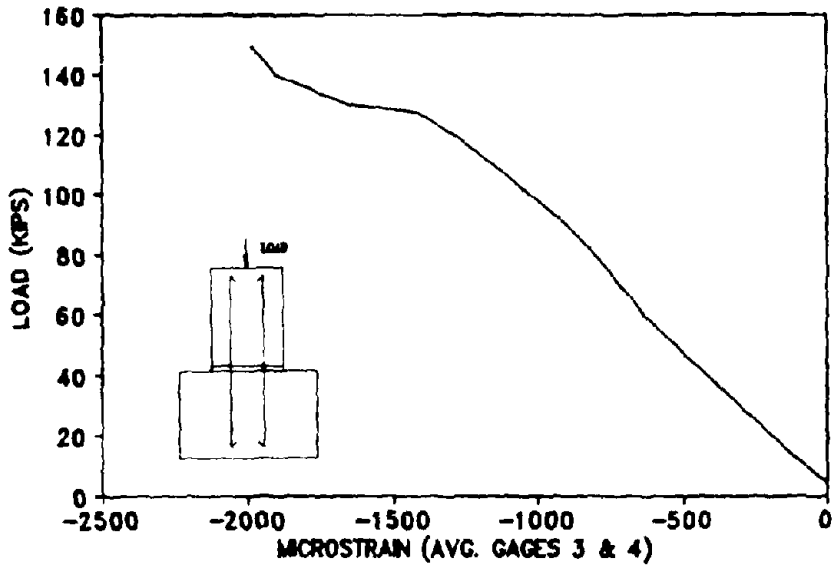

Figure 3-91. NCS1 Load-Strain Response (Average of Gages 3 & 4).

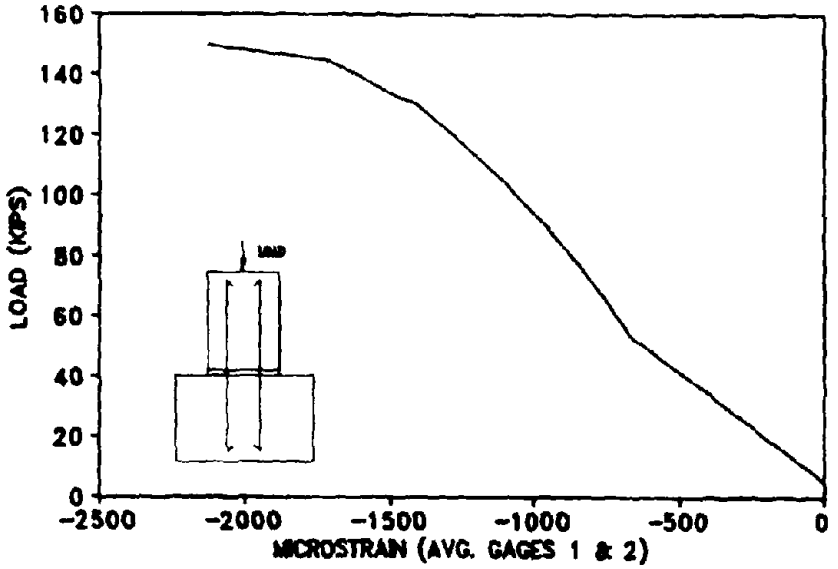

Figure 3-92. NCS2 Load-Strain Response (Average of Gages 1 & 2).

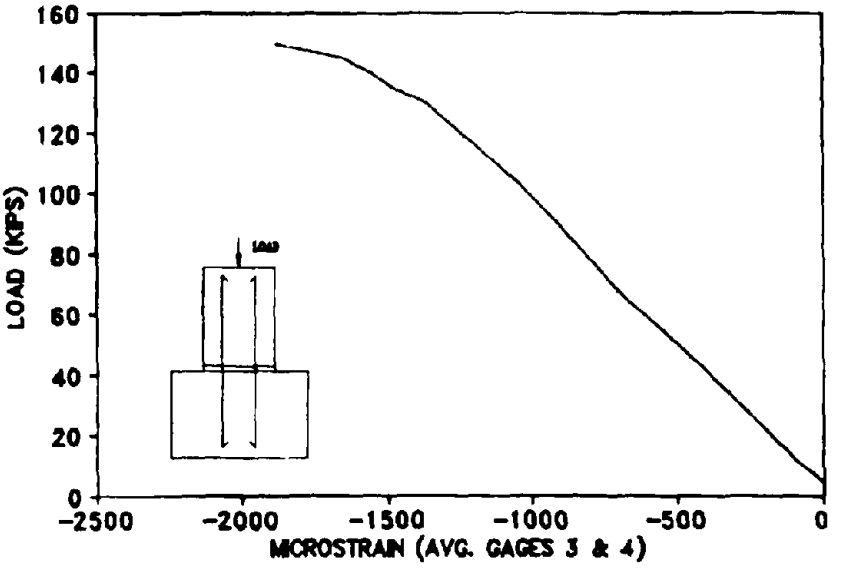

Figure 3-93. NCS2 Load-Strain Response (Average of Gages 3 & 4).

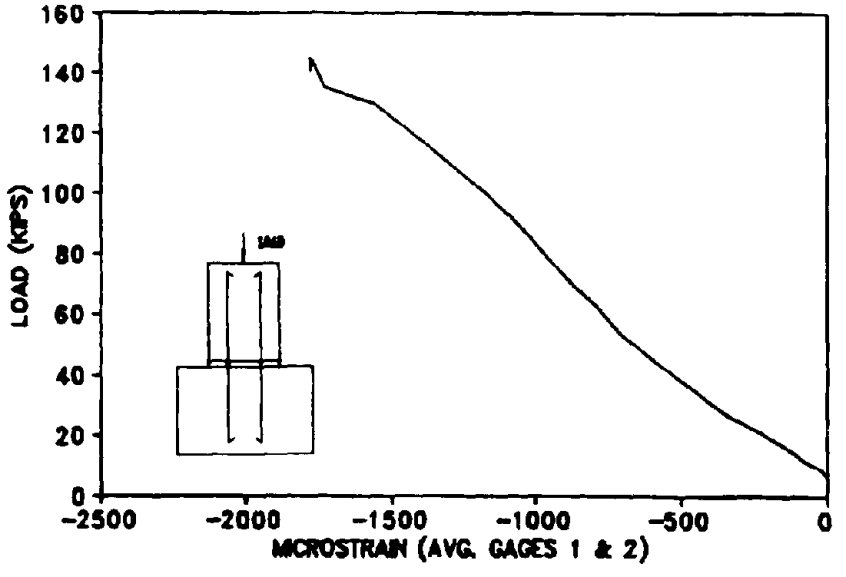

Figure 3-94. NCS3 Load-Strain Response (Average of Gages 1 & 2).

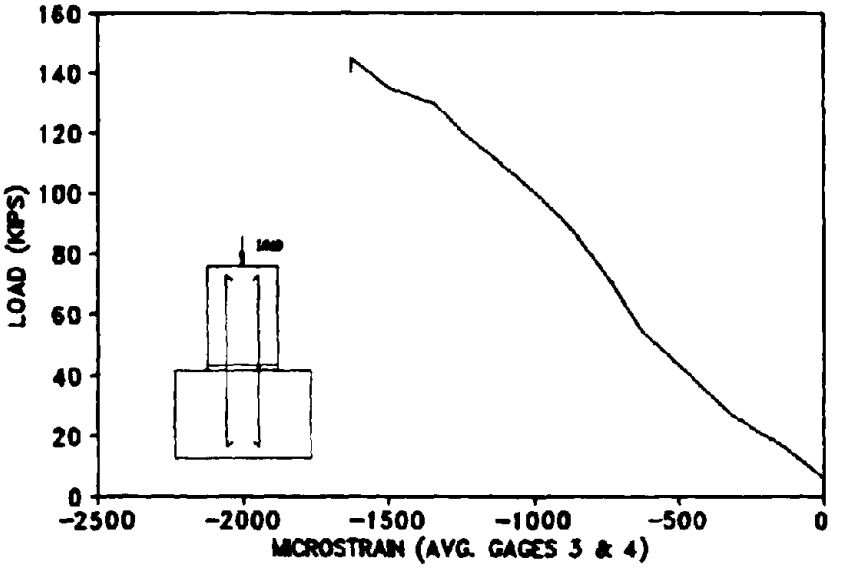

Figure 3-95. NCS3 Load-Strain Response (Average of Gages 3 & 4).

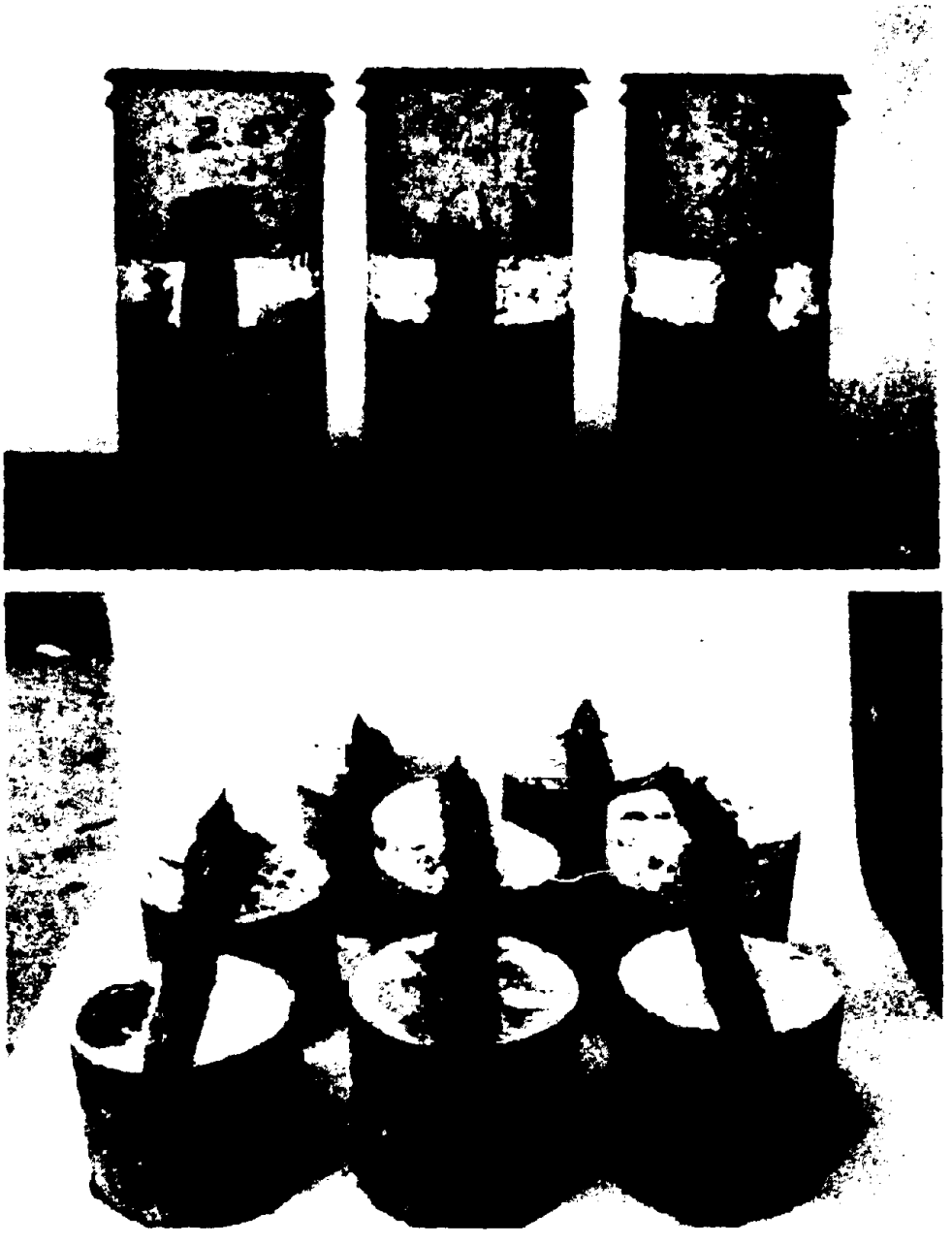

Figure 3-96. Typical Failed Plain Concrete Hinged Specimens.

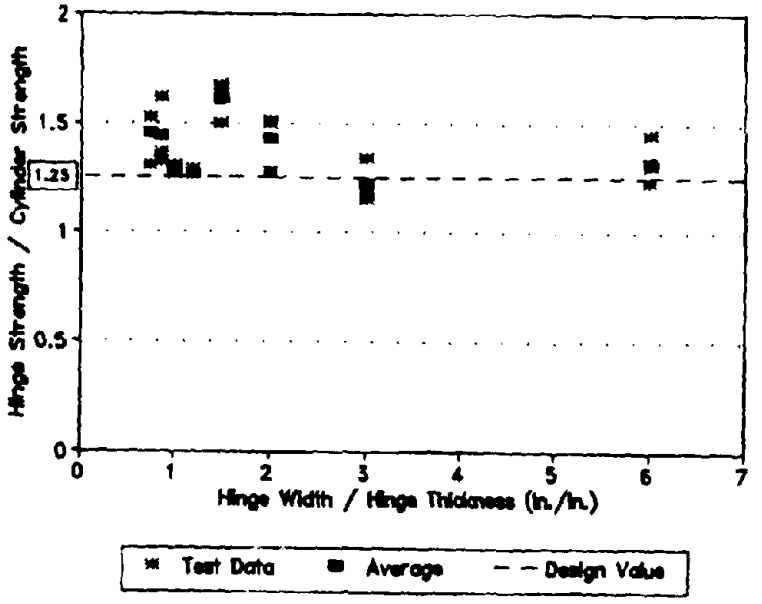

Figure 3-97. Relationship Between Hinge Strength and Hinge Size.

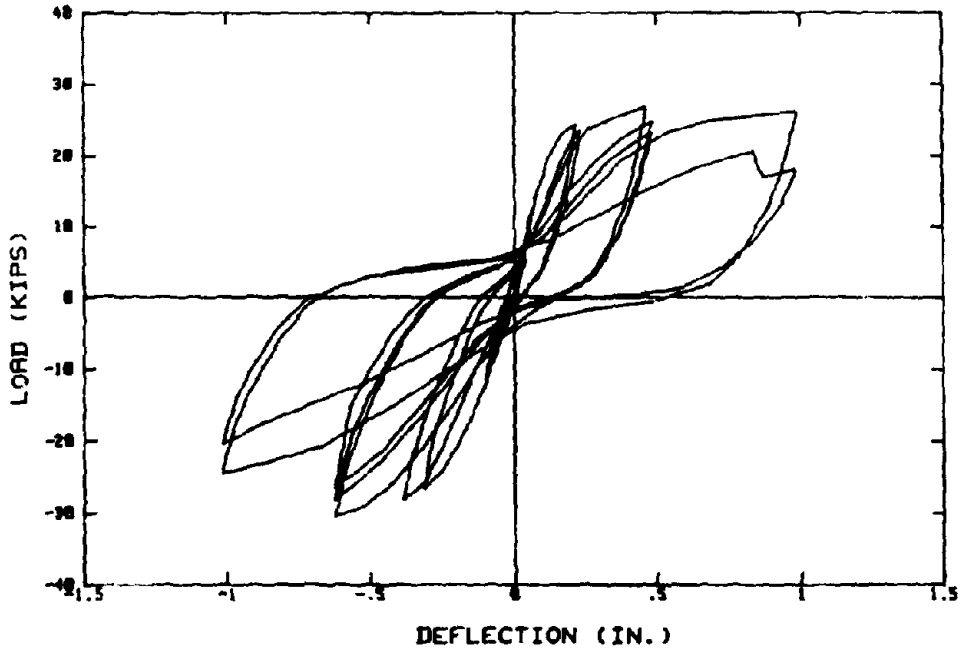

Figure 4-1. SD1C Load-Deflection Response (after Ref. 37).

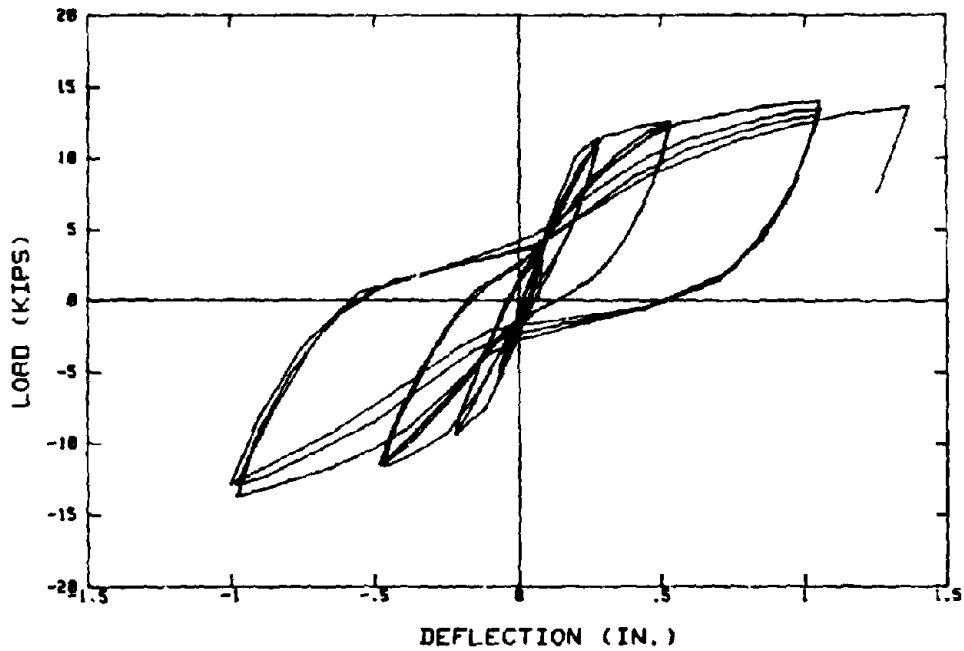

Figure 4-2. SD2C Load-Deflection Response (after Ref. 37).

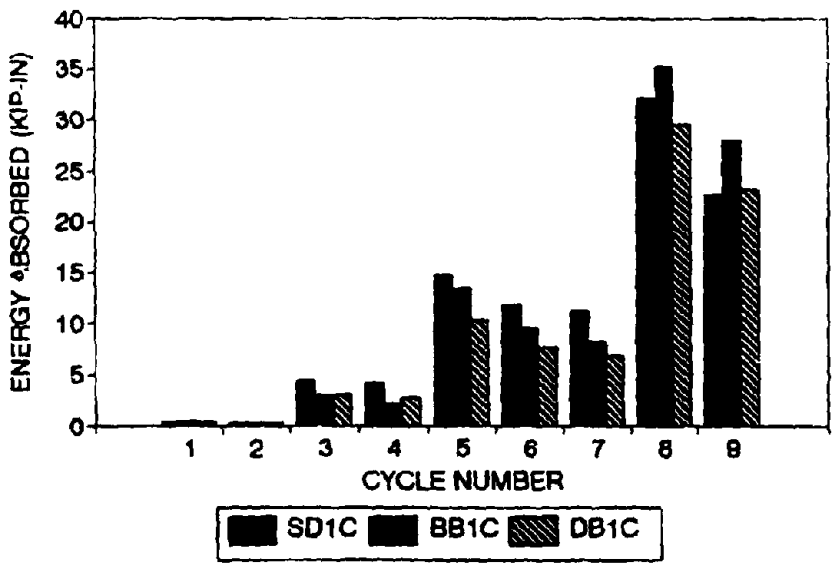

Figure 4-3. Short Column Specimen Energy Absorption Capacity.

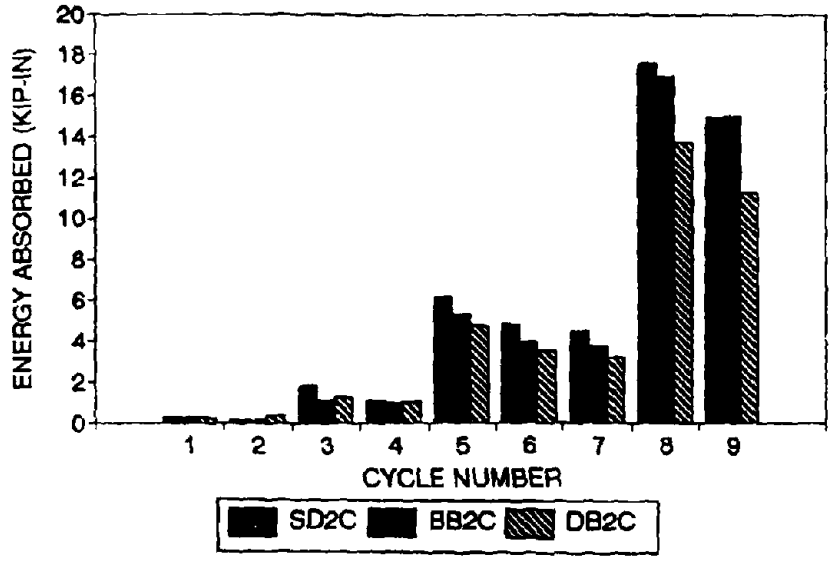

Figure 4-4. Long Column Specimen Energy Absorption Capacity.

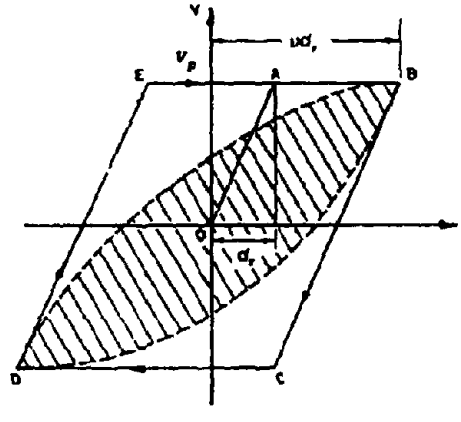

Figure 4-5. Actual and Idealized Elasto-Plastic Hysteresis Curves.

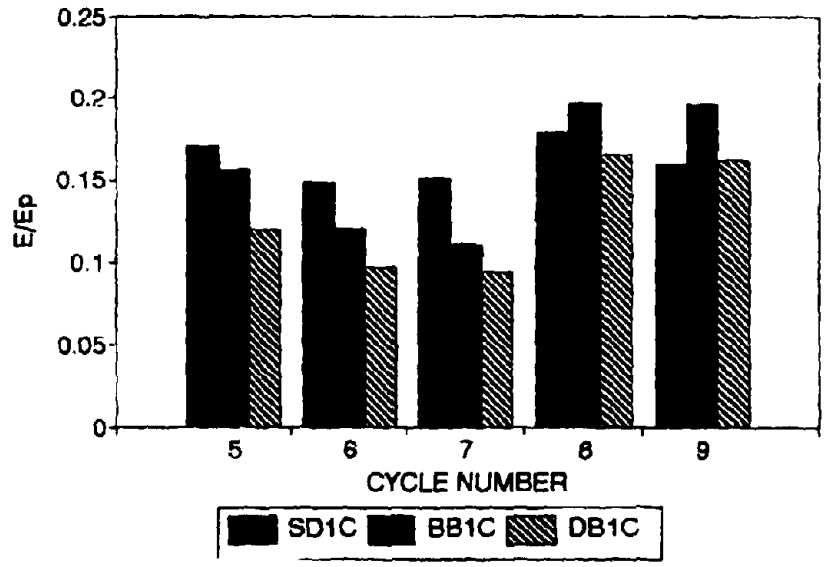

Figure 4-6. Short Column Specimen Relative Energy Absorption Capacity.

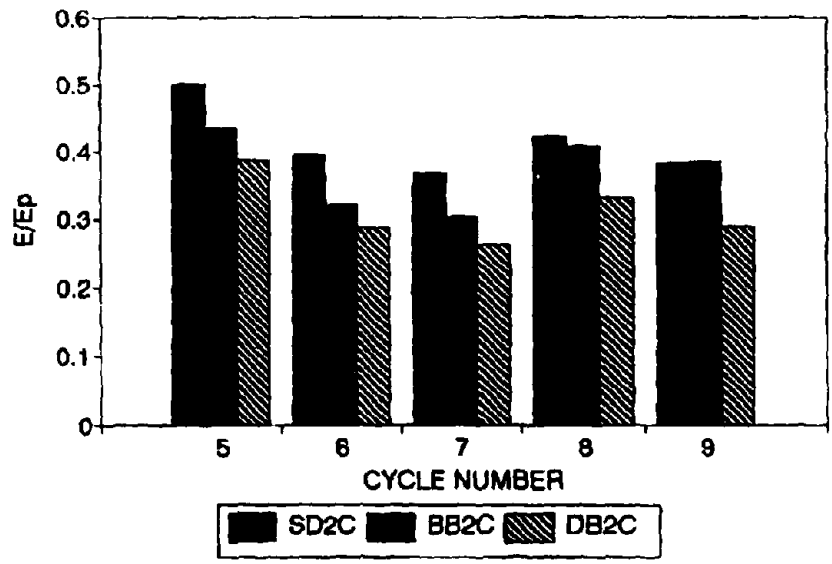

Figure 4-7. Long Column Specimen Relative Energy Absorption Capacity.

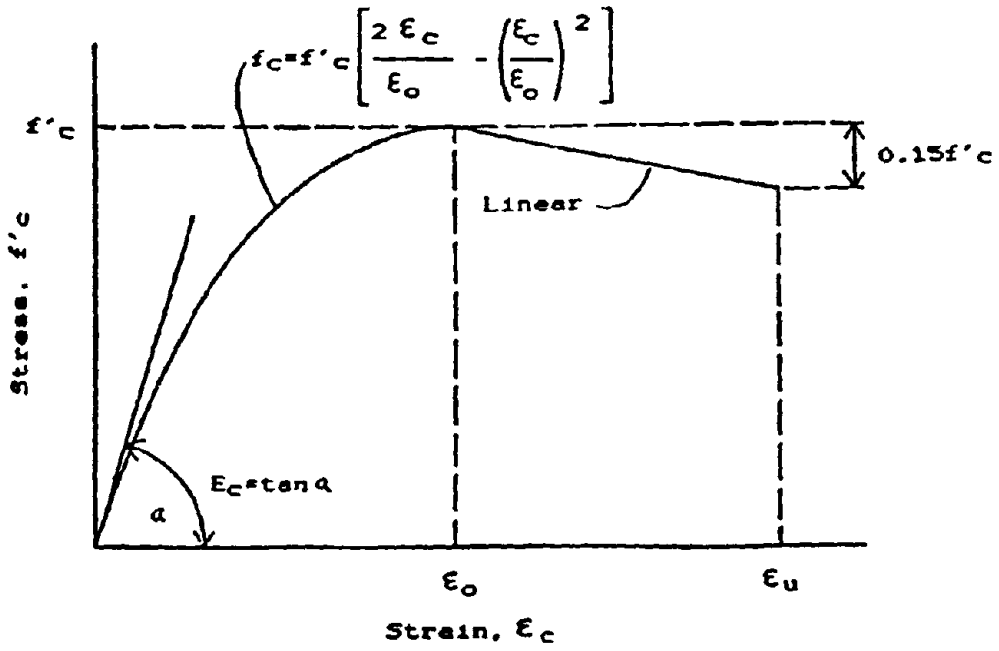

Figure 4-8. Hognestad Stress-Strain Model for Concrete.

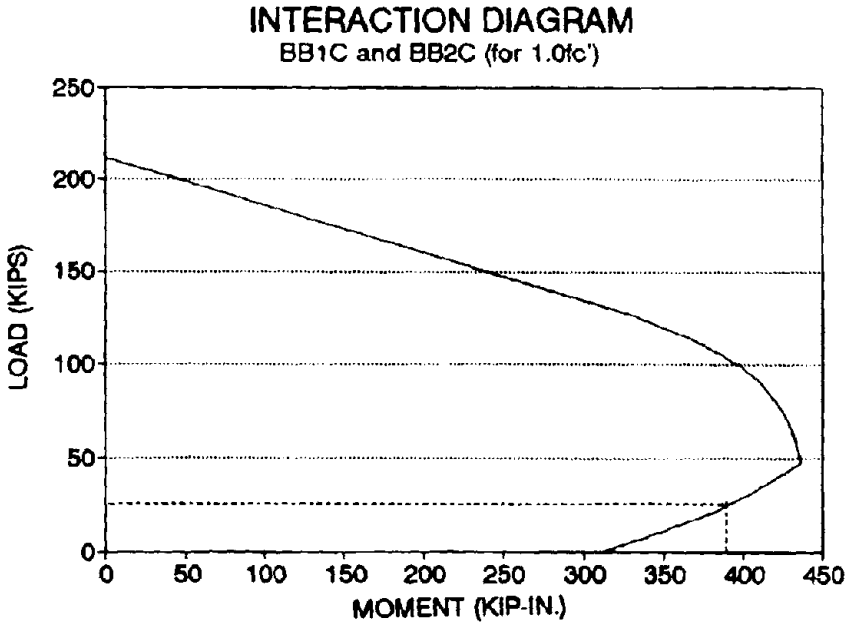

Figure 4-9. Bundled Bar Specimen Interaction Diagram (using f'_c).

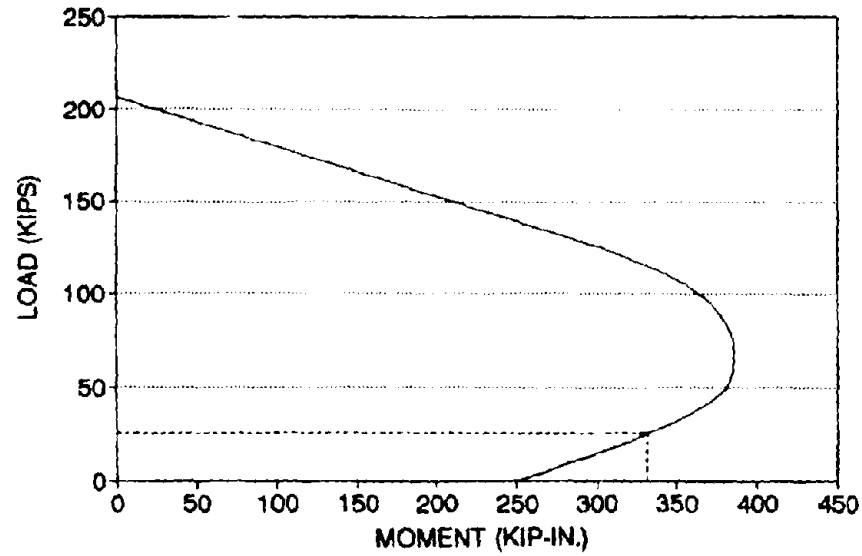

Figure 4-10. Diagonal Bar Specimen Interaction Diagram (using f'_c).

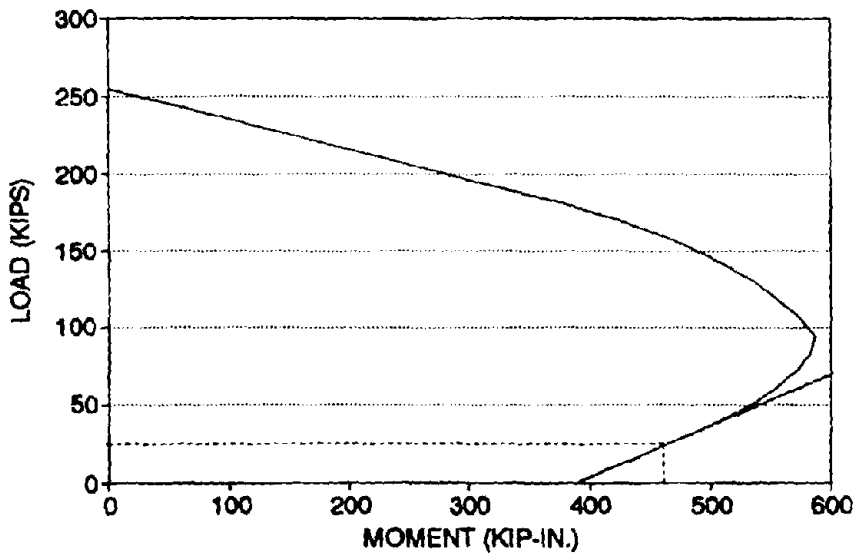

Figure 4-11. Bundled Bar Specimen Interaction Diagram (using $1.25f'_c$).

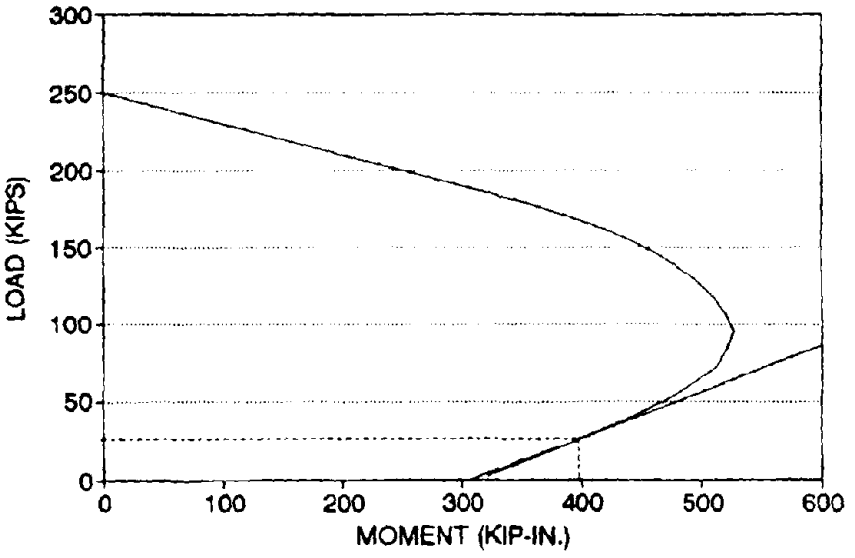

Figure 4-12. Diagonal Bar Specimen Interaction Diagram (using $1.25f'_c$).

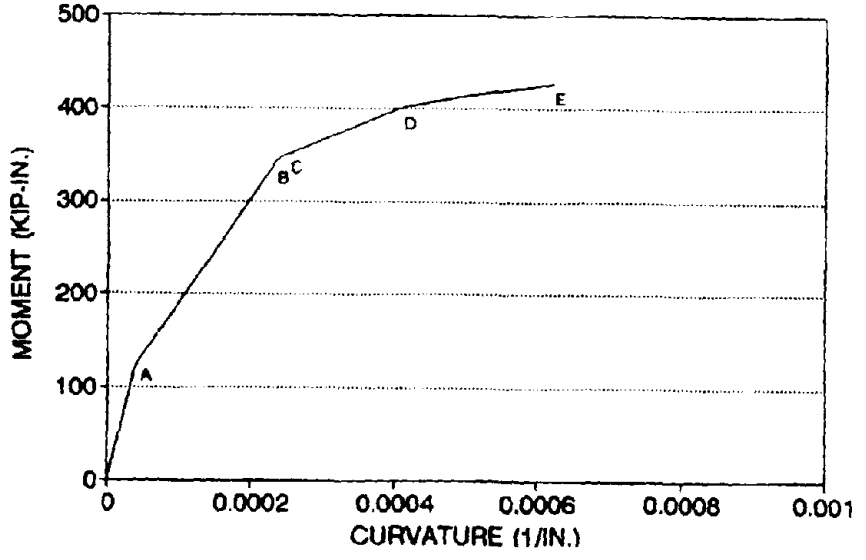

Figure 4-13. Bundled Bar Specimen Moment vs. Curvature (using f'_c).

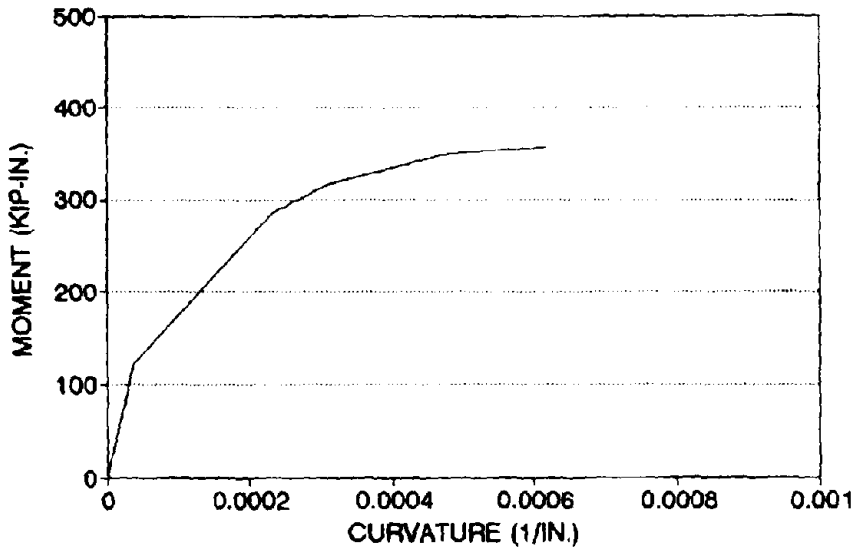

Figure 4-14. Diagonal Bar Specimen Moment vs. Curvature (using f'_c).

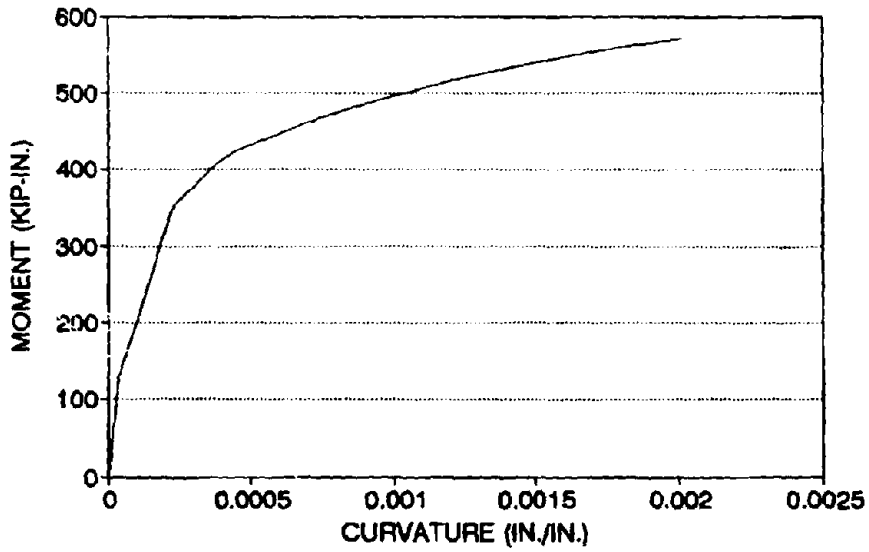

Figure 4-15. Bundled Bar Specimen Moment vs. Curvature (using $1.25f'_c$).

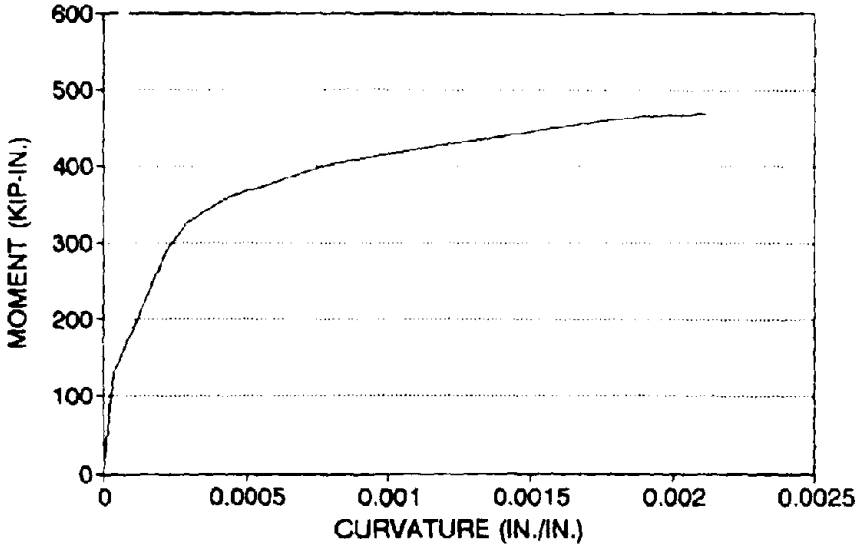

Figure 4-16. Diagonal Bar Specimen Moment vs. Curvature (using $1.25f'_c$).

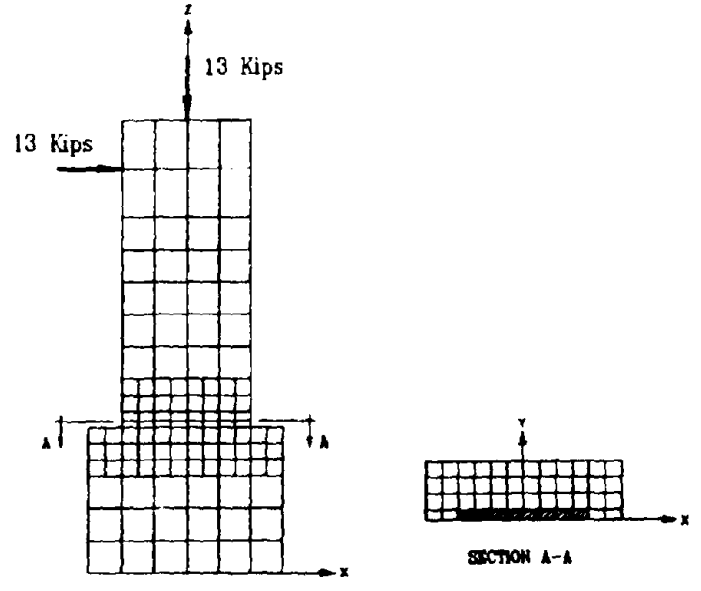

Figure 5-1. Long Column Specimen Finite Element Mesh.

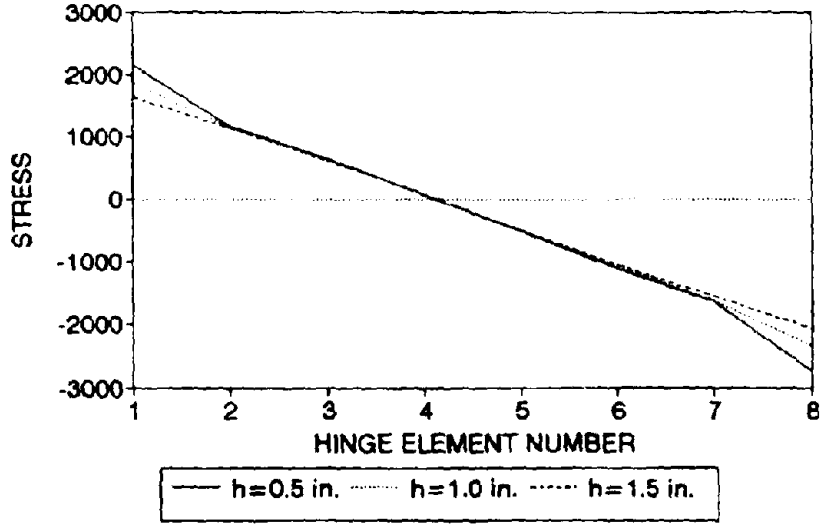

Figure 5-2. Column Specimen Hinge *x* Normal Stress Distribution.

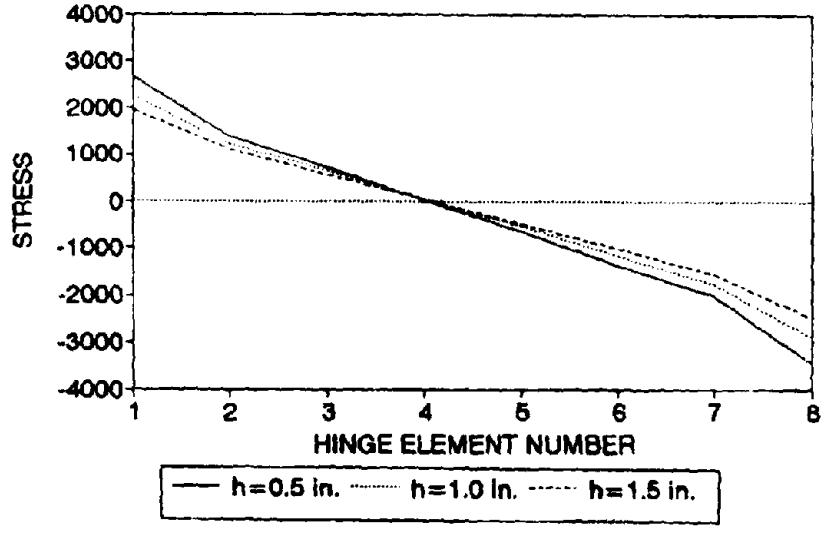

Figure 5-3. Column Specimen Hinge *y* Normal Stress Distribution.

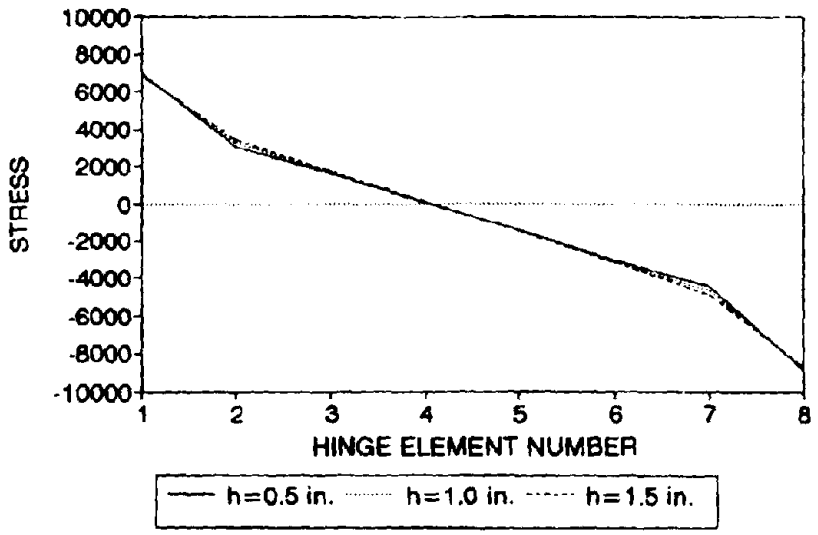

Figure 5-4. Column Specimen Hinge *z* Normal Stress Distribution.

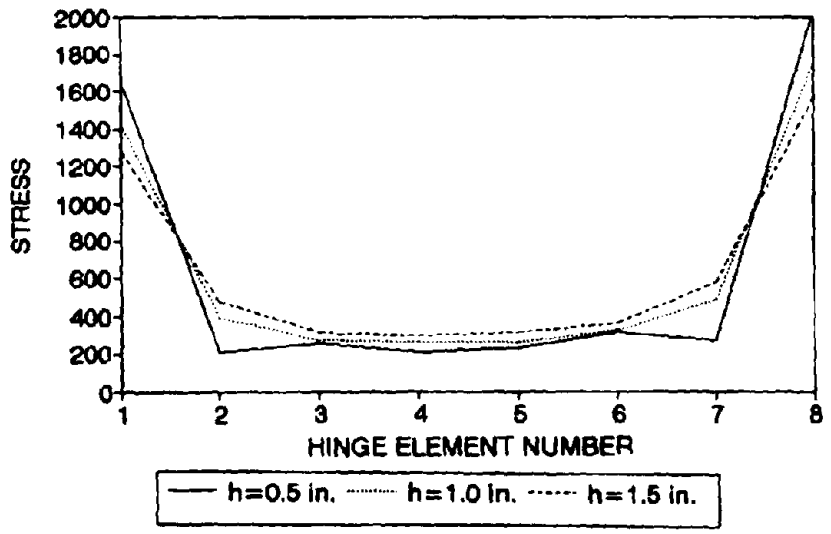

Figure 5-5. Column Specimen Hinge *x-z* Shear Stress Distribution.

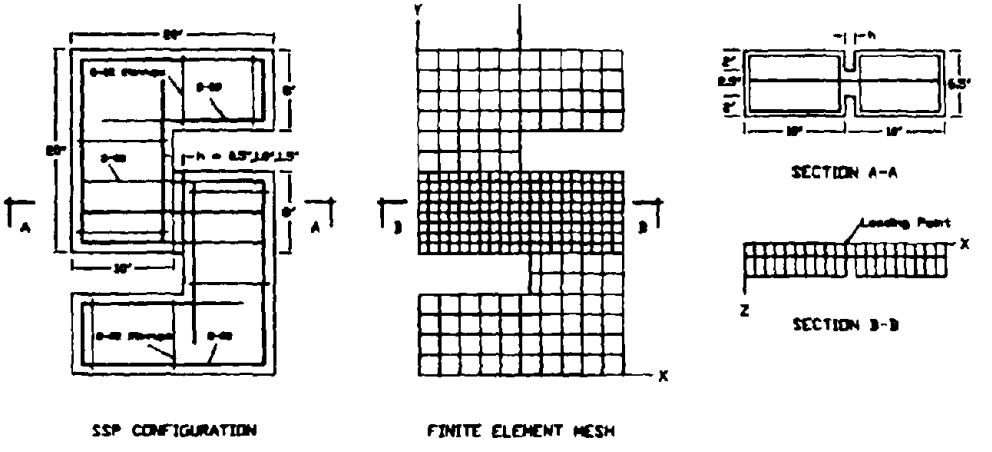

Figure 5-6. Shear Specimen Finite Element Mesh.

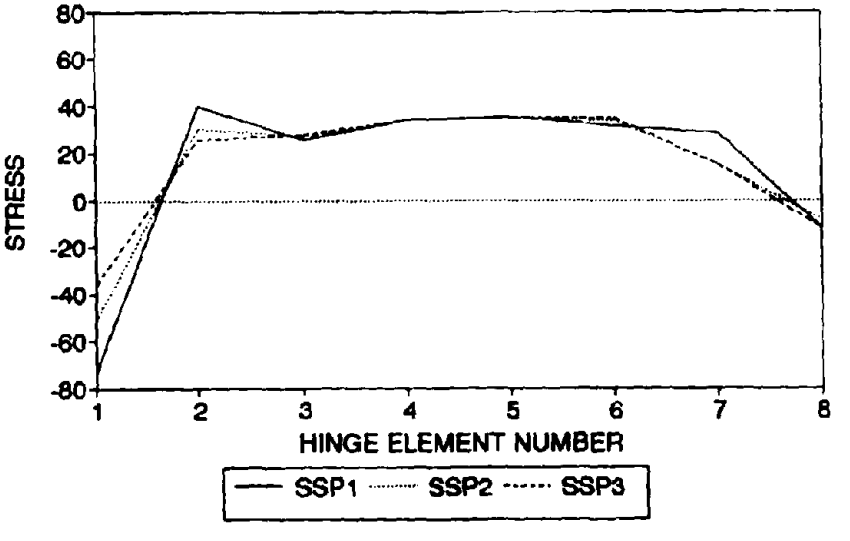

Figure 5-7. Shear Specimen Hinge *x* Normal Stress Distribution .

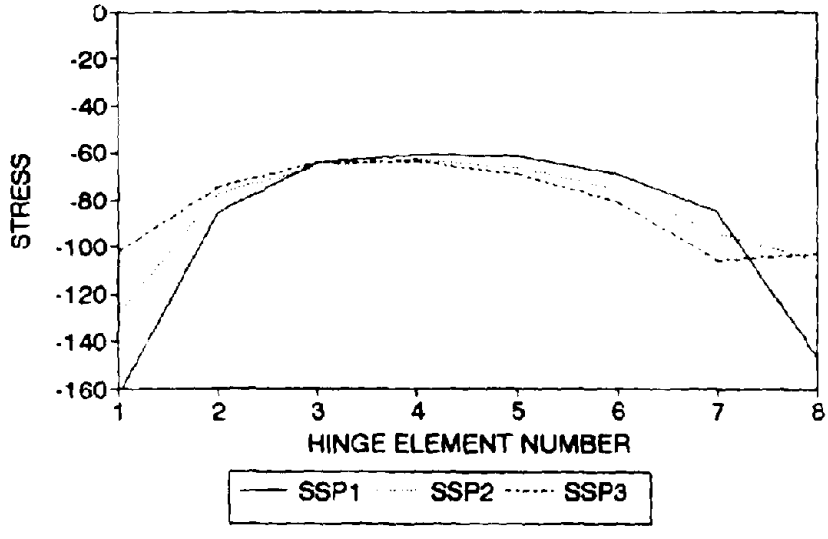

Figure 5-8. Shear Specimen Hinge *y* Normal Stress Distribution .

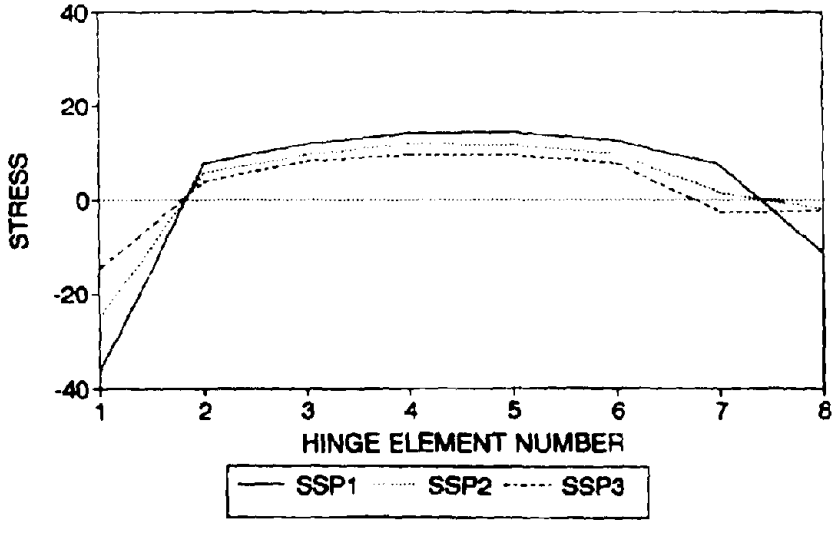

Figure 5-9. Shear Specimen Hinge *z* Normal Stress Distribution .

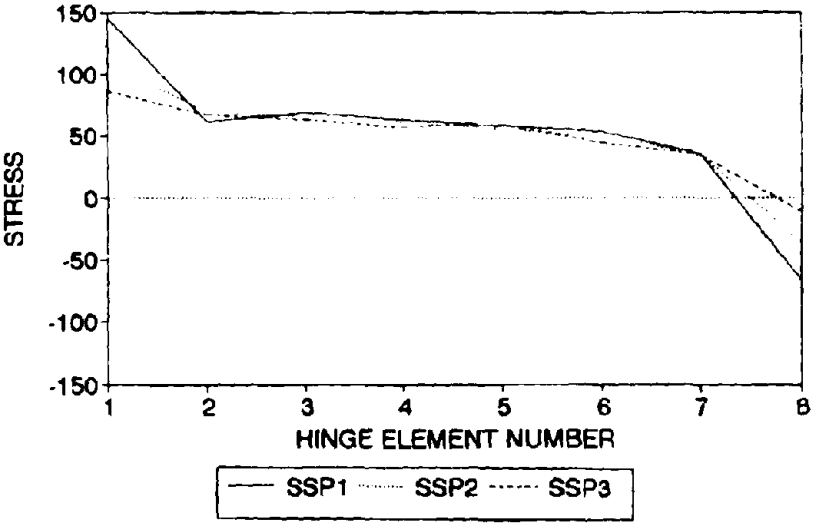

Figure 5-10. Shear Specimen Hinge *x-y* Shear Stress Distribution .

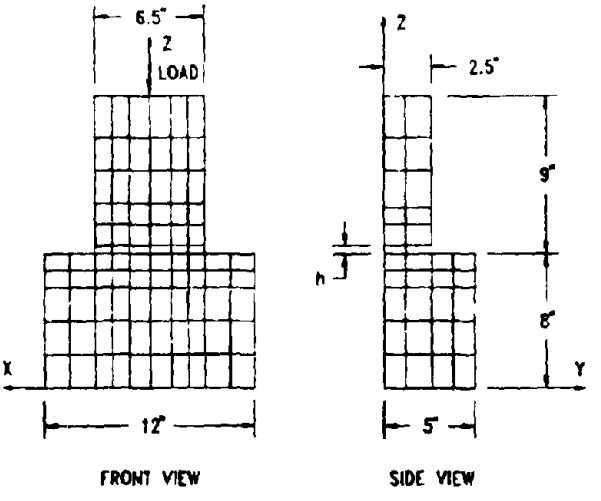

Figure 5-11. Compression Specimen Finite Element Mesh.

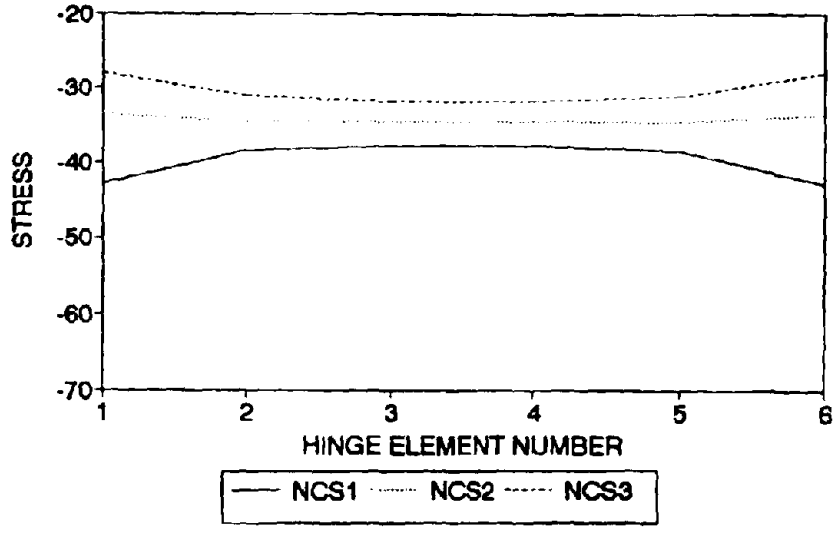

Figure 5-12. Compression Specimen Hinge *x* Normal Stress Distribution.

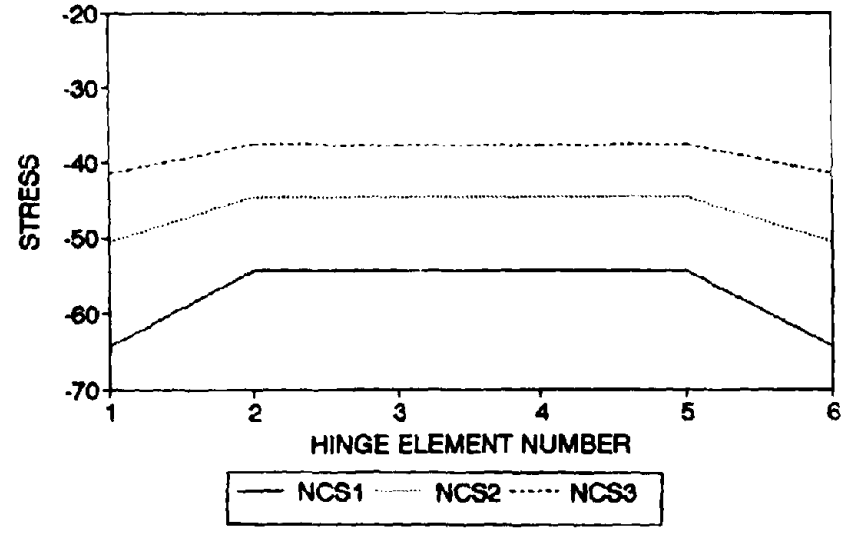

Figure 5-13. Compression Specimen Hinge *y* Normal Stress Distribution.

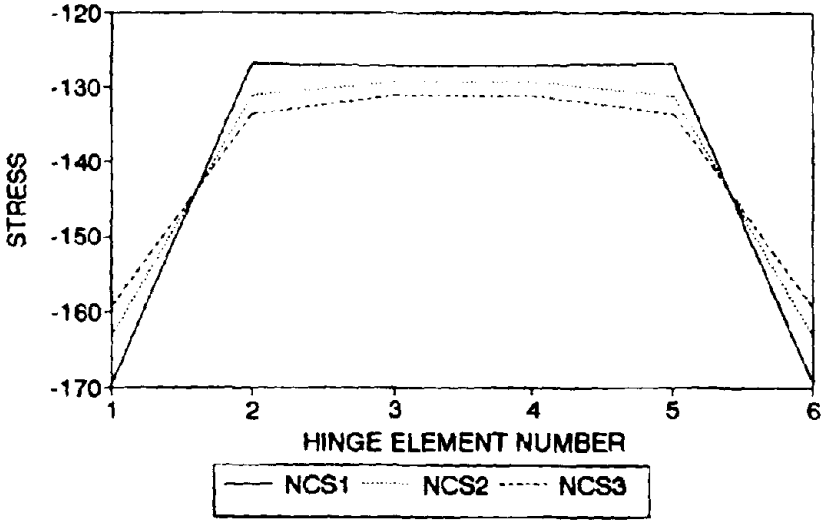

Figure 5-14. Compression Specimen Hinge *z* Normal Stress Distribution .

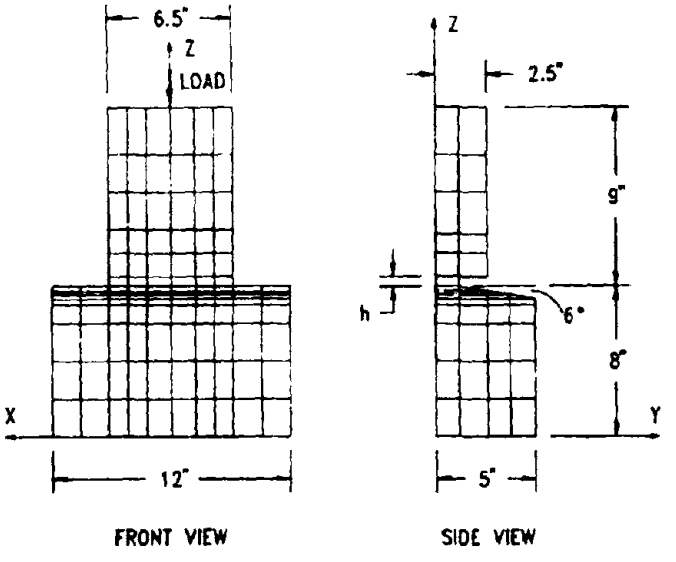

Figure 5-15. Compression Specimen (6° Footing Slope) Finite Element Mesh.

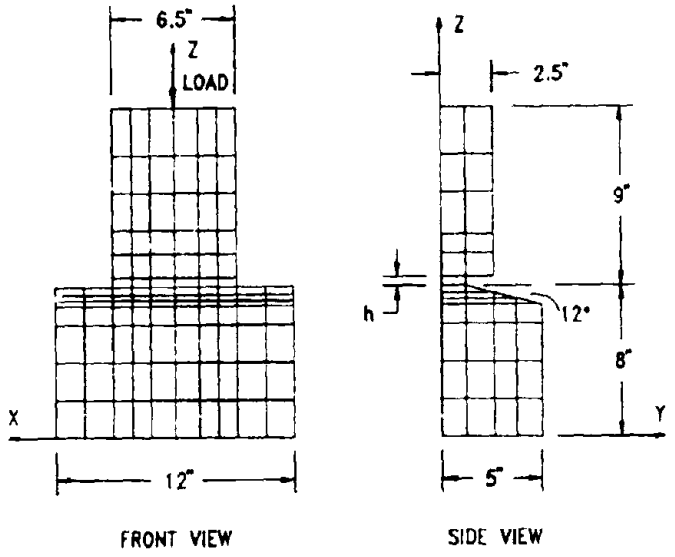

Figure 5-16. Compression Specimen (12° Footing Slope) Finite Element Mesh.

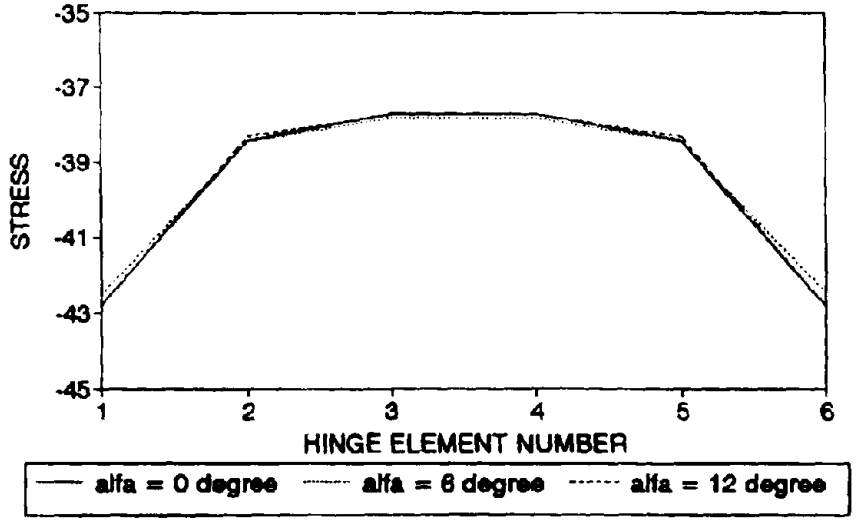

Figure 5-17. Sloped-Footing Compression Specimen Hinge *x* Normal Stress.

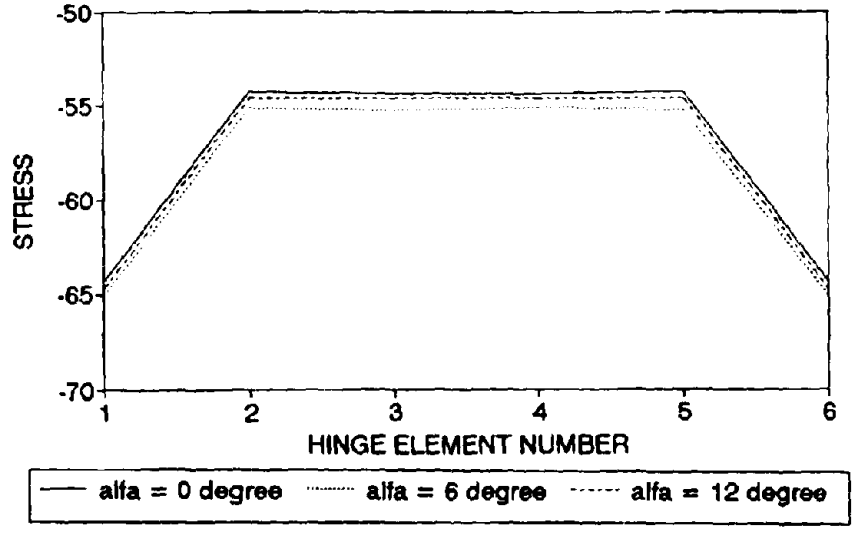

Figure 5-18. Sloped-Footing Compression Specimen Hinge *y* Normal Stress.

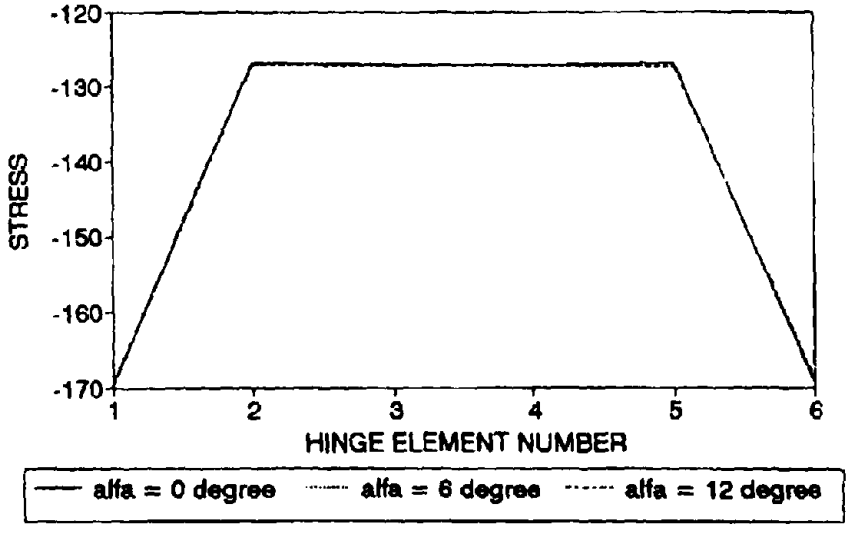

Figure 5-19. Sloped-Footing Compression Specimen Hinge *z* Normal Stress.

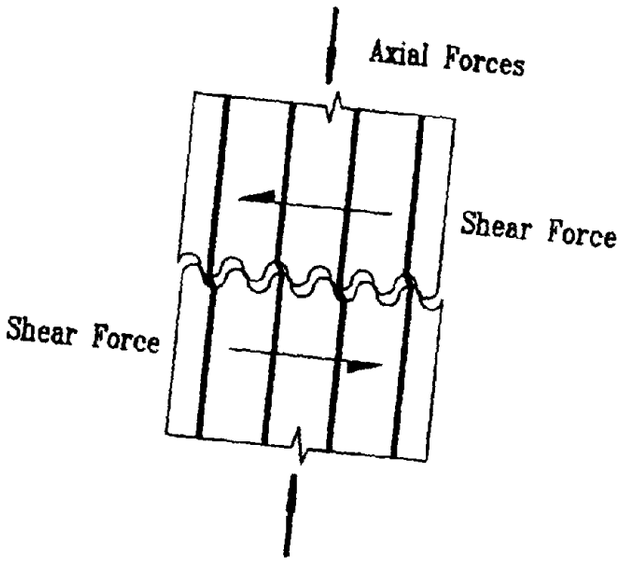

Figure 6-1. Shear Friction Mechanism.

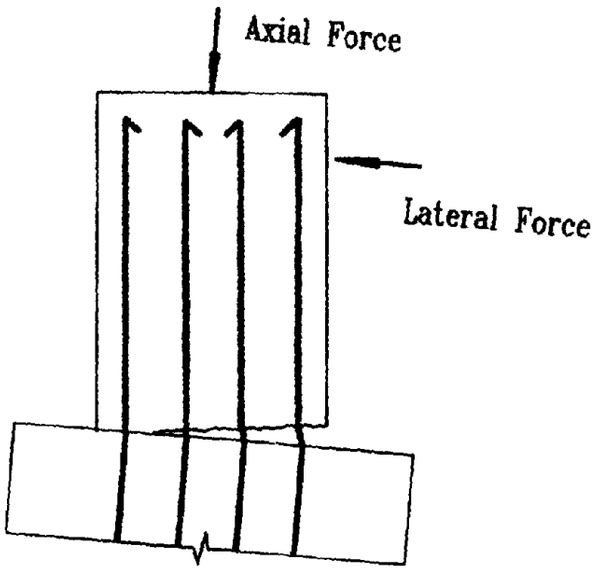

Figure 6-2. One-Way Hinge Failure Mechanism.

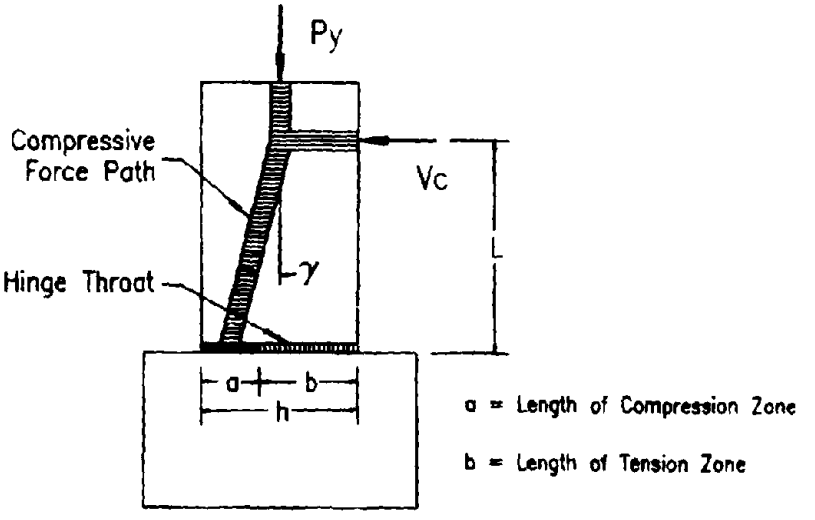

Figure 6-3. Compressive Force Path for a Hinge Column.

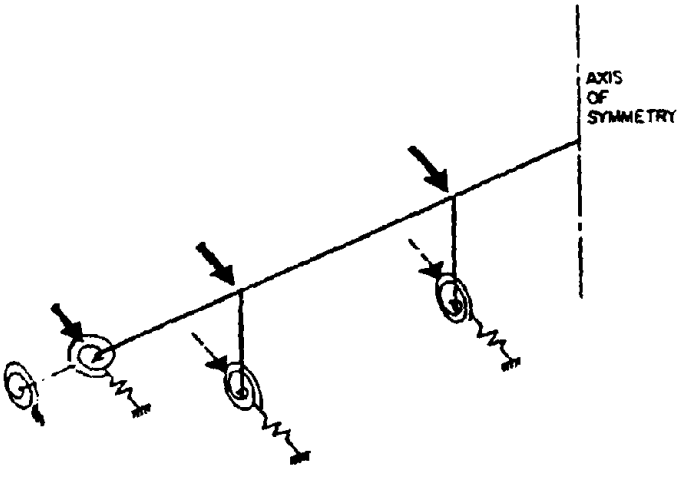

Figure 7-1. Schematic View of One-Half Bridge System (after Ref. 18).

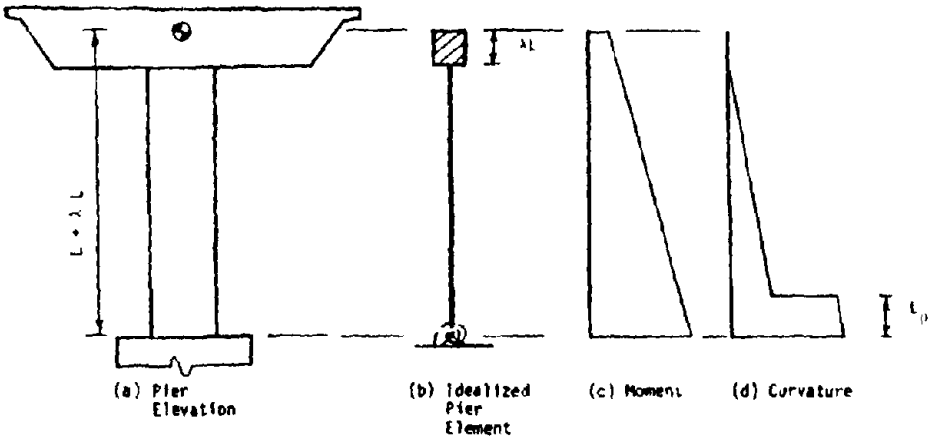

Figure 7-2. Pier Element (after Ref. 18).

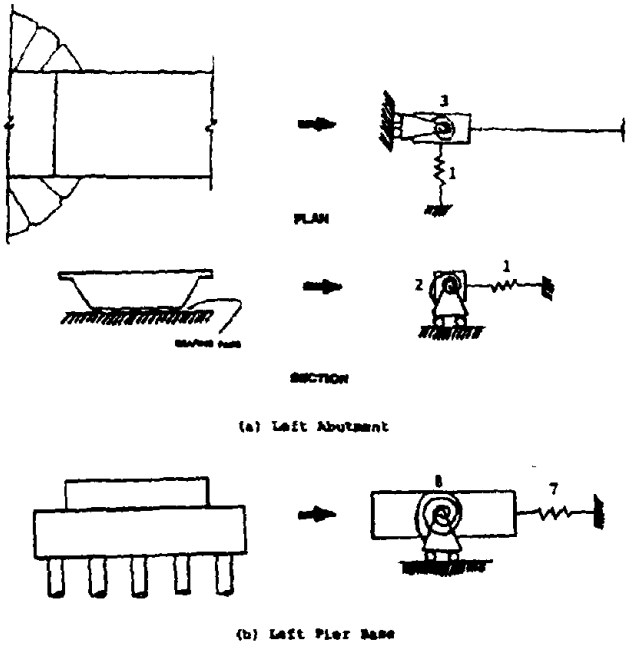

Figure 7-3. Boundary Spring Numbering (after Ref. 18).

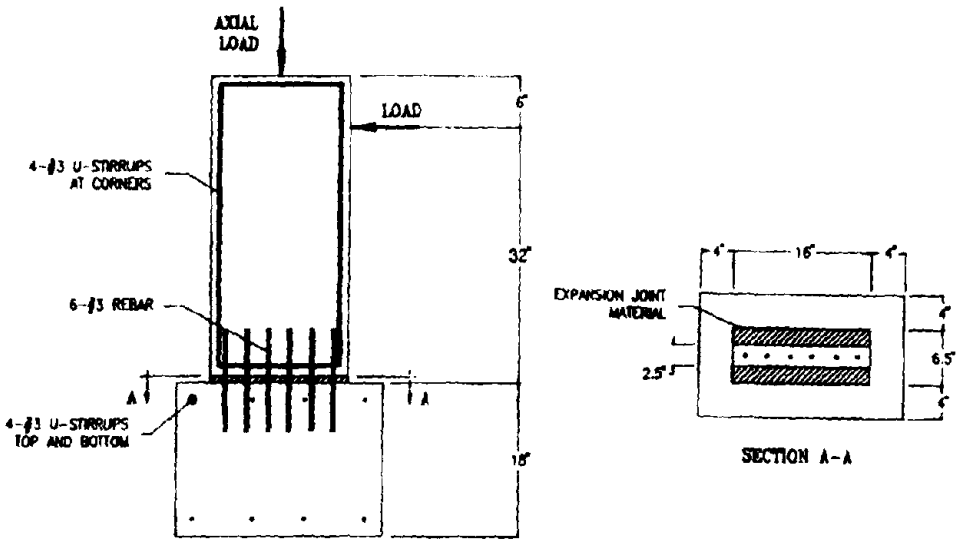

Figure 8-1. Details of Insufficient Development Length Specimen.

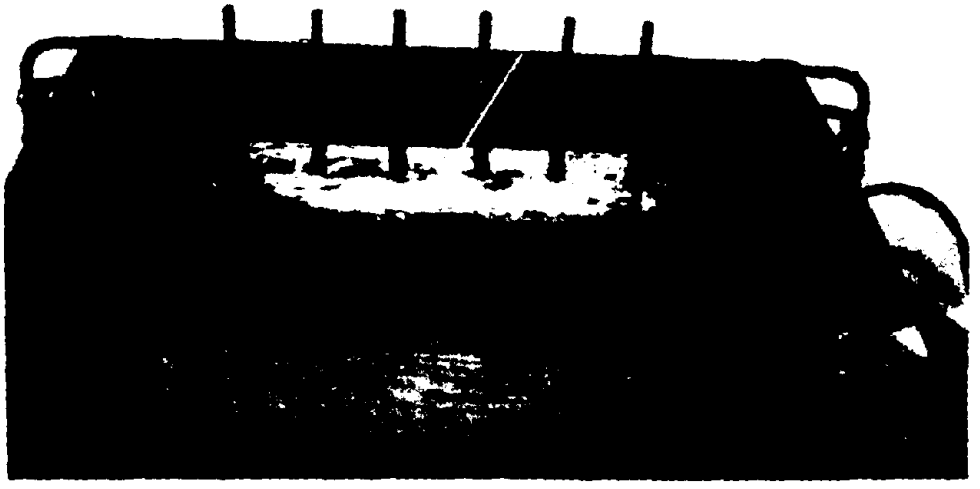

Figure 8-2. Insufficient Development Length Specimen before Pouring the Column.

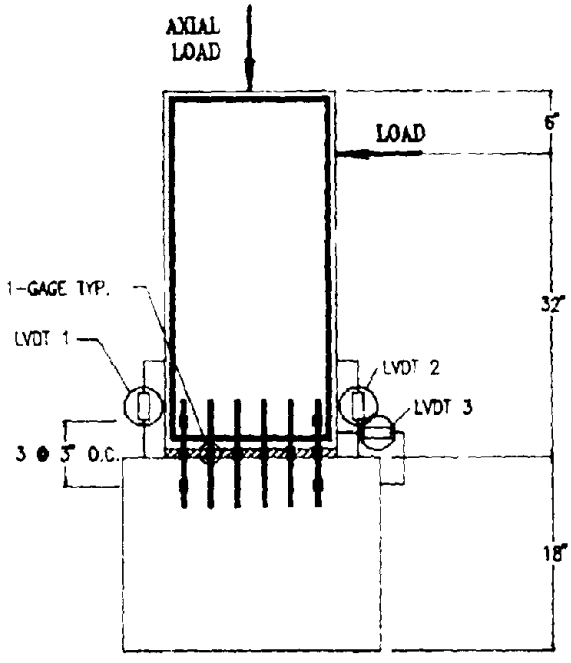

Figure 8-3. Insufficient Development Length Specimen Instrumentation Details.

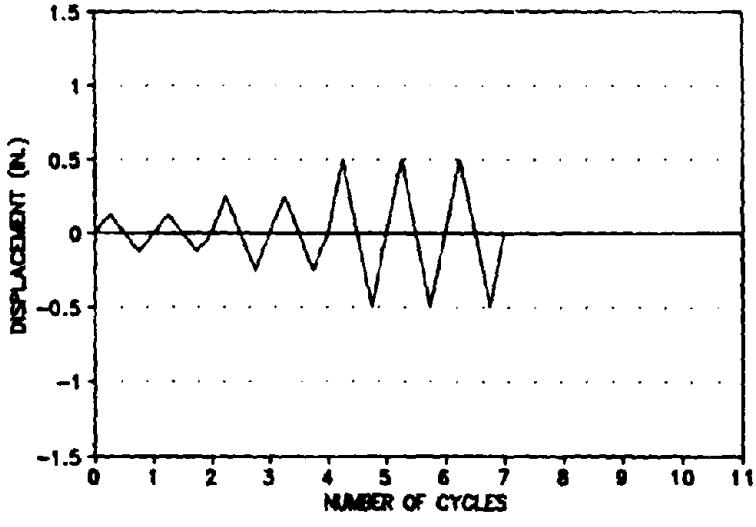

Figure 8-4. Original Specimen Lateral Displacement History.

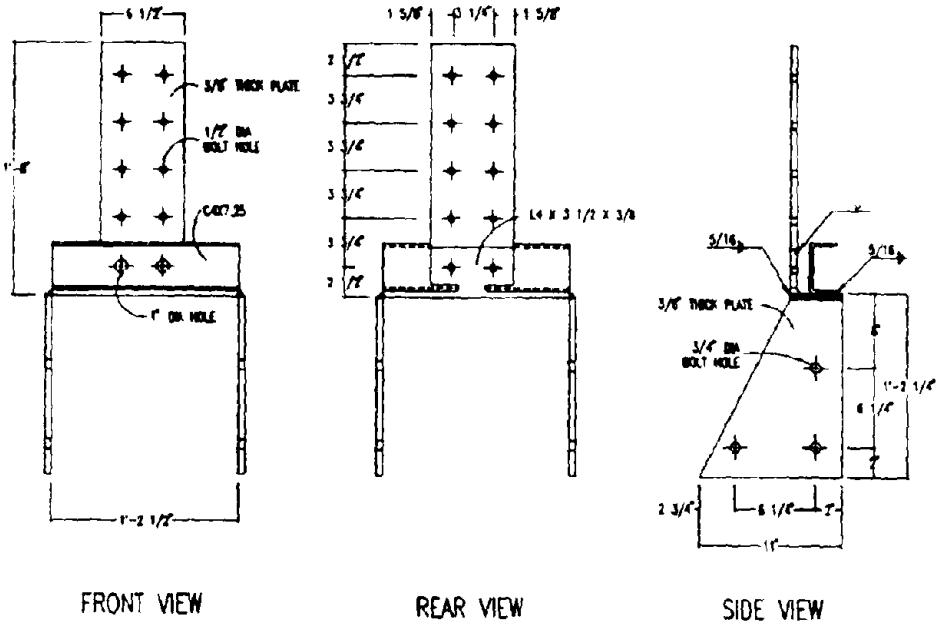

Figure 8-5. Details of Retrofit Steel Jacket.

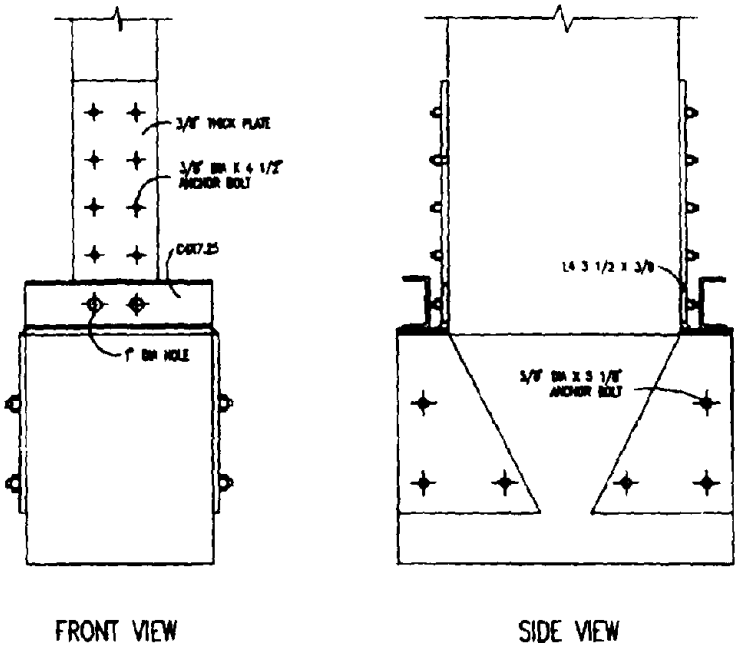

Figure 8-6. Column Repaired with Retrofit Steel Jacket.

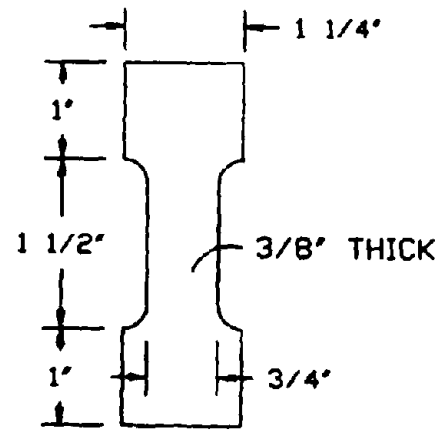

Figure 8-7. Tensile Strength Test Coupon.

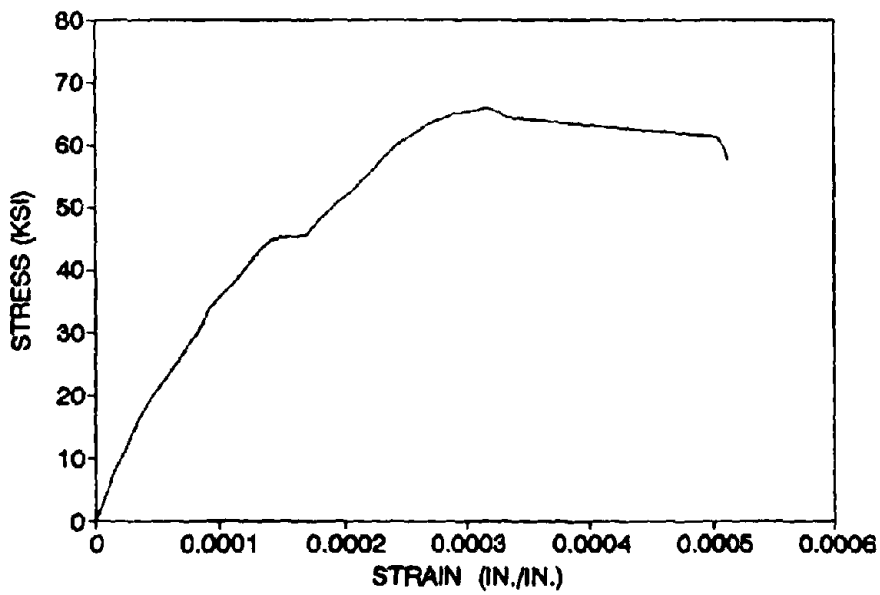

Figure 8-8. Steel Stress-Strain Curve.

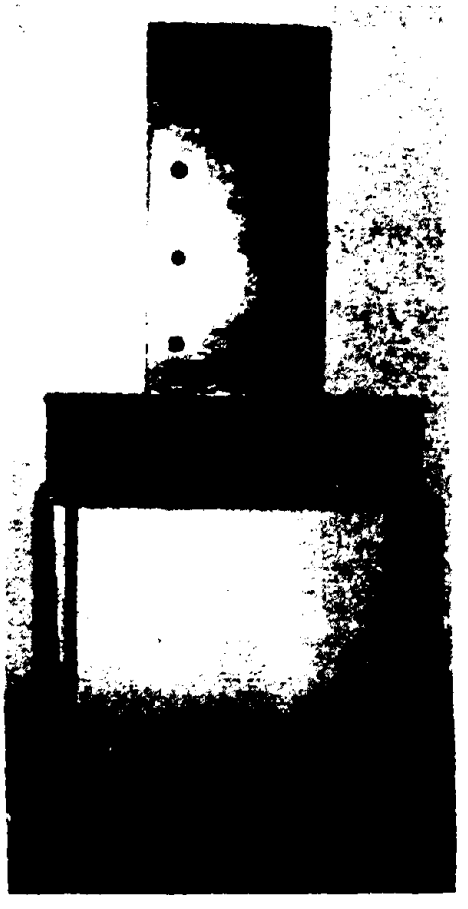

Figure 8-9. Front View of Retrofit Steel Jacket.

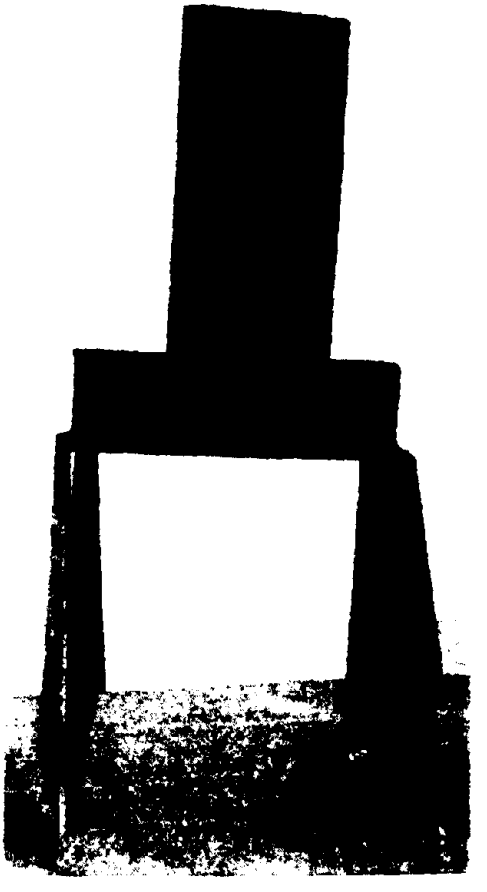

Figure 8-10. Back View of Retrofit Steel Jacket.

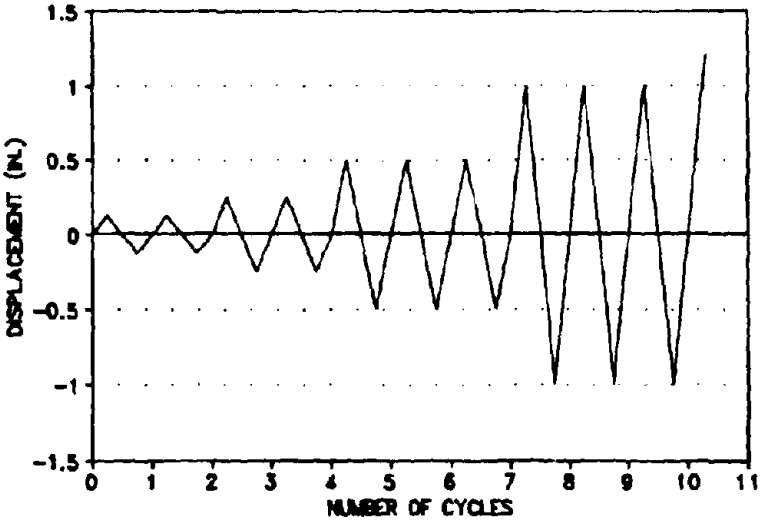

Figure 8-11. Repaired Specimen Lateral Displacement History.

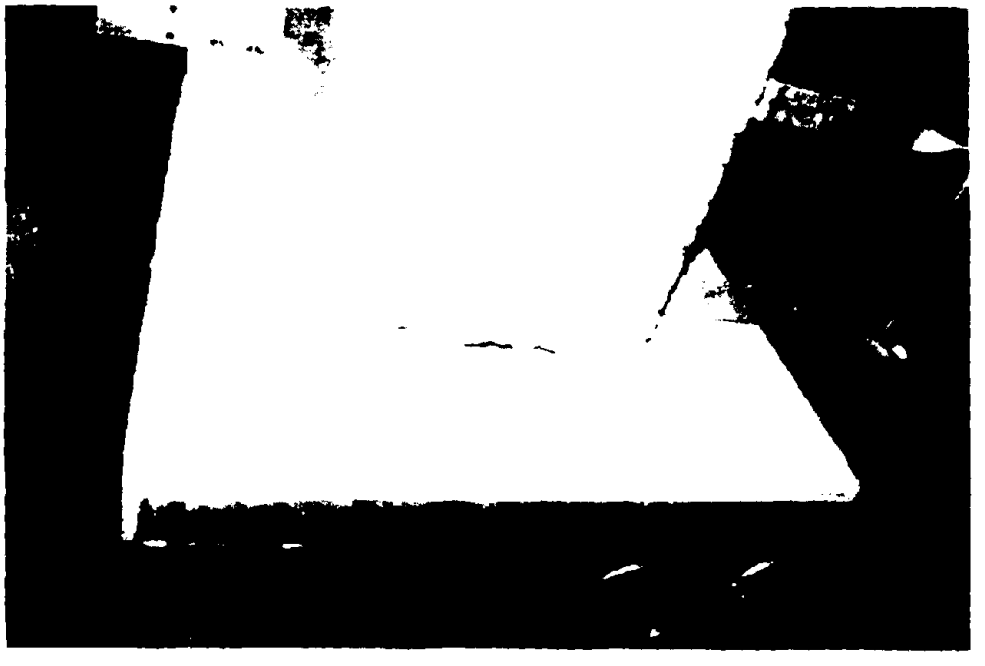

Figure 8-12. Original Specimen after Testing (1).

Figure 8-13. Original Specimen after Testing (2).

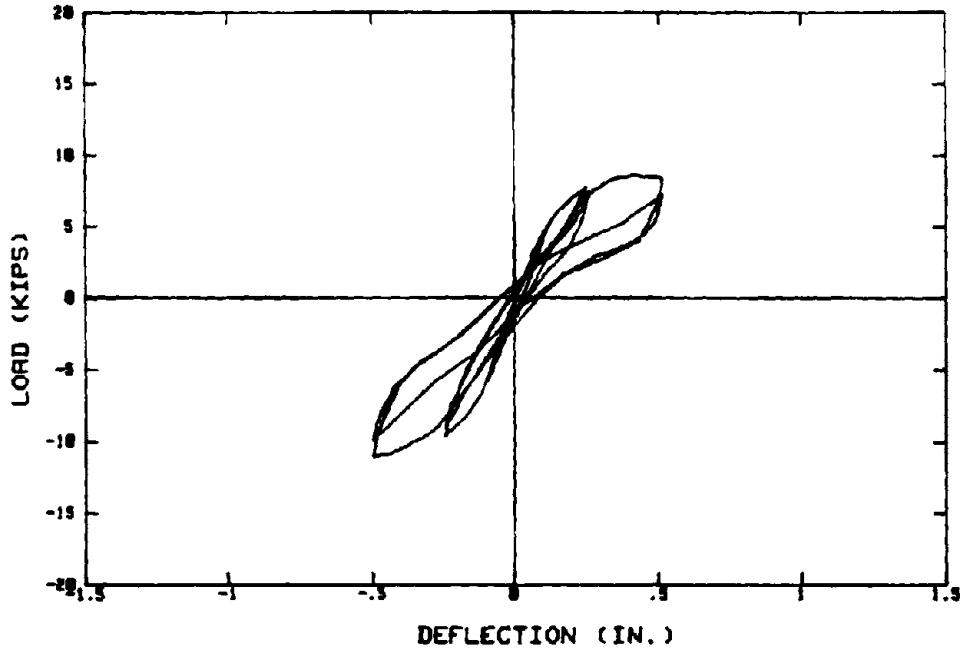

Figure 8-14. Original Specimen Load-Deflection Response.

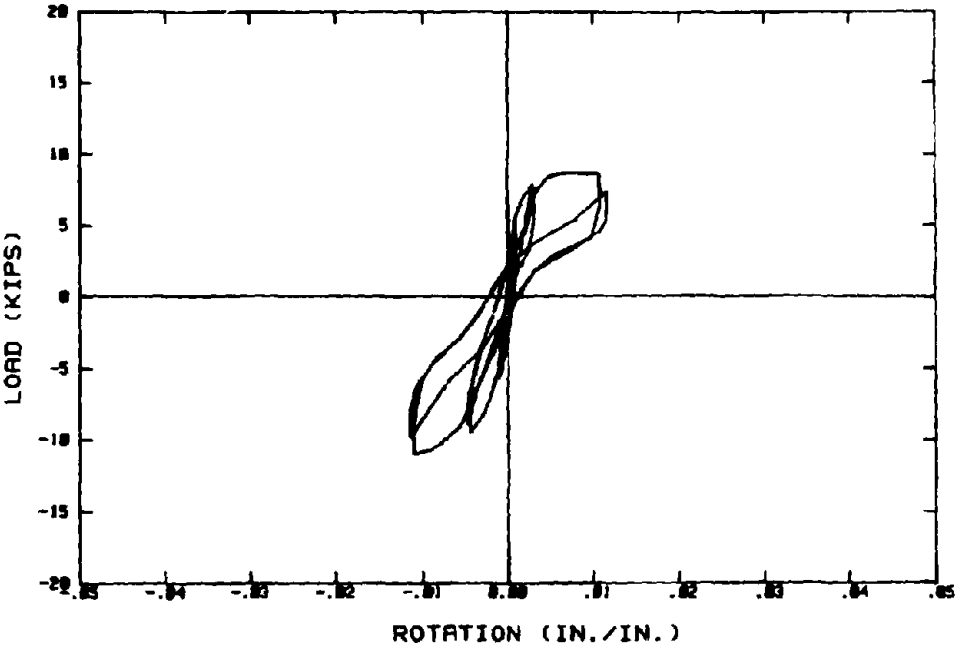

Figure 8-15. Original Specimen Load-Rotation Response.

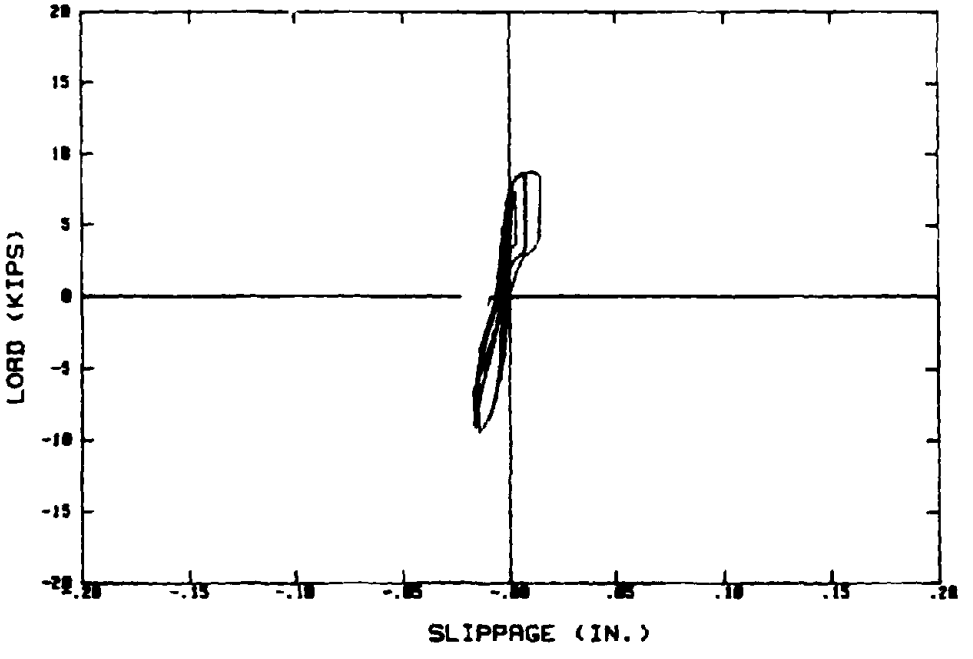

Figure 8-16. Original Specimen Load-Slippage Response.

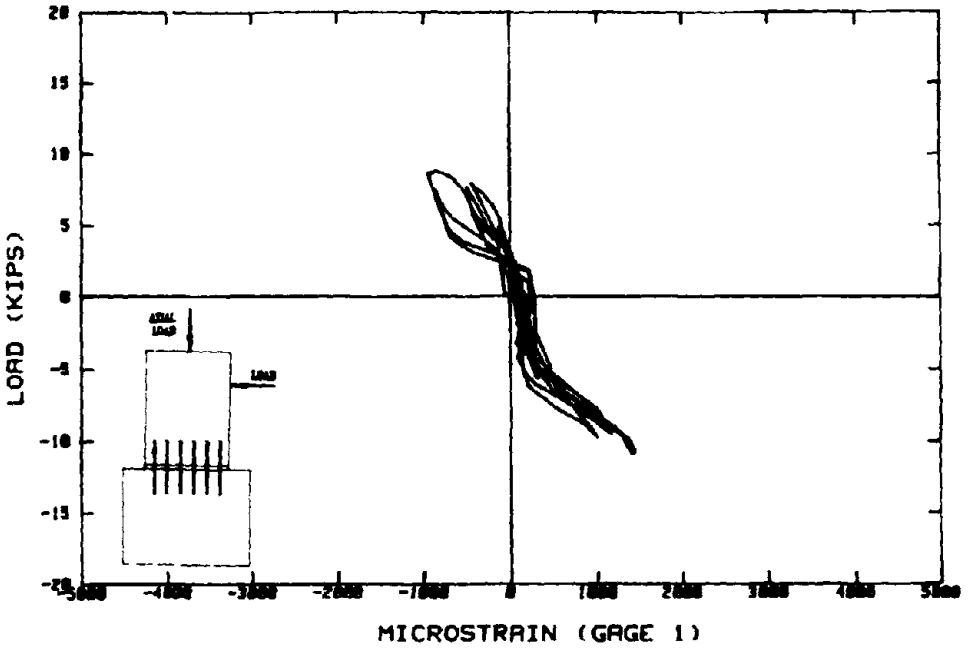

Figure 8-17. Original Specimen Load-Strain Response (Gage 1).

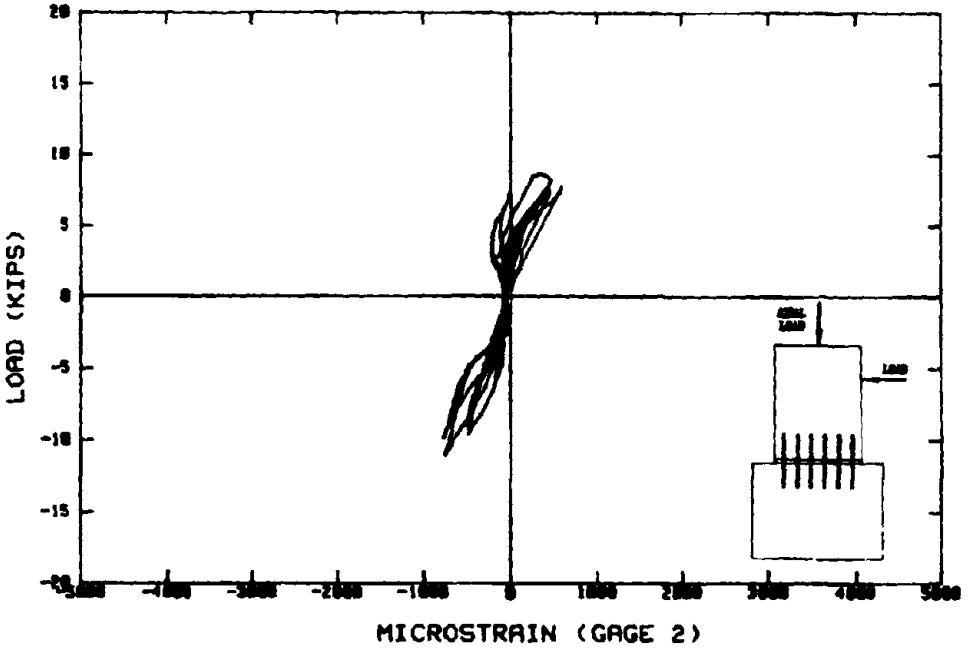

Figure 8-18. Original Specimen Load-Strain Response (Gage 2).

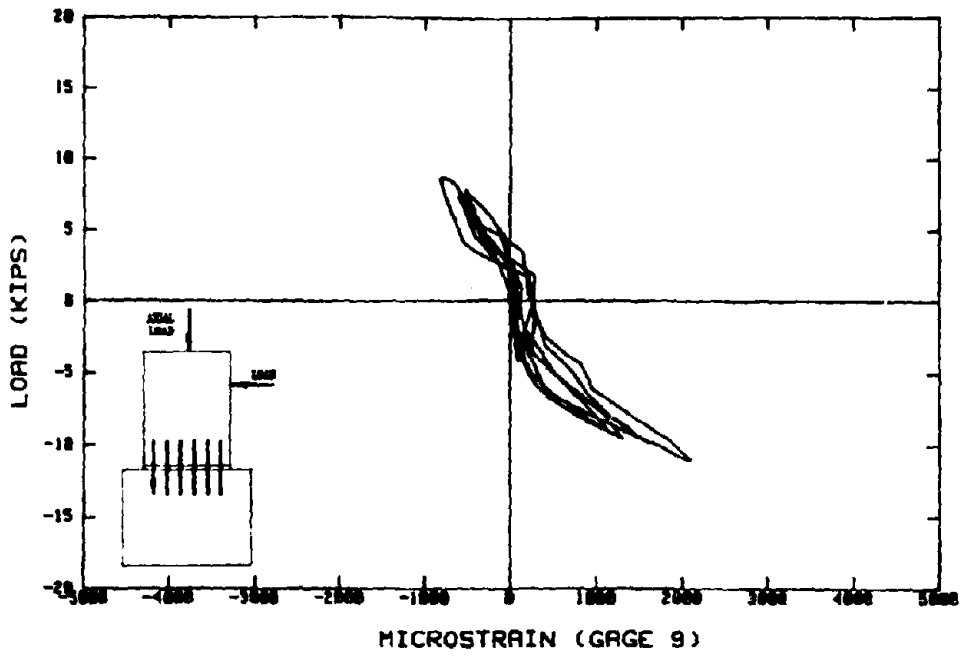

Figure 8-19. Original Specimen Load-Strain Response (Gage 9).

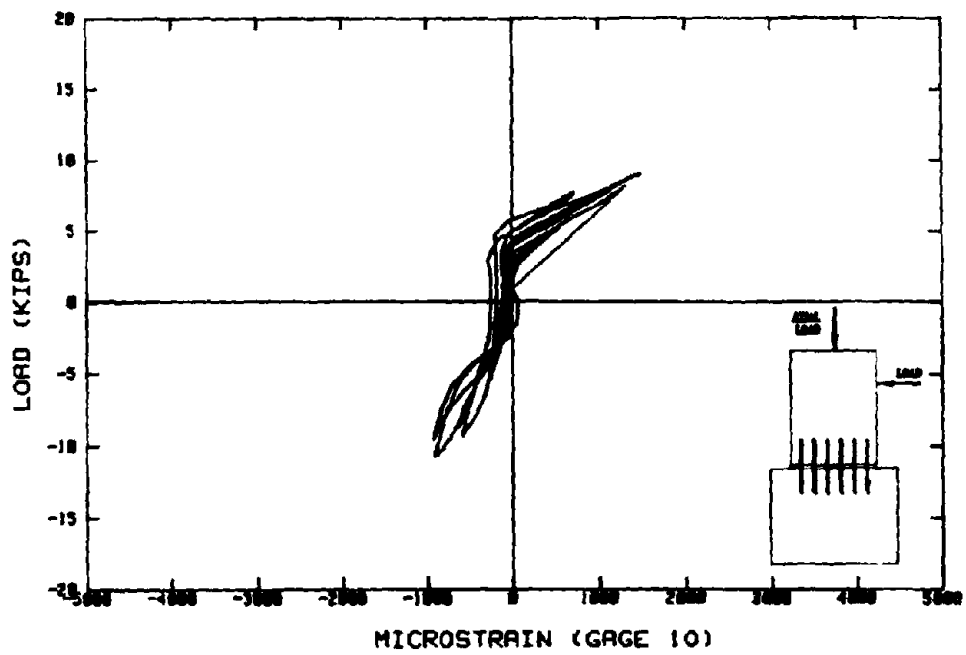

Figure 8-20. Original Specimen Load-Strain Response (Gage 10).

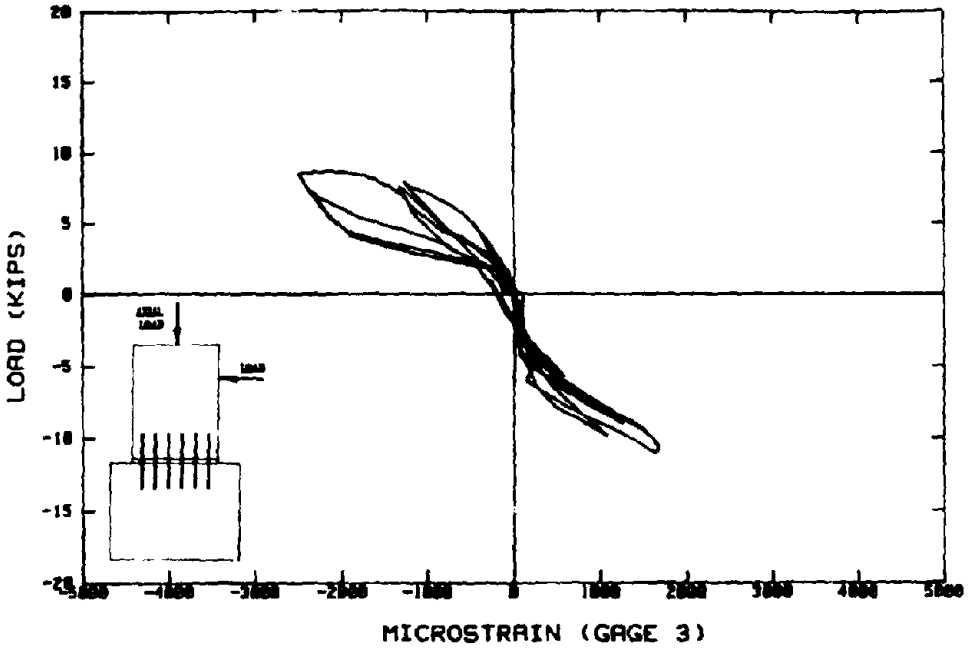

Figure 8-21. Original Specimen Load-Strain Response (Gage 3).

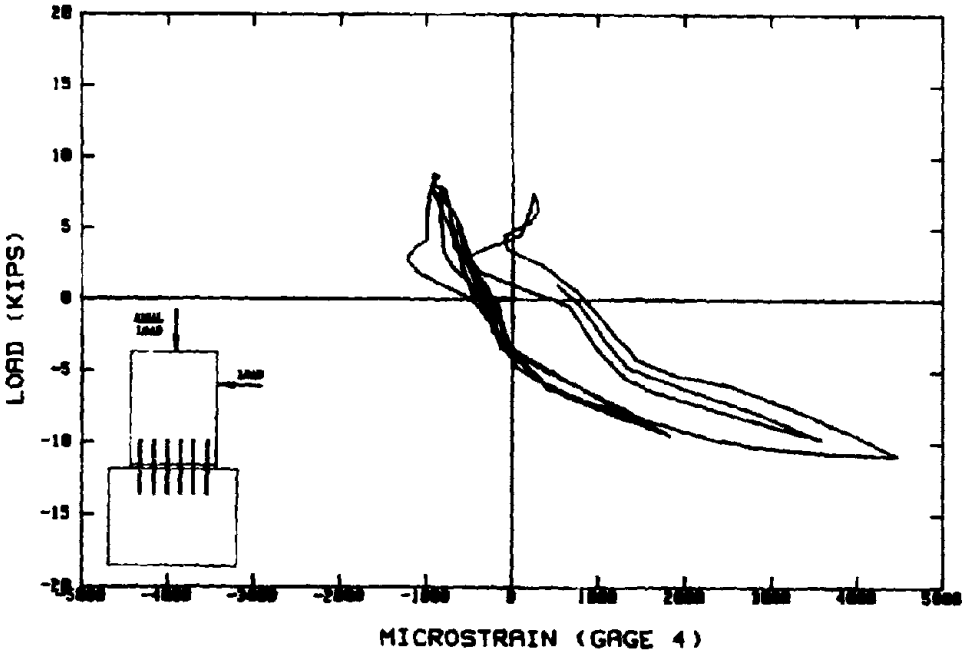

Figure 8-22. Original Specimen Load-Strain Response (Gage 4).

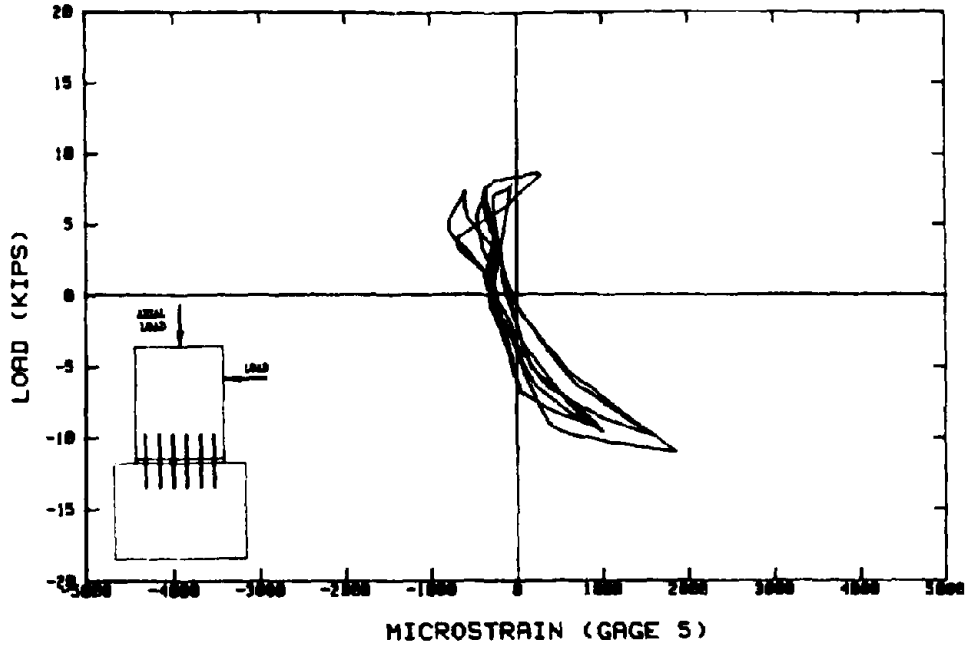

Figure 8-23. Original Specimen Load-Strain Response (Gage 5).

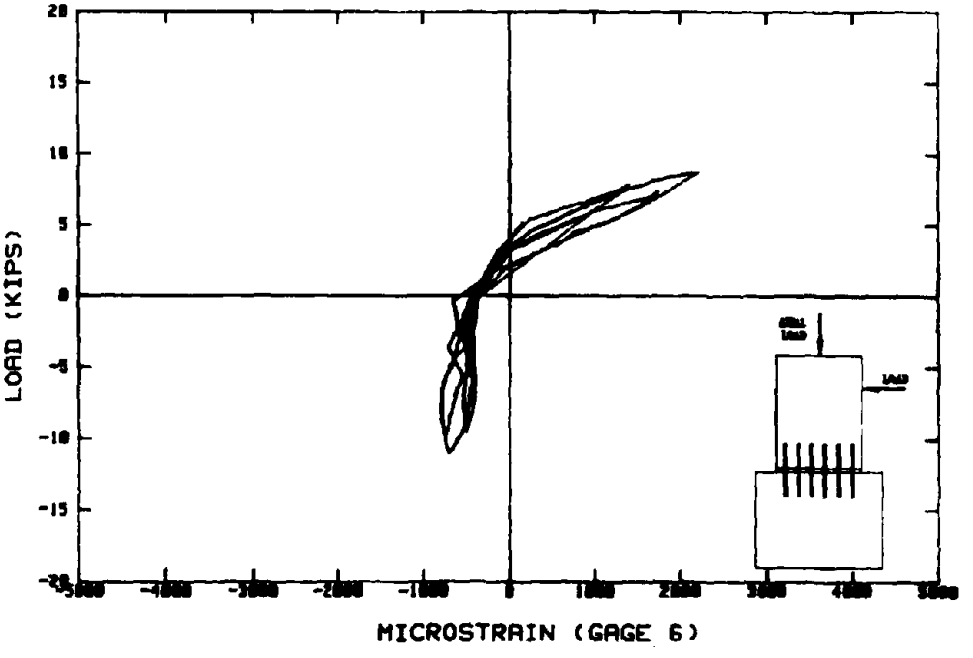

Figure 8-24. Original Specimen Load-Strain Response (Gage 6).

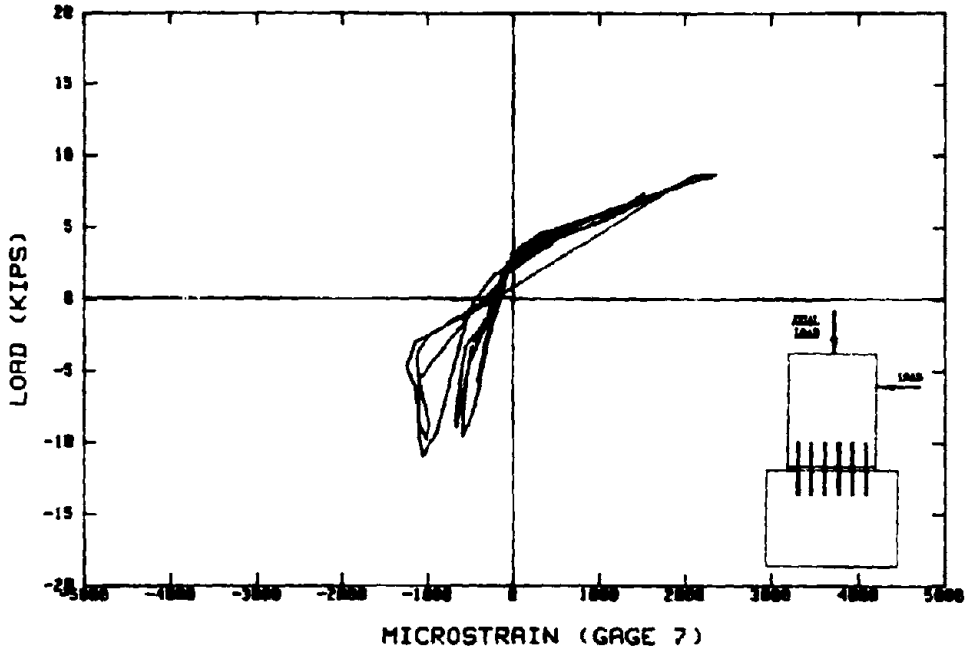

Figure 8-25. Original Specimen Load-Strain Response (Gage 7).

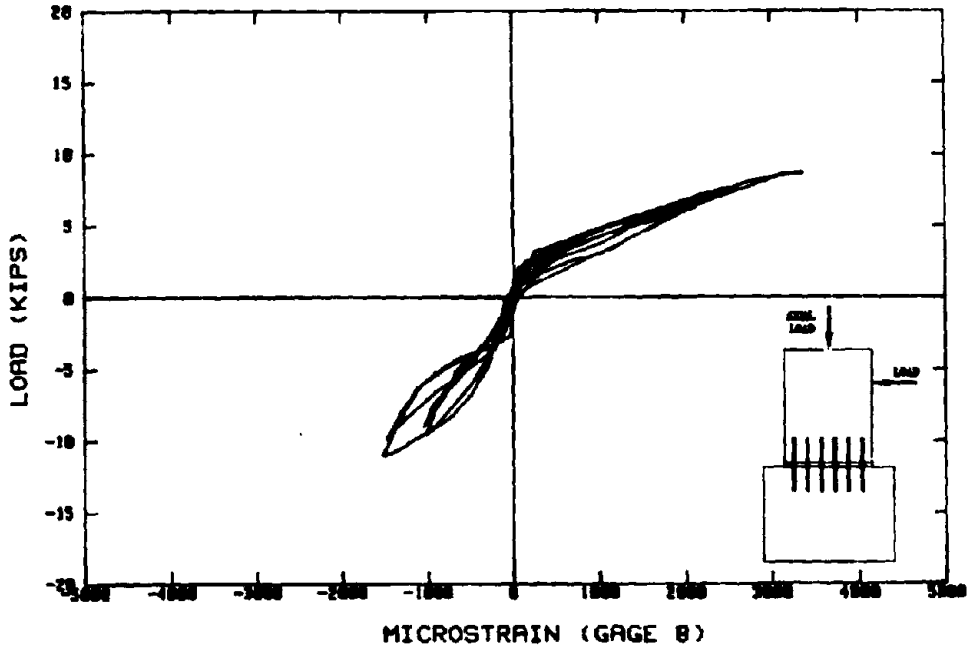

Figure 8-26. Original Specimen Load-Strain Response (Gage 8).

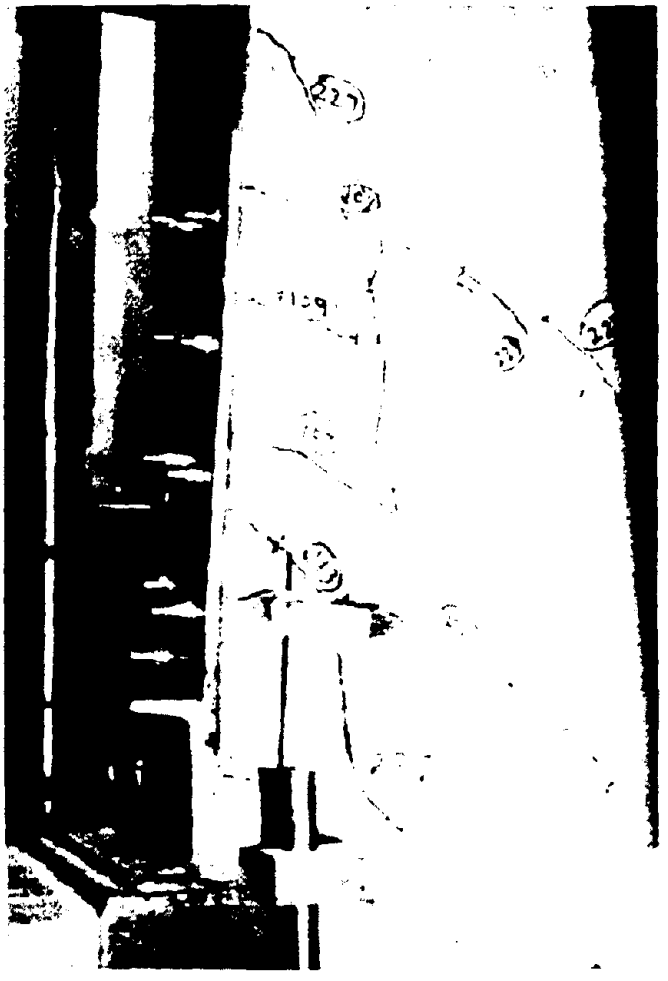

Figure 8-27. Repaired Specimen after Testing (1).

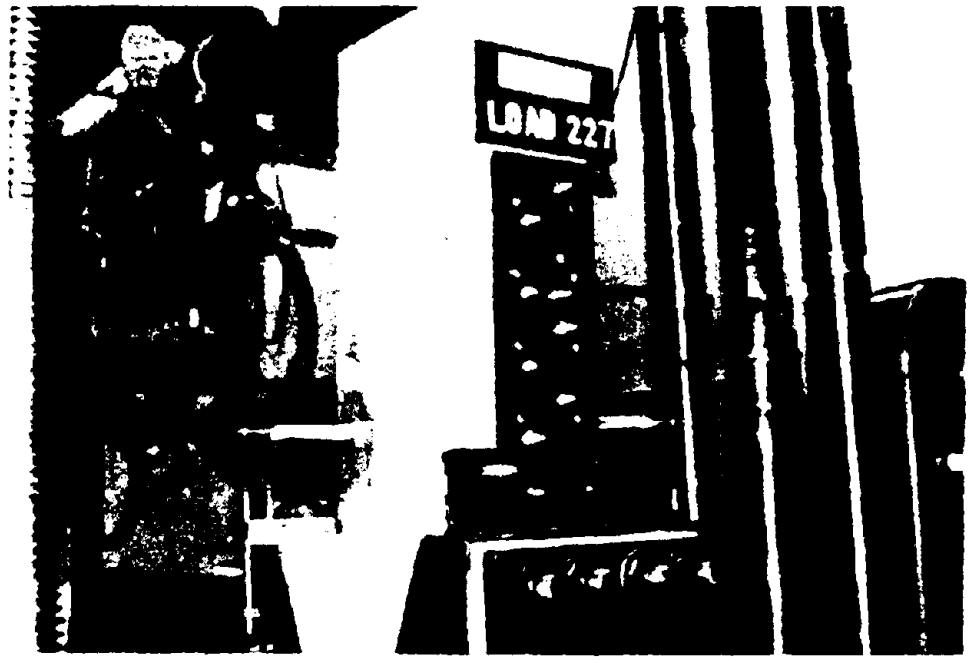

Figure 8-28. Repaired Specimen after Testing (2).

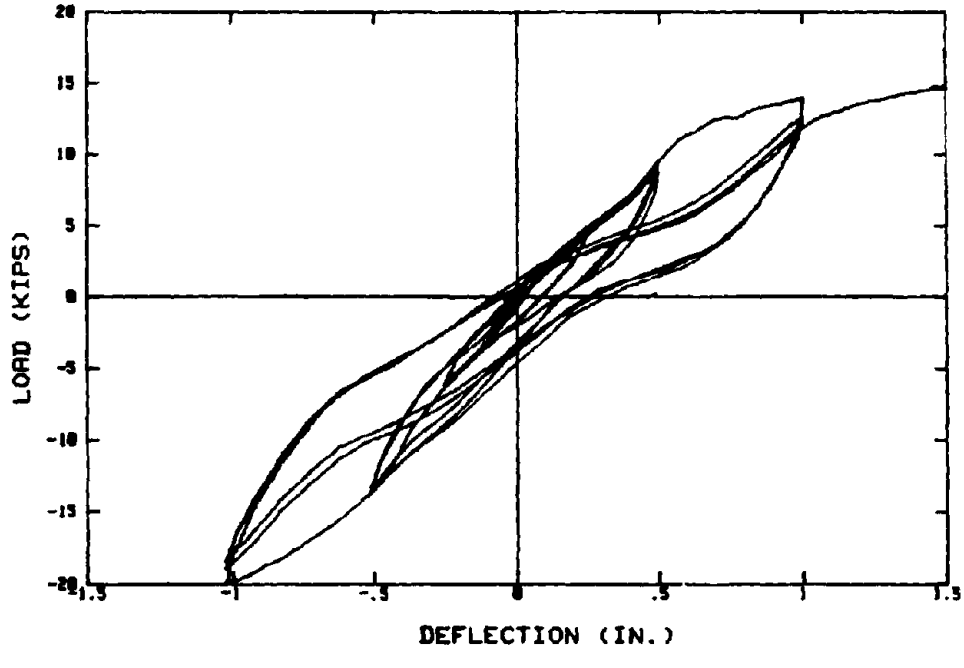

Figure 8-29. Repaired Specimen Load-Deflection Response.

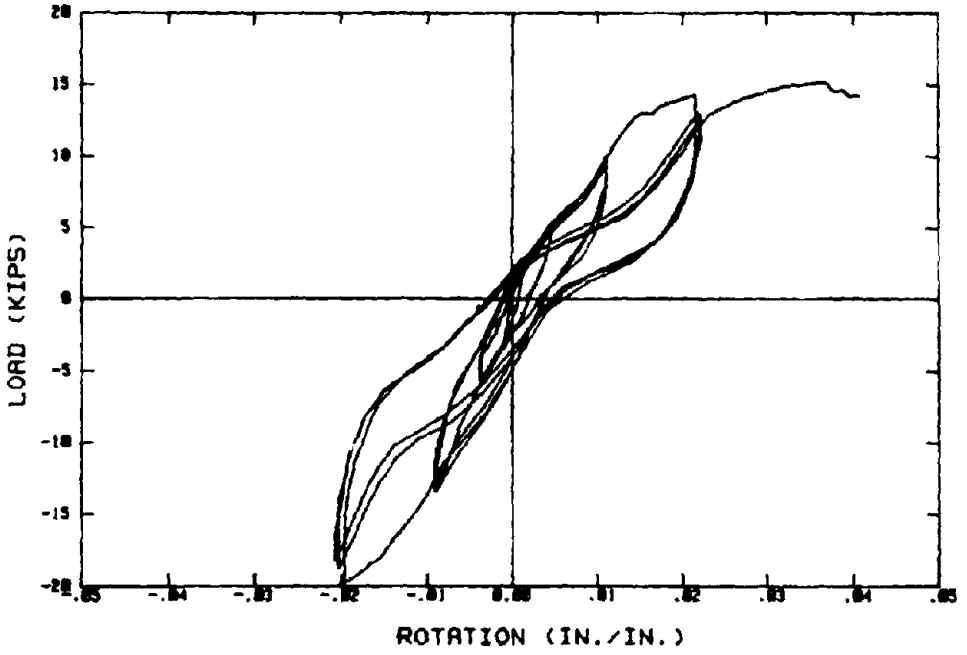

Figure 8-30. Repaired Specimen Load-Rotation Response.

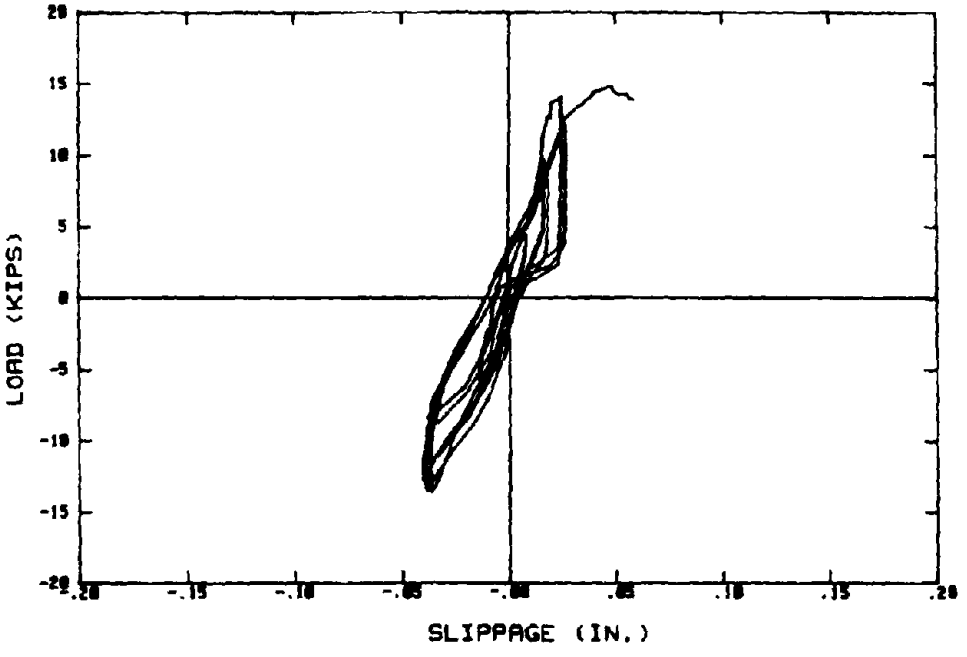

Figure 8-31. Repaired Specimen Load-Slippage Response.

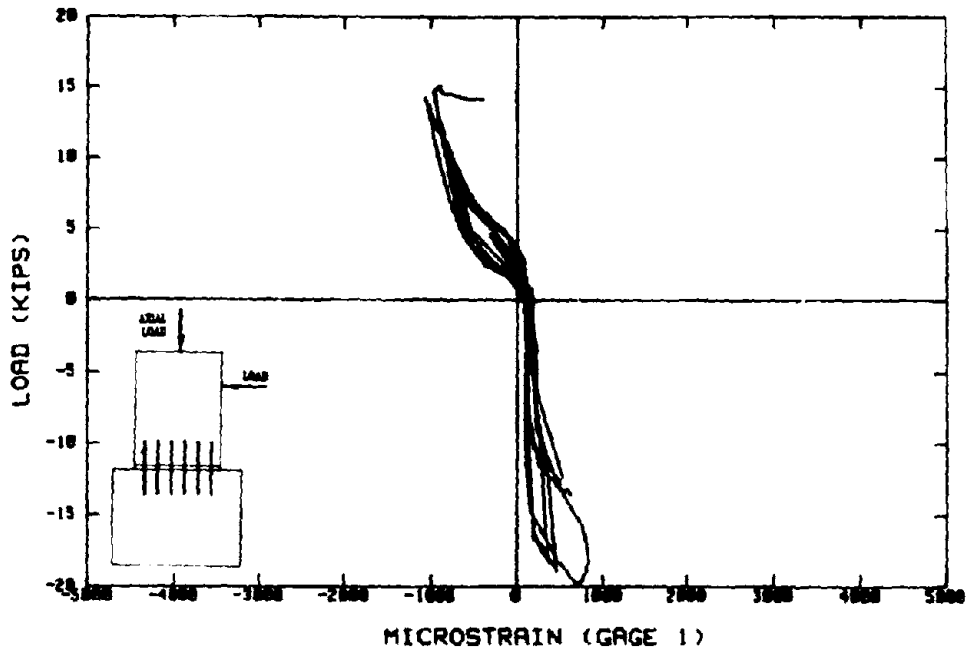

Figure 8-32. Repaired Specimen Load-Strain Response (Gage 1).

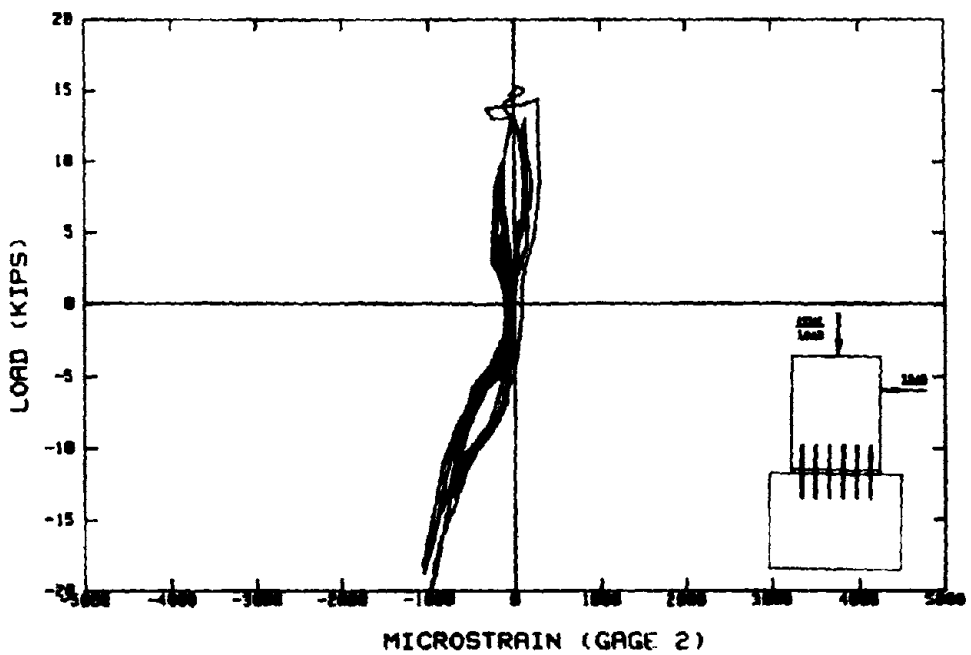

Figure 8-33. Repaired Specimen Load-Strain Response (Gage 2).

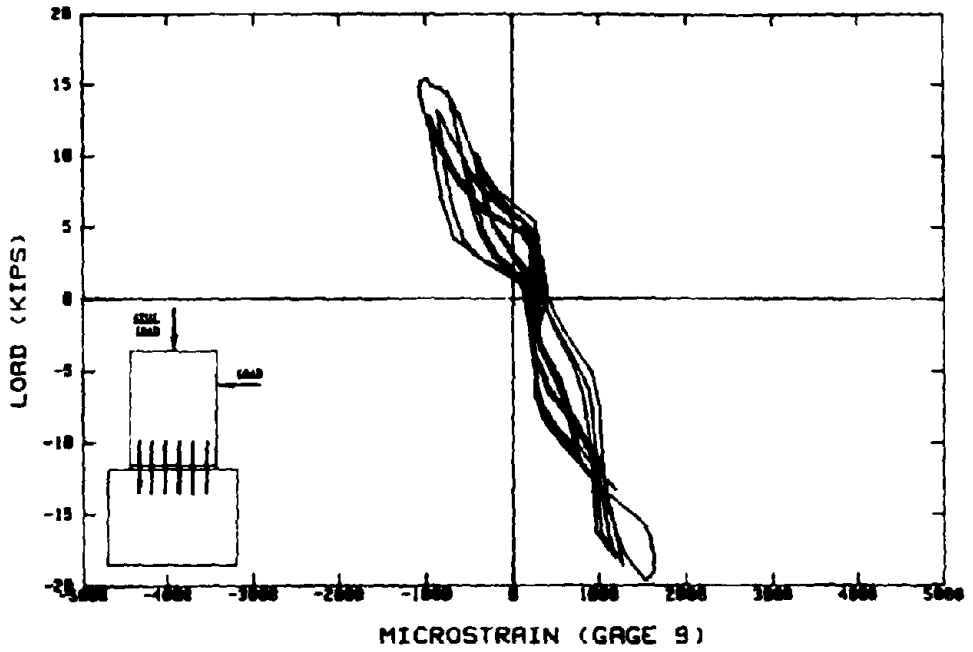

Figure 8-34. Repaired Specimen Load-Strain Response (Gage 9).

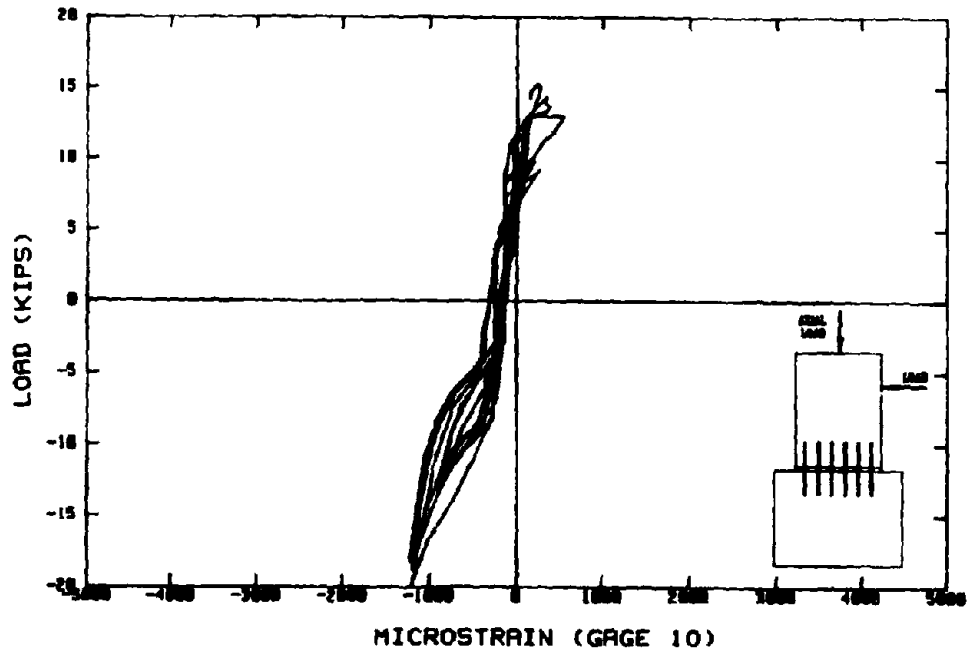

Figure 8-35. Repaired Specimen Load-Strain Response (Gage 10).

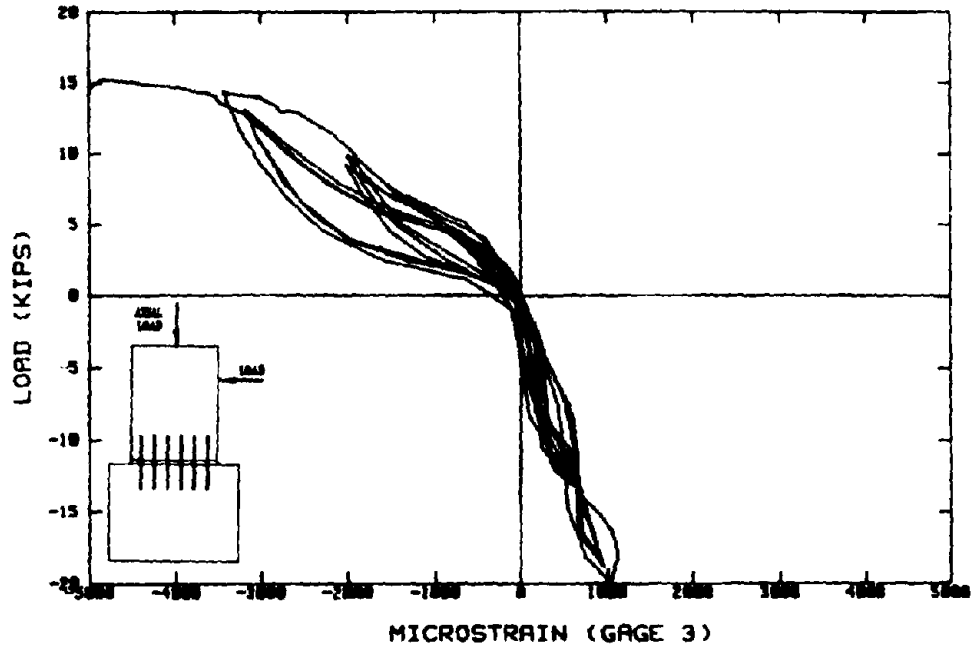

Figure 8-36. Repaired Specimen Load-Strain Response (Gage 3).

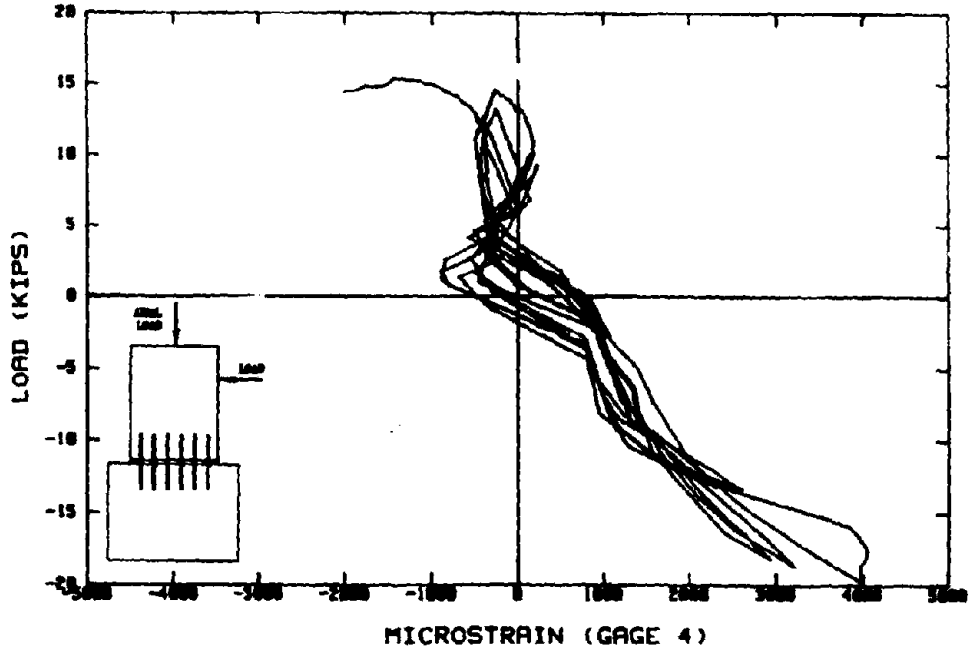

Figure 8-37. Repaired Specimen Load-Strain Response (Gage 4).

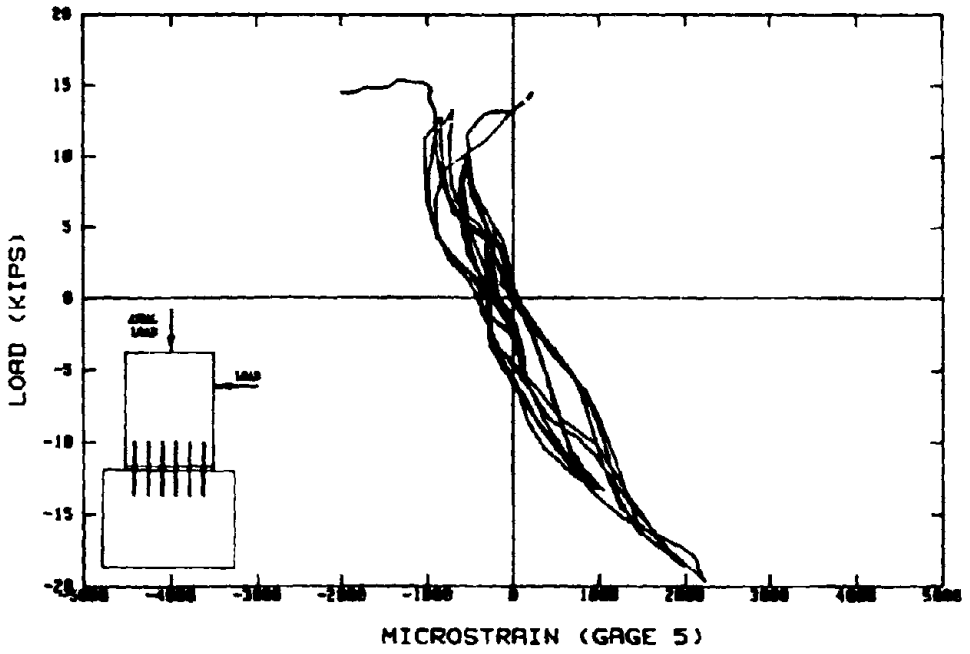

Figure 8-38. Repaired Specimen Load-Strain Response (Gage 5).

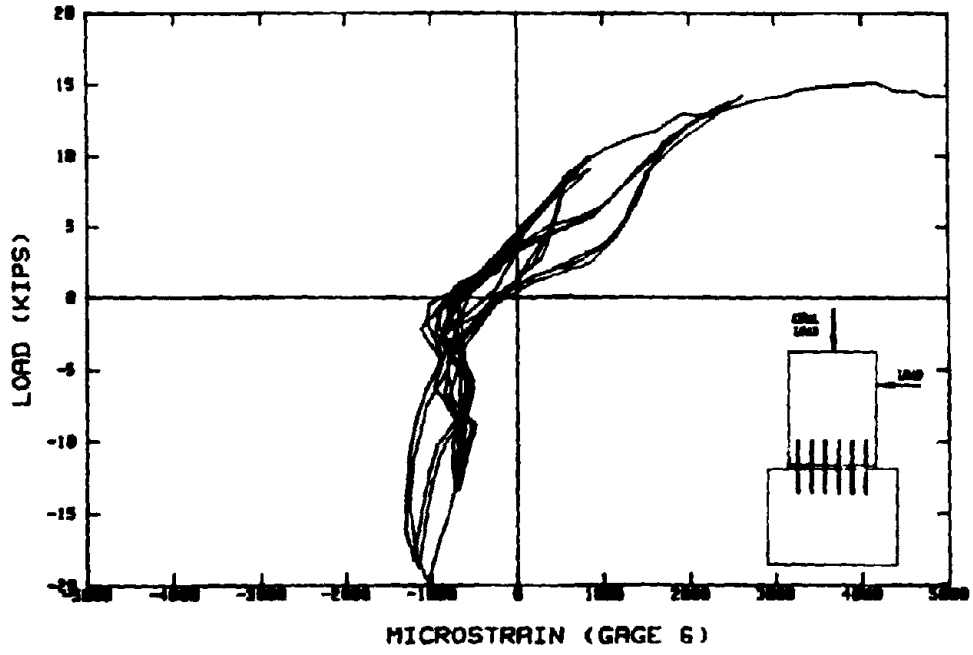

Figure 8-39. Repaired Specimen Load-Strain Response (Gage 6).

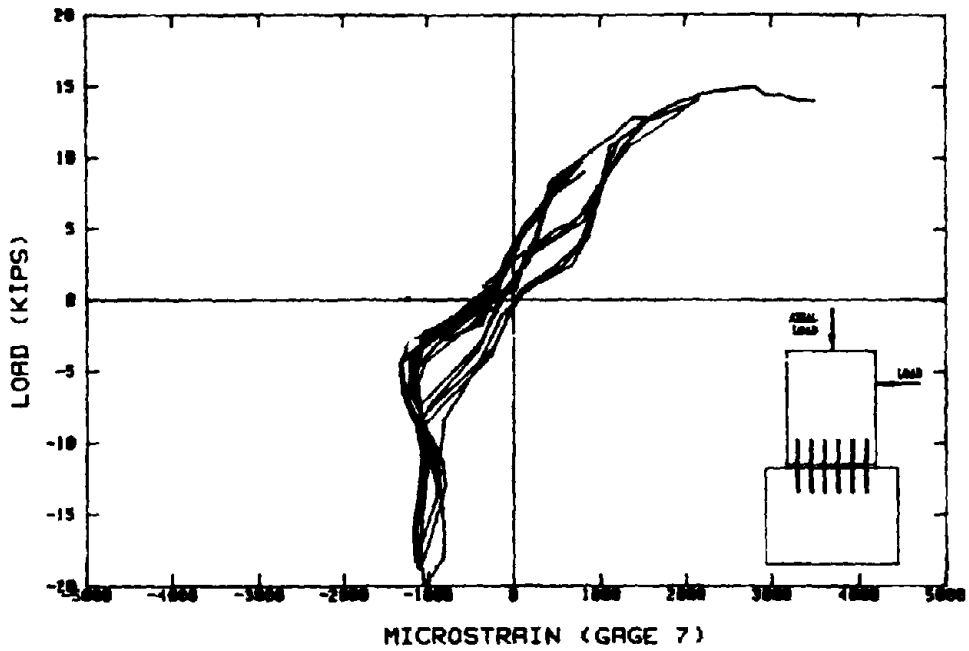

Figure 8-40. Repaired Specimen Load-Strain Response (Gage 7).

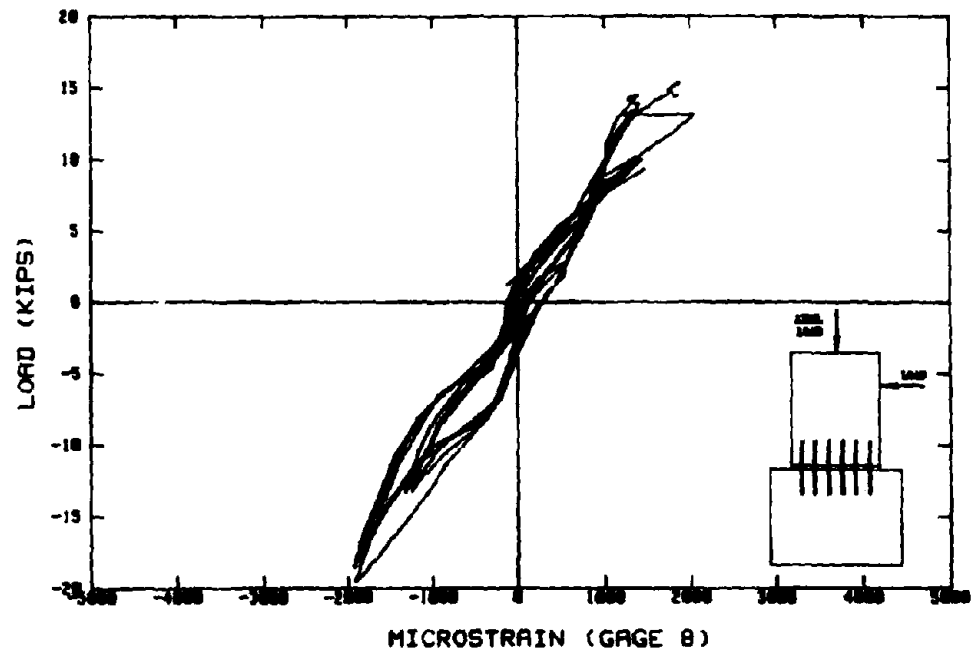

Figure 8-41. Repaired Specimen Load-Strain Response (Gage 8).

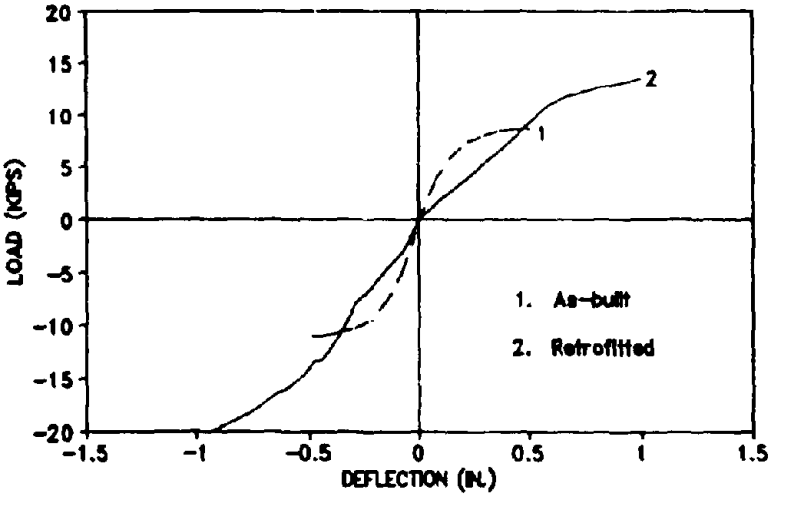

Figure 8-42. Response Comparison of Original and Repaired Column.

List of CCEER Publications

Report No.	Publication
CCEER-84-1	Saiidi, M., and R. A. Lawver. "User's manual for LZAK-C64, a computer program to implement the Q-model on Commodore 64." *Report number CCEER-84-1* Reno: University of Nevada, Department of Civil Engineering. January 1984.
CCEER-84-2	Douglas, B. M., and T. Iwasaki. "Proceedings of the first USA-Japan bridge engineering workshop," held at the Public Works Research Institute, Tsukuba, Japan. *Report number CCEER-84-2.* Reno: University of Nevada, Department of Civil Engineering. April 1984.
CCEER-84-3	Saiidi, M., J. D. Hart, and B. M. Douglas. "Inelastic static and dynamic analysis of short R/C bridges subjected to lateral loads." *Report number CCEER-84-3.* Reno: University of Nevada, Department of Civil Engineering. July 1984
CCEER-84-4	Douglas, B. "A proposed plan for a national bridge engineering laboratory." *Report number CCEER-84-4.* Reno: University of Nevada, Department of Civil Engineering. December 1984.
CCEER-85-1	Norris, G. M., and P. Abdollaholiaee. "Laterally loaded pile response: Studies with the strain wedge model." *Report number CCEER-85-1.* Reno: University of Nevada, Department of Civil Engineering. April 1985.
CCEER-86-1	Ghusn, G. E., and M. Saiidi. "A simple hysteretic element for biaxial bending of R/C columns and implementation in NEABS-86." *Report number CCEER-86-1.* Reno: University of Nevada, Department of Civil Engineering. July 1986.
CCEER-86-2	Saiidi, M., R. A. Lawver, and J. D. Hart. "User's manual of ISADAB and SIBA, computer programs for nonlinear transverse analysis of highway bridges subjected to static and dynamic lateral loads." *Report number CCEER-86-2.* Reno: University of Nevada, Department of Civil Engineering. September 1986.
CCEER-87-1	Siddharthan, R. "Dynamic effective stress response of surface and embedded footings in sand." *Report number CCEER-87-1.* Reno: University of Nevada, Department of Civil Engineering. June 1987.
CCEER-87-2	Norris, G., and R. Sack. "Lateral and rotational stiffness of pile groups for seismic analysis of highway bridges." *Report number CCEER-87-2.* Reno: University of Nevada, Department of Civil Engineering. June 1987.
CCEER-88-1	Orie, J., and M. Saiidi. "A preliminary study of one-way reinforced concrete pier hinges subjected to shear and flexure." *Report number CCEER-88-1.* Reno: University of Nevada, Department of Civil Engineering. January 1988.
CCEER-88-2	Orie, D., M. Saiidi, and B. Douglas. "A micro-CAD system for seismic design of regular highway bridges." *Report number CCEER-88-2.* Reno: University of Nevada, Department of Civil Engineering. June 1988.

CCEER-88-3 Orie, D., and M. Saiidi. "User's manual for Micro-SARB, a microcomputer program for seismic analysis of regular highway bridges." *Report number CCEER-88-3.* Reno: University of Nevada, Department of Civil Engineering. October 1988.

CCEER-89-1 Douglas, B., M. Saiidi, R. Hayes, and G. Holcomb. "A comprehensive study of the loads and pressures exerted on wall forms by the placement of concrete." *Report number CCEER-89-1.* Reno: University of Nevada, Department of Civil Engineering. February 1989.

CCEER-89-2a Richardson, J., and B. Douglas. "Dynamic response analysis of the Dominion Road Bridge test data." *Report number CCEER-89-2.* Reno: University of Nevada, Department of Civil Engineering. March 1989.

CCEER-89-2b Vrontinos, S., M. Saiidi, and B. Douglas. "A simple model to predict the ultimate response of R/C beams with concrete overlays." *Report number CCEER-89-2.* Reno: University of Nevada, Department of Civil Engineering. June 1989.

CCEER-89-3 Ebrahimpour, A., and P. Jagadish. "Statistical modeling of bridge traffic loads: A case study." *Report number CCEER-89-3.* Reno: University of Nevada, Department of Civil Engineering. December 1989.

CCEER-89-4 Shields, J., and M. Saiidi. "Direct field measurement of prestress losses in box girder bridges." *Report number CCEER-89-4.* Reno: University of Nevada, Department of Civil Engineering. December 1989.

CCEER-90-1 Saiidi, M., E. Maragakis, G. Ghusn, Jr., Y. Jiang, and D. Schwartz. "Survey and evaluation of Nevada's transportation infrastructure, task 7.2 - highway bridges, final report." *Report number CCEER-90-1.* Reno: University of Nevada, Department of Civil Engineering. October 1990.

CCEER-90-2 Abdel-Ghaffar, S., E. Maragakis, and M. Saiidi. "Analysis of the response of reinforced concrete structures during the Whittier earthquake of 1987." *Report number CCEER-90-2.* Reno: University of Nevada, Department of Civil Engineering. October 1990.

CCEER-91-1 Saiidi, M., E. Hwang, E. Maragakis, and B. Douglas. "Dynamic testing and analysis of the Flamingo Road Interchange." *Report number CCEER-91-1.* Reno: University of Nevada, Department of Civil Engineering. February 1991.

CCEER-91-2 Norris, G., R. Siddharthan, Z. Zafir, S. Abdel-Ghaffar, and P. Gowda. "Soil-foundation-structure behavior at the Oakland Outer Harbor Wharf." *Report number CCEER-91-2.* Reno: University of Nevada, Department of Civil Engineering. July 1991.

CCEER-91-3 Norris, G. M. "Seismic lateral and rotational pile foundation stiffness at Cypress." *Report number CCEER-91-3.* Reno: University of Nevada, Department of Civil Engineering. August 1991.

CCEER-91-4 O'Connor, D. N., and M. Saiidi. "A study of protective overlays for highway bridge decks in Nevada, with emphasis on polyester-styrene polymer concrete." *Report number CCEER-91-4.* Reno: University of Nevada, Department of Civil Engineering. October 1991.

CCEER-91-5 O'Connor, D. N., and M. Saiidi. "Laboratory studies of polyester-styrene polymer concrete engineering properties." *Report number CCEER-91-5.* Reno: University of Nevada, Department of Civil Engineering. November 1991.

CCEER-92-1 Straw, D. L., and M. "Saiid" Saiidi. "Scale model testing of one-way reinforced concrete pier hinges subjected to combined axial force, shear and flexure." *Report number CCEER-92-1.* Ed. by D. N. O'Connor. Reno: University of Nevada, Department of Civil Engineering. March 1992.

CCEER-92-2 Wehbe, N., M. Saiidi, and F. Gordaninejad. "Basic behavior of composite sections made of concrete slabs and graphite epoxy beams." *Report number CCEER-92-2.* Reno: University of Nevada, Department of Civil Engineering. August 1992.

CCEER-92-3 Saiidi, M., and E. Hutchens. "A study of prestress changes in a post-tensioned bridge during the first 30 months." *Report number CCEER-92-3.* Reno: University of Nevada, Department of Civil Engineering. April 1992.

CCEER-92-4 Saiidi, M., B. Douglas, S. Feng, E. Hwang, and E. Maragakis. "Effects of axial force on frequency of prestressed concrete bridges." *Report number CCEER-92-4.* Reno: University of Nevada, Department of Civil Engineering. August 1992.

CCEER-92-5 Siddharthan, R., and Zafir, Z. "Response of layered deposits to traveling surface pressure waves." *Report number CCEER-92-5.* Reno: University of Nevada, Department of Civil Engineering. September 1992.

CCEER-92-6 Norris, G., and Zafir, Z. "Liquefaction and residual strength of loose sands from drained triaxial tests." *Report number CCEER-92-6.* Reno: University of Nevada, Department of Civil Engineering. September 1992.

CCEER-92-7 Douglas, B. "Some thoughts regarding the improvement of the University of Nevada, Reno's national academic standing." *Report number CCEER-92-7.* Reno: University of Nevada, Department of Civil Engineering. September 1992.

CCEER-92-8 Saiidi, M., E. Maragakis, and S. Feng. "An evaluation of the current Caltrans seismic restrainer design method." *Report number CCEER-92-8.* Reno: University of Nevada, Department of Civil Engineering. October 1992.

CCEER-92-9 O'Connor, D. N., M. Saiidi, and E. A. Maragakis. "Effect of hinge restrainers on the response of the Madrone Drive Undercrossing during the Loma Prieta earthquake." *Report number CCEER-92-9.* Reno: University of Nevada, Department of Civil Engineering. February 1993.

CCEER-92-10 O'Connor, D. N., and M. Saiidi. "Laboratory studies of polyester concrete: Compressive strength at elevated temperatures and following temperature cycling, bond strength to portland cement concrete, and modulus of elasticity." *Report number CCEER-92-10.* Reno: University of Nevada, Department of Civil Engineering. February 1993.

CCEER-92-11 Wehbe, N., M. Saiidi, and D. O'Connor. "Economic impact of passage of spent fuel traffic on two bridges in north-east Nevada." *Report number CCEER-92-11.* Reno: University of Nevada, Department of Civil Engineering. December 1992.

CCEER-93-1 Jaing, Y., and M. Saiidi. "Behavior, design, and retrofit of reinforced concrete one-way bridge column hinges." *Report number CCEER-93-1*. Ed. by D. N. O'Connor. Reno: University of Nevada, Department of Civil Engineering. March 1993.